Aus dem Institut für Molekularbiologie Göttingen
(Prof. Dr. rer. nat. M. T. Bohnsack)
im Zentrum Biochemie und Molekulare Zellbiologie
der Medizinischen Fakultät der Universität Göttingen

Analysis of Expression of RNA Helicases and Cofactors in Human Tissues and Cancer

INAUGURAL-DISSERTATION

zur Erlangung des Doktorgrades
der Medizinischen Fakultät der
Georg-August-Universität zu Göttingen

vorgelegt von

Karolin Rathje

aus

Gifhorn

Göttingen 2022

Dekan: Prof. Dr. med. W. Brück

Betreuungsausschuss

Betreuer: Prof. Dr. rer. nat. M. T. Bohnsack

Ko-Betreuer: Prof. Dr. med. M. Dobbelstein

Prüfungskommission

Referent/in: Prof. Dr. rer. nat. M. T. Bohnsack

Ko-Referent/in: …..…….

Drittreferent/in: …..…….

Datum der mündlichen Prüfung: ……..

Hiermit erkläre ich, die Dissertation mit dem Titel "Analysis of Expression of RNA Helicases and Cofactors in Human Tissues and Cancer" eigenständig angefertigt und keine anderen als die von mir angegebenen Quellen und Hilfsmittel verwendet zu haben.

Göttingen, den …… ……

List of contents

List of figures

List of tables

List of abbreviations

APS	ammonium persulfate
ATP	adenosine triphosphate
ATPase	adenosine triphosphatase
BSA	bovine serum albumin
Bis-Tris	bis(2-hydroxyethyl)amino-tris(hydroxymethyl)methane
cDNA	complementary desoxyribonucleic acid
Ct	threshold cycle
CNP	Cerium oxide nanoparticles
D1	RecA-like domain 1
D2	RecA-like domain 2
DMEM	Dulbecco's Modified Eagle Medium
DMSO	dimethyl sulfoxide
DNA	deoxyribonucleic acid
dNTP	deoxynucleotide triphosphate
dsRNA	double-stranded RNA
DTT	dithiothreitol
EBV	Epstein-Barr virus
ECACC	European Collection of Authenticated Cell Cultures
EDTA	ethylenediaminetetraacetic acid
FCS	foetal calf serum
FMS	fibromyxosarcoma
fwd	forward
HCC	hepatocellular carcinoma
HIV-1	human immunodeficiency virus 1
HPV	human papillomavirus
miRNA	micro RNA
mRNA	messenger RNA
NCBI	National Center for Biotechnology Information
NGS	next generation sequencing
NS3hel	NSR helicase

NS3pro	NSR protease
NTP	nucleoside triphosphate
OB	oligonucleotide/oligosaccharide-binding
P38-MAPK	p38 mitogen-activated protein kinase
PAGE	polyacrylamide gel electrophoresis
PIPES	piperazine-N,N'-bis(2-ethanesulfonic acid)
PBS	phosphate buffered saline
PBS-T	phosphate buffered saline with Tween
pre-mRNA	precursor mRNA
pre-rRNA	precursor rRNA
qPCR	quantitative polymerase chain reaction
RBM	RNA binding motif
rev	reverse
RNA	ribonucleic acid
RNP	ribonucleoprotein
ROS	reactive oxygen species
RRM	RNA recognition motif
rRNA	ribosomal RNA
SCC	squamous cell carcinoma
SDS	sodium dodecyl sulphate
SDS-PAGE	SDS polyacrylamide gel electrophoresis
SF	superfamily
snRNP	small nuclear ribonucleoprotein
ssRNA	single stranded RNA
TBS	Tris-buffered saline
TBS-T	Tris-buffered saline with Tween
TEMED	tetramethylethylenediamine
Tris	tris(hydroxymethyl)aminomethane
VE-cadherin	vascular endothelial cadherin
WB buffer	western blot buffer
WH	winged helix
x	times

1. Introduction

1.1. RNA helicases

Historically, ribonucleic acid (RNA) helicases were first described as proteins that are characterized by their unwinding activity on double-stranded nucleic acids via nucleoside triphosphate (NTP) hydrolysis back in 1976 (Abdel-Monem and Hoffmann-Berling 1976; Abdel-Monem et al. 1976). It has recently been shown that this definition is far from sufficient, and the designation 'helicase' might be misleading. While some RNA helicases possess RNA unwinding ability, others lack this function and instead act in duplex annealing or as RNA clamps within ribonucleoprotein (RNP) complexes. Moreover, RNA helicase features are much more diverse than it was assumed some decades ago (Putnam and Jankowsky 2013).

1.1.1. Helicase families

RNA helicases can be divided into six superfamilies (SF), based on their shared conserved sequence motifs (Gorbalenya and Koonin 1993). These are harbored in the so-called RecA-like domains, which represent the core of the proteins (Hilbert et al. 2009). Hexameric SF 3, 4 and 5 helicases that are mostly found in viruses only consist of one RecA-like domain, while monomeric SF1 and SF2 helicases usually feature two of these conserved structures (Leitão et al. 2015). Especially SF2 helicases are characterized by their striking functions in RNA and RNP manipulation (Jarmoskaite and Russell 2014). They are subclassified into nine families and a small group (Fairman-Williams et al. 2010), most important amongst which are the DEAD-box, DEAH-box and Ski2-like helicases. Within human cells, the largest families are the 40 members of the DEAD-box protein family and the 15 members of the DEAH-box helicase family (Jarmoskaite and Russell 2014; Leitão et al. 2015; Putnam and Jankowsky 2013; Jankowsky 2011). Between these two types of helicase, not only their substrates but also their functional properties differ (Jarmoskaite and Russell 2014), as further described in section 1.1.3.

1.1.2. Overall architecture and conserved sequence motifs

As already mentioned in section 1.1.1, SF2 helicases all contain a conserved protein core, not only in human cells but in all forms of life as well as in viruses (Leitão et al. 2015). These two

RecA-like domains (D1 and D2) — the name deriving from the similarity to the *Escherichia coli* recombinase RecA (Story et al. 1992; Abdel-Monem et al. 1976; Story and Steitz 1992) — possess up to twelve identified conserved sequence motifs (Figure 1). These motifs are crucial for the protein's functions. For example, NTP and nucleic acid substrate binding take place here (Fairman-Williams et al. 2010; Hilbert et al. 2009; Jarmoskaite and Russell 2014). In many SF2 helicases, the RecA regions are framed by additional domains that can either be conserved or vary (Fairman-Williams et al. 2010).

More precisely, both DEAH-box as well as Ski2-like-helicases possess a conserved winged helix (WH) and ratchet domain, while a subset of Ski2-like-helicases feature an invariant arch domain component. DEAH-box helicases, on the other hand, share a common oligonucleotide/oligosaccharide-binding(OB)-fold domain (Weir et al. 2010; He et al. 2010). Alongside, these domains are located next to non-conserved structures (Figure 1). The importance of these auxiliary regions will be further exemplified in the following sections, as they significantly affect protein activities. Regulation of RNA helicase activity can also occur through the influence of either autoinhibitory effects, or the interaction with protein partners for adenosine triphosphatase (ATPase) activity regulation and with nucleic acids via RNA recognition domains (Fairman-Williams et al. 2010; Putnam and Jankowsky 2013; Ozgur et al. 2015).

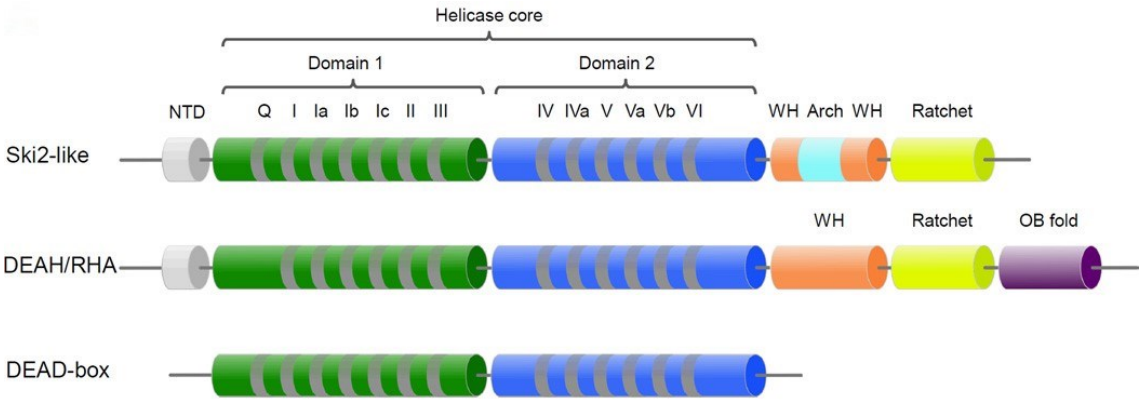

Figure 1: SF2 helicase conserved motifs. Conserved motifs of the helicase core are depicted in gray. The structural architecture of DEAH/RHA and Ski2-like is shown here for Mtr4 and Prp43, where domains are not to scale. DEAH-box and Ski2-like helicases possess a conserved WH and ratchet domain. A subset of Ski2-like-helicases also feature an invariant arch domain. DEAH-box helicases typically share a common OB-fold domain. The N-terminal domains (NTD) are not conserved. Modified from "Superfamily 2 (SF2) families involved in RNA chaperoning and RNP remodeling" by Jarmoskaite and Russell 2014, which is licensed from Annual Review of Biochemistry.

1.1.3. Molecular functions and mechanisms

Recent studies have revealed a constantly extending set of roles of structured RNAs and their importance for the cell's biological processes (Kapranov et al. 2007). In order to function properly, folded RNAs are dependent on their precisely formed three-dimensional conformations as well as association with RNA-binding proteins to form RNP complexes (Jarmoskaite and Russell 2014). To assemble such structures, they often face obstacles as their kinetically stable bonding of secondary local structures traps them in immature conformations (Russell 2008; Herschlag 1995). At this point, RNA helicase proteins perform key roles and their chaperoning function is indispensable at almost all steps of gene expression, as detailed in section 1.1.4 (Jankowsky 2011; Pan and Russell 2010). While RNA helicases possess nucleic acid-dependent nucleotide hydrolysis activity, their mechanistic capabilities vary within the SF2 helicase family, especially concerning their RNA processivity (Jarmoskaite and Russell 2014). DEAH-box and Ski2-like-helicases usually translocate from 3‘ to 5‘ and unwind RNA substrates in an adenosine triphosphate (ATP)-hydrolysis dependent manner (Bernstein et al. 2008). Crystal structure analysis of Prp43, which is a well-studied yeast DEAH-box helicase, revealed that this process is promoted by a β-turn of the RecA1-like domain containing a newly identified RF-motif (Tauchert et al. 2017). They are reliant on a 3'-single stranded RNA (ssRNA) overhang for helicase loading (Pena et al. 2009), and unwinding takes place directionally by translocating from 3' to 5'. RNA unwinding efficiency decreases when substrate RNA helices grow in length (Bernstein et al. 2008). Upon single-stranded nucleic acid and ATP binding to the helicase core (usually D1) movement of the two RecA-like domains (D1 and D2) is enabled. The helicase thereby shifts from a rigid ligand-free 'OFF' to the active 'ON' configuration (Figure 2a) (Bourgeois et al. 2016). Translocation takes place as D1 moves along the nucleic acid strand. ATP hydrolysis is then followed by product dissociation and RecA domain dissociation as well as simultaneous movement of D2 by one nucleotide along the substrate RNA. The open conformation enables the RNA helicase to re-bind ATP and perform another round of translocation (Jarmoskaite and Russell 2014; Tauchert et al. 2017). The ancillary winged-helix domain and ratchet domain also contact the substrate RNAs and this proximity is also suggested to be important for the unwinding process (Johnson and Jackson 2013).

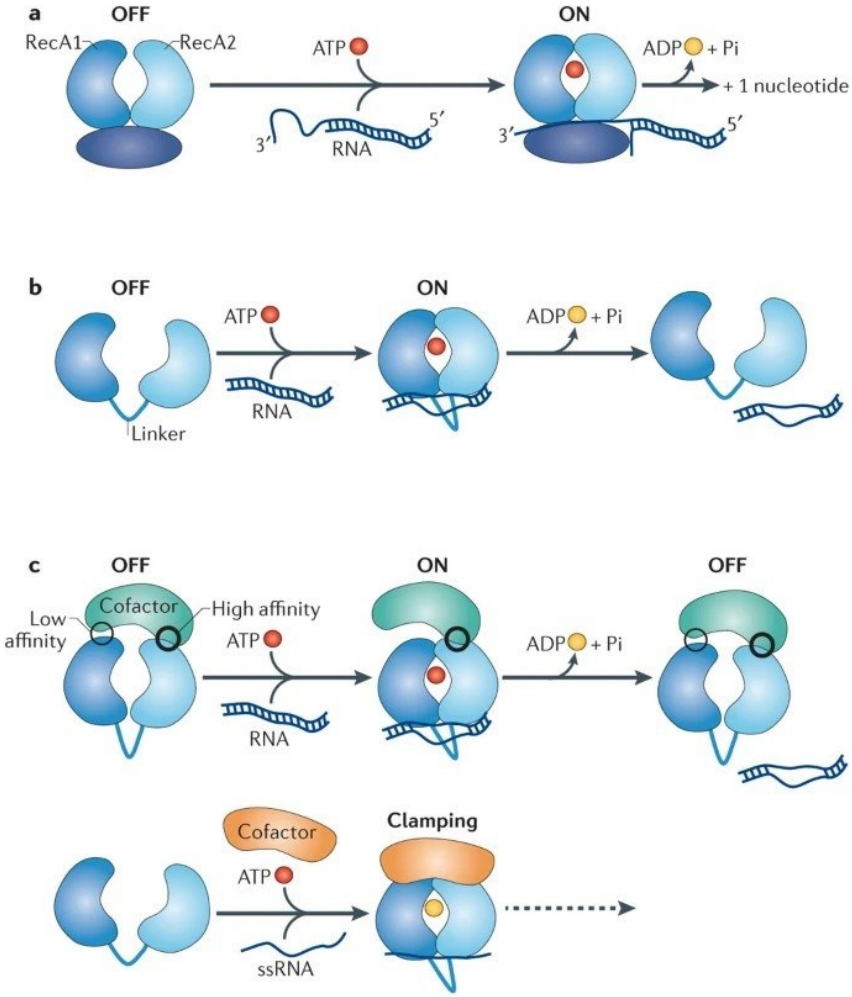

Figure 2: Molecular mechanisms of RNA helicases. Processive RNA helicases rely on a 3'-ssRNA overhang for helicase loading (Pena et al. 2009) and unwinding takes place directionally by translocating from 3' to 5'. Upon 3' single-stranded nucleic acid and ATP binding to the helicase core, movement of the two RecA-like domains is enabled. The helicase thereby shifts from the rigid ligand-free 'OFF' to the active 'ON' configuration. Translocation takes place as RecA1 moves along the nucleic acid strand. ATP hydrolysis is then followed by product dissociation and RecA domain dissociation as well as simultaneous movement of RecA2 by one nucleotide along the substrate RNA (not completely shown here). **b)** Non-processive RNA helicases such as DEAD-box helicases act locally, directly unwinding the double-stranded RNA region internally without translocating. A linker region and/or their short auxiliary domains allow for high mobility in the ligand-free 'OFF' conformation. Simultaneous docking of ATP and RNA causes closure of the two RecA-like domains and the conformational change from the flexible 'OFF' to the constant 'ON' formation (Bourgeois et al. 2016). This conformational change induces the distortion of the double-stranded RNA (dsRNA) strands, and thereby leads to local unwinding as well as ATP hydrolysis as a result of ATPase site formation. This is then followed by product release (Jarmoskaite and Russell 2014). **c)** The protein's binding site and its ATP hydrolysis activity are affected by interactions with different cofactors, which show varying affinities with the RecA domains. The upper panel shows helicase activation, resulting from the displacement of the weak binding of RecA1. Moreover, some cofactors have been associated with RNA helicase inhibition by trapping the RNA strand in the closed 'ON' conformation (lower panel). ATP hydrolysis occurs, but release of the inorganic phosphate is impeded. Thus, RNA dissociation cannot take place. „Mechanisms of action of RNA helicases" by Bourgeois et al. 2016 is licensed from Springer Nature.

The DEAD-box RNA helicases, in contrast to the other two families, perform their substrate unwinding activities non-processively (Mallam et al. 2012). It was shown that they do not need a single-stranded overhang for unwinding. They rather act locally, directly unwinding the double-stranded RNA region internally without translocating (Yang and Jankowsky 2006; Halls et al. 2007). Furthermore, an essential step for unwinding for DEAD-box helicases is ATP binding, whereas ATP hydrolysis follows unwinding and only facilitates the release of the RNA product. As the DEAD-box protein remains bound to its substrate RNA during the strand separation process, it is generally accepted that they are only capable of unwinding short stretches of double-stranded RNA (Chen et al. 2008). Mechanistically, it was revealed that D2 alone can bind the double-stranded RNA, whereas D1 is responsible for ATP binding (Schütz et al. 2010). Simultaneous docking of the ligands causes closure of the two RecA-like domains, a conformational change from the flexible 'OFF' to the constant 'ON' conformation (Mallam et al. 2012; Andersen et al. 2006; Bourgeois et al. 2016; Bono et al. 2006). This conformational change induces the distortion of one of the dsRNA strands, and thereby leads to local unwinding as well as ATP hydrolysis as a result of ATPase site formation. This is then followed by product release (Figure 2b) (Jarmoskaite and Russell 2014).

In addition, DEAD-box helicases can also chaperone the annealing process of single-stranded RNAs in an ATP-independent manner (Halls et al. 2007; Yang and Jankowsky 2005). In contrast to duplex unwinding, this function may be linked to poor ATPase and unwinding activities (Jarmoskaite and Russell 2014). Moreover, DEAD-box RNA helicases can perform RNA clamping by ATP-dependent binding to RNA substrates, but failure to release them due to impaired ATP hydrolysis. Thereby, they stay bound to the nucleic acid in the closed 'ON' conformation of the helicase (Bourgeois et al. 2016; Putnam and Jankowsky 2013; Linder and Jankowsky 2011).

Beside the unwinding and annealing activities, SF2 helicases can assist in RNP complex remodeling, in the form of protein displacement (Linder and Jankowsky 2011; Jarmoskaite and Russell 2014). Protein removal from structured RNA is dependent on ATP-hydrolysis (Fairman-Williams et al. 2010; Jankowsky 2011; Jankowsky et al. 2001). Depending on the type of RNA helicase involved, this can either occur by directional translocation (Jankowsky and Bowers 2006) or by induction of spontaneous protein detachment (Bowers et al. 2006).

1.1.4. Cellular functions – all steps of gene expression

Superfamily 2 helicase chaperoning and remodeling functions are indispensable for the biology of structured RNAs (Herschlag 1995). In the complex pathway of ribosome biogenesis, a lot of RNA helicases are needed to promote precursor ribosomal RNA (pre-rRNA) cleavages, modifications and folding as well as ribosomal RNA (rRNA) assembly with ribosomal proteins and trans-acting biogenesis factors (Strunk and Karbstein 2009; Shajani et al. 2011). They not only interact with pre-rRNAs, but can also modulate small nucleolar RNA (snoRNA) base pairing and assist in small nucleolar RNA-protein complex (snoRNP) function (Martin et al. 2013) in pre-rRNA folding and cleavages as well as installation of rRNA modifications (Watkins and Bohnsack 2012). Besides ribosome biogenesis, SF2 RNA helicases also play key roles in precursor mRNA (pre-mRNA) splicing (Cordin and Beggs 2013). Co- or post-transcriptionally, splice sites within immature transcripts can be recognized by a variety of splicing factors (Fu and Ares 2014; Witten and Ule 2011). Here, RNA helicases are not only crucial for secondary structure alterations and assembly of spliceosome complexes – consisting of small nuclear RNAs (snRNAs) and multiple proteins – but they also assist in spliceosome activation, small nuclear RNP (snRNP) disassembly and recycling as well as ATP-dependent proofreading of different steps in the splicing process and turnover of aberrant complexes and products (Cordin and Beggs 2013; Chang et al. 2013; Semlow and Staley 2012; Jarmoskaite and Russell 2014; Semlow et al. 2016; Bourgeois et al. 2016). Another major cellular pathway that requires RNA helicases is translation, especially for remodeling of the 5' untranslated region (5'UTR) during translation initiation, but also at later steps during the translation cycle (Jarmoskaite and Russell 2014; Gross et al. 2007). RNA helicases further function in RNA degradation, for example via interactions with the degradosome complex (Hardwick and Luisi 2013). Some RNA helicases play important roles in micro RNA (miRNA) biogenesis and their assembly with proteins to form micro RNP (miRNP) complexes as well as mRNA association of these complexes for gene silencing (Jonas and Izaurralde 2015; Bourgeois et al. 2016). SF2 members have also been implicated in various other pathways, such as in facilitating transcription, mRNA transport and storage in RNA granules (Hooper and Hilliker 2013; Hilliker 2012; Fuller-Pace 2013; Jarmoskaite and Russell 2014).

Besides the individual roles of RNA helicases at different steps of gene expression, multifunctional RNA helicases can also play key roles in coupling and orchestrating multiple biological processes (Bourgeois et al. 2016).

1.2. RNA helicase cofactors

The activity of a helicase can be influenced by protein partners, so-called helicase cofactors. As outlined earlier in section 1.1.2, these cofactors can bind to the N- and C-terminal ancillary regions of the RNA helicase or to the helicase core itself. A number of SF2 helicases were found to be multifunctional and it has been shown that they require cofactor proteins for identification of their substrates, suggesting that several such partner proteins can affect the activity of a multifunctional helicase (Linder and Jankowsky 2011; Ozgur et al. 2015). They do so by recruiting helicases to their respective RNA substrates and modulating their catalytic activity (Sloan and Bohnsack 2018). This is either performed through inducing changes in the tertiary structure or by regulating interactions with substrate RNAs (Napetschnig et al. 2009).

Either low or high-affinity interactions of cofactors with the two RecA domains determine the helicase's conformational changes and thereby its ATP hydrolysis activity. Moreover, some cofactors have been proposed as RNA helicase inhibitors by trapping the RNA strand in the closed 'ON' conformation. ATP hydrolysis occurs, but release of the inorganic phosphate is impeded. Thus, RNA dissociation cannot take place (Figure 2) (Bourgeois et al. 2016).

It has been shown that RNA helicases can regulate various steps in gene expression in a cell type-specific way (Dardenne et al. 2014). Besides cell type-specific signaling pathways, the expression of different sets of substrate nucleic acids and regulation of the expression of the RNA helicase itself, the availability of its cofactors likely represents additional means for cell type-specific functions of such enzymes (Bourgeois et al. 2016).

1.2.1. MIF4G domain cofactors and other examples of helicase-cofactor pairs

It has been revealed that some cofactors share the same, typical RNA helicase binding domain. A subset of DEAD-box helicases, namely the eukaryotic initiation factor-4A(eIF4A)-like helicases, are composed of the two RecA-like domains and usually lack any auxiliary regions (Ozgur et al. 2015). They interact with cofactors that share a conserved MIF4G domain (Ponting 2000). The latter consists of ten antiparallel α helices that make up five so-called HEAT repeats. Each HEAT repeat consists of 37 to 47 amino acids and together they associate in an arc-like structure to form the RNA helicase binding site (Sloan and Bohnsack 2018). While the N-terminal region of the MIF4G cofactors forms strong interactions with the RecA2 domain of the helicase, the interaction with the C-terminal region to the RecA1 domain is rather weak (Schütz et al. 2008). Upon cofactor binding, the

helicase changes into a 'half-open' conformation, promoting RNA substrate and ATP binding and formation of the closed conformation. This is then followed by double-stranded RNA unwinding, ATP hydrolysis and release of the substrate, ADP and phosphate (Hilbert et al. 2011). Interestingly, some MIF4G cofactors are also able to impede the helicase's unwinding activity and perform RNA clamping instead (Ballut et al. 2005). As their HEAT repeat domain features an additional α helix, this causes slight conformational changes resulting in altered affinity of RecA1 to the inhibiting cofactor and a different mode of RNA binding and subsequently the inhibition of the RNA helicase (Sloan and Bohnsack 2018; Alexandrov et al. 2012; Steckelberg et al. 2012). Overall, although MIF4G proteins share sequence and functional similarities, they also have individual characteristics that enable them to interact only with specific DEAD-box helicases in either a stimulatory or an inhibitory manner. As some helicases are multifunctional, the group of their interacting cofactors coordinate their distribution between substrates and functions (Sloan and Bohnsack 2018).

The cofactor-helicase interplay cannot only be observed for MIF4G-domain proteins but also for other proteins that are not part of one of the well-established cofactor families. OST-HTH/eLOTUS domain proteins, for example, are cofactors that regulate the Ded1-like helicase Vasa (Jeske et al. 2017). Interestingly, the interaction of eLOTUS with the helicase is only established by the binding of the RecA2 domain of Vasa (Sloan and Bohnsack 2018).

1.2.2. G-patch proteins

Similarly, many G-patch proteins have been found to act as regulators of DEAH-box helicases (Bohnsack et al. 2021).These protein cofactors, which feature a glycine-rich region ranging over 45 to 50 amino acids (Robert-Paganin et al. 2015), are found in many eukaryotes and display the largest family of RNA helicase cofactors (Aravind and Koonin 1999; Robert-Paganin et al. 2015). They share a consensus sequence $HHX_3GAX_2GXGHGX_4G$ (H = hydrophobic; A = aromatic; X = non-conserved) (Figure 3a) and often also contain other RNA binding regions, such as Zinc finger, RNA recognition motif (RRM) and R3H (Figure 3b) (Aravind and Koonin 1999; Robert-Paganin et al. 2015). Circular dichroism spectroscopy experiments revealed that before binding to the cognate RNA helicase the G-patch domain shows a disordered conformation and that the secondary structure only forms upon helicase binding (Christian et al. 2014). While N-terminal helices in the G-patch domain mainly interact with the helicase via hydrophobic interactions and are even sufficient for helicase binding, the less-conserved C-terminal G-patch domain can adopt different

conformations. The non-conserved middle section of the G-patch domain depicts a flexible linker region that does not directly take part in RNA helicase binding (Hamann et al. 2020). While other domains than the G-patch also participate in helicase cofactor binding (Christian et al. 2014; Banerjee et al. 2015), the latter has been shown to be essential for regulating the catalytic activity of the enzyme (Christian et al. 2014). Helicase cofactors can stimulate ATP hydrolysis in the presence or absence of RNA, but maximal stimulation usually requires the nucleic acid to be present (Lebaron et al. 2009).

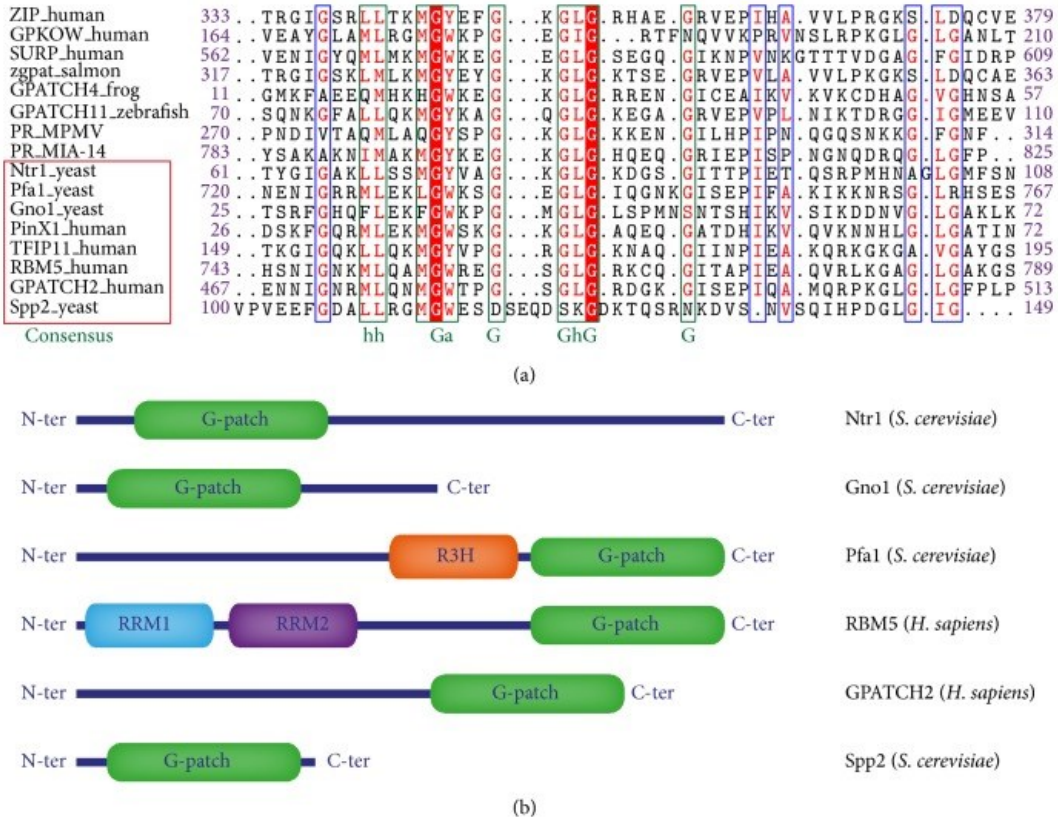

Figure 3: G-patch proteins and their G-patch domain sequence and organization. a) G-patch domain sequences of multiple G-patch proteins from different organisms. Encircled in the red box are some G-patch proteins from human and yeast. The consensus sequence of the G-patch is portrayed in green, while 'G' represents a glycine, 'a' an aromatic residue and 'h' depicts a hydrophobic residue. The G-patch protein consists of a glycine-rich, over 45 to 50 amino acids ranging domain with some invariant residues like the aromatic residue after the first glycine. **b)** Schematic representation of G-patch proteins with their respective domains. Beside the G-patch domain, some of them (here: Pfa1 in yeast and RBM5 in human) also contain other RNA binding domains, such as RRM and R3H. "Sequence organization of G-patch domains and G-patch protein partners" by Robert-Paganin et al. 2015 is licensed under CC BY-ND 4.0.

G-patch protein binding causes changes in intramolecular interactions between the RecA1 and RecA2 domains of the RNA helicase and facilitates ATP hydrolysis and further steps in the helicase cycle (Robert-Paganin et al. 2017; Tauchert et al. 2017). By cofactor binding, the ratchet domain of the helicase undergoes structural changes resulting in promoted RNA

binding (Christian et al. 2014). Recent structural studies of DEAH-box helicase G-patch domain complexes have revealed that the G-patch domain contacts both the RecA1 and RecA2 domain (Studer et al. 2020; Hamann et al. 2020). This binding enables it to act like a tether, promoting activity by holding the RecA-like domains in an optimal conformation for ATP hydrolysis (Bohnsack et al. 2021).

Some RNA helicases are multifunctional enzymes that can interact with several cofactors, which bind to the same sites on the helicase protein. Regarding G-patch proteins, the members of this cofactor family compete for binding of the helicase. Cofactor interactions can direct the helicase to various cellular compartments and different cofactors can also show differences in their affinities to the RNA helicase. Thus, changes in the levels of cofactors can result both in a different subcellular distribution and functions of the helicase, highlighting the importance of finetuning the interplay of helicase and cofactors for correct cellular function (Heininger et al. 2016).

G-patch proteins have largely been best characterized in yeast so far. Table 1 shows the yeast G-patch protein cofactors with the respective interacting helicase and the functions they are involved in.

Table 1: G-patch proteins in yeast and their interacting RNA helicases and functions

G-patch protein	Interacting helicase	Function
Ntr1	Prp43	Splicing
Gno1	Prp43	Ribosome biogenesis
Spp2	Prp2	Splicing
Pfa1	Prp43	Ribosome biogenesis
Cmg1	Prp43	Unknown

Modified from Robert-Paganin et al. (2015).

In humans, beside the homologues of the yeast G-patch proteins, additional G-patch proteins are expressed and are thought to act in gene expression (Sloan and Bohnsack 2018). More than 20 human G-patch proteins are known, however, the roles of only some of these proteins have been analyzed so far. RBM5, for example, plays a role in alternative pre-mRNA splicing via stimulation of the RNA helicase DHX15 (Niu et al. 2012). ZGPAT also interacts

with DHX15 and both of them assemble in spliceosome complexes (Chen et al. 2017), while NF-κB-repressing factor (NKRF) is implicated in pre-rRNA processing and turnover by activating DHX15 (Memet et al. 2017).

1.3. RNA helicases and their cofactors in disease

The importance of correct RNA helicase function and the physiological interplay between their cofactors to coordinate cellular processes is further emphasized by various findings that their dysregulation is linked to genetic diseases, tumorigenesis, autoimmune disorders, age-related diseases and infection.

Viral infections have been linked to numerous acute as well as chronic diseases and neurological disorders (Ahlquist 2006), also causing about 20 % of human cancers (Talbot and Crawford 2004). RNA helicases are not only involved in the life cycle of the biggest group consisting of RNA viruses, but helicases are also important in retro- and deoxyribonucleic acid(DNA)-viruses and are part of host-virus-interactions in general. RNA viruses can possess RNA helicases of their own, but multiple, especially retroviruses, are dependent on hijacking of host cell RNA helicases (Steimer and Klostermeier 2012). The former has been well described for the Hepatitis C virus, which encodes the NS3 helicase (NS3hel) that is essential for viral replication. It is a processive DEAH-box helicase that unwinds dsRNA as well as RNA-DNA-hybrids in a 3'- to 5'-dependant manner (Dumont et al. 2006; Levin et al. 2005). NS3hel facilitates viral particle assembly and homologues of NS3 are found in other viruses, such as the Yellow fever virus (Piccininni et al. 2002). Dengue virus (Luo et al. 2008), West Nile virus (Shiryaev et al. 2009) and Murray Valley encephalitis virus (Assenberg et al. 2009), encode proteins with structural similarity to NS3hel that also mediate processive unwinding. NS3hel is regulated by not only the NS3 protease (NS3pro) but also by NS4A, which binds NS3hel via its C-terminally located EFDEMEE motif (Shiryaev et al. 2009; Shiryaev et al. 2011). NS3pro as well as NS4A both enhance binding of the RNA substrate by NS3hel and further facilitate ATP hydrolysis and the unwinding process. Moreover, NS3pro protease activity is also stimulated by NS4A (Beran et al. 2009), indicating that the NS4A protein can be regarded as a cofactor not only for the helicase activity but also for the protease (Beran et al. 2009; Shiryaev et al. 2011). While NS3hel unwinding activity heavily relies on cofactor interactions, viral replication can only take place upon precise NS4A binding via its C-terminally located helicase interaction site (Phan et al. 2011).

The retrovirus human immunodeficiency virus 1 (HIV-1) is a well-known example of a virus that hijacks host RNA helicases for its viral replication cycle. Their expression levels highly vary upon HIV-1 infection and host RNA helicases are exploited for reverse transcription and integration of the viral genome into the host cell genome, transcription, RNA processing as well as nuclear export, translation and viral particle assembly (Ranji and Boris-Lawrie 2010).

Retroviral proteins containing a C-terminal G-patch domain were found in some betaretroviruses such as the Mason-Pfizer virus. It was shown that this G-patch domain is also responsible for nucleic acid binding (Svec et al. 2004) and contributes to viral infectivity. The proteinase and the reverse transcriptase of the virus interact and promote reverse transcriptase processivity (Křízová et al. 2012; Bauerová-Zábranská et al. 2005; Robert-Paganin et al. 2015). A G-patch protein derived from internal retroviral elements can also be found in human cells, however, whether it interacts with an RNA helicase or not, has not been studied yet (Sloan and Bohnsack 2018).

The fact that RNA helicases are required for various aspects of gene expression is emphasized by the fact that mutations within genes that encode for either the helicases themselves or their interacting cofactors can lead to genetic diseases. One example for aberrant cofactor function is the Klippel-Trenaunay syndrome, a congenital vascular disease that mainly alters the integrity of the capillary vessels and veins (Timur et al. 2005) and which coincides with high rates of mortality among children (Jacob et al. 1998). The AGGF1 gene, which is mutated in Klippel-Trenaunay syndrome patients, encodes for a G-patch domain containing protein that serves as an angiogenetic factor. 'AGGF1' is an acronym for 'AnGiogenic Factor with GPatch and FHA Domains 1'. The Klippel-Trenaunay syndrome chromosomal alteration causes an increase in AGGF1 expression levels, thus resulting in excessive vascularization (Tian et al. 2004; Hu et al. 2008). However, this cofactor is not only implicated in pathological tumor angiogenesis, but it is also essential for vascular development and stem cell differentiation, and lack of AGGF1 leads to early embryonic lethality (Zhang et al. 2016). Angiogenesis is stimulated by AGGF mediated activation of PI3K and AKT and the Klippel-Trenaunay syndrome pathogenesis is caused due to abnormalities of the AGGF1-PI3K-AKT signaling pathway (Zhang et al. 2016). Moreover, AGGF1 is implicated in vascular cohesion by coordinating phosphorylation and localization of vascular endothelial(VE)-cadherin to the membrane, where VE-cadherin protein is an important component of endothelial cell-to-cell adherent junctions (Zhang et al. 2016). Strikingly, a G-patch protein (AGGF1) therapy enabled reconstruction of cardiac function

by enhanced angiogenesis and reduced vessel permeability in a model with ischemia via reperfusion (Zhang et al. 2016).

Alterations in a G-patch domain containing protein can also be observed in patients born with the so-called TARP syndrome, the acronym deriving from its characteristic features. First described in 1970 as the Robin syndrome (Gorlin et al. 1970), the X-linked recessive hereditary disease, which received its label 'TARP' in 2003, is composed of the Pierre-Robin sequence with micrognathia glossoptosis and cleft palate, an atrial septal defect, talipes equivarus and the persistence of the left superior vena cava (Kurpinski et al. 2003; Gorlin et al. 1970). Although the incidence levels are very low, male patients suffering from the disease show a strongly reduced life expectancy, as the infantile mortality rate is very high (Gorlin et al. 1970). In 2010, the underlying mutation was found to be located in the RMB10 gene by massive parallel sequencing of DNA with exon recording (Johnston et al. 2010). RBM10 belongs to the RNA binding motif (RBM) gene family (Sutherland et al. 2005). RBM10 in particular plays a role in alternative splicing of pre-mRNAs, some of which encode proteins important for apoptosis (Johnston et al. 2014; Inoue et al. 2014). RBM10 possesses a zinc-finger domain, a G-patch domain and two RNA recognition motifs (Johnston et al. 2010). The first recorded cases of TARP syndrome showed high pre- and postnatal lethality, most of them holding nonsense mutations in the gene encoding RBM10 (Johnston et al. 2014), whereas recently, new cases where patients reached early child- and even adulthood were recorded. The underlying mutations of newly described cases caused a much milder phenotype (Wang et al. 2013; Højland et al. 2018).

During tumorigenesis, changes in expression levels are observed for a multitude of proteins, including several RNA helicases and cofactors. For example, the expression level of DDX1 – a DEAD-box helicase suggested to take part in transcription (Ishaq et al. 2009), mRNA processing (Bléoo et al. 2001), and translation (Kanai et al. 2004) – is upregulated in neuroblastoma and retinoblastoma cells (Godbout et al. 1998). DDX5, which is also known as p68 and takes part in miRNA processing and development (Fukuda et al. 2007), is enhanced in various types of cancer (Causevic et al. 2001). Interestingly, changes in expression were not only observed for RNA helicases but also their interacting cofactors. For example, it was shown that RBM5, a tumor suppressor and G-patch domain containing protein, interacts with DHX15, the human homologue of Prp43. The RNA helicase DHX15 has been implicated in several cellular processes, such as pre-mRNA splicing (Fouraux et al. 2002) and it is activated by the G-patch domain of RBM5 (Niu et al. 2012). RBM5 was also suggested to enhance apoptosis via regulation of alternative splicing (Rintala-Maki and

Sutherland 2004; Bonnal et al. 2008). Thus, decreased expression levels of RBM5 can be found in RAS-transformed cells (Edamatsu et al. 2000) as well as in numerous human neoplasms (Oh et al. 2002).

Another example for G-patch protein that is linked to cancer is GPATCH2, which has been implicated in breast cancer. Due to early diagnosis methods, improved health care organization and new treatments, breast cancer mortality rates have decreased in developed countries within the last few years, while incidences are constantly high (Early Breast Cancer Trialists' Collaborative Group 2005; Romond et al. 2005). This points out the need for further innovative breast cancer research and development of treatments. This necessity led to genome-wide expression analysis, which could recently reveal more oncogenes that are upregulated in abnormal proliferating breast cells (Nishidate et al. 2004), among them the G-patch domain containing protein GPATCH2. Usually, its expression is barely detectable in non-pathological tissues, except for testis. Importantly, it could be shown that GPATCH2 suppression results in lower proliferation rates of breast cancer cells. Moreover, the G-patch domain mediates interaction with the RNA helicase DHX15, and binding stimulates the ATPase activity of the helicase. These findings raise the possibility of new innovative treatment development in breast cancer therapy (Lin et al. 2009).

1.4 Aims of this work

RNA helicases are indispensable for cellular growth and homeostasis, as they play key roles in all pathways of RNA metabolism. Similarly, their cofactor interaction partners, whose binding can regulate the distribution and activity of cognate RNA helicases, are involved in various steps of gene expression and their functions are necessary for cellular metabolism. During viral infection and in other forms of disease, the expression levels and functions of certain helicases and their regulatory cofactors are altered. Some cofactors have even been categorized as tumor suppressors or oncogenes, affecting tumor growth. This work addresses the expression of RNA helicase cofactors in different cell types and in cancer. RNA helicase and cofactor levels are studied by quantitative PCR (qPCR) and western blotting and expression levels compared between various cell types. Not only cell culture cell lines but also tumor samples from patients and their matched-pair non-pathological tissues are analyzed. This provides the basis for studying the roles of differentially expressed proteins as well as differences in the regulation of RNA helicase functions in tumor cells.

2. Materials and Methods

2.1. Materials

2.1.1. Equipment

Equipment used is listed in Table 2.

Table 2: Equipment

Equipment	Company
Agarose gel electrophoresis chamber	UMG workshop
Allegra X-22 Series Benchtop Centrifuge	Beckman Coulter
Allegra X-15R Centrifuge	Beckman Coulter
Amersham Protran Premium 0.45 NC nitrocellulose Western blotting membranes	GE Healthcare Life Sciences
ARE Aluminum Hot Plate Stirrer	VELP Scientifica
Centrifuge 5425 R	Eppendorf AG
Centrifuge 5417 R	Eppendorf AG
CK40-F200 Microscope	Olympus
Cryo-Gloves®	Tempshield
CryoPure Tube 1.8 ml white	Sarstedt
Eppendorf® Research® plus pipette	Eppendorf AG
EM Techcolor measuring pipette	Hirschmann
Heracell 150i CO_2 Incubator	Thermo Fisher Scientific
HERAsafe KS	Thermo Scientific

Equipment	Company
HLC Cooling-ThermoMixer MKR 23	DITABIS
Image Studio™ Lite	LI-COR Biosciences
Kimtech Science™ Kimwipes™ Delicate Task Wipers	Kimberly-Clark
Kreisschüttler 3015	GLP
Mini-PROTEAN® Tetra Vertical Electrophoresis Cell	Bio-Rad Laboratories
Mini Trans-Blot® Cell	Bio-Rad Laboratories
LightCycler® 480 Instrument II	Roche Diagnostics
LightCycler® 480 Multiwell Plate 96	Roche Diagnostics
LightCycler® 480 Sealing Foil	Roche Diagnostics
LightCycler® 480 Software, Version 1.5	Roche Diagnostics
Microcentrifuge 1-15P	Sigma
Micro tube 1.5 ml	Sarstedt
NanoDrop 2000c Spectrophotometer	Thermo Fisher Scientific
Odyssey® Fc Imaging System	LI-COR Biosciences
Oregon Scientific Clock Timer TR 118	Eppendorf
PE 3600 Delta Range Analytical Digital Scale Balance	Mettler
Pipettierhelfer, PIPETBOY acu 2	Integra Biosciences
PowerPac™ Basic Power Supply	Bio-Rad Laboratories
SafeSeal tube 1.5ml	Sarstedt

Equipment	Company
Serological pipette (10ml)	Sarstedt
Thermo Scientific™ Mr. Frosty™ Freezing Container	Thermo Scientific
TC-Platte 6 Well, Standard, F	Sarstedt
TC Dish 60, Standard	Sarstedt
TC Dish 100, Standard	Sarstedt
Tube 15ml, 120x17mm, PP	Sarstedt
Tube 50ml, 114x28mm, PP	Sarstedt
Vortex Genie® 2 Mixer	Scientific Industries
Western Blot incubation boxes	LI-COR Biosciences
0.34 mm Whatman medium thickness 3MM Chr paper	GE Healthcare Life Sciences
1008 Waterbath	GFL

2.1.2. Chemicals

Chemicals used in this study are listed in Table 3.

Table 3: Chemicals

Chemical	Company
Acrylamide 4 K solution (30 %) - Mix 37.5:1	PanReac AppliChem
Agarose	SERVA Serving Scientists
Albumin Fraction V (pH 7.0)	PanReac AppliChem
Ammonium Persulfate (APS) 10 %	PanReac AppliChem

Chemical	Company
Chloroform z. A., ISO, Ph. Eur. (min. 99,5 %, stabilized with amylene)	ChemSolute
Dimethyl sulfoxide (DMSO)	Sigma-Aldrich
dNTP Mix (10 mM each dATP, dCTP, dGTP, dTTP, neutral pH)	Thermo Scientific
Ethanol, ≥ 99,8 %	Carl Roth
LightCycler® 480 SYBR Green I Master	Roche Diagnostics
Milk powder	Saliter
Oligo(dT)20-Primer	Thermo Fisher
PageRuler™ Plus Prestained Protein Ladder	Thermo Fisher Scientific
RiboLock RNase Inhibitor, 40 U/µL, 2,500 U	Thermo Scientific
SafeView™ Classic	Applied Biological Materials Inc.
SuperScript™ III Reverse Transcriptase	Invitrogen
Tetramethylethylenediamine (TEMED)	PanReac AppliChem
TRI Reagent RNA isolation reagent	Sigma-Aldrich
Trypsin-ethylenediaminetetraacetic acid (EDTA) (0.25 %)DM	Gibco
Tween® 20	Carl Roth
2-Propanol, ≥ 99,8 %	Carl Roth

Chemical	Company
6 M guanidine hydrochloride	Sigma-Aldrich

2.1.3. Media, buffer and solution recipes

Media, buffer and solution recipes that were used are listed in Table 4.

Table 4: Media, buffer and solution recipes

Acronym	Recipe
Dithiothreitol (DTT), 0.1 M Solution	Invitrogen
Dulbeccos Modified Eagle Medium (DMEM) + Pyruvate + 4.59 L/D-Glucose + L-Glutamine	Gibco
foetal calf serum (FCS) 10 %	Gibco
Laemmli buffer	250 mM Tris 1.92 M glycine 0.5 % SDS in H_2O
Phosphate-buffered saline (PBS) 10 times(x)	Gibco NaCl 1370 mM 27 mM KCl 80 mM Na_2HPO_4 80 mM H_2O 15 mM KH_2PO_4 pH 7.3
PBS-Tween (T)	1 x PBS 0.1 % Tween20

Acronym	**Recipe**
Resolving Gel Buffer	1.5 M Tris-HCl 0.4 % sodium dodecyl sulphate (SDS) pH 8.8
Stacking Gel Buffer	0.5 M Tris 14 mM SDS pH 6.8
TBS-Tween (T)	1 x TBS 0.1 % Tween20
Transfer buffer	1 x western blot (WB) buffer 20 % methanol (v/v)
Tris-buffered saline (TBS)	50 mM Tris 150 mM NaCl pH 7.6
WB buffer	250 mM Tris 1.93 M glycine
1 x SDS loading dye	60 mM Tris 2 % SDS 10 % glycerol 0.01 % bromophenol blue dye 1.25 % β-mercaptoethanol pH 6.8
5 x first-strand buffer	Invitrogen [250 mM Tris-HCl (pH 8.3), 375 mM KCl, 15 mM $MgCl_2$]

Acronym	Recipe
10 x BPTE buffer	100 mM PIPES (piperazine-N,N'-bis(2-ethanesulfonic acid)) 300 mM Bis-Tris (bis(2-hydroxyethyl)amino-tris(hydroxymethyl)methane) 10 mM EDTA pH 6.5
100 U/ml Penicillin-Streptomycin mix	Gibco

2.1.4. Oligonucleotides

Oligonucleotides used in this study were purchased from Sigma-Aldrich. They were used for qPCR amplification. Their names and sequences can be found in Table 5.

Table 5: Oligonucleotides

Name	Forward primer (5‘-3‘)	Reverse primer (5‘-3‘)
EMC7	GGGGCTGGACAGACTTTCTAA	TTGACTGCTCCATTTCCCGT
PSMB2	GGCCCCGACTATGTTCTTGT	GTCATGATCGTCCTTCATCTGGA
COPS6	CCCTATGACCAAGCACACAGA	CAGCATTGTGGCCTCTCCAT
DHX15	CAGCTCCCTGTTTGGGAATAC	TTGGGTACAGGCAACTCCTC
DHX35	GATGTGGGAAGAGCACACAGA	AGCTACTCTCCCTGCAACTGTA
AGGF1	CACAGAACGGCTGTACCAGA	TTACTGAGTTCTTCCACCTGCG
CHERP	CGCTCAGACAGGAGCAAGTGA	ATGTCTAGCTGGGTCTCCTCC

Name	Forward primer (5‘-3‘)	Reverse primer (5‘-3‘)
CMTR1	TGAGCCCTGGACTATGGGAT	CGGCCATAGTAGCAAATGTGAA
GPATCH1	TCAAAAGCCGAGCCACCTAA	TTGACGGTCTGATTTGCGGA
GPATCH2	ACTACTGCAGGATTTGTAGGTGA	GCGTCCAGCCCATATTCTGA
GPATCH3	TGGATTGGGGTACCATGGAG	GAGATGAGCCCCAAGCCATT
GPATCH4	TGAGGAAACTGTTTTAGGTGGTG	ATCCAAGATGTCCTCCTCCTCT
GPATCH11	AGCGAGCCTGTCAACAACTG	GCCTCAACCAGTACCATGCTT
GPKOW	AGACTGGAAGGGTGGGACAT	GGCAGATGGCATCGTAGTGA
PINX1	TGTCATCTCGGAGCAAAACAGA	CTGGTTGTCGTGGTTTCGTT
RBM5	TGACCCCAACTCGCAATACTAC	CACGTAGGTCTCTTTTTCCCCA
SUGP1	TCGCTCAGAAGAAACGGGAA	TGCATTTGTGATTTCGCCAGG
SUGP2	ACCCTGACCTGTGGTTTCTAC	TTGTGCGGAGATGACGTGAA
RBM6	GTCCGCCTTACTACTGCCAA	AATGGCGGATCAAGGTTCTGT
GPATCH8	TCTCCCGCTTCAACGAAGAC	GCGGTGTCCAATATTATCCGATT
GPANK1	CGGAAAACCGGTCTCCTACTC	GTGCGGTGGTTGGAATCTTG
RBM17	ACCTAGGAGTGGAGACCAGTG	TTTGGCTCTTTGCCTGAGTGA

Name	Forward primer (5‘-3‘)	Reverse primer (5‘-3‘)
TFIP11	ACCACCAAGGATCCAGATCCAGATATAATTC	GACATGGCCAGTCACTTAGAA
RBM10	AACGCCAATGACACCATCAT	ATGGTGGAGAGCTGGATGAA
SON	AGGAAAGGATTGATGCCTGGG	CAGGCTTGGGCACCAGTATT
NKRF	CACACGGTTTGGATGTGCAG	GGACCAGCCAACTGACCTTT
ZGPAT	TCCGTGTGCTTTACCTGTACC	CAGCTCATCCAGAGAGACCAC

2.1.5. Antibodies

Primary antibodies were used to detect proteins of interest by western blotting. Secondary antibodies were used to visualize the primary antibodies/proteins by fluorescence. A list of both is given in Table 6.

Table 6: Antibodies

Target	Supplier	Dilution	Organism	Conditions
KIAA0082/ CMTR1	Bethyl Laboratories	1:5,000	Rabbit	Blocking: 7.5 % milk; PBS-T Incubating: 3 % BSA; PBS-T
DHX16	Bethyl Laboratories	1:2,000	Rabbit	5 % milk; TBS-T
DHX15	Bethyl Laboratories	1:5,000	Rabbit	5 % milk; TBS-T
GPATCH4	Bethyl Laboratories	1:5,000	Rabbit	5 % milk; TBS-T
GPKOW	Bethyl Laboratories	1:1,000	Rabbit	5 % milk; TBS-T

Target	Supplier	Dilution	Organism	Conditions
GPATCH2	Sigma-Aldrich Chemie GmbH	1:500	Rabbit	5 % milk; TBS-T
NRF (NKRF)	Bethyl Laboratories	1:10,000	Rabbit	5 % milk; TBS-T
PINX1	Bethyl Laboratories	1:5,000	Rabbit	5 % milk; TBS-T
RBM6	Proteintech Group	1:5,000	Rabbit	Blocking: 7.5 % milk; PBS-T Incubating: 3 % BSA; PBS-T
Tubulin	Sigma-Aldrich	1:10,000	Mouse	5 % milk; TBS-T
Anti-Rabbit IgG IRDye® 800CW	LI-COR Biosciences	1:10,000	Donkey	Dependent on primary antibody conditions
Anti-Mouse IgG IRDye® 800CW	LI-COR Biosciences	1:10,000	Donkey	Dependent on primary antibody conditions
Anti-Mouse IgG IRDye® 680LT	LI-COR Biosciences	1:10,000	Goat	Dependent on primary antibody conditions

2.1.6. Cell lines

Cell lines that were used in the study with are listed in Table 7. Cell culturing is described in section 2.2.1. Their proteins and RNA were harvested for western botting and qPCR.

Table 7: Cell lines

Name	Genotype	Source
HEK293	Human embryonic kidney	Thermo Fisher Scientific

Name	Genotype	Source
HeLa	Cervical cancer	European Collection of Authenticated Cell Cultures (ECACC)
HCT116 wt p53	Colorectal cancer (carcinoma)	ECACC
HCT116 -/- p53	Colorectal cancer (carcinoma)	ECACC
A549	Lung cancer (adenocarcinoma)	ECACC
U2OS	Osteosarcoma	ECACC
CaCo-2	Colon cancer (adenocarcinoma)	ECACC
MCF-7	Breast cancer (adenocarcinoma)	ECACC

2.1.7. Tumor samples

Matched-pair normal tissue and tumor samples, listed in Table 8, were provided from the CEPA Biobank (Newcastle upon Tyne Hospitals NHS Trust, UK). Tissues were fresh frozen in liquid nitrogen within 15 min of removal and stored at -80 °C. Samples of adjacent tissue were formalin-fixed, paraffin-embedded and verified by histopathology. Frozen tissue samples were hand homogenized in TRI Reagent in the Biobank laboratory.

Table 8: Tumor samples

Sample	Genotype	Source
1	Squamous cell carcinoma (SCC)	Oral cavity
2	Squamous cell carcinoma	Oral cavity
3	Squamous cell carcinoma	Oral cavity
4	Squamous cell carcinoma	Oral cavity
5	Normal mucosal tissue	Oral cavity

Sample	Genotype	Source
6	Normal mucosal tissue	Oral cavity
7	Normal mucosal tissue	Oral cavity
8	Normal mucosal tissue	Oral cavity
9	Fibromyxosarcoma (FMS)	Limbs
10	Fibromyxosarcoma	Limbs
11	Fibromyxosarcoma	Limbs
12	Normal connective tissue (muscle/fascia)	Limbs
13	Normal connective tissue (muscle/fascia)	Limbs
14	Normal connective tissue (muscle/fascia)	Limbs

2.2. Methods

2.2.1. Cell culture

2.2.1.1. Culture conditions and passaging

The eight different cell lines listed in Table 7 were grown in DMEM complemented with 10 % fetal calf serum and 100 U/ml Penicillin-Streptomycin mix. They were incubated at 37 °C in humid conditions with 5 % CO_2. When cells were approximately 80 % confluent, media was removed, and cells were washed with PBS. Cells were detached with 0.25 % trypsin-EDTA and reseeded at a 1/10 ratio with fresh DMEM.

2.2.1.2. Thawing and preparing stocks

2.2.1.2.1.Thawing stocks

Cell stocks were taken out of liquid nitrogen and quickly thawed in a 37 °C water bath for two minutes, diluted to 1/10 with to 37 °C pre-warmed DMEM supplemented with 10 % fetal calf serum and 100 U/ml Penicillin-Streptomycin mix. After centrifuging the cells at 1100 g for 3 min, media was aspirated so only the pellet of cells remained. Fresh media was added, the solution resuspended, and cells were cultivated on a cell culture dish at a 37 °C in a humidified atmosphere as in section 2.2.1.1.

2.2.1.2.2.Preparing stocks

When 80 to 90 % confluence was reached, cells, detached as described in 2.2.1.1, were harvested by centrifugation at 1100 g for 3 min at room temperature. The supernatant was removed, Cryoprotectant Medium (DMEM supplemented only with 10 % fetal calf serum) was added to the cell pellet and gently resuspended by pipetting up and down. DMSO was added to a final concentration of 10 %, again resuspended and the cell suspension aliquoted into Cryo tubes. These were immediately placed in a freezing container filled with isopropanol and with a cooling rate of -1 °C/min. This was stored at -80 °C overnight, and the following day the tubes were transferred to liquid nitrogen.

2.2.2. Total RNA extraction

2.2.2.1. RNA extraction from cell lines

Total RNA from eight different human cell lines was extracted using TRI Reagent according to the manufacturer's instructions. For sample preparation, PBS was used to wash the cells, 500 µl of TRI Reagent was directly added onto the cell culture (six well plate) to lyse cells and was evenly distributed by swirling around. The samples were incubated for 5 min at room temperature. The cell lysate was transferred to a 1.5 ml tube, 100 µl of chloroform added, and vigorously shaken. The samples were incubated for 5 min again. They were centrifuged at 20,000 g for 15 min at 4 °C in order to separate into three different phases. The aqueous upper phase, containing RNA, was carefully transferred to a fresh 1.5 ml tube, and 250 µl of isopropanol were added and resuspended. The samples were incubated for 5 min at room temperature and then centrifuged at 20,000 g for 10 min at 4 °C, causing RNA pellets to form. The supernatant was then removed. For pellet washing, 500 µl of 70 % ethanol was added, the tube was vortexed, and again centrifuged at 20,000 g for 5 min (4 °C).

The supernatant was removed, and the pellet air-dried for approximately 10 min. 20 µl of ultrapure Milli-Q water was added, the inhomogeneous solution incubated at 60 °C for 5 min, gently pipetted up and down and then stored on ice. The RNA concentration and purity (260/280 ratio) was quantified using NanoDrop 2000c Spectrophotometer.

2.2.2.2. RNA extraction from tissue samples

Tissue samples already homogenized in TRI Reagent were taken out of the -80 °C freezer and defrosted. They were then centrifuged at 12,000 g (4 °C) for 10 min in order to separate the supernatant from any remaining insoluble material. The supernatant was transferred to a fresh tube. If needed, 500 µl of TRI Reagent was added to reach 1 ml for each tissue sample. The following steps were executed according to section 2.2.2.1.

2.2.3. Denaturing agarose gel electrophoresis to check RNA quality

1.2 % agarose was prepared in 1 x BPTE buffer by heating in the microwave until the agarose was dissolved completely. The gel was poured into the electrophoresis chamber and allowed to polymerize for 30 min. 1 µg of RNA was mixed with five-fold (v/v) excess of SafeView™ Classic stain. Samples were incubated at 55 °C for 20 min for denaturation. BPTE buffer was poured onto polymerized gel, filling up the chamber. Samples were loaded onto gel and separated by electrophorese at a constant voltage of 100 V for 30 to 40 min. RNA separation in the denaturing gel was visualized on a UV transilluminator. Intact total RNA showed well-defined 28 S and 18 S ribosomal RNA bands. If the upper 28 S rRNA band was observed to be twice as intense as the 18 S band, this implied good RNA quality.

2.2.4. cDNA synthesis

First-strand cDNA synthesis was performed using Superscript™ III reverse transcriptase according to the manufacturer's instructions. The total reaction volume was 40 µl. The starting point for cDNA synthesis was 4 µg of total RNA for each sample. Therefore, the appropriate volume of extracted RNA – dependent on the sample's RNA concentration – was added to a tube along with 2 µl of 50 µM oligo(dT)20 primer as well as 2 µl of 10 mM dNTP mix (10 mM dATP, 10 mM dTTP, 10 mM dGTP, 10 mM dCTP) and the volume was replenished to 26 µl with an appropriate amount of sterile distilled water. The mixture was incubated at 65 °C for 5 min, then stored on ice for several minutes. The tubes were briefly centrifuged. 8 µl of 5 x First-Strand-Buffer, 2 µl of 0.1 M DTT, 2 µl of RiboLock RNase Inhibitor and 2 µl of SuperScript™ III RT were added to each sample and gently

resuspended. The samples were incubated at 50 °C for 60 min. The tubes were briefly centrifuged, and the reaction inactivated by heating at 70 °C for 15 min. The samples again were centrifuged and stored at -80 °C until use.

2.2.5. Quantitative PCR

2.2.5.1. Primer design

Primers were designed using National Center for Biotechnology Information's (NCBI) Primer-BLAST. They were designed to span an exon-exon junction in order to only amplify mRNA and not the corresponding genomic DNA. The primer length was 20 to 25 nucleotides, while the length of the amplificon was 70 to 120 base pairs.

2.2.5.2. qPCR reaction

For qPCR, cDNA (prepared as in 2.2.4) was diluted in Milli-Q water and pipetted onto a 96-well plate. LightCycler 480 SYBR Green I Master, Milli-Q water and 16.6 µM primer mix (forward and reverse primer) were added to each well. The mixture was pipetted in triplicates for reliability reasons. The qPCR program was composed of 5 min pre-incubation at 95 °C, 50 cycles of denaturation for 10 s at 95 °C, 20 s annealing at 58 °C and 15 s amplification at 72 °C. The following melting curve analysis consisted of 10 s 95 °C, 1 min incubation at 55 °C and fluorescent detection at 97 °C.

2.2.5.3. qPCR primer testing

HEK293 cDNA was used for primer testing. To evaluate efficiency and specificity, several different primer pairs for each target were designed, ordered, and tested by establishing serial dilution (1:3, 1:15, 1:75 and 1:375) of HEK293 cDNA. Diluted cDNA was added to previously mentioned gene-specific primers (forward (fwd)/reverse (rev)), LightCycler 480 SYBR Green I Master and Milli-Q water. For verification of specific amplification, samples without cDNA were simultaneously run. The program setup was according to section 2.2.5.2. qPCR efficiency was represented by the incline of the linear standard curve from serial dilution. It was composed of the cDNA input in a logarithmic function over the matching threshold cycle (Ct) values ($E=10^{(-1/incline)}$) (Rasmussen 2001). Only primers with an efficiency between 1.8 and 2.0 were used for further experiments. The formation of the melting curves was also considered and only primers giving a single peak, corresponding to a single amplified product, were used.

2.2.5.4. qPCR data analysis

Gene expression analysis by qPCR from cell lines and tumor samples was performed by relative quantification. The Ct value of the target gene was normalized to an arithmetic average of the Cts from three different so called 'housekeeping genes' (EMC7, PSMB2, COPS6). These 'housekeeping genes' can be found ubiquitously and are expressed at a constant rate (Eisenberg and Levanon 2013). cDNA was diluted at a 1:15 ratio. For cell line qPCR, HEK293 served as the internal reference cell line (control). The pipetting setup for each plate was the following:

Table 9: Cell line qPCR pipetting setup

	1	2	3	4	5	6	7	8	9	10	11	12
Target 1	HEK 293	HEK 293	HEK 293	HeLa	HeLa	HeLa	HCT 116 wt p53	HCT 116 wt p53	HCT 116 wt p53	HCT 116 -/- p53	HCT 116 -/- p53	HCT 116 -/- p53
	A549	A549	A549	U2OS	U2OS	U2OS	CaCo-2	CaCo-2	CaCo-2	MCF-7	MCF-7	MCF-7
Target 2	HEK 293	HEK 293	HEK 293	HeLa	HeLa	HeLa	HCT 116 wt p53	HCT 116 wt p53	HCT 116 wt p53	HCT 116 -/- p53	HCT 116 -/- p53	HCT 116 -/- p53
	A549	A549	A549	U2OS	U2OS	U2OS	CaCo-2	CaCo-2	CaCo-2	MCF-7	MCF-7	MCF-7
Target 3	HEK 293	HEK 293	HEK 293	HeLa	HeLa	HeLa	HCT 116 wt p53	HCT 116 wt p53	HCT 116 wt p53	HCT 116 -/- p53	HCT 116 -/- p53	HCT 116 -/- p53
	A549	A549	A549	U2OS	U2OS	U2OS	CaCo-2	CaCo-2	CaCo-2	MCF-7	MCF-7	MCF-7
Reference gene	HEK 293	HEK 293	HEK 293	HeLa	HeLa	HeLa	HCT 116 wt p53	HCT 116 wt p53	HCT 116 wt p53	HCT 116 -/- p53	HCT 116 -/- p53	HCT 116 -/- p53
	A549	A549	A549	U2OS	U2OS	U2OS	CaCo-2	CaCo-2	CaCo-2	MCF-7	MCF-7	MCF-7
	A549	A549	A549	U2OS	U2OS	U2OS	CaCo-2	CaCo-2	CaCo-2	MCF-7	MCF-7	MCF-7

Cell line cDNA from HEK293, HeLa, HCT116 wt p53, HCT116 -/- p53, A549, U2OS, CaCo-2 and MCF-7 was diluted at a 1:15 ratio and pipetted on a 96-well plate according to the colored boxes above. Each cDNA was pipetted in triplicates. One plate accommodated three different targets genes, which were combined with one of the three housekeeping genes COPS6, EMC7 and PSMB2.

For tumor sample qPCR, each tumor sample was compared to the correlating matched-pair tissue sample. The pipetting setup was according to Table 9.

For ratio calculation, the following formula was used:

$r=2^{-\Delta\Delta Ct}$, with ΔCt = Ct(target gene) – Ct(reference gene) and $\Delta\Delta Ct$ = ΔCt(tumor sample) − Ct(control) (Pfaffl 2004).

For each target mRNA, three independent experiments were conducted, resulting in three relative expression rates, respectively.

The data generated from SCC RNA were not normalized to the Cts of the housekeeping genes, but internally among the 24 target mRNAs of the G-patch proteins and RNA helicases. Thus, for normalized cancer tissue Ct calculation, a correcting factor was determined by the average of all Cts from the cancer tissues over the normal tissues. According to this, the ratio was calculated as following:

$r = 2^{-\Delta\Delta Ct}$, with ΔCt = Ct(Ct [tumor sample]/(mean Ct [SCC tumor samples]/mean Ct[SCC normal samples])) and $\Delta\Delta Ct$ = ΔCt(tumor sample) − Ct(control).

For descriptive data analysis, first, means as well as standard deviation of these three independent experiments were determined. Null hypothesis H_0 was defined as *there is no difference in G-patch protein and RNA helicase mRNA expression levels in tumor and non-tumor samples*. Significance level α was set to 5 %, 1 % and 0.1 %, respectively. One sample two-legged student t-test was performed to report on *p*-values. All analyses were conducted utilizing Microsoft Excel 365.

2.2.6. Protein extraction from cell lines

2.2.6.1. Using TRI Reagent

Protein extraction using TRI Reagent was performed according to the manufacturer's instructions. After sample preparation (section 2.2.2.1), the mixture was separated into three phases. After transferring the upper layer to a fresh tube for RNA isolation, the interphase containing DNA was carefully discarded. 150 µl of 100 % ethanol was added to the lower phase, mixed by inversion, and incubated at room temperature for 2 min. The samples were centrifuged at 2,000 g for 5 min at 4 °C. The supernatant was transferred to two fresh tubes and the precipitated DNA pellet discarded. 750 µl of isopropanol was added to each tube, and the samples incubated for 10 min at room temperature. They were then centrifuged at 20,000 g for 10 min at 4 °C and the supernatant discarded. The remaining protein pellets

were washed three times with 1 ml of 0.3 M guanidine hydrochloride/95 % ethanol solution. Each washing step involved incubation at room temperature for 20 min each time, followed by centrifugation at 7,500 g for 5 min at 4 °C and removal of the supernatant. After the washing procedures, 1 ml of 100 % ethanol was added, the sample vortexed and again incubated for 20 min, at room temperature. The samples were centrifuged at 7,500 g for 5 min at 4 °C, the supernatant discarded, and the protein pellet dried under the extractor hood for 10 min. The protein pellet was dissolved in SDS loading dye, vortexed, resuspended, and centrifuged.

2.2.6.2. Whole cell protein extraction

For whole cell protein extraction, media was removed from adherent cell cultures and the cells were washed with PBS. An appropriate volume of 1 x SDS loading dye was added, the cell extract was resuspended and aliquoted into 1.5 ml tubes, which were vortexed and incubated at 95 °C for 10 min.

2.2.7. SDS-PAGE

For casting the gel, resolving gel buffer, Milli-Q water, 10 % acrylamide, 0.1 % APS (w/v) and 0.2 % TEMED were mixed and immediately poured between the 1.5 mm glass plates of the Mini-PROTEAN® Tetra Vertical Electrophoresis Cell. 600 µl of isopropanol was added in order to level the surface and prevent drying-out. After polymerization, the isopropanol was removed completely. The ingredients for the stacking gel (Milli-Q water, stacking gel buffer, 5 % acrylamide, 0.1 % APS, 0.2 % TEMED) were mixed and poured onto the resolving gel. A comb was placed into the stacking gel to form the wells.

For separating proteins, the Mini-PROTEAN® Tetra Vertical Electrophoresis Cell was filled with 1 x Laemmli buffer. The comb was removed carefully. The protein samples, dissolved in SDS loading dye, were denatured by incubation at 95 °C for 5 min and pipetted into the wells. A pre-stained ladder served as a size marker. The SDS-PAGE was run at 90 V for 10 min, then at 150 V until the dye front reached the bottom of the gel. Proteins were separated according to their molecular mass.

2.2.8. Western blotting

0.45 µm pore-sized nitrocellulose western blotting membrane was pre-soaked in Transfer Buffer for 2 min. The previously run gel (section 2.2.7) was placed in Mini Trans-Blot® Cell and filled with Transfer Buffer. The proteins were transferred from the gel to the membrane

at 100 V for 75 min at conditions optimized by cooling and stirring. For blocking, the membrane was incubated in either 5 % milk in TBS-T or 7.5 % PBS-T (see Table 6) for 1 h, shaking, at room temperature. The membrane was then incubated with primary antibody at varying dilutions in either 5 % milk in TBS-T or 3 % BSA in PBS-T (see Table 6) overnight at 4 °C, shaking. Tubulin served as a loading control that the other targets' expression levels were compared to. The following day, the membrane was washed with TBS-T/PBS-T three times for 10 min, shaking. It was then incubated with fluorescently labelled secondary antibody diluted 1:10,000 in 5 % milk in TBS-T or 3 % BSA in PBS-T (Table 6) for 60 min, shaking at room temperature under light-protected conditions. The membrane was washed three times for 10 min in TBS-T/PBS-T again, shaking at room temperature. For visualizing, an Odyssey® Fc Imaging System was used, detecting fluorescence in the 700/800 nm channels, scan intensity setting varying for each target protein from 2.5 to 9.0, depending on the amount of fluorescence. Protein bands were quantified using Image Studio™ Lite Software. The signaling intensity of each of the targets was normalized to the protein band of tubulin. HEK293 again served as the internal reference cell line.

For each target protein, three independent experiments were conducted, resulting in three relative expression rates, respectively.

For descriptive data analysis, first, means as well as standard deviation of these three independent experiments were determined. Null hypothesis H_0 was defined as *there is no difference in GPATCH and RNA helicase protein expression levels in tumor and non-tumor samples*. Significance level α was set to 5 %, 1 % and 0.1 %, respectively. One sample two-legged student t-test was performed to report on *p*-values. All analyses were conducted utilizing Microsoft Excel 365.

3. Results

3.1. Design and testing of primers for qPCR of G-patch protein mRNAs

There are 22 human proteins annotated as containing a G-patch domain in the Uniprot database (The UniProt Consortium 2021). Several of these proteins have been shown to function as regulatory cofactors of the RNA helicase DHX15. The Bohnsack laboratory has identified DHX35 as another RNA helicase that interacts with a single G-patch protein, GPATCH1, which was recently also confirmed in a separate publication (Sales-Lee et al. 2021). mRNA expression levels of these proteins have been analyzed in high-throughput studies in particular cell types but had not been systematically compared across different cell types or correlated with protein levels. To identify differences in expression levels of the human G-patch proteins and two G-patch protein-interacting helicases in different cancer cell lines and different tissues, first, a robust qPCR approach was developed to analyze the relevant mRNA levels.

Optimal primer design and quality are key basic requirements for reliable results of mRNA expression levels by qPCR. Primer characteristics can have a great effect on qPCR sensitivity as well as specificity (Robertson and Walsh-Weller 1998). Thus, the complete validation process included specific target identification, followed by primer design, complying with appropriately defined criteria, and lastly primer testing. Only if the primer pair passed through all these steps, good quality of qPCR results could be ensured and it was selected for further experiments (Bustin and Huggett 2017).

First of all, a suitable target sequence had to be identified (Bustin and Huggett 2017). A single gene often encodes for more than one protein isoform as a result of alternative pre-mRNA splicing, which occurs for more than half of the human genes (Johnson et al. 2003). 19 of the 22 genes encoding human G-patch proteins are alternatively spliced. Before designing primers to monitor the expression of these genes, it was therefore important to decide which of splice variants should be reflected in the outcome. The different transcripts encoding variants of all the human G-patch proteins were identified by using NCBI's Reference Sequencing for mRNA (O'Leary et al. 2016). Figure 4 shows an example of a gene (GPATCH11) that encodes for several protein isoforms. Primer pairs were selected that allow detection of mRNAs coding for all relevant protein isoforms, as shown for the primer pair used for GPATCH11 mRNA quantification. For some of the G-patch proteins with

several isoforms, a canonical protein and its corresponding mRNA sequence have been defined. A canonical isoform is a protein that is the most prevalent, the most similar to orthologous sequences existing in other species, and is often the longest (The UniProt Consortium 2019). This was considered during primer design. An example of a G-patch gene that is devoid of isoforms is AGGF1, where primers will only identify one mRNA sequence. Summing up, careful target sequence identification and selection was inevitable to receive valid and comparable qPCR results.

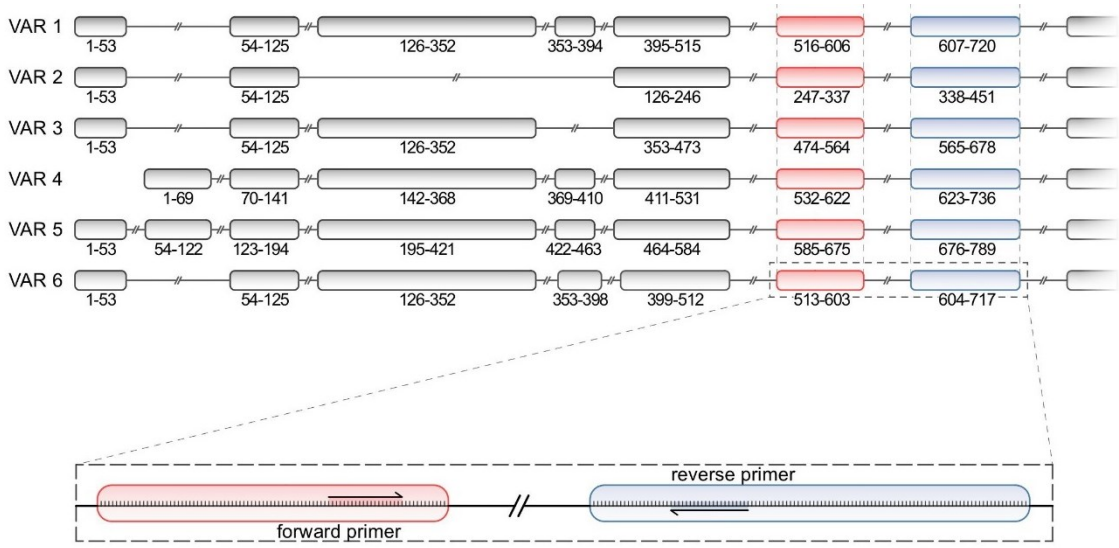

Figure 4: Schematic view of alternative splice variants of GPATCH11. Six representative splice variants (VAR) of GPATCH11 are exemplarily shown. Exons are illustrated by the boxes, respectively true to scale with the number of nucleotides written underneath. Corresponding base sequences are arranged in the rows above one another. Red boxes mark the segment our designed forward primer binds to, while the blue boxes show the reverse primer binding region. Introns are represented by the black connecting lines, respectively not to scale. Inside the black dashed lines, the primer binding exons are exemplarily shown in detail. Nucleotides are illustrated by the small vertical lines. Primer binding areas are highlighted in red and blue.

Poor PCR assay performances can result from primers that tend to form hairpin structures or primer-dimers and show low tolerance in temperature variations (Bustin and Huggett 2017). To avoid these issues, careful criteria-conforming primer design was performed using NCBI's primer-BLAST (Ye et al. 2012). The defined criteria included a primer length ranging between 17 and 23 nt for high target specificity (Mitsuhashi 1996) and a GC content of 40 to 60 %. In addition, primers had to span an exon-exon splicing junction to enable the amplification of spliced transcripts only (Raymaekers et al. 2009). Also, the product size had to range between 70 to 150 bp. The forward and reverse primer melting temperature had to be similar to prevent incorrect primer hybridization (Mitsuhashi 1996) and were in the range of 57 to 63 °C. To avoid possible self-complementarity, all designed primer sequences were

checked by OligoCalc (Kibbe 2007) and only primers possessing all the features were purchased from Sigma-Aldrich.

Even though all these criteria were considered during the primer designing, experimental validation was still necessary. Therefore, amplification efficiency and primer specificity were determined experimentally. Each primer pair was tested by serial dilution performance on HEK293 cDNA using qPCR (section 2.2.5.3). As a linear relation between the logarithm of the cDNA amount and its corresponding Ct value is implied, qPCR efficiency was determined by the incline of the linear regression of a plot of the two parameters (Rasmussen 2001). Figure 5 panel A shows the standard curve of one designed primer pair for the G-patch protein GPATCH4 as a representative example. Its efficiency was calculated to 1.53. Figure 5 panel B on the other hand demonstrates the efficiency of another GPATCH4 primer pair that equals 1.93. As an impeccable amplification cycle allows for doubling of cDNA copies and an efficiency value of 2, values for amplification efficiency close to this hallmark represent a well-established qPCR reaction (Bustin and Huggett 2017). This can be described by 2^n, with n presenting the cycle number. As qPCR efficiency is not only determined by primer characteristics but also relies on numerous other factors like PCR inhibitors and enhancers or nucleic acid degradation (Bustin and Nolan 2004; Wong and Medrano 2005; Yuan et al. 2006), the qPCR process usually does not reach full 100 % efficiency. Therefore, in this experimental setup, an efficiency greater than 1.8 was decided to be sufficient for further use.

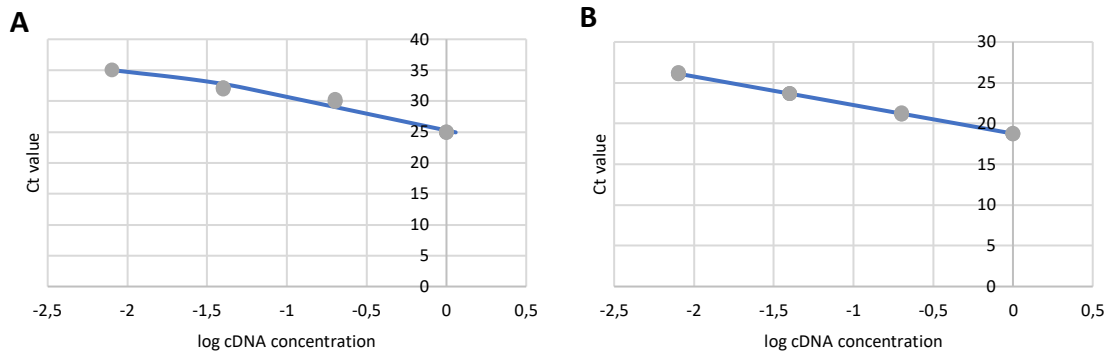

Figure 5: Standard curves of primers to evaluate amplification efficiency. Two target gene-specific primer pairs (fwd/rev) were designed, purchased, and amplification efficiency was evaluated by serial dilution and qPCR using HEK293 cDNA (1:3, 1:15, 1:75 and 1:375). The respective samples were pipetted in triplicates. qPCR primer efficiency is represented by the incline of the linear standard curve from serial dilution. It is composed of the cDNA input in a logarithmic function over the matching threshold cycle (Ct) values ($E = 10^{(-1/\text{incline})}$) (Rasmussen 2001)**.** Primers had to display an amplification efficiency greater than 1.8 in order to be selected for further qPCR experiments. Panel A shows the amplification efficiency of a GPATCH4 primer pair with a low value of 1.53, while Panel B shows the efficiency of another GPATCH4 primer pair with a high value of 1.93.

Another important point to consider was the specificity of the amplification reaction, as it is possible for primers to misalign, and non-specific amplification of any undesired products would influence the results obtained. Primer specificity was therefore checked by melting curve analysis. Figure 6 panel A shows a GPATCH4 primer pair with several melting peaks, while the melting peak of the second GPATCH4 primers possess only one single melting peak with overlapping melting curves (Figure 6 panel B). Only primers showing a single peak are specific as this implies amplification of only one product. Therefore, primers that showed more than one melting peak were detected and discarded. For all the 22 human G-patch proteins and the two G-patch protein-interacting RNA helicases, it was possible to establish an experimentally verified qPCR primer pair fulfilling all the above-described requirements.

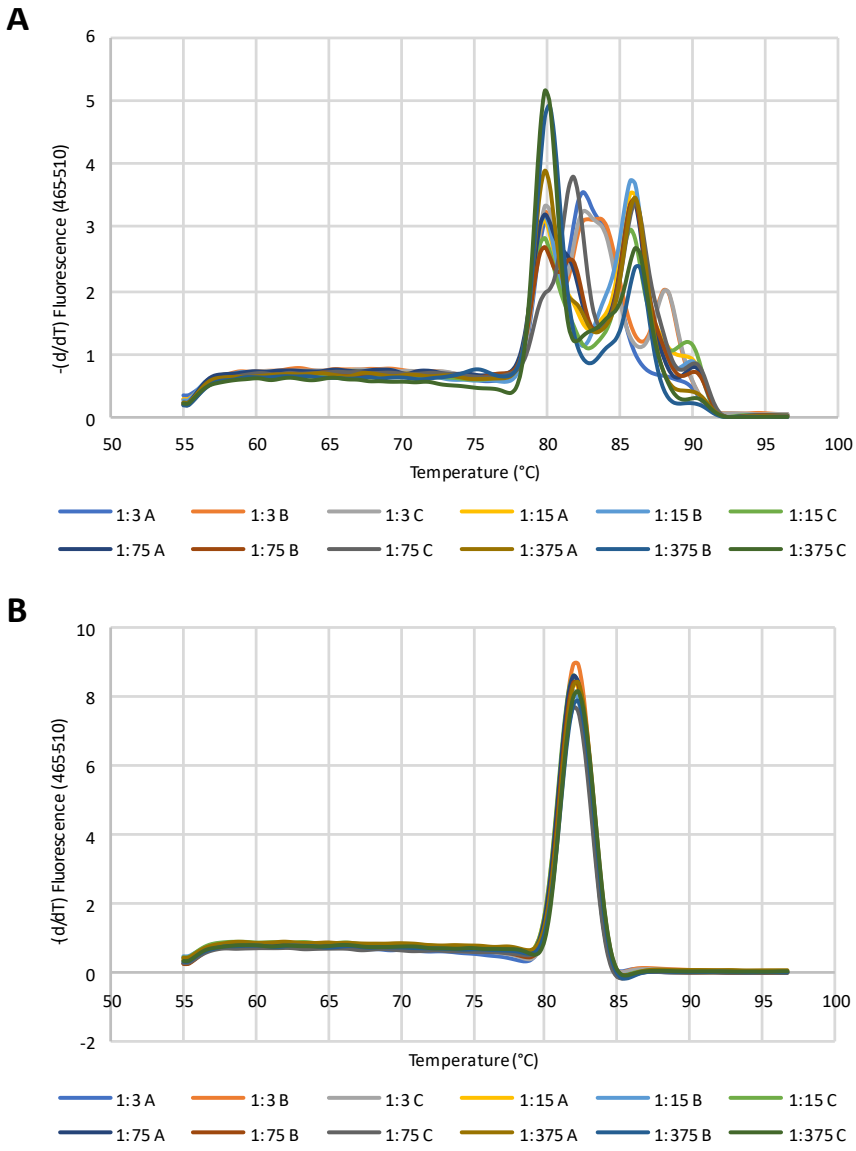

Figure 6: Melting curves of primers to evaluate primer specificity. Several target gene-specific primers (fwd/rev) were designed, purchased, and qPCR serial dilution was performed on HEK293 cDNA (1:3, 1:15, 1:75 and 1:375). The respective cDNA was pipetted in triplicates. Primer target binding specificity was evaluated via the respective melting peak formation analysis. Primers had to show a single melting curve to be selected for further qPCR experiments. Panel A shows the melting curves of a GPATCH4 primer with a weak target binding specificity, which is illustrated by several melting peaks, while Panel B shows the specificity of another GPATCH4 primer with a high target binding specificity.

3.2. Analysis of G-patch protein mRNA levels in human cancer cell lines

As already mentioned in section 1.1.4, there are different levels of gene expression regulation. Transcription, splicing, translation and (m)RNA stability are among them (Bourgeois et al. 2016). Differences in gene expression determine the identity of different cell types and dramatic changes in gene expression happen during development and in cancer. Cofactors, including G-patch proteins, can regulate the distribution and functional role of RNA helicases (Heininger et al. 2016). As changes in their expression levels are implicated in cancer, detailed information on how their expression level varies in different cancer cell lines could allow for a better understanding of RNA helicase regulation in tumors. Therefore, eight immortalized human cell lines coming from different origins were selected for further analysis. HEK293 cells are embryonic kidney cells, HeLa cells derived from cervical cancer cells, A549 are adenocarcinomic alveolar basal epithelial cells, U2OS cells come from osteosarcoma, CaCo-2 derive from a colon carcinoma and MCF-7 cells are of breast cancer origin (section 2.2.4 and 2.2.5.2). In addition, two types of HCT116 cells, colorectal carcinoma cells, either expressing wildtype p53 (wt) or lacking p53 (-/-) were included to get a more specific perspective on whether expression of the major tumor suppressor p53 affects G-patch protein expression.

To analyze G-patch protein and RNA helicase expression levels in these cell lines by qPCR, the cell lines were all cultured under optimal growth conditions and total RNA was harvested to serve as a template (section 2.2.3). To confirm RNA purity, the A_{260}/A_{280} ratio was checked using NanoDrop 2000c Spectrophotometer. This ratio is composed of the absorbance at 260 nm (A_{260}), which measures the nucleic acid concentration, over the absorbance at 280 nm (A_{280}), which measures protein contaminants (Kuang et al. 2018). RNA purity with a ratio greater than 1.8 was required for further experiments. RNA quality, which is dependent on RNA integrity, has great influence on the reliability of qPCR results, as the true changes in gene expression levels can deviate significantly from the values obtained for partially degraded RNA (Vermeulen et al. 2011). To check the integrity of the extracted RNAs, they were separated by agarose gel electrophoresis and the included fluorescent dye was visualized by a UV transilluminator (section 2.2.3) Nucleic acid mobility in the gel is reliant on its structural conformation as well as its molecular weight. Denaturation of the RNA leads to elimination of one of these factors and thereby increases the validity. As the phosphate backbone of the RNA molecule is negatively charged, it will migrate to the positively charged anode in an electric field. Figure 7 shows an agarose gel of the RNAs extracted from the

eight different cell lines, which were subsequently used for further qPCR experiments. In each lane, the upper band represents the 28S ribosomal RNA, whereas the lower bands represent the 18S ribosomal RNA. The detection of these sharp, long abundant intact RNAs indicates that the RNA is not degraded. Moreover, as the intensities of the upper bands are about twice as much as those of the lower bands due to the larger size of 28S versus 18S rRNAs, RNA integrity is confirmed. On the other hand, an altering ratio and a smear would imply low molecular weight components resulting from degradation (Kuang et al. 2018). Equal amounts of RNA from each cell line were then converted into cDNA by reverse transcription to serve as a template for qPCR reactions (section 2.2.4).

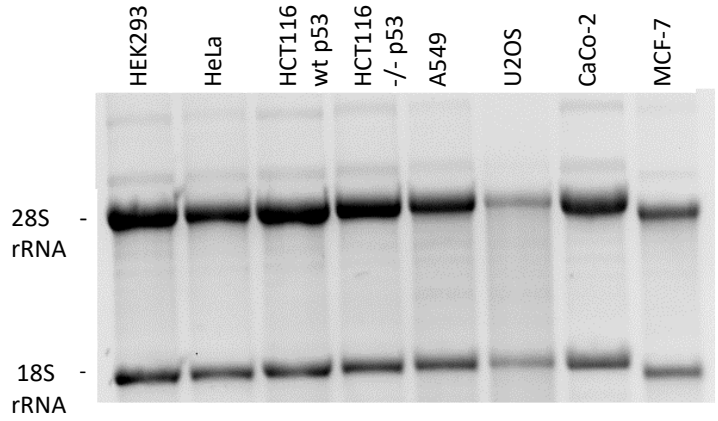

Figure 7: Agarose gel analysis of extracted RNAs to verify quality. RNA, extracted from eight different human cell lines (HEK293, HeLa, HCT116 wt p53, HCT116 -/- p53, A549, U2OS, CaCo-2, MCF-7), was separated by agarose gel electrophoresis and the rRNA bands visualized on a UV transilluminator. RNA size marker lane is not shown here.

The expression levels of the different G-patch protein and RNA helicase mRNAs were analyzed by relative quantification. The Ct values for the target genes were normalized to an arithmetic average of the Ct values obtained for the EMC7, PSMB2 and COPS6 mRNAs, which are three housekeeping genes. The expression levels of these three genes have been shown by RNA sequencing to be very consistent across different cell types and situations, making them good controls for the experiments performed here (Eisenberg and Levanon 2013). In contrast to classical housekeeping genes, such as actin, tubulin or GAPDH, these genes have been reported to be expressed at similar levels to the G-patch proteins, making them more comparable and therefore the qPCR data more reliable. Technical triplicates were performed to account for pipetting errors and samples deviating by > 0.5 Ct were discarded. HEK293 served as the internal reference cell line. These human cells were selected, as they are characterized as robust, can easily be cultured, and divide rapidly. In addition, they show a high and stable efficiency in protein production, which was a crucial feature for this study

(Swiech et al. 2012; Thomas and Smart 2005). The ratio of expression was calculated according to $r=2^{-\Delta\Delta Ct}$ (section 2.2.5.2 and 2.2.5.4). Figure 8 shows the mean values with their standard deviation for each target gene in each cell line, where the blue bars represent the average Ct ratios from three biologically independent assays (see also Supplemental table 1). Asterisks on top of the blue bars indicate significant differences in mRNA expression in the respective tumor cell line as compared to non-tumor HEK293, while α was set to 0.05, 0.01 and 0.001 for all analyzed variables.

In many cases, transcript levels in cancer cell lines were similar to those in HEK293 cells. In the following description, only remarkable variations in protein expression levels will be outlined. Means, standard deviations and *p*-values mentioned in text sections 3 and 4, were generally rounded to three decimal places.

AGGF1 mRNA levels were significantly decreased in comparison to HEK293 cells in HeLa cervical cancer ($M = 0.323$, $SD = 0.059$, $p = 0.003$), A549 lung cancer ($M = 0.433$, $SD = 0.102$, $p = 0.011$) and CaCo-2 colorectal cancer cells ($M = 0.525$, $SD = 0.169$, $p = 0.040$). The other tumor cell lines did neither show a significant up- nor downregulation of AGGF1 ratios (Figure 8a).

In A549 lung cancer cells, CHERP ($M = 0.241$, $SD = 0{,}159$, $p = 0.014$) as well as CMTR1 ($M = 0.261$, $SD = 0.107$, $p = 0.007$) mRNA levels were below 25% of those observed in HEK293 cells (Figure 8b, Figure 8c). The CMTR1 mRNA level was also notably lower in the three colorectal cancer cell lines − especially in CaCo-2 ($M = 0.275$, $SD = 0.145$, $p = 0.013$) − in comparison to HEK293 cells (Figure 8c), while CHERP mRNA levels were only mildly, albeit significantly reduced in HeLa cells ($M = 0.742$, $SD = 0.043$, $p = 0.009$).

GPANK1 mRNA levels were particularly elevated in HeLa cells, the level was significantly increased to a ratio of 1.287 ($SD = 0.005$, $p < 0.001$) (Figure 8d). A significant increase of mRNA levels was also observed for HCT116 wildtype ($M = 0.1.280$, $SD = 0.097$, $p = 0.038$), however not for p53 deletion cells.

GPATCH1 mRNA levels significantly were more than halved in HeLa cells in relation to HEK293 levels ($M = 0.387$, $SD = 0.016$, $p < 0.001$), while HCT116 -/- p53 ($M = 0.590$, $SD = 0.079$, $p = 0.012$) and A549 ($M = 0.793$, $SD = 0.082$, $p = 0.048$) also showed a significant, but minor decrease (Figure 8e).

a) AGGF1

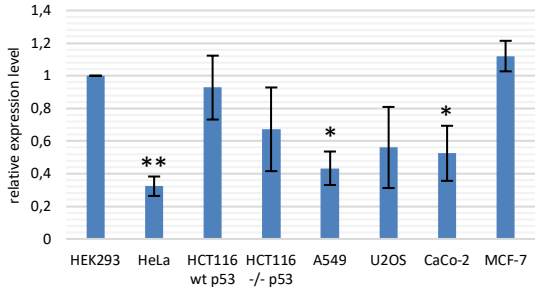

b) CHERP

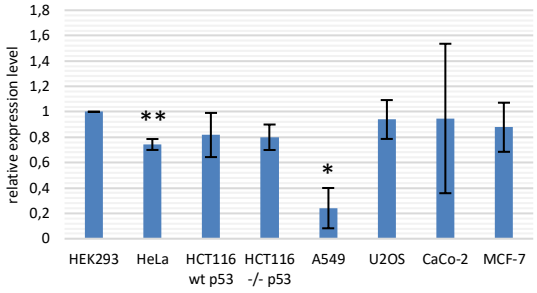

c) CMTR1

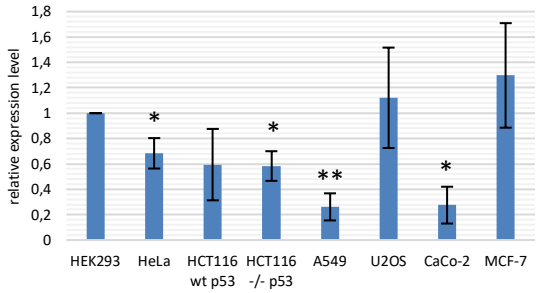

d) GPANK1

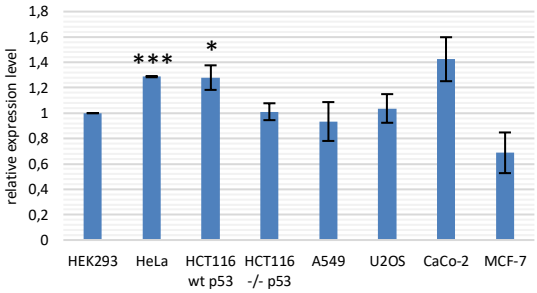

e) GPATCH1

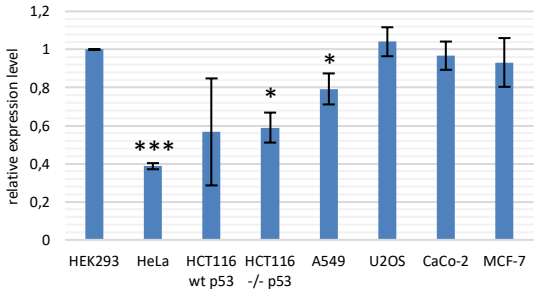

f) GPATCH2

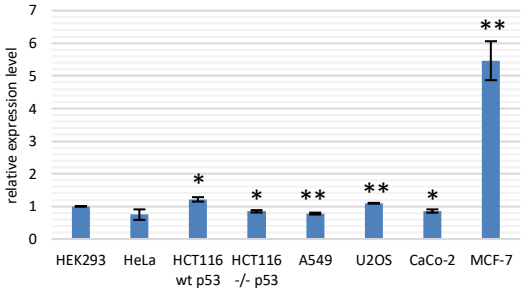

g) GPATCH3

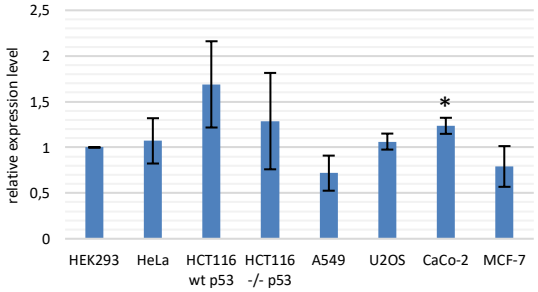

h) GPATCH4

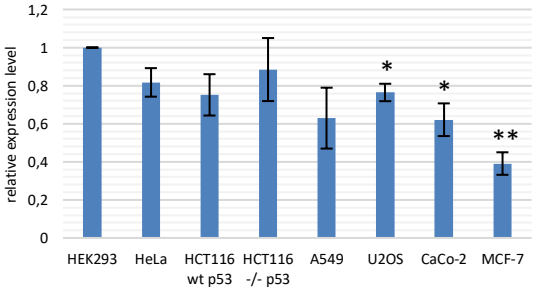

i) GPATCH8

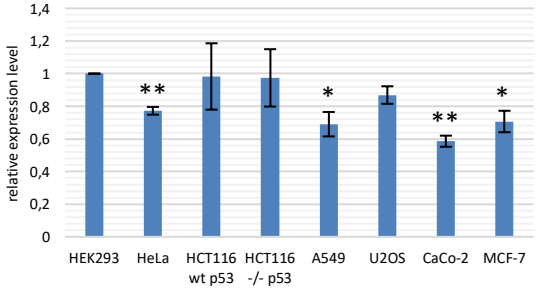

j) GPATCH11

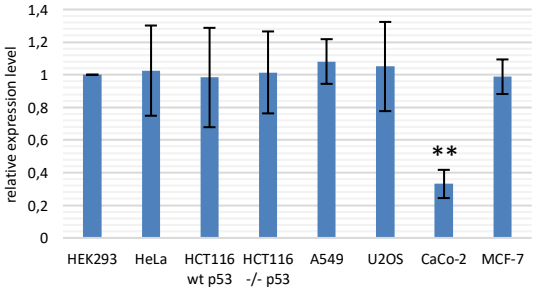

k) GPKOW

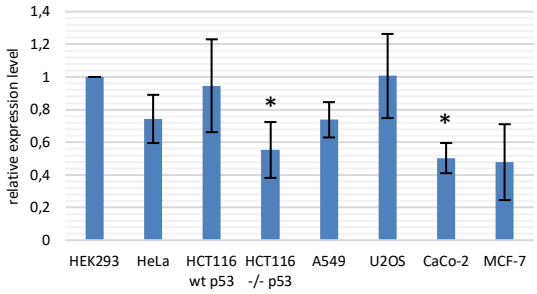

l) NKRF

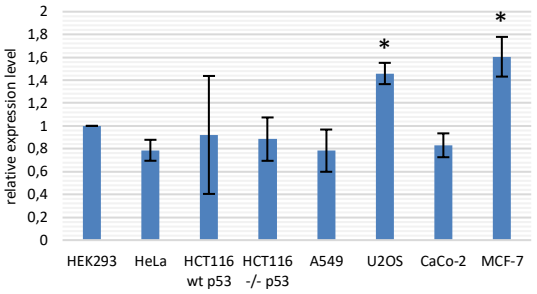

m) PINX1

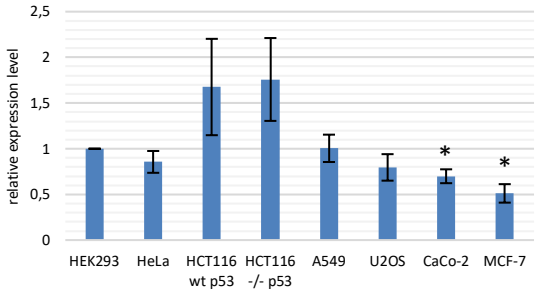

n) RBM5

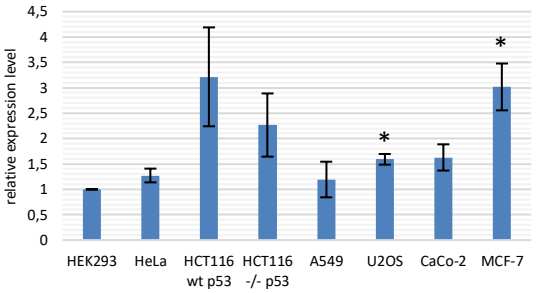

o) RBM6

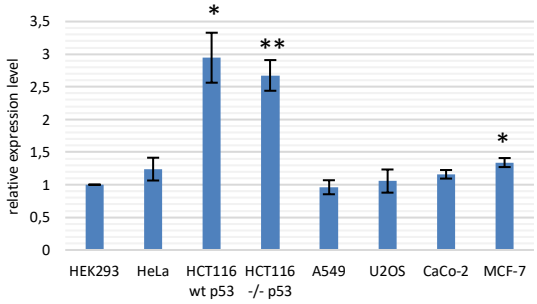

p) RBM10

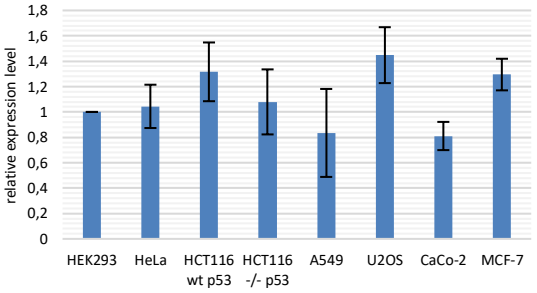

q) RBM17

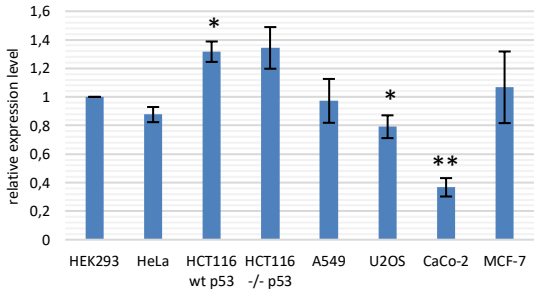

r) SON

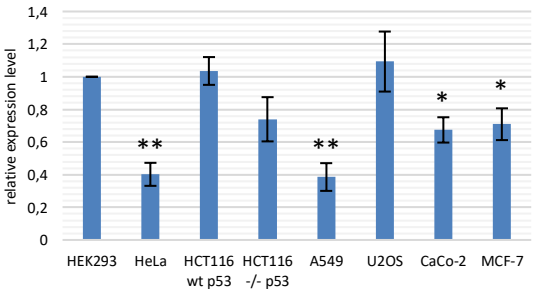

s) SUGP1

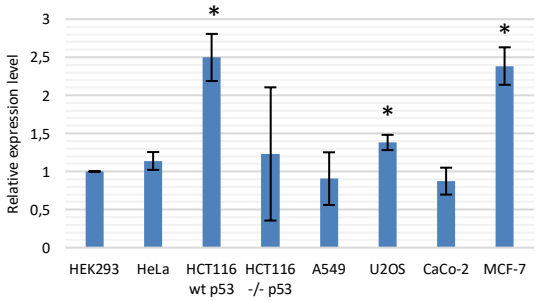

t) SUGP2

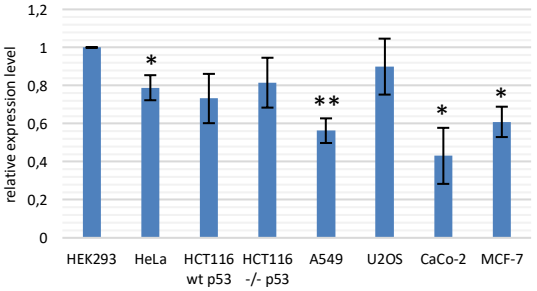

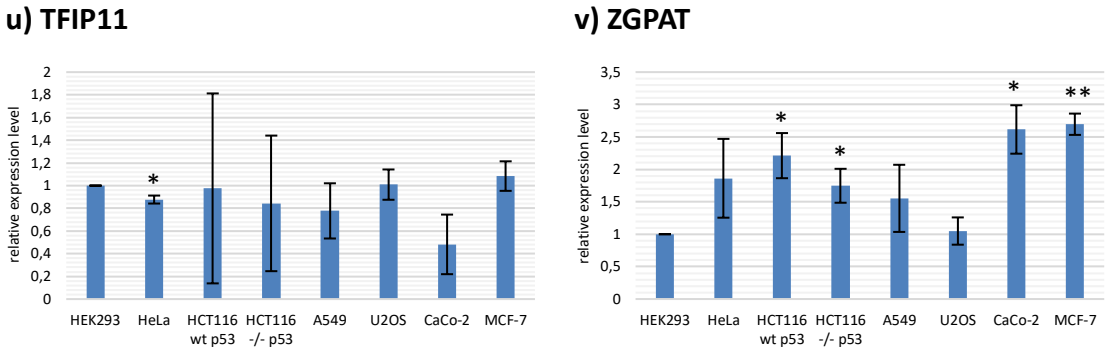

Figure 8: G-patch protein mRNA expression levels in human cancer cell lines. qPCR assays were performed. Gene expression levels from tumor cell lines were analyzed by relative quantification. The Ct value of each target gene was normalized to an arithmetic average of the Ct values from three different housekeeping genes (COPS6, EMC7, PSMB2). HEK293 served as an internal reference cell line. Ratios were calculated by $r = 2^{-\Delta\Delta Ct}$, with ΔCt = Ct(target gene) – Ct(reference gene) and ΔΔCt = ΔCt(tumor sample) − Ct(control). Data of three independent experiments were taken for mean value composition (blue bars) and are shown with standard deviation (black lined ranges). The error bars equal a 68 % confidence interval. Asterisks on top of the blue bars represent significant differences in mRNA expression in the respective tumor cell line as compared to non-tumor HEK293 (* = $p < 0.05$; ** = $p < 0.01$; *** = $p < 0.001$).

Remarkably, in the breast cancer cell line MCF-7, the GPATCH2 mRNA level was about five times higher than in all the other cell lines tested ($M = 5.464$, $SD = 0.597$, $p = 0.006$) (Figure 8f). In contrast, the MCF-7 GPATCH4 mRNA level was more than halved in comparison to most of the other cell lines ($M = 0.391$, $SD = 0.059$, $p = 0.003$). Also, GPATCH4 mRNA expression in CaCo-2 reflected a significant decrease to a ratio of about 0.621 ($SD = 0.086$, $p = 0.017$) and in U2OS, a minor but significant decrease to about 0.764 ($SD = 0.046$, $p = 0.012$) was observed (Figure 8h).

While a slight increase of GPATCH3 expression was observed for HCT116 cells, this was not statistically significant and the only significant variation among the eight cell lines was a minor increase in GPATCH3 levels in the case of CaCo-2 cells (Figure 8g).

GPATCH8 relative expression in HeLa ($M = 0.773$, $SD = 0.024$, $p = 0.004$), A549 ($M = 0.690$, $SD = 0.075$, $p = 0.019$), CaCo-2 ($M = 0.586$, $SD = 0.034$, $p = 0.002$) and MCF-7 ($M = 0.707$, $SD = 0.066$, $p = 0.016$) was rather slightly, but significantly decreased to a ratio greater than 0.6, as compared to the HEK293 level (Figure 8i).

CaCo-2 colorectal cells appeared to significantly show low expression of the G-patch protein GPATCH11 mRNA, as the GPATCH11 mRNA level only amounted to 1/3 of that in HEK293 cells ($M = 0.331$, $SD = 0.087$, $p = 0.006$) compared to the reference genes (Figure 8j).

GPKOW mRNA levels were about halved in HCT116 -/- p53 (M = 0.553, SD = 0.171, p = 0.455), CaCo-2 (M = 0.503, SD = 0.092, p = 0.011) and, albeit not significantly, in MCF-7 (M = 0.478, SD = 0.232, p = 0.060) as compared to HEK293 (Figure 8k).

The NKRF mRNA level in U2OS osteosarcoma (M = 1.459, SD = 0.093, p = 0.013) and MCF-7 cells (M = 1.606, SD = 0.174, p = 0.026) showed a significant increase to about 1.5-fold in relation to HEK293 cells (Figure 8l).

In colorectal cancer cells HCT116 wildtype p53 (M = 1.675, SD = 0.527, p = 0.157) and HCT116 -/- p53 (M = 1.758, SD = 0.453, p = 0.101), PINX1 levels were descriptively, but not statistically significantly, up to a ratio of more than 1.5, whereas in MCF-7 and CaCo-2 cells they were significantly downregulated to a ratio of 0.5 (M = 0.511, SD = 0.101, p = 0.014) and 0.7 (M = 0.699, SD = 0.076, p = 0.021), respectively (Figure 8m).

Remarkably, in HCT116 (albeit not significantly) and MCF-7 cells (M = 3.017, SD = 0.461, p = 0.017) RBM5 mRNA levels were increased up to threefold, as compared to HEK293 cells (Figure 8n). Similarly, an almost threefold increase of RBM6 mRNA levels was detected in HCT116 wildtype (M = 2.946, SD = 0.383, p = 0.013) and HCT116 -/- p53 (M = 2.675, SD = 0.235, p = 0.006) (Figure 8o), while a small increase was observed for MCF-7 cells (M = 1.340, SD = 0.070, p = 0.014). In contrast, RBM10 mRNA expression did not show any significant change to HEK293 in none of the seven tumor cell lines (Figure 8p).

Especially in CaCo-2 cells, as compared to HEK293 cells, the RBM17 mRNA level was significantly decreased to less than 0.4-fold (M = 0.367, SD = 0.064, p = 0.003) and in U2OS to about 0.8-fold (M = 0.791, SD = 0.080, p = 0.045), whereas both colorectal cancer HCT116 lines showed an increase to a ratio of almost 1.5 (M = 1.317, SD = 0.071, p = 0.017 for the wildtype and M = 1.343, SD = 0.146, p = 0.055 for the p53 -/- cells), even though the p53 -/- cells nonsignificant (Figure 8q).

Significant down-leveling to a ratio of less than 0.5 was also observed for SON mRNA expression in HeLa (M = 0.402, SD = 0.071, p = 0.005) and A549 lung cancer cells (M = 0.386, SD = 0.085, p = 0.006). Two other cell lines, CaCo-2 (M = 0.674, SD = 0.078, p = 0.018) and MCF-7 (M = 0.709, SD = 0.097, p = 0.035), also showed a significant, but minor decrease in relation to HEK293 (Figure 8r).

In HCT116 wildtype p53 (M = 2.498, SD = 0.310, p = 0.014) and MCF-7 cells (M = 2.385, SD = 0.246, p = 0.014), SUGP1 mRNA levels were about 2.5 times higher as compared to the reference cell line HEK293. Moreover, did the U2OS osteosarcoma cell line show a minor, but significant increase of the expression level (M = 1.381, SD = 0.100, p = 0.022) as

compared to HEK293 (Figure 8s). In contrast, not only in A549 (M = 0.563, SD = 0.065, p = 0.007), CaCo-2 (M = 0.431, SD = 0.0.147, p = 0.022) and also MCF-7 cells (M = 0.609, SD = 0.090, p = 0.014), SUGP2 mRNA expression was reduced approximately by half in relation to HEK293 cells, but also HeLa cells showed a smaller but significant reduction for this mRNA (M = 0.789, SD = 0.066, p = 0.031) (Figure 8t).

For TFIP11, colorectal cancer HCT116 ratios conspicuously exhibited wide ranging standard deviations of more than 0.5 (SD = 0.837 and SD = 0.597), limiting its statistical power, and only a slight but significant reduction in expression could be observed for Hela cells (M = 0.877, SD = 0.035, p = 0.026) (Figure 8u).

ZGPAT was significantly expressed at a 2.5-fold higher level in MCF-7 (M = 2.696, SD = 0.164, p = 0.003) and CaCo-2 cells (M = 2.615, SD = 0.374, p = 0.017), while a smaller but significant increase was observed in both HCT116 cell lines (M = 2.212, SD = 0.348, p = 0.026 for the wildtype and M = 2.615, SD = 0.374, p = 0.017 for the p53 -/- cells) (Figure 8v).

Not only cofactor levels but also RNA helicase expression levels can vary upon tumorigenesis (Steimer and Klostermeier 2012). To receive better insights into these mRNA expression variations in cancer, qPCR assays, targeting G-patch protein-interacting RNA helicases, were performed for the previously mentioned cancer cell lines. The experimental setup remained according to the cofactor qPCR assays (section 2.2.5.4).

DHX15 levels in both HCT116 wildtype p53 (M= 2.329, SD = 0.413, p = 0.031) and HCT116 -/- p53 cells (M = 1.992, SD = 0.256, p = 0.021) more than doubled in comparison to HEK293 cells. Additionally, mRNA expression in MCF-7 cells also significantly increased more than 1.7-fold over the control level (M = 1.709, SD = 0.165, p = 0.018), and in CaCo-2 cells a similar upregulation could be observed (M = 1.830, SD = 0.479, p = 0.095), while HeLa cells showed a small but significant increase (M = 1.192, SD = 0.067, p = 0.038) (Figure 9a).

DHX35 helicase levels were significantly upregulated by more than twofold in HeLa (M = 2.235, SD = 0.134, p = 0.004) and HCT116 -/- p53 (M = 2.394, SD = 0.417, p = 0.029), and approximately threefold in HCT116 wildtype p53 cells (M= 3.121, SD = 0.842, p = 0.049) as compared to HEK293. CaCo-2 colon cancer cells even showed an almost sixfold higher DHX35 mRNA level as the control level (M= 5.546, SD = 0.391, p = 0.003) (Figure 9b).

Together these data illustrate that different tumor cell lines express G-patch protein and RNA helicase mRNAs at variable levels. While some G-patch protein mRNAs appear to be similarly expressed across the range of cell lines tested, other G-patch protein mRNAs were observed to increase or decrease in different cancer cell lines, suggesting a complex picture of gene expression regulation.

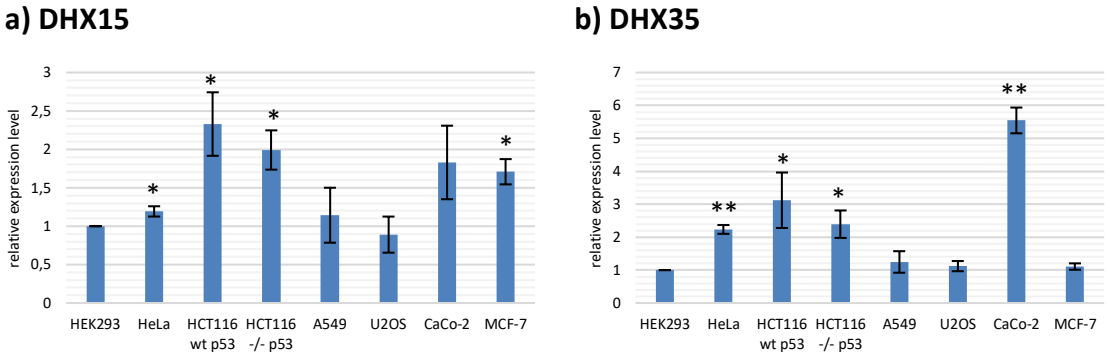

Figure 9: RNA helicase mRNA expression levels in human cancer cell lines. qPCR assays were performed. Gene expression levels from tumor cell lines were analyzed by relative quantification. The Ct value of each target gene was normalized to an arithmetic average of the Ct values from three different housekeeping genes. HEK293 served as an internal reference cell line. Ratios were calculated by $r = 2^{-\Delta\Delta Ct}$, with ΔCt = Ct(target gene) – Ct(reference gene) and $\Delta\Delta Ct = \Delta Ct$(tumor sample) − Ct(control). Data of three independent experiments were taken for mean value composition (blue bars) and the standard deviation was calculated (black lined range). The error bars equal a 68 % confidence interval Asterisks on top of the blue bars show significant differences in mRNA expression in the respective tumor cell line as compared to non-tumor HEK293 (***** = $p < 0.05$; ****** = $p < 0.01$; ******* = $p < 0.001$).

3.3. Analysis of G-patch protein levels in human cancer cell lines

mRNAs are templates for ribosomes to produce cellular proteins. While monitoring mRNA levels can be a good indicator of gene expression, direct analysis of protein levels is another important approach, as gene expression can also be controlled at the translational level. So, protein expression was directly analyzed by western blotting for G-patch proteins, where antibodies were available, and the two RNA helicases DHX15 and DHX16, as this allows for at least semi-quantitative target protein detection (Vallejo-Illarramendi et al. 2013). Thus, protein was harvested from the cancer cell lines (section 2.2.6) and separated by SDS-PAGE (section 2.2.7). This was followed by protein transfer onto a nitrocellulose membrane and then blocking of the membrane. The membrane was then incubated with primary antibodies against selected G-patch proteins and RNA helicases, followed by labeling with the secondary antibody and subsequent target visualizing (section 2.2.8). In each case, tubulin was also immunodetected to serve as a loading control, accounting for potential differences

in the amount of protein loaded in each lane. HEK293 again served as the internal reference cell line. Protein bands were quantified using Image Studio™ Lite Software.

Figure 10, left column exemplarily shows one of the three analyzed Western blot pictures for each target protein, respectively combined with tubulin bands for normalization. The diagram on the right side visualizes the mean values with their standard deviation for each target protein, while the blue bars again represent the average ratios from three biologically independent assays (see also Supplemental table 3). Asterisks on top of the blue bars once more indicate significant differences in protein expression in the respective tumor cell line as compared to non-tumor HEK293, while α was again set to 0.05, 0.01 and 0.001 for all analyzed variables.

For CMTR1 protein levels, a slight decrease to a ratio of about 0.6 in HCT 116 -/- p53 (M = 0.676, SD = 0.259, p = 0.163) and CaCo-2 cells (M = 0.631, SD = 0.227, p = 0.106), as compared to HEK293 cells, could be described. Yet overall, protein expression across all seven tumor cell lines did not show any significant variation (Figure 10a).

GPATCH2 protein levels were two times higher in CaCo-2 cells than they were in HEK293 cells (M = 2.032, SD = 0.315, p = 0.030). Also, GPATCH2 expression in A549 lung cancer cells significantly amounted to a ratio of 1.75 (M = 1.787, SD = 0.303, p = 0.046), while U2OS (M = 0.847, SD = 0.048, p = 0.031) and HCT116 wildtype p53 cells (M = 0.761, SD = 0.019, p = 0.002) showed a significant reduction in protein levels. Statistical power for MCF-7 seems limited, as relative expression rates of the three independent MCF-7 blots widely lie apart from each other, resulting in a standard deviation greater than 7.5 (SD = 7.580) (Figure 10b).

GPATCH4 protein expression, in relation to HEK293, had significantly been reduced by about half in colorectal cancer cell lines HCT116 wildtype p53 (M = 0.693, SD = 0.104, p = 0.036) as well as CaCo-2 (M = 0.559, SD = 0.138, p = 0.031). The A549 protein level descriptively showed a remarkable major increase in protein expression. The respective standard deviation amounted to 26, thus indicating limited statistical power (M = 15.663, SD = 25.984, p = 0.432) (Figure 10c).

a) CMTR1

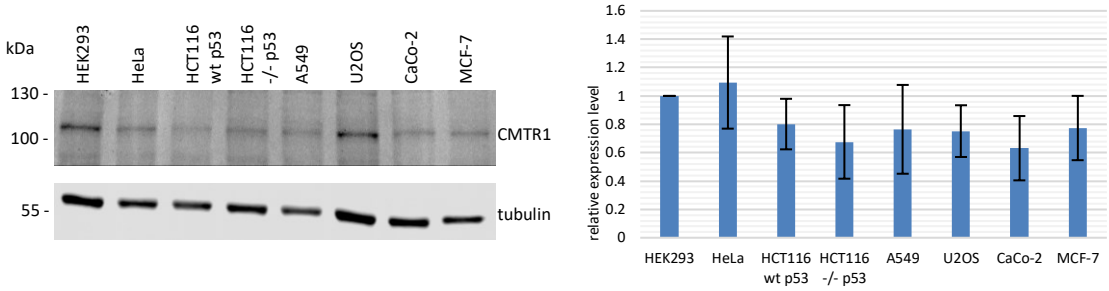

b) GPATCH2

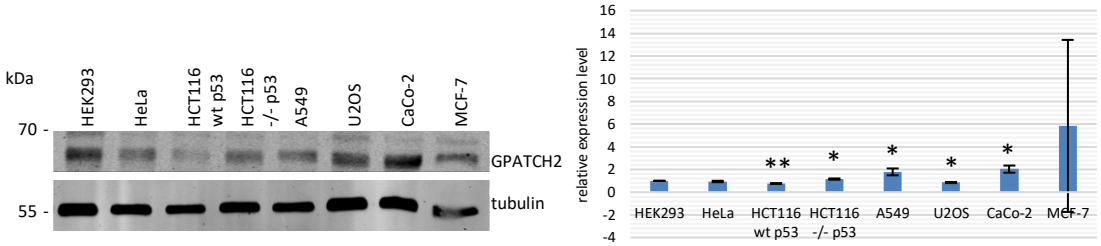

c) GPATCH4

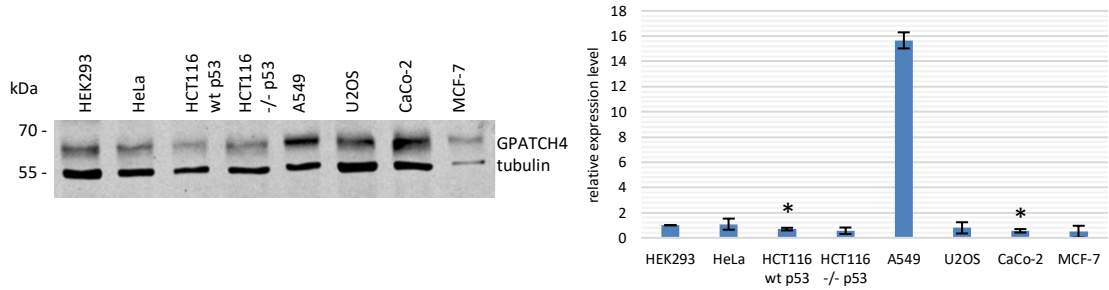

d) GPATCH11

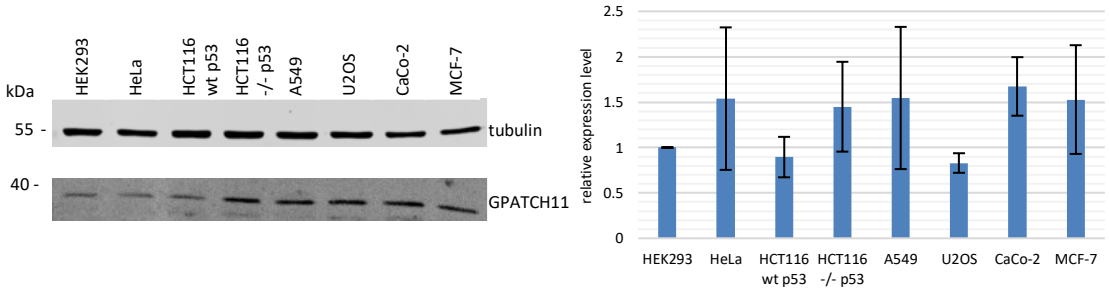

e) GPKOW

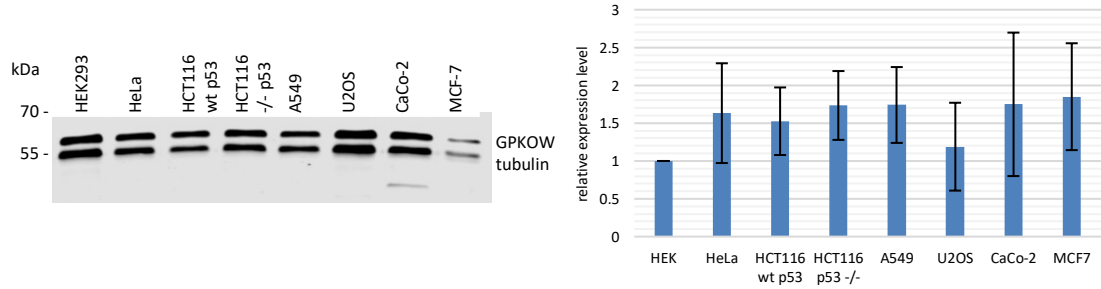

f) NKRF

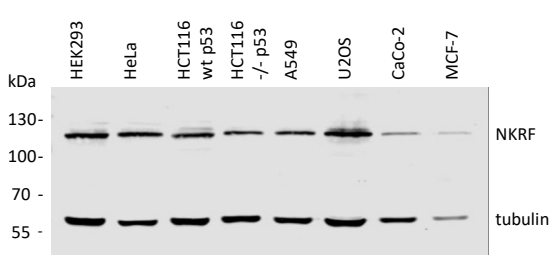

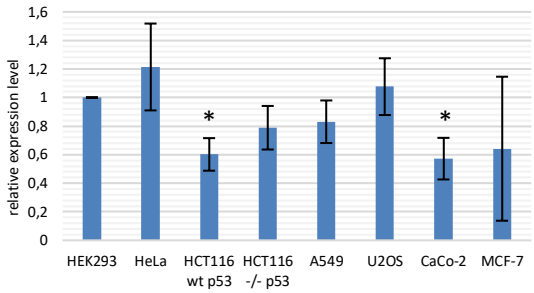

g) PINX1

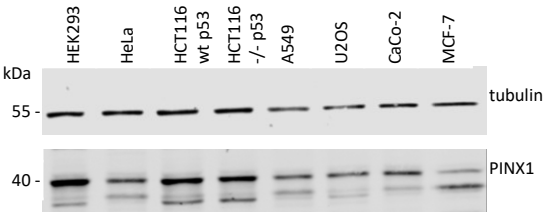

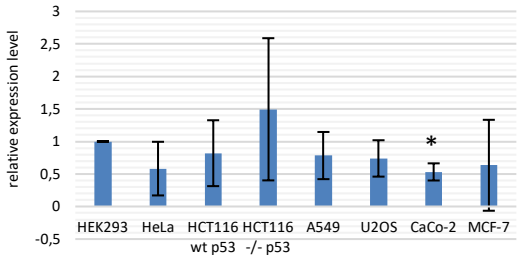

h) RBM6

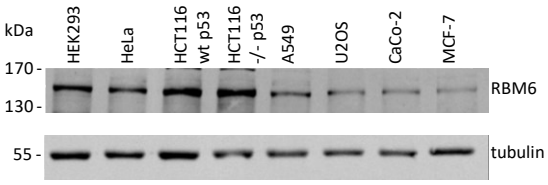

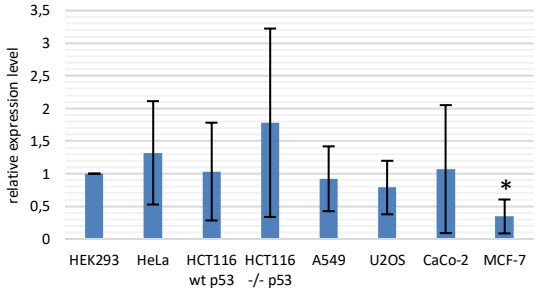

i) DHX15

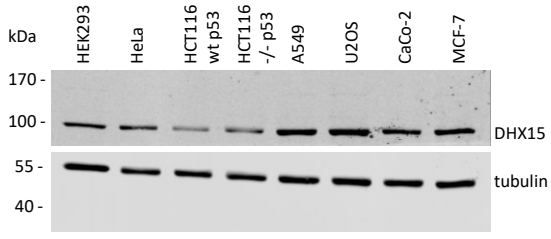

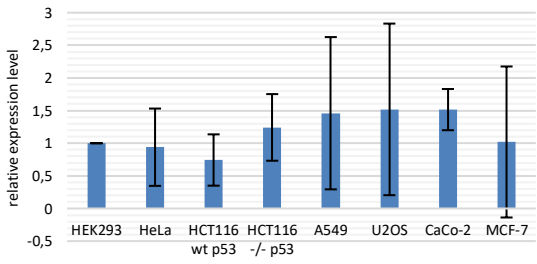

j) DHX16

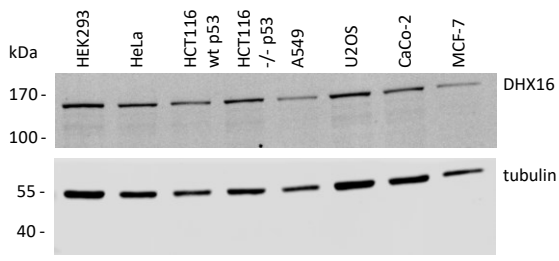

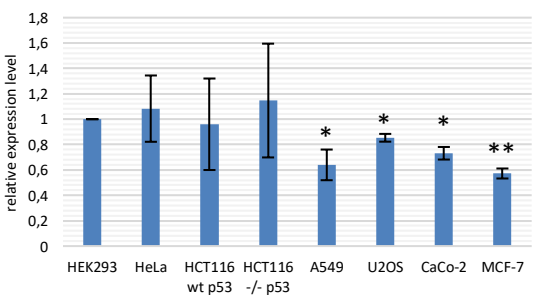

Figure 10: G-patch protein and RNA helicase expression levels in human cancer cell lines. SDS-PAGE and western blotting was performed. Tubulin served as the reference gene (left column). Protein bands were quantified using Image Studio™ Lite Software. Protein size marker is indicated on the left. The signaling intensity of each of the targets was normalized to the protein band of tubulin. HEK293 again served as the internal reference cell line. Data of three independent experiments were taken for mean value composition of the ratios (right column, blue diagram bars) and the respective standard deviation was calculated (black lined range). The error bars equal a 68 % confidence interval. Asterisks on top of the blue bars show significant differences in mRNA expression in the respective tumor cell line as compared to non-tumor HEK293 (***** = $p < 0.05$; ****** = $p < 0.01$; ******* = $p < 0.001$).

Neither for GPATCH11, nor for GPKOW, any significant changes in protein expression could be observed (Figure 10d, Figure 10e). NKRF expression levels were significantly decreased to a ratio of 0.6 in colorectal cancer cell lines HCT116 wildtype p53 ($M = 0.602$, $SD = 0.114$, $p = 0.026$) and CaCo-2 ($M = 0.572$, $SD = 0.146$, $p = 0.037$) (Figure 10f).

In general, PINX1 relative expression levels were low in six of the seven cancer cell lines − HCT116 -/- p53 excluded −, whereupon the mean ratio in CaCo-2 cells again showed a significant reduce by about half ($M = 0.532$, $SD = 0.132$, $p = 0.026$) (Figure 10g).

Also, G-patch protein RBM6 mean ratio in breast cancer cell line MCF-7 was significantly reduced to approximately one third of the amount in HEK293 cells ($M = 0.345$, $SD = 0.260$, $p = 0.049$), while the other cell lines did not show significant variations (Figure 10h).

In none of the seven cancer cell lines, significant changes in RNA helicase DHX15 expression – again as compared to HEK293 − could be observed (Figure 10i), while DHX16 expression levels were significantly lowered in A549 ($M = 0.640$, $SD = 0.121$, $p = 0.036$), U2OS ($M = 0.853$, $SD = 0.031$, $p = 0.014$), CaCo-2 ($M = 0.731$, $SD = 0.050$, $p = 0.011$) and MCF-7 ($M = 0.572$, $SD = 0.039$, $p = 0.003$) cells compared to HEK293 protein expression (Figure 10j).

Apart from the fact that for some of the target proteins' statistical power might have been limited, these data illustrate varying levels of cofactor and RNA helicase proteins in different types of cancer cell lines. Strikingly, protein levels analyzed by western blotting do not necessarily correspond to the respective mRNA levels that were analyzed by qPCR (section 3.2).

3.4. Analysis of G-patch protein mRNA levels in matched-pair squamous cell carcinoma and fibromyxosarcoma tissue samples

In sections 3.2 and 3.3, RNA helicase and their interacting cofactor expression levels have been analyzed from human cancer cell lines. These data allow for comparisons in gene expression between multiple cancer cell lines, and favorably for conclusions on the role of G-patch proteins in tumorigenesis. The reference cell line initially originates from embryonic kidney cells, while the other cell lines descend from different human tumor tissues. Thus, these cell lines are likely to possess different characteristics due to cell differentiation, resulting in different gene expression programs and varying protein expression levels. Accordingly, it was shown that RNA helicases regulate gene expression steps in a cell type specific way (Dardenne et al. 2014), while the availability of cofactors display one of the main reasons for cell type specific processes of the helicases (Bourgeois et al. 2016). Apart from this, in this study, mRNA levels in matched-pair tumor and normal tissue were analyzed for the purpose of detecting either expression differences or similar tendencies within the same tissue. RNA for qPCR analysis was extracted from tissues from patients suffering from cancer (Table 8). Thus − other than in section 3.2 and 3.3 − an *in vivo* rather than *in vitro* situation was analyzed. The tissues were provided from the CEPA Biobank (Newcastle upon Tyne Hospitals NHS Trust, UK) and two different tumor types were obtained − squamous cell carcinoma from oral cavity and fibromyxosarcoma from limbs. For both of them, four/three different matched-pair tumor and normal tissue sets from patients were provided. Total RNA was extracted, and qPCR assays were performed (section 2.2.5). Gene expression levels were again analyzed by relative quantification through normalization of the Ct values from the target genes to an arithmetic average of the Cts from EMC7, PSMB2 and COPS6. Normal non-tumor tissue served as reference for each sample and the ratio was calculated according to $r = 2^{-\Delta\Delta Ct}$.

Figure 11 and Figure 12 show the analyses of G-patch protein and RNA helicase mRNA expression levels, respectively, in three samples of fibromyxosarcoma tissues from three different patients (see also Supplemental table 5). As only a limited amount of tissue could be obtained, the analyses could only be performed for nine G-patch protein and two helicase mRNAs.

a) GPATCH1

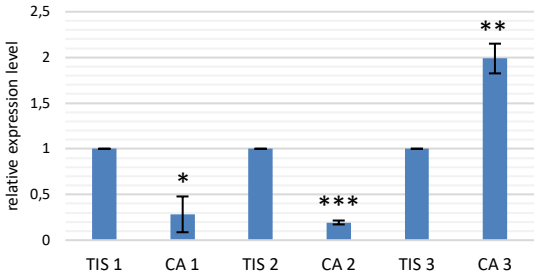

b) GPATCH3

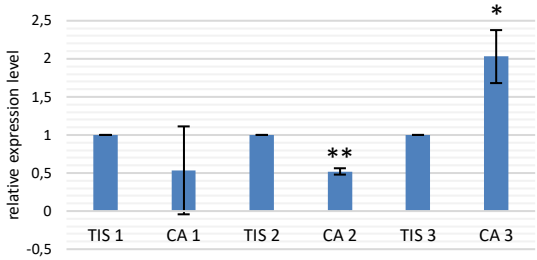

c) GPATCH4

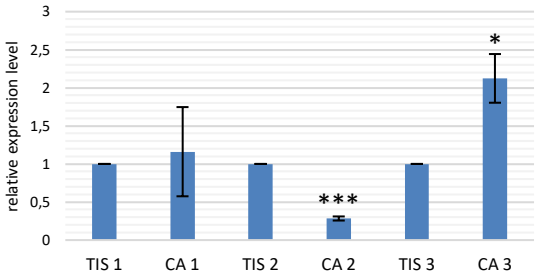

d) NKRF

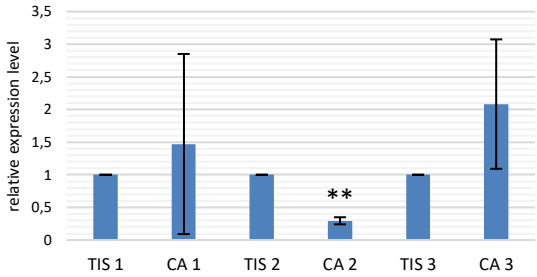

e) RBM5

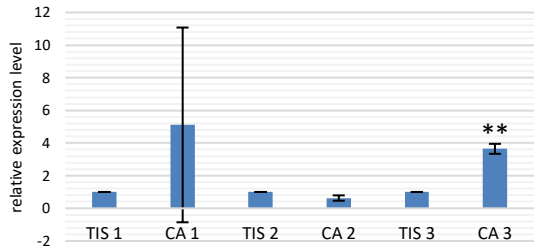

f) SUGP1

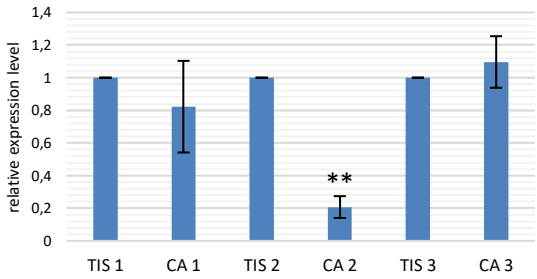

g) SUGP2

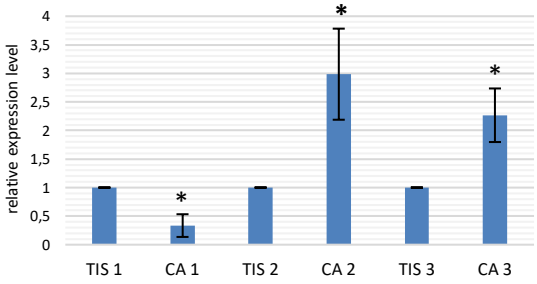

h) TFIP11

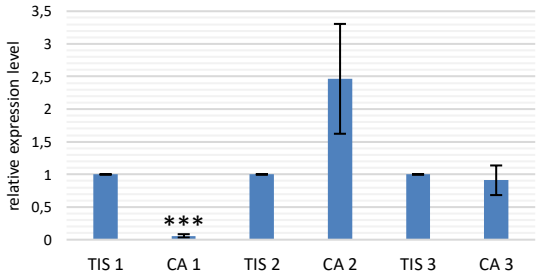

i) ZGPAT

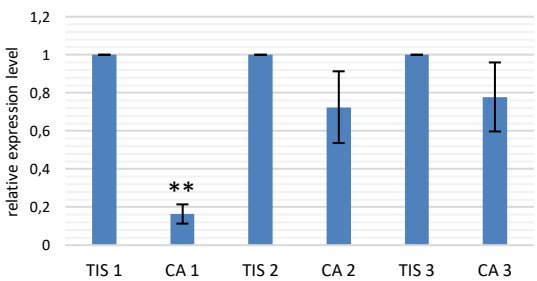

Figure 11: G-patch protein mRNA expression levels in matched-pair fibromyxosarcoma tissue samples. qPCR assays were performed. Gene expression levels from three different fibromyxosarcoma tissue samples (CA) and their respective matched-pair normal tissue (TIS) were analyzed by relative quantification. The Ct value of each target gene was normalized to an arithmetic average of the Cts from three different housekeeping genes. The respective non-pathogenic tissue (TIS) served as each internal reference. Ratios were calculated by $r = 2^{-\Delta\Delta Ct}$, with ΔCt = Ct(target gene) – Ct(reference gene) and ΔΔCt = ΔCt(tumor sample) − Ct(control). Data of three independent experiments were taken for mean value composition (blue bars) and the standard deviation was calculated (black lined range). The error bars equal a 68 % confidence interval. Asterisks on top of the blue bars show significant differences in mRNA expression in the respective tumor tissue (CA) as compared to its matched-pair non-tumor tissue (TIS) (***** = p <0.05; ****** = p < 0.01; ******* = p < 0.001).

For GPATCH1, expression levels were significantly downregulated in cancer sample 1 and 2 to a ratio of less than 0.3 (M = 0.283, SD = 0.196, p = 0.024 and M = 0.194, SD = 0.022, p < 0.001), while the level in cancer sample 3 showed a twofold increase in relation to its matched-pair normal tissue (M = 1.988, SD = 0.163, p = 0.009) (Figure 11a). Similarly, GPATCH3 ratios in cancer sample 2 were significantly reduced (M = 0.521, SD = 0.042, p = 0.003), whereas mRNA expression in cancer sample 3 again doubled as compared to its normal tissue (M = 2.029, SD = 2.0.348, p = 0.036) (Figure 11b). GPATCH4 relative expression levels behaved likewise, as in cancer sample 2 the ratio was significantly lowered (M = 0.284, SD = 0.027, p < 0.001) and in cancer sample 3, it went up again (M = 2.124, SD = 0.320, p = 0.026) (Figure 11c).

For NKRF (M = 0.295, SD = 0.055, p = 0.002) and SUGP1 (M = 0.207, SD = 0.067, p = 0.002) ratios significantly decreased in sample 2, while RBM5 mRNA levels showed an almost fourfold increase in sample 3 (M = 3.644, SD = 0.306, p = 0.004) (Figure 11d, Figure 11f, Figure 11e). In contrast, a more than twofold increase of SUGP2 expression levels occurred in samples 2 (M = 2.985, SD = 0.797, p = 0.050) and 3 (M = 2.266, SD = 0.469, p = 0.043), whereas cancer sample 1 ratios showed a significant decrease compared to its matched-pair sample (M = 0.334, SD = 0.199, p = 0.029) (Figure 11g).

For TFIP11 (M = 0.059, SD = 0.026, p < 0.001) and ZGPAT (M = 0.164, SD = 0.051, p = 0.001), relative expression levels in cancer sample 1 significantly were reduced in relation to their respective normal tissue (Figure 11h, Figure 11i).

Likewise, RNA helicase ratios in Figure 12 showed varying expression levels. While DHX15 expression did not show any significant variation between the three independent FMS tissues, DHX35 mRNA was significantly downregulated in cancer sample 1 (M = 0.065, SD = 0.023, p = <0.001). In cancer sample 3, the DHX35 mRNA was significantly upregulated by twofold (M = 2.049 SD = 0.167, p = 0.008).

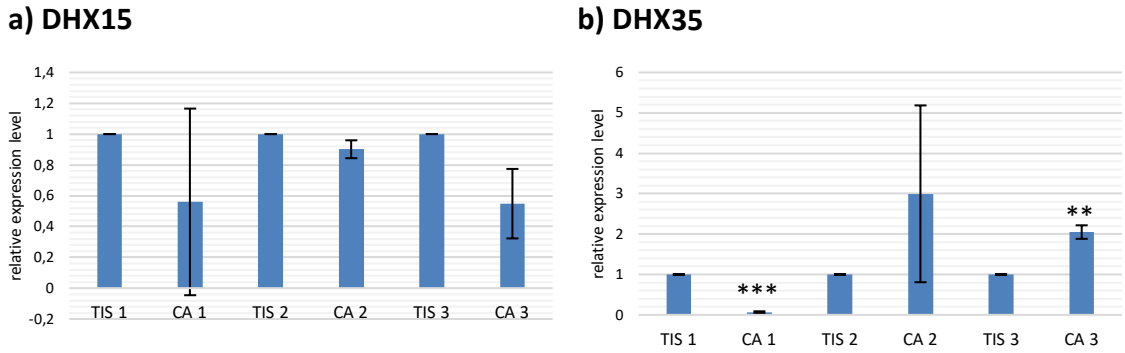

Figure 12: RNA helicase mRNA expression levels in matched-pair fibromyxosarcoma tissue samples. qPCR assays were performed. Gene expression levels from three different fibromyxosarcoma tissue samples (CA) and their respective matched-pair normal tissue (TIS) were analyzed by relative quantification. The Ct value of each target gene was normalized to an arithmetic average of the Cts from three different housekeeping genes. The respective non-pathogenic tissue (TIS) served as each internal reference. Ratios were calculated by $r = 2^{-\Delta\Delta Ct}$, with ΔCt = Ct(target gene) – Ct(reference gene) and $\Delta\Delta Ct = \Delta Ct$(tumor sample) − Ct(control). Data of three experiments were taken for mean value composition (blue bars) and the standard deviation was calculated (black lined range). The error bars equal a 68 % confidence interval. Asterisks on top of the blue bars show significant differences in mRNA expression in the respective tumor tissue (CA) as compared to its matched-pair non-tumor tissue (TIS) (* = $p < 0.05$; ** = $p < 0.01$; *** = $p < 0.001$).

For the squamous cell carcinoma samples, the analyses of the qPCR data revealed that the mRNA levels of the reference genes showed strong up- or downregulation in the patient samples, which then lead to high correction factors during normalization of mRNA levels for the genes of interest. Therefore, normalization was also performed among the 24 target mRNAs (see section 2.2.5.4), which led to results that were more consistent across the tissue samples (see below). Including the three reference genes in these analyses illustrated a strong mRNA accumulation for all three reference genes COPS6 (Figure 13a), EMC7 (Figure 13b) and PSMB2 (Figure 13c) in squamous cell carcinoma from patients 1 and 2, while in the other two patients all three mRNA levels were reduced. In contrast, this expression pattern was not observed for the majority of G-patch protein mRNAs (see below), indicating that it did not reflect systematic differences between samples.

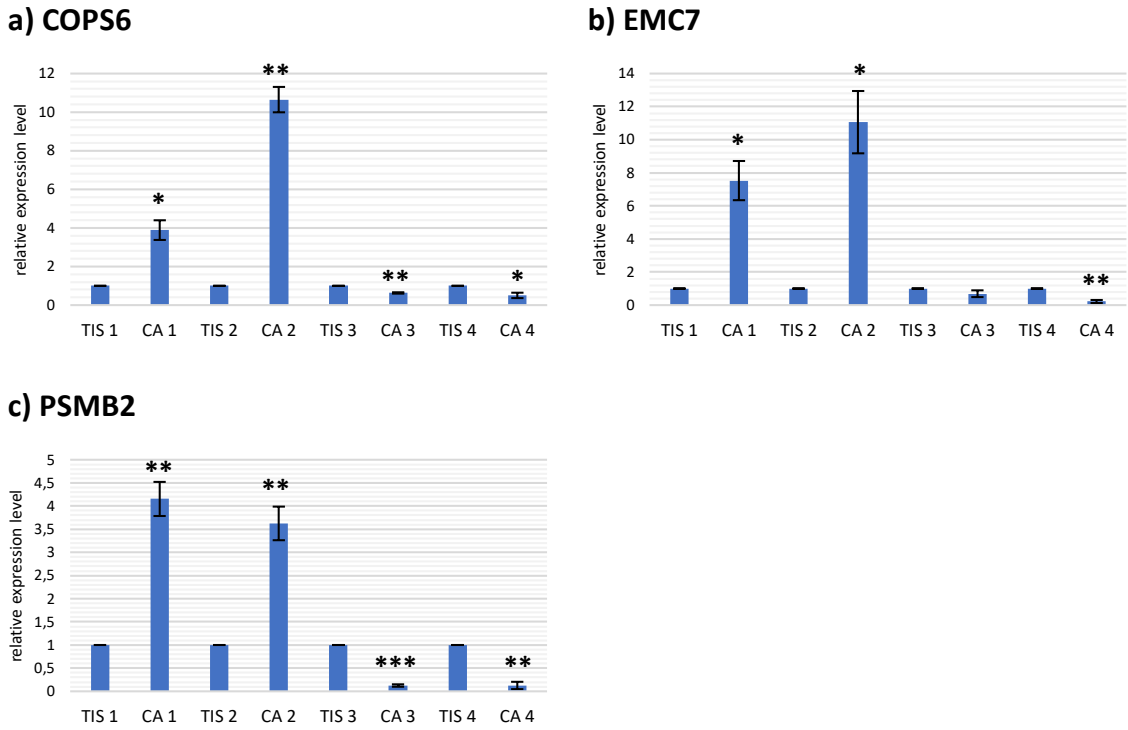

Figure 13: Reference gene mRNA expression levels in matched-pair squamous cell carcinoma tissue.qPCR assays were performed. Gene expression levels from four different squamous cell carcinoma tissue samples (CA) and their respective matched-pair normal tissue (TIS) were analyzed by relative quantification. The normalization was performed among 27 mRNAs, including 24 target mRNAs and the three reference genes COPS6, EMC7 and PSMB2. The respective non-pathogenic tissue (TIS) served as reference. Ratios were calculated by $r = 2^{-\Delta\Delta Ct}$, with ΔCt = Ct(Ct [tumor sample]/(mean Ct [SCC tumor samples]/mean Ct [SCC normal samples])) and ΔΔCt = ΔCt(tumor sample) − Ct(control). Data of three experiments were taken for mean value composition (blue bars) and the standard deviation was calculated (black lined range). The error bars equal a 68 % confidence interval. Asterisks on top of the blue bars show significant differences in mRNA expression in the respective tumor tissue (CA) as compared to its matched-pair non-tumor tissue (TIS) (* = $p < 0.05$; ** = $p < 0.01$; *** = $p < 0.001$).

Therefore, both normalization approaches, normalization to the three reference genes and internal normalization of G-patch protein and helicase data, were performed and the results of the calculations compared. Figure 14 and Figure 15 exemplarily show the results of both analyses for the mRNAs of the G-patch proteins AGGF1 and RBM5. For AGGF1 mRNA, normalization to the reference genes indicated a highly significant reduction of mRNA in tumor compared to healthy tissue for patients 1 and 2 ($M = 0.131$, $SD = 0.043$, $p < 0.001$ and $M = 0.246$, $SD = 0.089$, $p = 0.005$), while little change was observed in patient 3 and a strong accumulation was calculated for patient 4 ($M = 3.735$, $SD = 0.811$, $p = 0.028$) (Figure 14a). In the internal normalization over all G-patch proteins and helicases analyzed, no significant changes in AGGF1 mRNA levels were detected, besides a reduction in tumor of patient 3 ($M = 0.272$, $SD = 0.163$, $p = 0.016$) (Figure 15a).

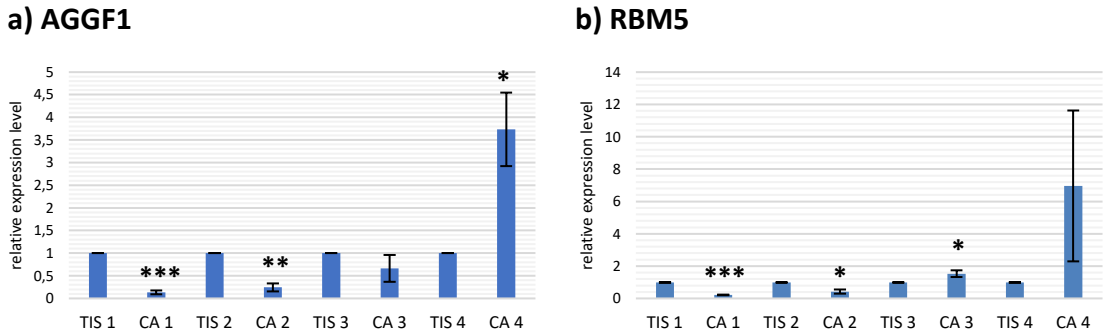

Figure 14: Normalization to the three reference genes − AGGF1 and RBM5 mRNA expression levels in matched-pair squamous cell carcinoma tissue. qPCR assays were performed. Gene expression levels from four different squamous cell carcinomas (CA) and their respective matched-pair normal tissue (TIS) were analyzed by relative quantification. The Ct value of each target gene was normalized to an arithmetic average of the Cts from three different housekeeping genes. The respective non-pathogenic tissue (TIS) served as each internal reference. Ratios were calculated by $r = 2^{-\Delta\Delta Ct}$, with ΔCt = Ct(target gene) – Ct(reference gene) and $\Delta\Delta Ct$ = ΔCt(tumor sample) − Ct(control). Data of three experiments were taken for mean value composition (blue bars) and the standard deviation was calculated (black lined range). The error bars equal a 68 % confidence interval. Asterisks on top of the blue bars show significant differences in mRNA expression in the respective tumor tissue (CA) as compared to its matched-pair non-tumor tissue (TIS) (* = $p < 0.05$; ** = $p < 0.01$; *** = $p < 0.001$).

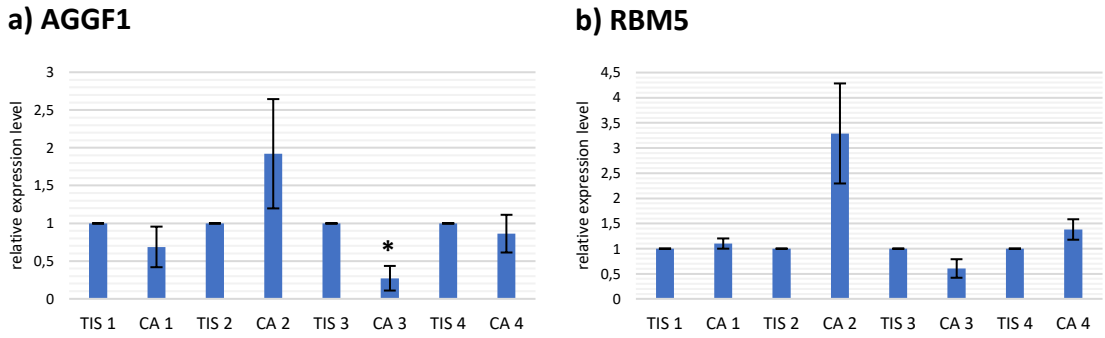

Figure 15: Internal normalization − AGGF1 and RBM5 mRNA expression levels in matched-pair squamous cell carcinoma tissue. qPCR assays were performed. Gene expression levels from four different squamous cell carcinoma tissue samples (CA) and their respective matched-pair normal tissue (TIS) were analyzed by relative quantification. The normalization was performed among the 24 target mRNAs. The respective non-pathogenic tissue (TIS) served as each internal reference. Ratios were calculated by $r = 2^{-\Delta\Delta Ct}$, with ΔCt = Ct(Ct [tumor sample]/(mean Ct [SCC tumor samples]/mean Ct [SCC normal samples])) and $\Delta\Delta Ct$ = ΔCt(tumor sample) − Ct(control). Data of three experiments were taken for mean value composition (blue bars) and the standard deviation was calculated (black lined range). The error bars equal a 68 % confidence interval. Asterisks on top of the blue bars show significant differences in mRNA expression in the respective tumor tissue (CA) as compared to its matched-pair non-tumor tissue (TIS) (* = $p < 0.05$; ** = $p < 0.01$; *** = $p < 0.001$).

In case of RBM5, a significant reduction in mRNA levels was again calculated for the tumors of patients 1 and 2 ($M = 0.217$, $SD = 0.017$, $p < 0.001$ and $M = 0.427$, $SD = 0.136$, $p = 0.018$), while patient 3 showed a small but significant increase ($M = 1.533$, $SD = 0.215$, $p = 0.050$) and patient 4 a strong but not significant increase when normalized to the reference genes ($M = 6.962$, $SD = 4.669$, $p = 0.158$ for sample 4) (Figure 14b). When RBM5 data were analyzed in comparison to the other G-patch protein mRNAs, an increase in the tumor of patient 2 was observed, but overall, no significant change was detected (Figure 15b). Together, these analyzes indicate that normalization of the G-patch protein and RNA helicase expression data to the three reference samples lead to the uniform expression pattern (see Figure 14a and Figure 14b, Supplemental figure 1 and

Supplemental table 8) and that the calculated values do not necessarily represent genuine expression levels.

Further analyses of the squamous cell carcinoma samples were therefore performed by internal normalization among the 24 G-patch protein and RNA helicase mRNAs. Figure 16 and Figure 17 show mean ratios based on the average of the Cts from three independent experiments with their respective standard deviation for each target gene (see also Supplemental table 7). Asterisks on top of the blue bars again indicate significant differences in mRNA expression in the respective tumor sample as compared to its matched-pair normal tissue, while α was set to 0.05, 0.01 and 0.001 for all analyzed variables.

Several analyzed target mRNA levels in squamous cell carcinoma matched-pair samples were specifically increased in cancer tissue 2 as compared to their matched-pair normal tissue (Figure 16b, Figure 16c, Figure 16j, Figure 16k, Figure 16l, Figure 16m, Figure 16o, Figure 16p, Figure 16q, Figure 16s, Figure 16t), while some factors showed a reduction of mRNA levels in cancer sample 3 (Figure 16b, Figure 16d, Figure 16f, Figure 16g, Figure 16h, Figure 16j, Figure 16k, Figure 16o, Figure 16q, Figure 16r, Figure 16s). Only for mRNA levels of GPKOW (Figure 16j), RBM6 (Figure 16m), SON (Figure 16p), TFIP11 (Figure 16s) and ZGPAT (Figure 16t), similar patterns were observed, however, most of these changes were not statistically significant.

The analyses of the results for the individual genes of interest revealed that no significant changes in mRNA levels were observed for CHERP (Figure 16a) and GPATCH2 (Figure 16c). For CMTR1, a significant increase in cancer 2 ($M = 11.880$, $SD = 4.276$, $p = 0.048$) and a decrease in cancer sample 3 were observed ($M = 0.503$, $SD = 0.119$, $p = 0.019$), while GPANK1 mRNA levels only increased in cancer sample 2 ($M = 13.306$, $SD = 4.699$, $p = 0.045$) (Figure 16b, Figure 16c).

Cancer sample 1 and 3 significantly showed low expression of GPATCH1 (M = 0.497, SD = 0.043, p = 0.002 and M = 0.346, SD = 0.055, p = 0.002), while GPATCH3 (M =0.397, SD = 0.067, p = 0.004) and GPATCH4 (M = 0.176, SD = 0.083, p = 0.003) only showed a reduction in cancer sample 3 as compared to their matched-pair normal tissue (Figure 16d, Figure 16f, Figure 16g).

a) CHERP

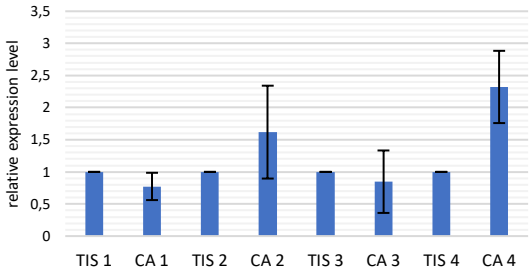

b) CMTR1

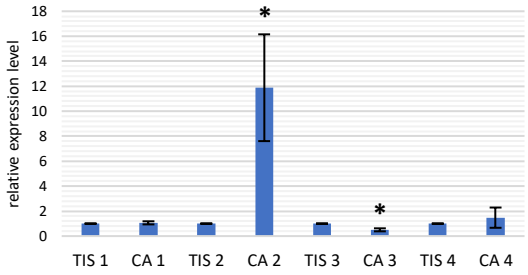

c) GPANK1

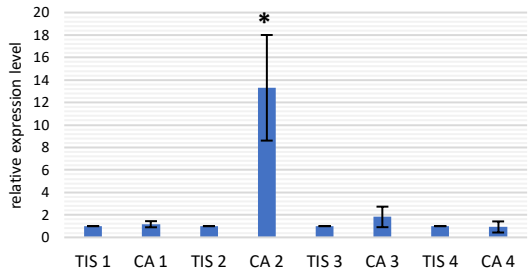

d) GPATCH1

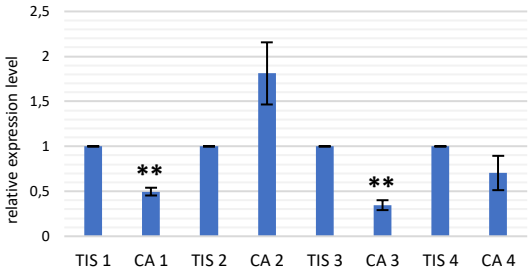

e) GPATCH2

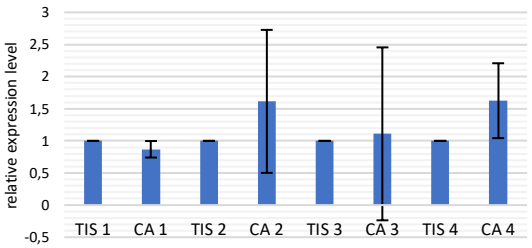

f) GPATCH3

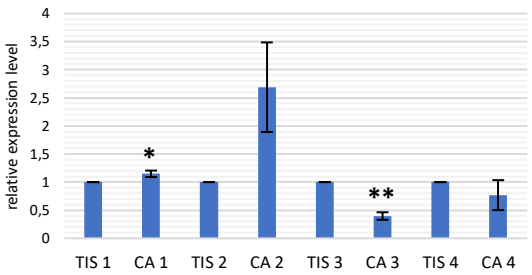

g) GPATCH4

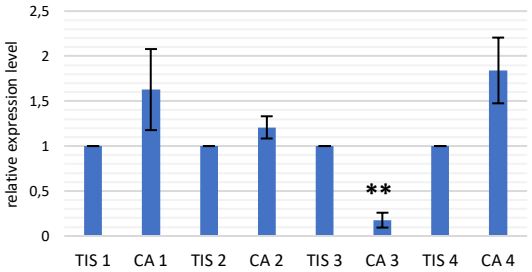

h) GPATCH8

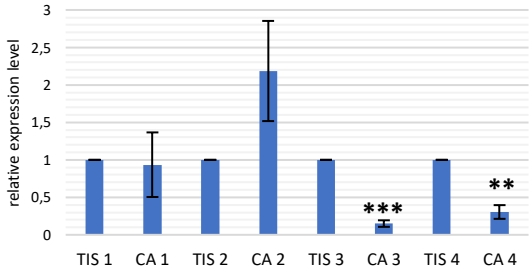

i) GPATCH11

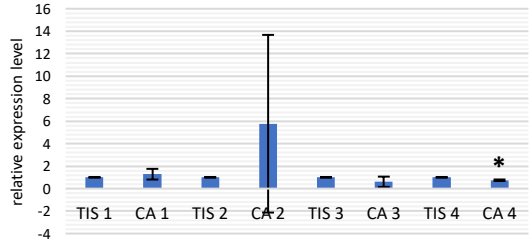

j) GPKOW

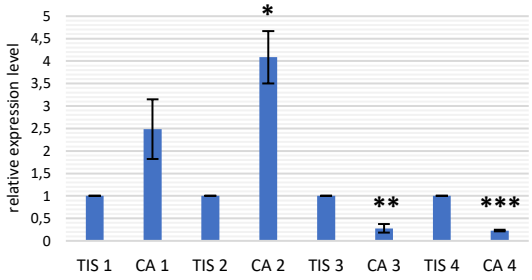

k) NKRF

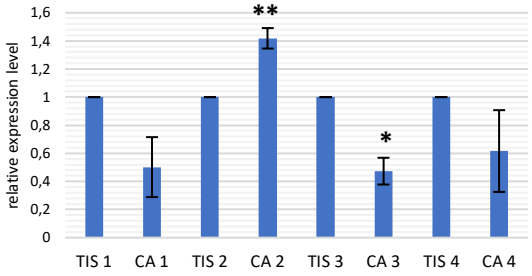

l) PINX1

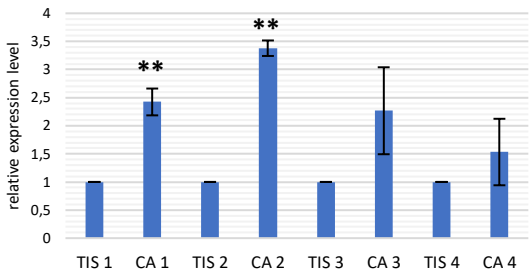

m) RBM6

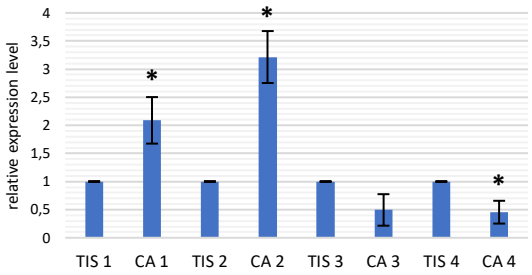

n) RBM10

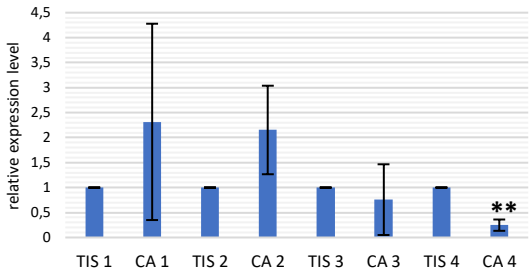

o) RBM17

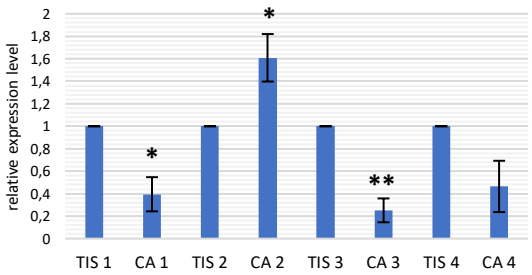

p) SON

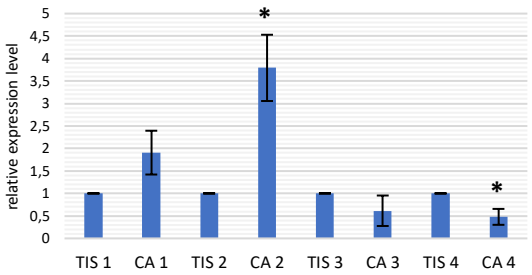

q) SUGP1

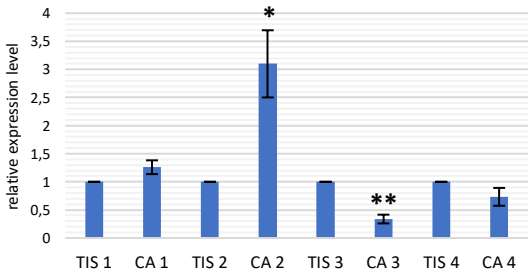

r) SUGP2

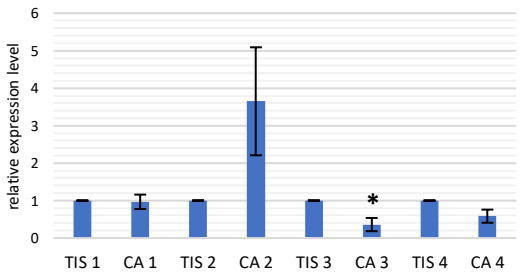

s) TFIP11

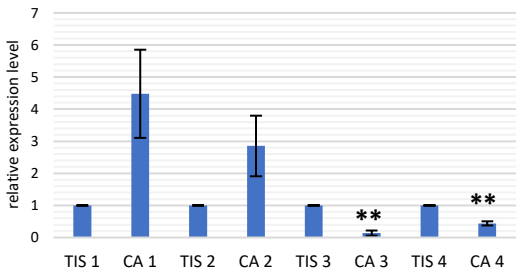

t) ZGPAT

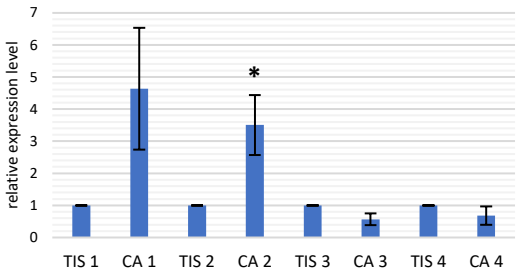

Figure 16: G-patch protein mRNA expression levels in matched-pair squamous cell carcinoma tissue samples. qPCR assays were performed. Gene expression levels from four different squamous cell carcinoma tissue samples (CA) and their respective matched-pair normal tissue (TIS) were analyzed by relative quantification. The Ct value of each target gene was normalized to an arithmetic average of the Cts from all analyzed target genes. The respective non-pathogenic tissue (TIS) served as each internal reference. Ratios were calculated by $r = 2^{-\Delta\Delta Ct}$, with ΔCt = Ct(Ct [tumor sample]/(mean Ct [SCC tumor samples]/mean Ct [SCC normal samples])) and $\Delta\Delta Ct = \Delta Ct$(tumor sample) − Ct(control). Data of three experiments were taken for mean value composition (blue bars) and the standard deviation was calculated (black lines range). The error bars equal a 68 % confidence interval. Asterisks on top of the blue bars show significant differences in mRNA expression in the respective tumor tissue (CA) as compared to its matched-pair non-tumor tissue (TIS) (* = $p < 0.05$; ** = $p < 0.01$; *** = $p < 0.001$).

GPATCH8 mRNA levels decreased in comparison to the normal tissue in cancer sample 3 ($M = 0.150$, $SD = 0.044$, $p < 0.001$) and sample 4 ($M = 0.305$, $SD = 0.092$, $p = 0.006$) (Figure 16h), while GPATCH11 mRNA only showed a significant reduction in cancer sample 4 ($M = 0.743$, $SD = 0.069$, $p = 0.023$) (Figure 16i).

For GPKOW ($M = 4.086$, $SD = 0.582$, $p = 0.012$) and NKRF ($M = 1.419$, $SD = 0.073$, $p = 0.010$) a significant increase in cancer sample 2 was observed, while for GPKOW samples 3 and 4 showed strongly reduced mRNA levels ($M = 0.280$, $SD = 0.098$, $p = 0.006$ and $M = 0.230$, $SD = 0.020$, $p < 0.001$), and for NKRF a significant reduction in sample 3 occurred ($M = 0.473$, $SD = 0.095$, $p = 0.011$) (Figure 16j, Figure 16k).

Interestingly, PINX1 showed an upregulation of its mRNA level in all squamous cell carcinoma samples, even though this was only statistically significant for samples 1 and 2 ($M = 2.423$, $SD = 0.238$, $p = 0.009$ and $M = 3.379$, $SD = 0.138$, $p = 0.001$). Similar to PINX1, RBM6 relative mRNA expression levels in cancer sample 1 and 2 were significantly upregulated ($M = 2.089$, $SD = 0.414$, $p = 0.045$ and $M = 3.215$, $SD = 0.462$, $p = 0.014$) in comparison to the normal tissue. However, RBM6 was significantly reduced in sample 4 ($M = 455$, $SD = 0.203$, $p = 0.043$) (Figure 16l, Figure 16m)

RBM10 ($M = 0.247$, $SD = 0.114$, $p = 0.008$) and SON ($M = 0.479$, $SD = 0.177$, $p = 0.036$) showed mRNA downregulation in sample 4, while only for SON a significant upregulation in sample 2 was observed ($M = 3.792$, $SD = 0.737$, $p = 0.023$) (Figure 16nFigure 16p).

For cancer sample 3, RBM17 ($M = 0.252$, $SD = 0.106$, $p < 0.007$), SUGP1 ($M = 0.338$, $SD = 0.078$, $p < 0.005$) and SUGP2 ($M = 0.359$, $SD = 0.176$, $p = 0.024$) mRNA ratios were lowered, while only RBM17 showed a significant reduction in sample 1 ($M = 0.395$, $SD = 0.152$, $p = 0.020$). And RBM17 ($M = 1.609$, $SD = 0.211$, $p = 0.038$) and SUGP1 ($M = 3.099$, $SD = 0.598$, $p = 0.026$) mRNA showed a statistically significant increase in

sample 2 as compared to the matched-pair normal tissue (Figure 16o, Figure 16q, Figure 16r).

The mRNA levels of both TFIP11 and ZGPAT showed patterns similar to the reference genes. However, only the upregulation in cancer sample 1 ($M = 4.479$, $SD = 1.370$, $p = 0.048$) and the downregulation in samples 3 ($M = 0.143$, $SD = 0.078$, $p = 0.003$) and 4 ($M = 0.438$, $SD = 0.066$, $p = 0.005$) were significant for TFIP11 as well as the upregulation in cancer sample 2 ($M = 3.503$, $SD = 0.931$, $p = 0.043$) for ZGPAT (Figure 16s, Figure 16t).

RNA helicase relative expression levels in squamous cell carcinoma were presented similarly as to the G-patch protein tendencies outlined in the previous paragraphs in this section 3.4. While DHX15 mRNA showed an upregulation in samples 1 ($M = 2.885$, $SD = 0.728$, $p = 0.046$) and 2 ($M = 3.435$, $SD = 0.430$, $p = 0.010$) and a downregulation in samples 3 ($M = 0.148$, $SD = 0.025$, $p < 0.001$) and 4 ($M = 0.539$, $SD = 0.131$, $p = 0.026$), DHX35 mRNA levels were significantly increased in cancer sample 2 ($M = 3.778$, $SD = 0.733$, $p = 0.022$) and reduced in sample 3 ($M = 0.192$, $SD = 0.063$, $p = 0.002$) in comparison to their respective normal tissue (Figure 17a and Figure 17b).

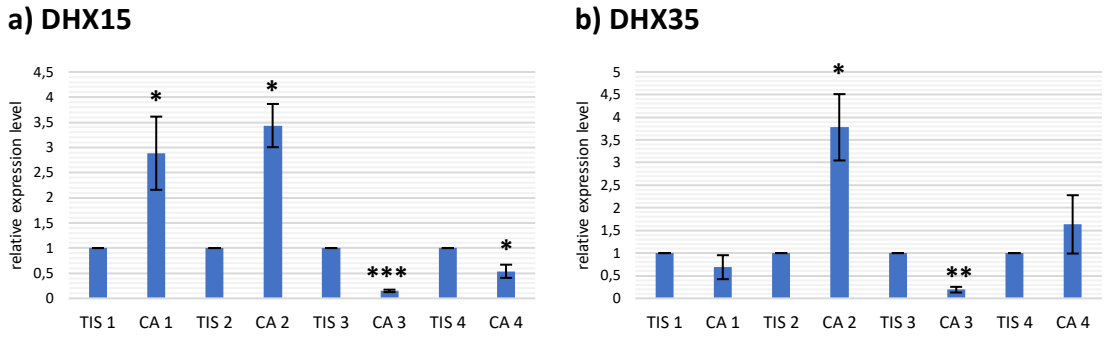

Figure 17: RNA helicase mRNA expression levels in matched-pair squamous cell carcinoma tissue samples. qPCR assays were performed. Gene expression levels from four different squamous cell carcinoma tissue samples (CA) and their respective matched-pair normal tissue (TIS) were analyzed by relative quantification. The Ct value of each target gene was normalized to an arithmetic average of the Cts from all analyzed target genes. The respective non-pathogenic tissue (TIS) served as each internal reference. Ratios were calculated by $r = 2^{-\Delta\Delta Ct}$, with $\Delta Ct = Ct(Ct\ [tumor\ sample]/(mean\ Ct\ [SCC\ tumor\ samples]/mean\ Ct\ [SCC\ normal\ samples]))$ and $\Delta\Delta Ct = \Delta Ct(tumor\ sample) - Ct(control)$. Data of three experiments were taken for mean value composition (blue bars) and the standard deviation was calculated (black lines range). The error bars equal a 68 % confidence interval. Asterisks on top of the blue bars show significant differences in mRNA expression in the respective tumor tissue (CA) as compared to its matched-pair non-tumor tissue (TIS) (* = $p < 0.05$; ** = $p < 0.01$; *** = $p < 0.001$).

In summary, for most of the G-patch proteins relative expression levels highly varied between the three provided independent fibromyxosarcoma tissues. The data were slightly more consistent for the squamous cell carcinoma tissues, especially after internal normalization within the mRNA expression data for the 24 genes of interest. However, overall, multiple examples of high variation in the expression of specific genes between samples from different patients were observed, suggesting a complex picture of gene expression regulation or sample diversity.

4. Discussion

RNA helicases have been functionally implicated in many cellular pathways, especially the different processes of gene expression. They have been found to be indispensable for the metabolism of a multitude of structured RNAs and the biogenesis and function of various RNA-protein complexes (Kapranov et al. 2007; Jarmoskaite and Russell 2014; Jankowsky and Bowers 2006). Many RNA helicases are multifunctional and influenced by specific cofactors, which regulate helicase activity and also the distribution within the cell (Bourgeois et al. 2016; Linder and Jankowsky 2011; Bohnsack et al. 2021; Sloan and Bohnsack 2018). It has been shown that changes in the levels of the different cofactors can result in changes in the distribution and function of such multifunctional helicases (Heininger et al. 2016). Thus, changes in gene expression programs, for example in cancer, can affect the helicases themselves and their regulating cofactors and could then further impact proteins with important roles as tumor suppressors or oncogenes (Sloan and Bohnsack 2018). This model was the starting point of this thesis. G-patch protein mRNA expression levels had been analyzed in high-throughput studies in particular cell types, but they had not been compared across different cell types or correlated with protein levels. The present study aimed at identifying differences in expression levels of the human G-patch proteins and G-patch protein-interacting helicases in different cancer cell lines and in matched-pair samples from patients with fibromyxosarcoma in limbs or squamous cell carcinoma in the oral cavity.

4.1. RNA helicase and G-patch protein expression in human cancer cell lines

The expression of the 22 human G-patch proteins and the RNA helicases DHX15 and DHX35 was analyzed systematically in the human cancer cell lines HeLa (cervical cancer), HCT116 wildtype p53 as well as a HCT116 p53 deletion cell line (colorectal carcinoma), A549 (adenocarcinomic alveolar basal epithelial cells), U2OS (osteosarcoma), CaCo-2 (colon carcinoma) and MCF-7 (breast cancer). mRNA levels were quantified by qPCR, normalized to the reference genes COPS6, EMC7 and PSMB2, and mRNA levels compared to their expression in HEK293 cells. For the G-patch proteins CMTR1, GPATCH2, GPATCH4, GPATCH11, GPKOW, NKRF, PINX1, RBM6 and the RNA helicases DHX15 and DHX16, for which specific antibodies were available, the protein levels were investigated by western blotting.

While in most cases the G-patch protein and RNA helicase mRNA and protein levels did not change significantly, individual changes were observed, as described in the results section of this thesis (see section 3.2 and 3.3).

For GPATCH2, its mRNA levels showed a strong and significant increase in MCF-7 cells (Figure 8f), which was also supported by an increase – even though not statistically significant due to large error bars – in protein levels in this cell line (Figure 10b). This is in line with previous findings implicating GPATCH2 with breast cancer. It might even be a key player in tumor growth, as GPATCH2 depletion resulted in downregulated proliferation rates in breast cancer cells (see section 1.3) (Lin et al. 2009). Thus, our findings once more emphasize the compelling potential of new treatment development in breast cancer therapy. Moreover, GPATCH2 has been implicated in colon cancer liver metastasis, where an upregulation had been detected previously (Liu et al. 2018). However, our study's GPATCH2 mRNA analysis in colon cancer cell lines HCT116 -/- p53 and CaCo-2 did not show an increase. As cancer cell lines might not reflect the heterogeneity primary malignancies naturally feature and are lacking the environmental conditions of *in vivo* tumors (Vargo-Gogola and Rosen 2007), they are differing from colon cancer liver metastasis conditions. Only for the HCT116 wildtype cells a slight but significant increase could be described (Figure 8f). However, as opposed to the mRNA levels, GPATCH2 protein expression in HCT16 -/- p53 and CaCo-2 cells was significantly upregulated, while the HCT116 wildtype p53 cells showed a minor decrease (Figure 10b). This might be due to technical reasons or a possible divergence in mRNA and the respective protein expression levels under certain circumstances.

For the G-patch protein PINX1, with the exception of HCT116 cells, mRNA levels were presented lower in the other cell lines analyzed, as compared to HEK293 cells, especially for CaCo-2 and MCF-7 cells (Figure 8m). This is mirrored by protein expression levels with especially CaCo-2 cells showing a significantly lower expression of PINX1 than HEK293 cells (Figure 10g). PINX1 plays an important role in telomere length preservation and stability of chromosomes (Zhou and Lu 2001; Yoo et al. 2014). It has been described as a haploinsufficient tumor suppressor required for chromosome stability, and was previously shown to be reduced in its expression in breast cancer (Zhou et al. 2011), which is further supported by the data obtained here. This gene locus has previously been identified as being among the most frequent loss of heterozygosity regions in epithelial tumors like breast, liver, colon and lung cancer (Emi et al. 1992; Yokota et al. 1999). The loss of heterozygosity thus caused telomerase activation and chromosome instability (Zhou et al. 2011). PINX1 expression has been found downregulated in several human cancers and might even be involved in tumorigenesis (Cai et al. 2010; Zhou et al. 2011), while the exact mechanisms still

have to be identified. Decreased PINX1 levels have also been associated with poor prognoses for multiple tumor types (Cai et al. 2010; Feng et al. 2017; Qian et al. 2016). However, PINX1 regulation might also depend on the specific cancer type, as different extends of up- or downregulation in its expression were observed in different forms of cancer (Li et al. 2014; Qian et al. 2013; Tian et al. 2014; Bai et al. 2015).

Another G-patch protein that showed strong alterations in its expression level is GPATCH4. Here, mRNA levels were found to be lower in all other cell lines as compared to HEK293, with the lowest expression in CaCo-2 and MCF-7 cells (Figure 8h). A reduced expression in relation to HEK293 cells was also generally observed on the protein level, as analyzed by western blotting (Figure 10c). Interestingly however, high protein levels of this G-patch protein were observed in A549 cells (Figure 10c), indicating that the high expression of this protein might be regulated at the translation level. Hirawake-Mogi et al. (2021) implicated GPATCH4 in cell growth regulation and nucleolar structure. They found the G-patch protein, which has previously been identified as a component of the pre-ribosomes, localized to the nucleolus as well as to the site of RNP processing and maturation. Knockdown of GPATCH4 did not result in significant changes in pre-rRNA processing, but did have a negative effect on the number of nucleolar components and cell growth (Hirawake-Mogi et al. 2021). As a feature of tumors is the uncontrolled division, assuming the findings of (Hirawake-Mogi et al. 2021) to be generally valid, one would expect the GPATCH4 levels to be increased in cancer cells as compared to non-tumor cells, which was only the case for A549 protein levels in this study (Figure 10c).

Interestingly, RBM5 mRNA levels showed a significant increase, especially in breast cancer cell line MCF-7 (Figure 8n), which underlines previous findings of RBM5 upregulation in breast cancer (Oh et al. 1999). RBM5 is involved in alternative splicing of genes that are associated with apoptosis (Mourtada-Maarabouni et al. 2006; Bonnal et al. 2008; Rintala-Maki and Sutherland 2004). Upregulation of RBM5 RNA was also recorded in 5-fluorouracil-resistant colorectal and breast cancer cells as well as in breast and ovarian cancer cells (Wang et al. 2004; Oh et al. 1999; Rintala-Maki et al. 2007). Additionally, a protein level increase was observed in breast tumor by Rintala-Maki et al. (2007). However, RBM5 has also been proposed as a tumor suppressor (Oh et al. 2006). A decrease of the RBM5 level has previously been found in multiple tumors (Oh et al. 2002; Edamatsu et al. 2000; Zhao et al. 2012) and has been implicated in enhanced metastasis (Ramaswamy et al. 2003), while its upregulation led to impeded growth and apoptosis initiation (Oh et al. 2002; Oh et al. 2006; Mourtada-Maarabouni et al. 2003). Its gene locus was identified to be located within the tumor suppressor region 3p21.3, which is often affected by loss of heterozygosity or deletion

in lung cancer and also other tumor entities (Angeloni 2007). Together, these data indicate different expression levels of RBM5 in various tumors, while the data presented here for MCF-7 cells are well in line with previous findings of its upregulation in breast cancer.

Beside the wildtype HCT116 cell line, a derivative cell line, in which the expression of the tumor suppressor p53 is abolished, was included in the analyses. p53 is a ubiquitously occurring tumor suppressor and key player of the cell's metabolic regulation, cell proliferation and death (Kruiswijk et al. 2015). A hallmark of cancer is the activation of oncogenes and/or repression of tumor suppressors (Pavlova and Thompson 2016). Thus, p53 indeed is the most commonly mutated gene in human cancers. Most of these mutations are loss of function mutations (Muller and Vousden 2013; Hollstein et al. 1991). Correspondingly, knockdown of p53 in mice for example resulted in spontaneous tumor development (Donehower et al. 1992), while mutant p53 cells showed restored expression of p53-responsive genes and growth inhibition by the help of an adaptor protein that reactivates mutant p53 (Roth et al. 2003). However, G-patch protein and RNA helicase mRNA levels in the HCT116 wildtype and the HCT116 -/- p53 cell lines were usually either unaffected or both up- and downregulated, and only in few cases slight differences between the expression of the genes of interest in the two cell lines were observed (Figure 8 and Figure 9). At protein level, only for GPATCH2 a lower expression in HCT116 wildtype p53 versus a slight increase in expression in the HCT116 -/- p53 cell line was observed, while for all other factors no significant differences of their expression in the two cell lines occurred (Figure 10). This indicates that in HCT116 cells under the conditions tested, the presence of the tumor suppressor p53 generally does not strongly affect G-patch protein expression.

Taken together, findings of this study revealed that different tumor cell lines expressed G-patch protein and RNA helicase mRNAs as well as proteins at variable levels. While some appeared to be similarly expressed across the range of cell lines tested, others were observed to significantly diverge in their expression levels. For several of the examples discussed above, changes in expression of the factors analyzed here are well in line with previous findings. Other significant changes in expression levels detected here provide the basis for future functional analyses of the proteins in the corresponding cell lines and tumors.

4.2. RNA helicase and G-patch protein expression in tissue samples

Besides the analysis of G-patch protein and RNA helicase mRNA and protein levels in different cancer cell lines, this work also analyzed changes in their expression in matched-pair samples from patients that had developed fibromyxosarcoma in limbs or squamous cell

carcinoma in the oral cavity. Tissue samples were obtained from the CEPA Biobank (Newcastle upon Tyne Hospitals NHS Trust, UK) and total RNA was extracted followed by qPCR to analyze the mRNA levels of the target genes.

For the samples from fibromyxosarcoma patients analyzed here, the amount of RNA extracted from the material originally obtained from the CEPA Biobank turned out to be limiting. This restricted the number of G-patch protein mRNAs that could be analyzed to GPATCH1, GPATCH3, GPATCH4, NKRF, RBM5, SUGP1, SUGP2, TFIP11 and ZGPAT (Figure 11) as well as the RNA helicases DHX15 and DHX35 (Figure 12). While most of the data showed no consistent changes among the samples from different patients, both the mRNAs of ZGPAT and DHX15 showed a small and in most cases non-significant reduction in the tumor samples from all patients. While both RNA helicases DHX15 and DHX35 have previously been shown to be part of spliceosomal complexes, DHX15 was found involved in splicing during spliceosome disassembly and splice-site proofreading, and it was also implicated in ribosome biogenesis (Arenas and Abelson 1997; Koodathingal et al. 2010; Bohnsack et al. 2009). Decreased DEAH-box helicase DHX15 levels have previously been reported in human glioma cell lines (Ito et al. 2017). DHX15 was observed to be upregulated in several cancers (Xie et al. 2019; Jing et al. 2018; Nakagawa et al. 2006; Albrecht et al. 2004; Pan et al. 2017), while conversely, DHX15 depletion resulted in enhanced proliferation of mouse astrocytes, and DHX15-transduced glioma cell lines showed impeded growth, thus suggesting DHX15 to act as a putative tumor suppressor (Ito et al. 2017). Similarly, it was shown that ZGPAT is capable of suppressing tumorigenesis and tumor growth in breast cancer via the inhibition of the oncogene EGFR, while ZGPAT depletion resulted in tumor proliferation. Consequently, ZGPAT was also proposed as a putative tumor suppressor (Li et al. 2009; Ordway et al. 2006).

In the case of the samples from squamous cell carcinoma patients, the amount of RNA obtained allowed analyses of the mRNA levels for all 22 G-patch proteins and the RNA helicases DHX15 and DHX35. Importantly, analysis of the results obtained for the three reference genes revealed that their mRNA levels showed strong differences between the samples from the different squamous cell carcinoma patients (Figure 13), while the results for the G-patch protein mRNAs were more consistent. It is currently unknown why the three reference genes, which usually do not change much in their expression in various tissues and conditions, would show differences in their expression specifically in squamous cell carcinoma. However, these observations ruled out the possibility that the data obtained for the G-patch protein mRNAs could be normalized to those of the reference genes, as stronger systematic errors would be introduced. As data were available for 22 G-patch

protein and two RNA helicase mRNAs, this large number of individual mRNAs allowed an internal normalization within this group of genes, which is based on the assumption that not all different mRNAs are uniformly up- or downregulated in the samples from cancer patients. Based on this normalization, more consistent data were obtained and only few genes showed strongly divergent effects between the different patients. In contrast to the normalization using the three reference genes, the levels of multiple G-patch protein mRNAs, including CHERP, GPANK1, GPATCH2 and RBM5, were calculated not to change much in cancer samples, besides a general increase in cancer sample 2 (Figure 16a, Figure 16c, Figure 16e and Figure 15b). Interestingly, the mRNAs of AGGF1, GPATCH1, GPATCH8, NKRF, RBM17 and SUGP2 showed a general downregulation (Figure 15a and Figure 16d, Figure 16h, Figure 16k, Figure 16o, Figure 16r), while the level of the PINX1 mRNA was increased in all cancer samples, as compared to the matched-pair tissue (Figure 16l).

Among the G-patch proteins showing a reduction in their mRNA levels in the cancer samples, AGGF1, which is mutated in Klippel-Trenaunay syndrome patients (Tian et al. 2004; Hu et al. 2008), has previously been linked to a variety of cancers. Modified expression levels have been detected in multiple types of cancer, including hepatocellular, gastric, serous ovarian and colorectal cancer, and were associated with cancer progression and matastasis (Yao et al. 2019; Zhao et al. 2019; Li et al. 2019; Zhang et al. 2019). Remarkably, Zhang et al. (2019) found that AGGF1 protein expression in colorectal cancer increased as compared to the respective normal tissue, while the mRNA level in normal and matched-pair malignant tissue did not show any significant difference. They assumed this might be due to malignant processes mainly taking place on the protein level. Strikingly, AGGF1 has recently been proposed as a tumor suppressor by directly and indirectly enhancing p53 function and can thereby inhibit tumor growth (Si et al. 2021). In this study, AGGF1 mRNA cancer cell line and tumor sample levels generally showed a decrease or invariant expression as compared to HEK293 or matched-pair tissue expression, respectively (Figure 15a). These observations are in line with the suggestion of Zhang et al. (2019) that AGGF1 upregulation can only be observed on the protein level. This could be consolidated by future analyses that compare protein levels in matched-pair samples from patients.

GPATCH1 was recently shown to specifically interact with the RNA helicase DHX35 and to copurify with spliceosomal complexes (Sales-Lee et al. 2021). However, little is known about its molecular function, and a potential role in pre-mRNA splicing will need to be consolidated. So far, GPATCH1 has not been directly implicated in tumorigenesis. Similarly, a missense mutation in a highly conserved region of the GPATCH8 gene was associated to

juvenile-onset hyperuricemia (Kaneko et al. 2011), but other than this, GPATCH8 has also not been linked to diseases and its function has so far remained elusive.

In contrast to the less characterized G-patch proteins AGGF1, GPATCH1 and GPATCH8, the NF-kappa-B-repressing factor NKRF is a well-known protein involved in ribosome biogenesis and as a regulator of the transcription factor NF-κB. NKRF is required for correct pre-rRNA processing and fragment turnover, inhibits abnormal rRNA precursor formation and enhances the degradation of discarded fragments (Coccia et al. 2017). Increased ribosome biogenesis has been linked to cell proliferation and is therefore associated with tumorigenesis. The upregulation is mediated by multiple tumor suppressors or oncogenes like c-MYC and RAS (Stumpf and Ruggero 2011; Dai et al. 2012). NKRF is also an antagonist of NF-κB, a transcription factor whose activation can be triggered by inflammation, carcinogens and other stress conditions, including bacterial and viral infection. Thus, it coordinates the expression of a number of inflammatory cytokines, chemokines, immunoreceptors and cell adhesion molecules (Pahl 1999). This emphasizes the importance of NKRF in immune system stability, which can be dysregulated upon malignant invasion. These and other findings imply that tumor cells might possess low NKRF levels in order to result in an increase in NF-κB expression and thus in tumor proliferation. This is in line with the data presented here, where NKRF expression is downregulated in squamous cell carcinoma samples of three out of four patients (Figure 16k).

RBM17 represents a component of spliceosomal complexes and has been copurified with the U2 snRNP (De Maio et al. 2018), suggesting that variations in RBM17 expression could result in splicing variations and might therefore be linked to dysregulation of gene expression (Fu and Ares 2014). It was further identified as an interaction partner of U2SURP and CHERP, and together, these proteins were suggested to synergistically regulate the expression of a set of transcripts (De Maio et al. 2018). The role of RBM17 in tumorigenesis is controversially discussed and might depend on the type of cancer investigated. While RBM17 had been found overexpressed in several cancer tissues like breast, bladder, ovarian, colon, prostate and hepatocellular carcinomas and was implicated in cell migration and invasion in ovarian cancer (Liu et al. 2013; Sampath et al. 2003; Li et al. 2020), overexpression of RBM17 was also shown to restrain cell proliferation and was suggested to be involved in DNA repair (Al-Ayoubi et al. 2012; Chaouki and Salz 2006). Interestingly, in this study, a partly significant reduction of RBM17 mRNA was observed in squamous cell carcinoma samples of three out of four patients as compared to their normal tissues (Figure 16o). Here, CHERP mRNA level was not co-regulated with that of RBM17 in the patient samples (Figure 16a and Figure 16o). However, future investigations should also analyze protein

levels for possible changes of these two factors, as De Maio et al. (2018) proposed post-transcriptional dependencies from one another rather than on the mRNA level.

SUGP2, also known as SFRS14, is also involved in pre-mRNA splicing (Sampson and Hewitt 2003) and has recently been shown to interact with the multifunctional nucleoporin Tpr. Similar to Tpr, depletion of SUGP2 was reported to cause transcription-dependent replication stress, DNA breaks, and genomic instability (Kosar et al. 2021). As the cell's ability to prevent genotoxic stress is fundamental for cellular function, the lack of this ability in turn leads to genomic instability and pathologies, such as developmental defects, neurodegeneration, immunodeficiency, premature aging, and cancer (Jackson and Bartek 2009). The observation of a downregulation of SUGP2 mRNA levels in squamous cell carcinoma (Figure 16r) is in line with recent findings of Kosar and colleagues, who associated SUGP2 depletion with genomic instability, which again is a hallmark of cancer (Kosar et al. 2021). It will be interesting to complement these analyses by studying protein levels of SUGP2 in these cancers and by analyzing the effects of SUGP2 depletion on tumorigenesis.

In contrast to the factors discussed previously, mRNA levels of PINX1 show a systematic upregulation in squamous cell carcinoma samples from all patients analyzed in this study (Figure 16l). While several types of cancer have previously been reported to show reduced levels of this G-patch protein (Qian et al. 2016; Zhou et al. 2011; Cai et al. 2010; Feng et al. 2017), other studies also reported opposing effects (Qian et al. 2013; Tian et al. 2014; Bai et al. 2015). Just recently, PINX1 has been proposed to exhibit oncogenic functions in prostate cancer, as it was said to enhance proliferation and migration of malignant cells and to act as a co-activator of the androgen receptor, which itself holds a key position in cancer evolution (Flores-Ramírez et al. 2021). Another study found high PINX1 expression levels in patients with papillary thyroid carcinoma (Kang et al. 2018). This raises the question of whether the role of PINX1 in tumor growth is more complex and its functions more diverse than it has been thought so far, leading to the proposal of tumor entity specificity (Li et al. 2016) and indicating the requirement for more detailed investigation and the potential for other modes of regulation.

Taken together, the limited amount of material especially for the patient cancer samples restricted the number of G-patch protein mRNAs that could be analyzed for the fibromyxosarcoma samples and the number of repetitions that could be performed for the squamous cell carcinoma samples, especially in cases where divergent results had been obtained. Some of the data showed significant variations between different patients, which could be due to biological differences or unequal treatment of samples, for example during

sample collection for pathology or deposition in the database. Overall, however, multiple examples of specific up- or downregulation of expression of mRNAs analyzed here could be observed. Many of them could be correlated with independent reports from other researchers on up- or downregulation of the specific factors in other cancer types. However, this study also highlights several significant changes in gene expression of G-patch proteins in fibromyxosarcoma and squamous cell carcinoma, which were not previously reported and can be further investigated in future studies.

4.3. Conclusions and perspectives

Superfamily 2 RNA helicases have been found to be indispensable for RNA and RNP metabolism and play key roles in all major gene expression processes, which in turn determine the cellular structure and functions. These proteins share sequence similarities in their conserved domains and often possess ancillary regions that can have an influence on their activity or interactions with other proteins. SF2 helicases are subdivided into nine families, one of them being the DEAH-box family of RNA helicases. DEAH-box RNA helicases, some of which are multifunctional, can interact with specific cofactors, whose expression levels and availability can regulate the distribution and activities of the RNA helicases and provide for a state at equilibrium in salubrious tissue. Some DEAH-box helicases can interact with so-called G-patch proteins, named after their conserved glycine-rich helicase binding domain. RNA helicases and their cofactors have previously been implicated in disease, where the helicases themselves and their regulating cofactors often show modified expression levels and function. Some cofactors even represent tumor suppressors or oncogenes, or interact with such proteins, thereby directly affecting tumorigenesis or tumor growth. This was the starting point of this study. By analyzing different DEAH-box RNA helicase and cofactor levels, conclusions about protein expression changes should be drawn. The observations could then be the basis for future studies on the differences in the regulation of RNA helicase function in different cells, tissues and in cancer. Not only cell culture cell lines but also tumor samples from patients and their matched-pair non-pathological tissues were analyzed. This allowed conclusions to be drawn concerning candidates that might play key roles in malignancy, which in the long term could then be expanded to potential targets for disease treatment.

mRNA analysis by qPCR of the different tumor cell lines provided some interesting observations on G-patch gene expression levels in different tumor cells. While some results match well with previous findings from other studies, others differ from previous

observations. Similarly, some of the results observed for G-patch protein expression on the protein level could be correlated to the data obtained here for the corresponding mRNAs and/or previous observations on protein expression, for example concerning upregulation of GPATCH2 in MCF-7 and breast cancer cells. Interestingly, this work revealed a potential regulation of GPATCH4 expression at the level of translation in A549 cells. This could be further analyzed on the functional level and a potential general upregulation of GPATCH4 in lung cancer could be investigated.

The analyses of the limited number of matched-pair tumor and normal samples from patients suffering from squamous cell carcinoma or fibromyxosarcoma showed that an increased amount of material and a larger dataset will be required to obtain more reliable data and to perform more sensitive analyses. Also, faster sample collection and freezing as well as reduced sample manipulation could improve the reproducibility of the results. With the development of novel and further improvement of the next generation sequencing (NGS) technologies, future analyses will most likely be performed using these technologies, rather than the significantly more laborious qPCR approach. However, significant hits identified by NGS can still be confirmed using the specific qPCR setup.

Recently, a compendium of papers in the Pan-Cancer Analysis of Whole Genomes project within the International Cancer Genome Consortium provided detailed information on whole-genome sequencing data of 2,658 primary tumors from 38 tumor types (Campbell 2020). While squamous cell carcinoma samples from oral cavity and fibromyxosarcoma samples from limbs were not among the analyzed sample types, these analyses not only outlined somatic alterations but also RNA level variations in multiple other cancers. This illustrates that, since the beginning of the study presented here, a large amount of sequencing data and a multitude of corresponding analysis tools have become available (Cortés-Ciriano et al. 2021). As a further outlook, it would be beneficial to conduct high-throughput sequencing analyses of various cancer samples in large sample sizes in comparison to matched-pair normal tissue to alleviate general differences in gene expression levels between individuals. The combination of whole-genome and exome sequencing as well as high-throughput mass spectrometry could provide comprehensive information on gene expression regulation in healthy tissues and in disease.

5. Supplemental material

5.1 G-patch protein and RNA helicase mRNA levels in human cancer cell lines

Supplemental table 1: Ratios of G-patch protein and RNA helicase mRNA levels in human cancer cell lines

	round 1	round 2	round 3	mean value	standard deviation	t value	p value
AGGF1							
HEK293	1	1	1	1	0		
HeLa	0.2545187	0.35831701	0.35655839	0.32313137	0.05942681	-19.727977	0.00255956
HCT116 wt p53	0.83826672	1.15198023	0.79220871	0.92748522	0.19577753	-0.6415408	0.58688216
HCT116 -/- p53	0.95881404	0.46512918	0.59167638	0.6718732	0.25642705	-2.2163508	0.15699527
A549	0.5339722	0.32901686	0.43642844	0.43313917	0.10251725	-9.5772342	0.01072723
U2OS	0.45267181	0.84494632	0.38436263	0.56066025	0.24855676	-3.0615091	0.09217711
CaCo-2	0.6334755	0.61017829	0.33025491	0.52463623	0.16874171	-4.8793756	0.03952847
MCF-7	1.18406225	1.01310949	1.16457583	1.12058252	0.09358296	2.23176388	0.1553115
CHERP							
HEK293	1	1	1	1	0		
HeLa	0.76441368	0.69291409	0.76988623	0.74240466	0.04294735	-10.388725	0.00913882
HCT116 wt p53	1.0062177	0.66335551	0.78155206	0.81704176	0.17416446	-1.8195043	0.2104467
HCT116 -/- p53	0.88959035	0.69118332	0.81668953	0.7991544	0.10035909	-3.4663005	0.07409601
A549	0.18206975	0.42052357	0.11957668	0.24072333	0.15881574	-8.2807017	0.01427217
U2OS	0.76659405	1.05779624	0.99325896	0.93921642	0.15293831	-0.6883838	0.56233481
CaCo-2	0.43103682	1.58835036	0.82246613	0.94728443	0.5886666	-0.1551065	0.89097688
MCF-7	1.09984674	0.7428728	0.7914852	0.87806825	0.19359769	-1.0908807	0.38922603
CMTR1							
HEK293	1	1	1	1	0		
HeLa	0.81987754	0.63507708	0.59536234	0.68343899	0.11981621	-4.5761736	0.04458322
HCT116 wt p53	0.62443376	0.85969309	0.29923141	0.59445275	0.28143111	-2.4959161	0.12995705
HCT116 -/- p53	0.67421368	0.45133532	0.62394959	0.5831662	0.11690233	-6.175902	0.02522999
A549	0.38205413	0.22146178	0.18025992	0.26125861	0.10662113	-12.000788	0.00687204
U2OS	1.43018552	1.25739495	0.67518815	1.12092287	0.3955676	0.52947856	0.64937098
CaCo-2	0.42416532	0.13478223	0.26657421	0.27517392	0.14488309	-8.665163	0.01305794
MCF-7	1.07802482	0.8391642	0.87844272	0.93187725	0.12808214	-0.9212219	0.45418595
GPANK1							
HEK293	1	1	1	1	0		
HeLa	1.28828362	1.29177872	1.28225277	1.28743837	0.0048189	103.313685	9.3675E-05
HCT116 wt p53	1.19507762	1.38512372	1.25965741	1.27995292	0.09663494	5.01777823	0.03749736

HCT116 -/- p53	1.06296856	0.93615248	1.03446152	1.01119419	0.06653275	0.29141894	0.79817612
A549	0.79846992	1.0999689	0.90319636	0.93387839	0.15307334	-0.7481772	0.53236817
U2OS	0.90933564	1.12370616	1.07731956	1.03678712	0.1127867	0.56493507	0.62903412
CaCo-2	1.56186477	1.23028199	1.48233085	1.42482587	0.17310951	4.25060418	0.05113908
MCF-7	0.63146995	0.86853167	0.56270971	0.68757044	0.16044381	-3.3727936	0.0777877
GPATCH1							
HEK293	1	1	1	1	0		
HeLa	0.36855262	0.39583545	0.39676823	0.3870521	0.01602781	-66.238444	0.00022784
HCT116 wt p53	0.78070688	0.67157603	0.24872898	0.56700396	0.28098329	-2.6690952	0.11637137
HCT116 -/- p53	0.65335744	0.61416206	0.50167429	0.58973127	0.07873749	-9.0250056	0.01205579
A549	0.82219453	0.85561129	0.70067898	0.79282827	0.08153397	-4.401012	0.0479464
U2OS	1.10906078	0.9587117	1.05423454	1.040669	0.07608698	0.92579282	0.45228874
CaCo-2	0.90106957	1.04779712	0.95353988	0.96746885	0.07434888	-0.757854	0.52766256
MCF-7	1.07802482	0.8391642	0.87844272	0.93187725	0.12808214	-0.9212219	0.45418595
GPATCH2							
HEK293	1	1	1	1	0		
HeLa	0.62956846	0.68356165	0.93124709	0.74812573	0.16086917	-2.711887	0.11332345
HCT116 wt p53	1.14268156	1.27503017	1.22697664	1.21489613	0.06699621	5.55570215	0.03090428
HCT116 -/- p53	0.80535436	0.87023431	0.86889338	0.84816068	0.03707743	-7.0930865	0.01930241
A549	0.79045985	0.80369221	0.7471268	0.78042629	0.02958743	-12.853866	0.00599807
U2OS	1.0859214	1.09090123	1.11164923	1.09615729	0.01364551	12.2054323	0.0066458
CaCo-2	0.83073315	0.9170234	0.82487253	0.85754303	0.0515948	-4.7823178	0.04105076
MCF-7	5.78299506	5.83424558	4.7759086	5.46438308	0.5967868	12.9569526	0.00590384
GPATCH3							
HEK293	1	1	1	1	0		
HeLa	0.88717068	0.97334099	1.35279558	1.07110242	0.2477289	0.49712811	0.66837016
HCT116 wt p53	2.23363517	1.39850188	1.4355929	1.68924332	0.47182179	2.530202	0.12709724
HCT116 -/- p53	1.8946113	1.02252297	0.94473339	1.28728922	0.52739253	0.94350885	0.44501486
A549	0.84790972	0.80851986	0.49722092	0.7178835	0.19211161	-2.543522	0.12600992
U2OS	1.13324372	0.96500036	1.09154187	1.06326198	0.08761433	1.25062837	0.33754698
CaCo-2	1.28804151	1.28485017	1.13408298	1.23565822	0.08798121	4.63930878	0.04345544
MCF-7	1.04617269	0.69065137	0.63595099	0.79092502	0.22273653	-1.6258154	0.24550043
GPATCH4							
HEK293	1	1	1	1	0		
HeLa	0.79368495	0.75680387	0.90110372	0.81719752	0.07496827	-4.2234291	0.05174893
HCT116 wt p53	0.87527615	0.70714509	0.67253471	0.75165198	0.10845124	-3.9663115	0.05808324
HCT116 -/- p53	1.05148807	0.88186351	0.72028335	0.88454498	0.16561864	-1.2074364	0.35068135
A549	0.79046588	0.62691606	0.47088818	0.62942337	0.1598036	-4.0165398	0.05676017
U2OS	0.81703865	0.7366537	0.73877097	0.76415444	0.04581131	-8.9169362	0.01234436
CaCo-2	0.71347691	0.60640855	0.54365554	0.62118033	0.08586896	-7.6411185	0.01669937
MCF-7	0.45388649	0.38254529	0.33629521	0.390909	0.05924011	-17.808484	0.00313832
GPATCH8							
HEK293	1	1	1	1	0		
HeLa	0.75972039	0.75789631	0.79991858	0.77251176	0.02375251	-16.588609	0.00361427

HCT116 wt p53	0.75115789	1.06565164	1.13159241	0.98280065	0.20329983	-0.1465331	0.89693723
HCT116 -/- p53	0.79717906	0.97658459	1.14871167	0.97415844	0.17577887	-0.2546318	0.82279753
A549	0.60387848	0.73430834	0.73281468	0.69033383	0.07487626	-7.1632526	0.01893674
U2OS	0.9119937	0.8086485	0.88601475	0.86888565	0.05375976	-4.2242879	0.05172949
CaCo-2	0.58707244	0.61960585	0.55148817	0.58605549	0.03407023	-21.043973	0.00225049
MCF-7	0.64540266	0.69896063	0.77622178	0.70686169	0.06576648	-7.7202004	0.01636732
GPATCH11							
HEK293	1	1	1	1	0		
HeLa	1.29919176	1.03013547	0.74631697	1.02521473	0.27647024	0.15796708	0.88899078
HCT116 wt p53	1.19532725	0.63424071	1.11954435	0.98303744	0.30443411	-0.096507	0.93191758
HCT116 -/- p53	1.15324793	0.72451108	1.16525568	1.01433823	0.25106947	0.09891504	0.93022696
A549	1.1740623	1.14542795	0.92388307	1.08112444	0.13692559	1.02618988	0.41270047
U2OS	1.13474266	1.27167797	0.74488878	1.05043647	0.27332648	0.31961239	0.77955942
CaCo-2	0.25428653	0.42465714	0.31343356	0.33079241	0.08650164	-13.399764	0.00552327
MCF-7	1.05856514	1.03917676	0.86608309	0.98794167	0.10597694	-0.1970773	0.86197903
GPKOW							
HEK293	1	1	1	1	0		
HeLa	0.91347043	0.65333854	0.66244727	0.74308541	0.14762802	-3.0142592	0.09468881
HCT116 wt p53	1.22384161	0.65542488	0.95987889	0.94638179	0.28444863	-0.3264894	0.77505387
HCT116 -/- p53	0.72684361	0.38469041	0.54698908	0.55284103	0.17115165	-4.5252385	0.04552462
A549	0.80231006	0.79822576	0.61300367	0.7378465	0.10813634	-4.1989878	0.05230653
U2OS	1.30070871	0.82254889	0.89529469	1.0061841	0.25764617	0.04157319	0.97061601
CaCo-2	0.60636757	0.47367952	0.42893272	0.50299327	0.09227813	-9.3287637	0.0112965
MCF-7	0.74637827	0.34339751	0.3448048	0.47819353	0.23225586	-3.8913778	0.06014198
NKRF							
HEK293	1	1	1	1	0		
HeLa	0.79832762	0.8716023	0.68968539	0.78653844	0.09152966	-4.0394149	0.05617213
HCT116 wt p53	1.09407355	1.32814713	0.34015987	0.92079352	0.51628401	-0.2657252	0.81533545
HCT116 -/- p53	1.08205661	0.70342806	0.86714069	0.88420845	0.18989044	-1.0561714	0.40162884
A549	0.59063747	0.95905498	0.80037347	0.78335531	0.1847974	-2.030546	0.17940938
U2OS	1.55614258	1.44946384	1.37069304	1.45876649	0.09307409	8.53735801	0.01344391
CaCo-2	0.71032382	0.90294192	0.87753269	0.83026615	0.10464716	-2.8093228	0.10679093
MCF-7	1.73975116	1.66772272	1.40907361	1.60551583	0.17389417	6.03116349	0.02640735
PINX1							
HEK293	1	1	1	1	0		
HeLa	0.99331517	0.78105258	0.79275373	0.85570716	0.11931556	-2.0946348	0.17121281
HCT116 wt p53	2.24226998	1.58385391	1.19968899	1.67527096	0.52726804	2.21823346	0.15678826
HCT116 -/- p53	2.22301916	1.73315451	1.31744623	1.7578733	0.45329223	2.89586932	0.10142659
A549	0.99909146	1.15624822	0.85742661	1.00425543	0.14947772	0.04930918	0.96515432
U2OS	0.96188634	0.69638391	0.72855727	0.79560917	0.14489601	-2.443237	0.13452886
CaCo-2	0.78244142	0.63361248	0.68027812	0.69877734	0.07611951	-6.8541294	0.02062967
MCF-7	0.62790677	0.45316486	0.45270284	0.51125816	0.10102093	-8.3797061	0.0139439
RBM5							

HEK293	1	1	1	1	0		
HeLa	1.17471202	1.42693787	1.21538295	1.27234428	0.13541756	3.48340445	0.07344816
HCT116 wt p53	4.16495549	3.26502741	2.21901262	3.21633184	0.97388493	3.94173812	0.05874692
HCT116 -/- p53	2.87686471	2.28996824	1.63317098	2.26666797	0.62217417	3.52623651	0.07186123
A549	0.87014756	1.56689027	1.14542767	1.19415517	0.3509179	0.95830566	0.43903549
U2OS	1.52204416	1.71128744	1.54047049	1.59126736	0.10434796	9.81432769	0.01022302
CaCo-2	1.84083078	1.70314349	1.34045788	1.62814405	0.25848007	4.20913464	0.05207398
MCF-7	3.48383771	3.00776531	2.56073924	3.01744742	0.4616254	7.56960399	0.01700836
RBM6							
HEK293	1	1	1	1	0		
HeLa	1.17635151	1.10432896	1.43639632	1.2390256	0.17468032	2.37006936	0.14125829
HCT116 wt p53	3.3140916	2.97288824	2.54995778	2.94564587	0.38279464	8.80356512	0.0126583
HCT116 -/- p53	2.84517187	2.77202566	2.4065898	2.67459578	0.23496382	12.34439	0.00649847
A549	0.85724818	1.07210357	0.9543442	0.96123198	0.10759317	-0.6240933	0.59626473
U2OS	0.85388846	1.188603	1.12494451	1.05581199	0.17774402	0.54386755	0.64105584
CaCo-2	1.11133168	1.23410087	1.13368281	1.15970512	0.06539066	4.23022759	0.05159537
MCF-7	1.29803336	1.41967697	1.30143563	1.33971532	0.06926971	8.49439375	0.01357749
RBM10							
HEK293	1	1	1	1	0		
HeLa	1.23112719	1.00455043	0.89698283	1.04422015	0.17056781	0.4490387	0.69737066
HCT116 wt p53	1.36709073	1.06357756	1.51809275	1.31625368	0.23148287	2.36634121	0.14161358
HCT116 -/- p53	1.23839175	0.7836838	1.21549968	1.07919174	0.25617322	0.53543505	0.64591862
A549	0.87889553	1.15739146	0.46815636	0.83481445	0.34672555	-0.8251765	0.49602939
U2OS	1.6323386	1.20380176	1.50702018	1.44772018	0.22033684	3.51949364	0.07210775
CaCo-2	0.91857864	0.81675066	0.69663319	0.81065416	0.11109825	-2.9519512	0.09815266
MCF-7	1.42766243	1.18057229	1.27659717	1.29494397	0.12456259	4.10121486	0.05462713
RBM17							
HEK293	1	1	1	1	0		
HeLa	0.82208336	0.92811688	0.87880119	0.87633381	0.0530598	-4.0368812	0.05623682
HCT116 wt p53	1.3938126	1.2529592	1.3028833	1.3165517	0.07141455	7.67747744	0.01654547
HCT116 -/- p53	1.31622143	1.50028805	1.21267532	1.3430616	0.1456728	4.07900517	0.05517516
A549	1.14707488	0.86002349	0.90888992	0.9719961	0.1535787	-0.3158262	0.78204602
U2OS	0.7920935	0.87049584	0.71095335	0.7911809	0.07977516	-4.5338086	0.0453642
CaCo-2	0.35340842	0.43688401	0.31017596	0.36682279	0.06441034	-17.026694	0.00343162
MCF-7	0.91109453	1.35676929	0.93377864	1.06721416	0.25101847	0.46378393	0.68838421
SON							
HEK293	1	1	1	1	0		
HeLa	0.4721058	0.40363137	0.33093556	0.40222424	0.07059564	-14.666317	0.00461681
HCT116 wt p53	1.1320036	0.970487	1.00424724	1.03557928	0.08519493	0.7233426	0.54462824
HCT116 -/- p53	0.77615227	0.85289487	0.58946146	0.73950287	0.13548681	-3.3301713	0.07955875
A549	0.35801765	0.4812136	0.31808213	0.38577113	0.08503329	-12.511284	0.00632789
U2OS	1.18217754	0.88175417	1.21611425	1.09334865	0.18403014	0.87857677	0.47229506
CaCo-2	0.72064608	0.71785323	0.58481818	0.67443917	0.07762661	-7.2641057	0.01842891

MCF-7	0.6117542	0.70999648	0.80637148	0.70937405	0.09731013	-5.1729342	0.03539793
SUGP1							
HEK293	1	1	1	1	0		
HeLa	1.00605174	1.22929795	1.17955286	1.13830085	0.11720074	2.04387868	0.17766108
HCT116 wt p53	2.52337028	2.79343683	2.17600675	2.49760462	0.3095204	8.38047284	0.0139414
HCT116 -/- p53	1.83077127	1.63420126	0.2269773	1.23064995	0.87474512	0.45670152	0.69269031
A549	0.51735078	1.17796524	1.02376128	0.9063591	0.34560139	-0.4693002	0.68504354
U2OS	1.33650512	1.3112244	1.49599635	1.38124196	0.10018087	6.59138248	0.02225155
CaCo-2	0.6770968	1.02009957	0.92292129	0.87337256	0.1767881	-1.2406104	0.34054048
MCF-7	2.48468096	2.10436084	2.56532893	2.38479024	0.2461839	9.74282679	0.01037129
SUGP2							
HEK293	1	1	1	1	0		
HeLa	0.86438463	0.75535723	0.74608448	0.78860878	0.06578739	-5.5655095	0.03080043
HCT116 wt p53	0.85936987	0.60047501	0.7355382	0.73179436	0.12948803	-3.5875578	0.06967416
HCT116 -/- p53	0.94877572	0.68701155	0.8092698	0.81501902	0.13097676	-2.4462085	0.13426506
A549	0.6055036	0.59477344	0.48845862	0.56291189	0.06470124	-11.700839	0.00722502
U2OS	1.06290872	0.85658807	0.77856372	0.8993535	0.14691726	-1.1865512	0.35724891
CaCo-2	0.35019321	0.34116537	0.60053613	0.43063157	0.14721089	-6.6990632	0.02156474
MCF-7	0.67697944	0.62907758	0.52130705	0.60912136	0.07973181	-8.4912371	0.01358738
TFIP11							
HEK293	1	1	1	1	0		
HeLa	0.84130488	0.87880119	0.91155245	0.87721951	0.03515048	-6.0500463	0.02624919
HCT116 wt p53	1.63855768	1.2529592	0.03491895	0.97547861	0.8370549	-0.0507402	0.96414437
HCT116 -/- p53	1.16350912	1.21267532	0.15421457	0.84346634	0.59741554	-0.4538286	0.69444246
A549	0.50354422	0.96839673	0.86002349	0.77732148	0.24321119	-1.5858256	0.2536645
U2OS	1.13693714	0.87049584	1.01904453	1.00882584	0.13351426	0.11449559	0.91930342
CaCo-2	0.35178852	0.78441012	0.31017596	0.48212487	0.26261223	-3.4156294	0.07606439
MCF-7	1.15755363	1.16080543	0.93377864	1.0840459	0.13014542	1.11853166	0.37965649
ZGPAT							
HEK293	1	1	1	1	0		
HeLa	2.13138451	1.16656349	2.28902281	1.8623236	0.60767924	2.45785638	0.13323792
HCT116 wt p53	2.48092928	2.33554288	1.81864811	2.21170676	0.34807417	6.02957027	0.02642076
HCT116 -/- p53	1.74846928	1.48457462	2.00769762	1.74691384	0.26156497	4.94597092	0.03853148
A549	1.97668426	1.70612522	0.97573387	1.55284779	0.51777978	1.84935853	0.2056418
U2OS	0.99372272	0.87121037	1.28088034	1.04860447	0.21027691	0.40035504	0.72761082
CaCo-2	2.88353059	2.18866866	2.77382947	2.61534291	0.3735596	7.4897179	0.01736367
MCF-7	2.78370572	2.79770138	2.50638765	2.69593158	0.16429896	17.8786263	0.00311386
DHX15							
HEK293	1	1	1	1	0		
HeLa	1.14073531	1.26793713	1.16842852	1.19236698	0.06689442	4.98082486	0.03802437
HCT116 wt p53	1.88973963	2.71007468	2.38852556	2.32944662	0.41334627	5.5707993	0.03074464
HCT116 -/- p53	1.8321818	2.28656604	1.85625581	1.99166788	0.2556728	6.71803628	0.02144699
A549	1.48282064	1.17591347	0.76959134	1.14277515	0.35776755	0.69121365	0.56088198

U2OS	0.78796476	1.15886869	0.72349343	0.89010896	0.23497443	-0.8100323	0.50297774
CaCo-2	2.27192787	1.89523827	1.32130271	1.82948962	0.47871099	3.00122242	0.09539899
MCF-7	1.68090441	1.88529484	1.55990357	1.70870094	0.16446688	7.46354551	0.01748249
DHX35							
HEK293	1	1	1	1	0		
HeLa	2.30988313	2.08032376	2.31393054	2.23471247	0.13371987	15.9930217	0.00388688
HCT116 wt p53	2.1866053	3.82168341	3.35546802	3.12125224	0.84232588	4.36187081	0.04874856
HCT116 -/- p53	1.92032502	2.55803834	2.70436844	2.39424394	0.41689624	5.79257159	0.0285334
A549	0.86916929	1.44343282	1.42778596	1.24679602	0.32712791	1.30671591	0.3213588
U2OS	1.272726	1.1252299	0.96366754	1.12054115	0.15458257	1.35062702	0.30933808
CaCo-2	5.87007675	5.1109348	5.65538233	5.54546462	0.39132538	20.1187455	0.00246146
MCF-7	1.02607766	1.08186505	1.21440406	1.10744892	0.09673473	1.92389009	0.19426674

Supplemental table 2: Raw data of G-patch protein and RNA helicase mRNA levels in human cancer cell lines as quantified by RT-qPCR

	target/reference	Ct value	target/reference	Ct value
round 1				
HEK293	GPATCH1	22.7445863	GPKOW	22.4726102
HeLa	GPATCH1	24.6782371	GPKOW	22.9612429
HCT116 wtp53	GPATCH1	23.6829761	GPKOW	23.0201269
HCT116 -/- p53	GPATCH1	24.0553528	GPKOW	23.6349674
A549	GPATCH1	24.3028518	GPKOW	24.0661955
U2OS	GPATCH1	22.8366072	GPKOW	22.1906547
CaCo-2	GPATCH1	24.7993682	GPKOW	23.5741362
MCF-7	GPATCH1	23.4670261	GPKOW	23.1847854
HEK293	GPATCH2	24.8072634	PINX1	22.6941863
HeLa	GPATCH2	25.4368545	PINX1	23.0511506
HCT116 wt p53	GPATCH2	24.8290081	PINX1	23.1983791
HCT116 -/- p53	GPATCH2	25.6006582	PINX1	22.7120684
A549	GPATCH2	26.8588142	PINX1	23.9713148
U2OS	GPATCH2	24.929703	PINX1	22.6780798
CaCo-2	GPATCH2	28.1905408	PINX1	24.6687093
MCF-7	GPATCH2	22.3974504	PINX1	23.7289239
HEK293	GPATCH3	28.189627	RBM5	22.9609287
HeLa	GPATCH3	27.4685054	RBM5	23.4873912
HCT116 wt p53	GPATCH3	28.6993863	RBM5	22.5717804
HCT116 -/- p53	GPATCH3	28.4381276	RBM5	22.6068337
A549	GPATCH3	29.0830706	RBM5	24.4374139
U2OS	GPATCH3	28.2505281	RBM5	22.5962777
CaCo-2	GPATCH3	29.3111947	RBM5	23.9850639
MCF-7	GPATCH3	28.9553361	RBM5	21.5181958
HEK293	GPATCH4	19.7412112	SUGP1	23.7947197
HeLa	GPATCH4	19.5961198	SUGP1	24.5447849
HCT116 wt p53	GPATCH4	20.8933247	SUGP1	24.1285206

HCT116 -/- p53	GPATCH4	20.8391812	SUGP1	23.2010507
A549	GPATCH4	21.3562533	SUGP1	26.0213221
U2OS	GPATCH4	20.2740943	SUGP1	23.9886036
CaCo-2	GPATCH4	21.2361406	SUGP1	26.2617779
MCF-7	GPATCH4	21.3980852	SUGP1	23.0205492
HEK293	GPATCH8	22.3049272	DHX15	19.3929756
HeLa	GPATCH8	23.4601564	DHX15	19.9617812
HCT116 wt p53	GPATCH8	24.3868919	DHX15	20.1439409
HCT116 -/- p53	GPATCH8	23.8023539	DHX15	19.6898154
A549	GPATCH8	24.3084142	DHX15	22.1160131
U2OS	GPATCH8	22.6791907	DHX15	19.9781319
CaCo-2	GPATCH8	24.977809	DHX15	22.5921521
MCF-7	GPATCH8	23.7674859	DHX15	19.474568
HEK293	GPANK1	28.6619996	DHX35	24.7539164
HeLa	GPANK1	29.055319	DHX35	24.1576111
HCT116 wt p53	GPANK1	30.074048	DHX35	25.2943764
HCT116 -/- p53	GPANK1	29.7443031	DHX35	24.9829683
A549	GPANK1	30.7564475	DHX35	26.2320245
U2OS	GPANK1	29.201432	DHX35	24.6473538
CaCo-2	GPANK1	29.9232222	DHX35	25.9419052
MCF-7	GPANK1	30.1560437	DHX35	25.5476066
HEK293	AGGF1	23.2043219	TFIP11	22.5097092
HeLa	AGGF1	25.9372479	TFIP11	22.9663282
HCT116 wt p53	AGGF1	22.6506998	TFIP11	22.4386304
HCT116 -/- p53	AGGF1	24.4354013	TFIP11	23.1695124
A549	AGGF1	25.3853025	TFIP11	24.775336
U2OS	AGGF1	24.5891438	TFIP11	21.9280396
CaCo-2	AGGF1	25.7674533	TFIP11	25.9214211
MCF-7	AGGF1	23.791407	TFIP11	23.1294603
HEK293	CMTR1	21.8852826	CHERP	27.3423943
HeLa	CMTR1	22.9305719	CHERP	28.4887385
HCT116 wt p53	CMTR1	22.9291168	CHERP	29.0026046
HCT116 -/- p53	CMTR1	23.6244072	CHERP	28.6815837
A549	CMTR1	24.5492508	CHERP	28.7159346
U2OS	CMTR1	21.6104396	CHERP	27.9672189
CaCo-2	CMTR1	25.0270762	CHERP	27.9901279
MCF-7	CMTR1	21.4495246	CHERP	28.0359219
HEK293	RBM17	20.6107896	GPATCH11	22.9457983
HeLa	RBM17	21.6522027	GPATCH11	22.8673859
HCT116 wt p53	RBM17	21.6368841	GPATCH11	24.3575455
HCT116 -/- p53	RBM17	21.3847898	GPATCH11	23.9104981
A549	RBM17	22.646817	GPATCH11	23.9901065
U2OS	RBM17	21.1884062	GPATCH11	22.4493197
CaCo-2	RBM17	24.0158735	GPATCH11	25.1365658
MCF-7	RBM17	21.5759471	GPATCH11	23.6945184
HEK293	GPKOW	22.8015978	RBM10	25.2214819
HeLa	GPKOW	23.5234753	RBM10	25.6802717

HCT116 wt p53	GPKOW	23.9691038	RBM10	26.4395256
HCT116 -/- p53	GPKOW	24.3785886	RBM10	26.0834165
A549	GPKOW	23.9075078	RBM10	26.6835354
U2OS	GPKOW	23.1117047	RBM10	24.7559008
CaCo-2	GPKOW	24.7662821	RBM10	27.2484989
MCF-7	GPKOW	24.2688632	RBM10	25.5386571
HEK293	ZGPAT	27.3341614	SON	19.8478283
HeLa	ZGPAT	25.8220342	SON	20.7993265
HCT116 wt p53	ZGPAT	27.6924336	SON	21.3381026
HCT116 -/- p53	ZGPAT	27.6984714	SON	20.3852423
A549	ZGPAT	27.6268961	SON	22.6055428
U2OS	ZGPAT	27.5846054	SON	19.8477409
CaCo-2	ZGPAT	27.7108173	SON	23.0575122
MCF-7	ZGPAT	26.6879848	SON	20.8090418
HEK293	RBM6	22.1178936	SUGP2	23.3166792
HeLa	RBM6	22.1786282	SUGP2	23.6976222
HCT116 wt p53	RBM6	22.0584329	SUGP2	23.9023967
HCT116 -/- p53	RBM6	21.7797802	SUGP2	24.3733057
A549	RBM6	23.6159259	SUGP2	25.3521516
U2OS	RBM6	22.5871333	SUGP2	22.9200642
CaCo-2	RBM6	23.8700963	SUGP2	25.7146227
MCF-7	RBM6	22.5723962	SUGP2	23.3486284
HEK293	NKRF	21.7109936	COPS6	19.9718317
HeLa	NKRF	22.1690815	COPS6	20.8366522
HCT116 wt p53	NKRF	23.5987953	COPS6	21.9817741
HCT116 -/- p53	NKRF	22.957257	COPS6	21.369705
A549	NKRF	23.7106033	COPS6	21.6149886
U2OS	NKRF	21.8643352	COPS6	20.4314737
CaCo-2	NKRF	24.0961445	COPS6	21.6612472
MCF-7	NKRF	23.1046398	COPS6	19.6845734
HEK293	COPS6	19.9718317	COPS6	19.7281693
HeLa	COPS6	20.8366522	COPS6	20.6727235
HCT116 wtp53	COPS6	21.9817741	COPS6	21.4943935
HCT116 p53 -/-	COPS6	21.369705	COPS6	21.439834
A549	COPS6	21.6149886	COPS6	20.4265761
U2OS	COPS6	20.4314737	COPS6	19.4203578
CaCo-2	COPS6	21.6612472	COPS6	21.9746292
MCF7	COPS6	19.6845734	COPS6	20.2355228
HEK293	COPS6	19.5362358	COPS6	20.2895473
HeLa	COPS6	20.4247248	COPS6	20.9456885
HCT116 wt p53	COPS6	21.6685335	COPS6	21.5063128
HCT116 -/- p53	COPS6	21.7235831	COPS6	21.264677
A549	COPS6	21.3580685	COPS6	21.0462403
U2OS	COPS6	19.6345978	COPS6	19.8401703
CaCo-2	COPS6	21.9007337	COPS6	22.1460646
MCF-7	COPS6	20.9466451	COPS6	20.5435404
HEK293	EMC7	20.1200047	EMC7	19.7585156

HeLa	EMC7	20.213975	EMC7	20.1846711
HCT116 wt p53	EMC7	21.5037843	EMC7	21.6012209
HCT116 -/- p53	EMC7	20.5812705	EMC7	20.813936
A549	EMC7	20.1965721	EMC7	20.6746993
U2OS	EMC7	19.8901163	EMC7	20.4884855
CaCo-2	EMC7	21.4881488	EMC7	21.1571347
MCF-7	EMC7	20.0997836	EMC7	20.5012849
HEK293	EMC7	18.5966172	PSMB2	18.8866471
HeLa	EMC7	20.3393145	PSMB2	19.5298059
HCT116 wt p53	EMC7	21.8531123	PSMB2	20.0611991
HCT116 -/- p53	EMC7	20.9409978	PSMB2	18.7780884
A549	EMC7	20.0491482	PSMB2	20.5813369
U2OS	EMC7	20.0610329	PSMB2	18.682995
CaCo-2	EMC7	20.8306924	PSMB2	20.5023463
MCF-7	EMC7	20.6320958	PSMB2	19.6983062
HEK	PSMB2	18.6879594	PSMB2	19.3401463
HeLa	PSMB2	19.5652037	PSMB2	19.7564407
HCT116 wtp53	PSMB2	19.8577837	PSMB2	20.2383664
HCT116 p53 -/-	PSMB2	19.9112436	PSMB2	19.8173297
A549	PSMB2	20.571817	PSMB2	21.1552192
U2OS	PSMB2	19.1869048	PSMB2	19.6165971
CaCo-2	PSMB2	21.1750709	PSMB2	21.3823342
MCF7	PSMB2	19.9350874	PSMB2	20.4920285
HEK293	PSMB2	18.8602896		
HeLa	PSMB2	19.6577254		
HCT116 wt p53	PSMB2	19.8783236		
HCT116 -/- p53	PSMB2	19.8931059		
A549	PSMB2	20.5960097		
U2OS	PSMB2	18.7647116		
CaCo-2	PSMB2	20.7445226		
MCF-7	PSMB2	20.0577149		
round 2				
HEK293	AGGF1	23.2443901	GPATCH2	24.101119
HeLa	AGGF1	25.1040616	GPATCH2	25.1476638
HCT116 wt p53	AGGF1	24.3680731	GPATCH2	24.7778598
HCT116 -/- p53	AGGF1	24.7801978	GPATCH2	24.8449345
A549	AGGF1	25.5891352	GPATCH2	25.1813334
U2OS	AGGF1	23.5723392	GPATCH2	24.3345727
CaCo-2	AGGF1	25.8060997	GPATCH2	24.8709004
MCF-7	AGGF1	23.9052835	GPATCH2	22.2489856
HEK293	CMTR1	22.0306166	GPATCH3	27.018619
HeLa	CMTR1	23.064593	GPATCH3	27.5703154
HCT116 wt p53	CMTR1	23.5791605	GPATCH3	27.4039011
HCT116 -/- p53	CMTR1	23.6098562	GPATCH3	27.4179969
A549	CMTR1	24.9464655	GPATCH3	27.997615
U2OS	CMTR1	22.059153	GPATCH3	27.4289919
CaCo-2	CMTR1	25.4241529	GPATCH3	27.1556784

MCF-7	CMTR1	22.0728657	GPATCH3	28.232273
HEK293	CHERP	26.9539325	RBM5	22.8361618
HeLa	CHERP	27.553704	RBM5	22.7022192
HCT116 wt p53	CHERP	28.4152425	RBM5	21.9982309
HCT116 -/- p53	CHERP	27.9183033	RBM5	22.0723453
A549	CHERP	30.1523479	RBM5	22.9292362
U2OS	CHERP	27.2318449	RBM5	21.9658115
CaCo-2	CHERP	28.6702879	RBM5	22.5702003
MCF-7	CHERP	28.0624289	RBM5	21.7151679
HEK293	GPATCH1	22.7211687	SUGP1	23.585638
HeLa	GPATCH1	24.5402061	SUGP1	23.6667834
HCT116 wt p53	GPATCH1	23.9474801	SUGP1	22.9727611
HCT116 -/- p53	GPATCH1	23.7667354	SUGP1	23.1446976
A549	GPATCH1	23.4823272	SUGP1	24.0903196
U2OS	GPATCH1	22.7205672	SUGP1	23.5261469
CaCo-2	GPATCH1	23.1560477	SUGP1	24.0591665
MCF-7	GPATCH1	23.6538272	SUGP1	22.952261
HEK293	DHX15	19.6300555	GPKOW	21.7598069
HeLa	DHX15	19.6665522	GPKOW	22.269357
HCT116 wt p53	DHX15	19.0608871	GPKOW	22.3375543
HCT116 -/- p53	DHX15	18.868384	GPKOW	22.6516011
A549	DHX15	19.8026899	GPKOW	21.9623252
U2OS	DHX15	19.4938101	GPKOW	21.7394832
CaCo-2	DHX15	18.9483769	GPKOW	22.9837809
MCF-7	DHX15	19.3949489	GPKOW	22.8615116
HEK293	DHX35	24.7292111	PINX1	22.4402506
HeLa	DHX35	23.9003712	PINX1	22.8289071
HCT116 wt p53	DHX35	23.664167	PINX1	22.6459756
HCT116 -/- p53	DHX35	23.8056843	PINX1	22.0783614
A549	DHX35	24.9406856	PINX1	22.971778
U2OS	DHX35	24.9179655	PINX1	22.8552865
CaCo-2	DHX35	22.6780701	PINX1	23.2964344
MCF-7	DHX35	24.9298795	PINX1	23.7913119
HEK293	GPATCH8	23.0232473	RBM17	21.1658292
HeLa	GPATCH8	23.8021548	RBM17	21.6524307
HCT116 wt p53	GPATCH8	23.8006756	RBM17	21.5559568
HCT116 -/- p53	GPATCH8	23.4889415	RBM17	21.0121007
A549	GPATCH8	24.2097679	RBM17	21.7088481
U2OS	GPATCH8	23.6886368	RBM17	21.5349799
CaCo-2	GPATCH8	24.1109585	RBM17	22.8627454
MCF-7	GPATCH8	24.2196477	RBM17	21.4053373
HEK293	GPANK1	29.3789996	TFIP11	22.9548296
HeLa	GPANK1	29.3886206	TFIP11	23.583109
HCT116 wt p53	GPANK1	29.6165003	TFIP11	23.1115674
HCT116 -/- p53	GPANK1	29.9056953	TFIP11	23.1678582
A549	GPANK1	30.4446682	TFIP11	23.742138
U2OS	GPANK1	29.875089	TFIP11	23.1286513

CaCo-2	GPANK1	29.5822491	TFIP11	23.807388
MCF-7	GPANK1	30.1425812	TFIP11	23.419387
HEK293	GPATCH4	19.3597786	GPATCH11	21.7675113
HeLa	GPATCH4	20.0721202	GPATCH11	21.7688768
HCT116 wt p53	GPATCH4	20.4211327	GPATCH11	23.2935731
HCT116 -/- p53	GPATCH4	19.9726624	GPATCH11	22.6639427
A549	GPATCH4	20.7744129	GPATCH11	22.3126031
U2OS	GPATCH4	20.1596943	GPATCH11	21.9441203
CaCo-2	GPATCH4	20.3490784	GPATCH11	24.2452227
MCF-7	GPATCH4	21.1790587	GPATCH11	23.1164182
HEK293	RMB10	24.7281568	NKRF	21.6867168
HeLa	RMB10	24.5962304	NKRF	22.2759514
HCT116 wt p53	RMB10	25.5083958	NKRF	23.2917049
HCT116 -/- p53	RMB10	25.5113244	NKRF	22.6598216
A549	RMB10	24.7578974	NKRF	23.1772832
U2OS	RMB10	24.8195332	NKRF	21.6333404
CaCo-2	RMB10	25.5224277	NKRF	23.7027322
MCF-7	RMB10	25.168354	NKRF	23.0350905
HEK293	SON	19.0094786	ZGPAT	28.8273506
HeLa	SON	20.4712765	ZGPAT	28.1145397
HCT116 wtp53	SON	19.9218621	ZGPAT	28.4727569
HCT116 p53 -/-	SON	19.8065781	ZGPAT	28.6888121
A549	SON	19.8853486	ZGPAT	28.7976056
U2OS	SON	19.5500045	ZGPAT	27.8578889
CaCo-2	SON	19.9843543	ZGPAT	27.2642097
MCF7	SON	20.3981382	ZGPAT	27.2498338
HEK293	SUGP2	22.9617754	RBM6	22.3501976
HeLa	SUGP2	23.6657025	RBM6	22.4948583
HCT116 wtp53	SUGP2	23.7012299	RBM6	21.6474966
HCT116 p53 -/-	SUGP2	23.9008117	RBM6	21.3107681
A549	SUGP2	23.7630685	RBM6	22.9907319
U2OS	SUGP2	22.7852303	RBM6	22.4599049
CaCo-2	SUGP2	23.6113087	RBM6	22.5489757
MCF7	SUGP2	22.9035795	RBM6	22.5243185
HEK293	EMC7	20.1769801	PSMB2	19.197841
HeLa	EMC7	20.6722553	PSMB2	20.0061278
HCT116 wt p53	EMC7	22.080405	PSMB2	19.7431467
HCT116 -/- p53	EMC7	21.080606	PSMB2	19.3665445
A549	EMC7	21.1469711	PSMB2	20.7829394
U2OS	EMC7	20.5474496	PSMB2	19.886188
CaCo-2	EMC7	21.5468462	PSMB2	19.8116023
MCF-7	EMC7	20.8701719	PSMB2	20.3951522
HEK293	COPS6	19.7050619	COPS6	19.5892064
HeLa	COPS6	20.0871645	COPS6	19.7545711
HCT116 wt p53	COPS6	20.6764414	COPS6	20.2311032
HCT116 -/- p53	COPS6	20.6500095	COPS6	20.2397748
A549	COPS6	20.1120192	COPS6	20.0439966

U2OS	COPS6	20.2674032	COPS6	19.3857878
CaCo-2	COPS6	20.234947	COPS6	19.7752687
MCF-7	COPS6	19.8473701	COPS6	19.7011261
HEK293	PSMB2	19.2575637	EMC7	19.7716094
HeLa	PSMB2	19.6370183	EMC7	19.7744842
HCT116 wt p53	PSMB2	19.5472753	EMC7	20.641003
HCT116 -/- p53	PSMB2	19.0576012	EMC7	19.8820567
A549	PSMB2	20.5131054	EMC7	19.9074555
U2OS	PSMB2	19.7551055	EMC7	20.1256678
CaCo-2	PSMB2	19.7013231	EMC7	19.9062236
MCF-7	PSMB2	20.4067454	EMC7	20.1241783
HEK293	PSMB2	18.7933547	COPS6	19.7226299
HeLa	PSMB2	19.3715205	COPS6	20.5244849
HCT116 wt p53	PSMB2	19.0676069	COPS6	20.8822635
HCT116 -/- p53	PSMB2	18.81013	COPS6	20.7471595
A549	PSMB2	19.9142654	COPS6	20.5042994
U2OS	PSMB2	18.9133345	COPS6	20.0904704
CaCo-2	PSMB2	19.3354522	COPS6	20.2604528
MCF-7	PSMB2	19.8275866	COPS6	20.0234505
HEK293	EMC7	19.5705281		
HeLa	EMC7	19.3679681		
HCT116 wt p53	EMC7	20.7380081		
HCT116 -/- p53	EMC7	19.8344926		
A549	EMC7	19.5285299		
U2OS	EMC7	20.044136		
CaCo-2	EMC7	19.7328052		
MCF-7	EMC7	20.7061458		
round 3				
HEK293	AGGF1	24.6625924	GPKOW	22.6279268
HeLa	AGGF1	25.7832337	GPKOW	23.7451827
HCT116 wt p53	AGGF1	25.219543	GPKOW	23.9984911
HCT116 -/- p53	AGGF1	24.6883688	GPKOW	24.4568523
A549	AGGF1	25.3495062	GPKOW	23.8198815
U2OS	AGGF1	25.0715869	GPKOW	23.0756795
CaCo-2	AGGF1	25.8765266	GPKOW	24.2071805
MCF-7	AGGF1	25.1581072	GPKOW	24.8852947
HEK293	CHERP	27.3815512	PINX1	22.8006146
HeLa	CHERP	28.4139614	PINX1	23.6602815
HCT116 wt p53	CHERP	28.4982039	PINX1	23.2990207
HCT116 -/- p53	CHERP	28.1243868	PINX1	22.8535657
A549	CHERP	29.4981162	PINX1	23.889353
U2OS	CHERP	27.5572355	PINX1	23.4885858
CaCo-2	CHERP	27.215259	PINX1	23.9601788
MCF-7	CHERP	28.4342363	PINX1	24.657826
HEK293	CMTR1	22.7295439	RBM5	22.7231729
HeLa	CMTR1	23.9808626	RBM5	22.9449205
HCT116 wt p53	CMTR1	23.7087168	RBM5	22.3343216

HCT116 -/- p53	CMTR1	23.8607377	RBM5	22.4661923
A549	CMTR1	24.1670808	RBM5	23.39411
U2OS	CMTR1	23.4621084	RBM5	22.1140168
CaCo-2	CMTR1	23.9268694	RBM5	22.8016839
MCF-7	CMTR1	22.8468197	RBM5	21.8498003
HEK293	GPATCH1	22.670945	SUGP1	23.8524161
HeLa	GPATCH1	24.5111309	SUGP1	24.1173346
HCT116 wt p53	GPATCH1	24.006389	SUGP1	23.4917997
HCT116 -/- p53	GPATCH1	23.824949	SUGP1	23.5945257
A549	GPATCH1	23.7627411	SUGP1	24.6853603
U2OS	GPATCH1	22.8977021	SUGP1	23.6274276
CaCo-2	GPATCH1	23.2408168	SUGP1	24.4693735
MCF-7	GPATCH1	23.5732442	SUGP1	23.4943534
HEK293	GPATCH2	24.3024274	DHX15	19.7389446
HeLa	GPATCH2	25.3544426	DHX15	20.0175337
HCT116 wt p53	GPATCH2	24.7129626	DHX15	19.2438909
HCT116 -/- p53	GPATCH2	24.9536468	DHX15	19.2972443
A549	GPATCH2	25.4845359	DHX15	20.3719862
U2OS	GPATCH2	24.5833938	DHX15	19.6921536
CaCo-2	GPATCH2	24.9286338	DHX15	19.3178023
MCF-7	GPATCH2	22.4732006	DHX15	19.8128071
HEK293	GPATCH3	28.1013961	DHX35	25.0293209
HeLa	GPATCH3	28.6435374	DHX35	24.4756714
HCT116 wt p53	GPATCH3	28.340816	DHX35	24.0438734
HCT116 -/- p53	GPATCH3	28.6341122	DHX35	24.0447244
A549	GPATCH3	29.2748645	DHX35	25.3823646
U2OS	GPATCH3	28.6132906	DHX35	24.6564312
CaCo-2	GPATCH3	28.2410329	DHX35	23.1769706
MCF-7	GPATCH3	29.4697279	DHX35	25.6311197
HEK293	GPATCH4	20.0230243	GPATCH8	22.3481601
HeLa	GPATCH4	20.9281915	GPATCH8	22.9135823
HCT116 wt p53	GPATCH4	21.2840128	GPATCH8	22.9308723
HCT116 -/- p53	GPATCH4	20.9470831	GPATCH8	22.5988386
A549	GPATCH4	21.9763914	GPATCH8	23.6634633
U2OS	GPATCH4	20.8112931	GPATCH8	22.6886835
CaCo-2	GPATCH4	21.2458992	GPATCH8	23.5399744
MCF-7	GPATCH4	22.1246412	GPATCH8	23.4289386
HEK293	RBM10	25.2376052	GPANK1	29.1964061
HeLa	RBM10	25.7342137	GPANK1	29.0262989
HCT116 wt p53	RBM10	25.3964118	GPANK1	29.4874579
HCT116 -/- p53	RBM10	25.4067509	GPANK1	29.5982214
A549	RBM10	25.8935518	GPANK1	29.9257669
U2OS	RBM10	24.8118325	GPANK1	29.1940673
CaCo-2	RBM10	25.4853926	GPANK1	29.1297755
MCF-7	RBM10	25.1889937	GPANK1	30.1150751
HEK293	SON	19.1029121	GPATCH11	22.250918
HeLa	SON	20.9149605	GPATCH11	22.7112425

HCT116 wt p53	SON	19.8578643	GPATCH11	22.8490729
HCT116 -/- p53	SON	19.7831676	GPATCH11	22.4809667
A549	SON	21.0249863	GPATCH11	23.2319593
U2OS	SON	18.9865594	GPATCH11	22.0701106
CaCo-2	SON	20.0823882	GPATCH11	23.9877845
MCF-7	SON	20.3123477	GPATCH11	22.9107962
HEK293	RBM17	20.5941993	TFIP11	20.5941993
HeLa	RBM17	21.2837491	TFIP11	21.2837491
HCT116 wt p53	RBM17	21.0299264	TFIP11	21.0299264
HCT116 -/- p53	RBM17	20.7667012	TFIP11	20.7667012
A549	RBM17	21.6785748	TFIP11	21.6785748
U2OS	RBM17	20.960216	TFIP11	20.960216
CaCo-2	RBM17	22.7842774	TFIP11	22.7842774
MCF-7	RBM17	21.4083661	TFIP11	21.4083661
HEK293	SUGP2	23.0647643	ZGPAT	28.091623
HeLa	SUGP2	23.766181	ZGPAT	28.3725167
HCT116 wt p53	SUGP2	23.416416	ZGPAT	27.9898232
HCT116 -/- p53	SUGP2	23.7211216	ZGPAT	28.2960587
A549	SUGP2	24.2528426	ZGPAT	28.9938869
U2OS	SUGP2	22.7757849	ZGPAT	28.456456
CaCo-2	SUGP2	23.7544765	ZGPAT	27.4628063
MCF-7	SUGP2	23.2853367	ZGPAT	27.3227004
HEK293	NKRF	21.6556764	RBM6	22.4407396
HeLa	NKRF	22.5636039	RBM6	22.8007281
HCT116 wt p53	NKRF	22.8598708	RBM6	21.8513328
HCT116 -/- p53	NKRF	22.411679	RBM6	21.6244445
A549	NKRF	23.5561916	RBM6	23.3749815
U2OS	NKRF	22.0449289	RBM6	22.4368118
CaCo-2	NKRF	23.7083702	RBM6	22.7609594
MCF-7	NKRF	23.3107905	RBM6	22.775955
HEK293	PSMB2	19.4202599	PSMB2	19.0292432
HeLa	PSMB2	19.9143147	PSMB2	19.6044215
HCT116 wt p53	PSMB2	19.4709555	PSMB2	19.1509588
HCT116 -/- p53	PSMB2	19.1962845	PSMB2	18.9053083
A549	PSMB2	20.5598891	PSMB2	20.2238209
U2OS	PSMB2	19.6966653	PSMB2	18.9037634
CaCo-2	PSMB2	19.7883583	PSMB2	19.4583678
MCF-7	PSMB2	20.1235347	PSMB2	19.9435548
HEK293	EMC7	19.9209996	COPS6	19.5667806
HeLa	EMC7	20.2282996	COPS6	20.2169917
HCT116 wt p53	EMC7	21.0178051	COPS6	20.6640015
HCT116 -/- p53	EMC7	20.577967	COPS6	20.7384659
A549	EMC7	20.396151	COPS6	20.5732446
U2OS	EMC7	20.2636508	COPS6	19.5283973
CaCo-2	EMC7	20.1162394	COPS6	20.1256357
MCF-7	EMC7	20.8922295	COPS6	20.1301667
HEK293	COPS6	19.6162195	EMC7	19.627325

HeLa	COPS6	20.2362696	EMC7	20.0701596
HCT116 wt p53	COPS6	20.533478	EMC7	20.754847
HCT116 -/- p53	COPS6	20.5791083	EMC7	20.0712174
A549	COPS6	20.3329923	EMC7	20.2520517
U2OS	COPS6	19.7578993	EMC7	20.0098538
CaCo-2	COPS6	20.0720126	EMC7	19.9914627
MCF-7	COPS6	19.9340776	EMC7	20.4305105
HEK293	PSMB2	18.8680391	EMC7	19.8369696
HeLa	PSMB2	19.4365746	EMC7	20.3574474
HCT116 wt p53	PSMB2	18.9927342	EMC7	20.8811956
HCT116 -/- p53	PSMB2	18.8544921	EMC7	20.4405787
A549	PSMB2	19.9535141	EMC7	20.3333273
U2OS	PSMB2	18.7969146	EMC7	20.1993403
CaCo-2	PSMB2	19.7243097	EMC7	20.4142916
MCF-7	PSMB2	19.9516055	EMC7	20.4780123
HEK293	COPS6	19.7353918		
HeLa	COPS6	20.0851768		
HCT116 wt p53	COPS6	21.0048521		
HCT116 -/- p53	COPS6	20.3140634		
A549	COPS6	20.7976488		
U2OS	COPS6	19.9580781		
CaCo-2	COPS6	20.4416828		
MCF-7	COPS6	20.1754111		

5.2 G-patch protein and RNA helicase protein levels in human cancer cell lines

Supplemental table 3: Ratios of G-patch protein and RNA helicase protein levels in human cancer cell lines

	blot 1	**blot 2**	**blot 3**	**mean value**	**standard deviation**	**t value**	***p* value**
GPATCH2							
HEK293	1	1	1	1	0		
HeLa	0.88103131	0.94046254	1.00685451	0.94278279	0.06294368	-1.5744728	0.25604554
HCT116 wt p53	0.73971354	0.77328073	0.76989247	0.76096225	0.01847974	-22.404298	0.00198629
HCT116 -/- p53	1.13705507	1.11096161	1.21237963	1.15346543	0.05266288	5.04738696	0.03708281
A549	1.79225146	1.48155127	2.08797268	1.78725847	0.30324154	4.49665203	0.04606577
U2OS	0.90238055	0.82156611	0.81774781	0.84723149	0.04779863	-5.5357827	0.03111679
CaCo-2	1.67908674	2.13160026	2.28561828	2.03210176	0.31526987	5.67022998	0.02972301
MCF-7	1.31550164	1.61144949	14.5899659	5.83897233	7.58002718	1.1057145	0.38405846
GPATCH4							
HEK293	1	1	1	1	0		
HeLa	1.24435666	1.42615101	0.58846154	1.08632307	0.44063803	0.33931693	0.76668837

HCT116 wt p53	0.80793012	0.66468824	0.60617604	0.69293147	0.10379999	-5.1238764	0.03604262
HCT116 -/- p53	0.85244149	0.38092359	0.45234131	0.56190213	0.25413571	-2.9858368	0.09624692
A549	1.11503897	45.6618526	0.21081886	15.6625701	25.9840742	0.97738008	0.4314551
U2OS	0.9094905	0.30082873	1.16913688	0.79315204	0.4456913	-0.803855	0.50583977
CaCo-2	0.7095118	0.43963907	0.52660824	0.55858637	0.13774895	-5.5503208	0.03096148
MCF-7	1.02777505	0.25112659	0.20213025	0.4936773	0.46319053	-1.8933389	0.19882538
GPKOW							
HEK293	1	1	1	1	0		
HeLa	1.27332913	2.39339594	1.23029418	1.63233975	0.65944514	1.66085775	0.238623
HCT116 wt p53	1.54395138	1.96296925	1.07015301	1.52569122	0.44668813	2.03838838	0.17837821
HCT116 -/- p53	1.26351587	2.17167794	1.76673321	1.73397567	0.45496635	2.79423557	0.10776703
A549	1.21160274	2.2085818	1.80114231	1.74044228	0.50125361	2.55855245	0.12479853
U2OS	0.89109694	0.81780056	1.85829373	1.18906374	0.58072771	0.56389251	0.62962473
CaCo-2	1.15710383	1.24692118	2.84288061	1.74896854	0.94841948	1.36780359	0.304786
MCF7	1.17191685	1.79649015	2.58168202	1.85002967	0.70640591	2.08420478	0.17251164
GPATCH11							
HEK293	1	1	1	1	0		
HeLa	1.01427227	1.16064116	2.44148015	1.53879786	0.78516396	1.18857374	0.35660661
HCT116 wt p53	0.68807769	0.86486486	1.13085726	0.89459994	0.22288241	-0.8190788	0.49881544
HCT116 -/- p53	1.49449046	0.93399522	1.92070175	1.44972914	0.49487385	1.57404504	0.25613582
A549	2.44463587	1.00740741	1.18608882	1.54604403	0.7833149	1.20740204	0.35069203
U2OS	0.8051482	0.94708793	0.73535227	0.82919613	0.10789683	-2.7418876	0.11125332
CaCo-2	1.44874635	1.52808989	2.0424312	1.67308915	0.32231043	3.61708617	0.0686552
MCF-7	0.91584708	1.55622289	2.11272098	1.52826365	0.5989266	1.52769886	0.26616212
NKRF							
HEK293	1	1	1	1	0		
HeLa	1.54094973	1.1628695	0.93933197	1.21438373	0.30409911	1.22106085	0.34647376
HCT116 wt p53	0.47956731	0.70540521	0.62034381	0.60177211	0.11405863	-6.0473367	0.0262718
HCT116 -/- p53	0.61280138	0.88728458	0.8662214	0.78876912	0.15275601	-2.3950783	0.13890661
A549	0.7625	1.00184888	0.7278169	0.83072193	0.14921145	-1.9649848	0.18835296
U2OS	1.29290736	1.0347941	0.90199451	1.07656532	0.19877586	0.66715863	0.57334117
CaCo-2	0.62008399	0.68773958	0.40843652	0.5720867	0.1457064	-5.0867195	0.03654248
MCF-7	1.22341418	0.37468833	0.32706968	0.64172406	0.50432076	-1.2304711	0.34360254
PINX1							
HEK293	1	1	1	1	0		
HeLa	0.32280739	0.3677543	1.05787045	0.58281071	0.41202715	-1.7537511	0.22156488
HCT116 wt p53	0.72820409	0.3655058	1.36631295	0.82000761	0.50668003	-0.6152916	0.60104698
HCT116 -/- p53	0.58546366	1.19146204	2.70778384	1.49490318	1.09321459	0.78410723	0.51509773
A549	0.45020197	0.73042571	1.17053749	0.78372172	0.36311316	-1.031648	0.41065979
U2OS	0.42631356	0.96412057	0.828908	0.73978071	0.27976214	-1.611058	0.24847329
CaCo-2	0.42503639	0.49134146	0.67951064	0.53196283	0.13201082	-6.1408915	0.02550754
MCF-7	0.15930661	1.43715688	0.30590289	0.63412213	0.69930053	-0.9062185	0.46047258

RBM6							
HEK293	1	1	1	1	0		
HeLa	2.23385387	0.83988095	0.88536575	1.31970019	0.7920069	0.69915676	0.5568224
HCT116 wt p53	0.67429955	0.52894823	1.89338897	1.03221225	0.74933354	0.07445717	0.94742365
HCT116 -/- p53	1.4098709	0.55880497	3.37314653	1.78060746	1.44333427	0.93675583	0.4477727
A549	1.46958729	0.49964061	0.79725841	0.92216211	0.49689017	-0.2713259	0.81158002
U2OS	1.24897656	0.65124459	0.4641644	0.78812852	0.40992126	-0.895226	0.46513665
CaCo-2	2.20151859	0.53896104	0.4697628	1.07008081	0.98046453	0.12380206	0.91279224
MCF-7	0.64475013	0.18729566	0.20306644	0.34503741	0.25967858	-4.3685871	0.04860953
DHX15							
HEK293	1	1	1	1	0		
HeLa	0.39217034	0.85598985	1.56783744	0.93866588	0.59217799	-0.1793951	0.87415697
HCT116 wt p53	0.42249314	1.18178964	0.62406937	0.74278405	0.39332261	-1.1326862	0.3748624
HCT116 -/- p53	0.94184546	1.83101278	0.95290975	1.24192266	0.510197	0.82129519	0.49780095
A549	0.85221167	0.72204026	2.80462325	1.45962506	1.16661958	0.68239379	0.56542138
U2OS	0.77891539	0.73998746	3.03580864	1.51823716	1.31439957	0.68290733	0.56515616
CaCo-2	1.73472732	1.15321055	1.65697832	1.51497206	0.31569728	2.82535786	0.10576718
MCF-7	0.36353827	0.33836461	2.35417685	1.01869324	1.15663122	0.02799306	0.98020979
DHX16							
HEK293	1	1	1	1	0		
HeLa	0.79157216	1.16156223	1.29597861	1.08303767	0.26121074	0.55061081	0.6371881
HCT116 wt p53	0.54732276	1.21347632	1.11887484	0.95989131	0.36041221	-0.1927523	0.86495213
HCT116 -/- p53	0.62941658	1.41808878	1.39283869	1.14678135	0.44822887	0.56719407	0.62775594
A549	0.53592516	0.77243372	0.6112491	0.63986932	0.12082389	-5.1625933	0.0355324
U2OS	0.83796954	0.8336354	0.88873523	0.85344672	0.03063748	-8.2852011	0.014257
CaCo-2	0.7851117	0.6874175	0.72178559	0.73143826	0.04955724	-9.3863704	0.01116057
MCF-7	0.56536402	0.61435933	0.53644185	0.57205507	0.03938732	-18.818808	0.00281178

Supplemental table 4: Raw data of G-patch protein and RNA helicase protein levels in human cancer cell lines obtained by quantification of western blot

cell line	target protein	signal target protein	reference protein	signal reference protein
HEK293	NKRF	104000	tubulin	305000
HeLa	NKRF	59900	tubulin	114000
HCT116 wt p53	NKRF	39900	tubulin	244000
HCT116 -/- p53	NKRF	28000	tubulin	134000
A549	NKRF	31200	tubulin	120000
U2OS	NKRF	123000	tubulin	279000
CaCo-2	NKRF	12200	tubulin	57700
MCF-7	NKRF	5590	tubulin	13400
HEK293	NKRF	380000	tubulin	254000
HeLa	NKRF	254000	tubulin	146000
HCT116 wt p53	NKRF	78200	tubulin	74100

HCT116 -/- p53	NKRF	150000	tubulin	113000
A549	NKRF	128000	tubulin	85400
U2OS	NKRF	370000	tubulin	239000
CaCo-2	NKRF	178000	tubulin	173000
MCF-7	NKRF	52300	tubulin	93300
HEK293	NKRF	163000	tubulin	689000
HeLa	NKRF	136000	tubulin	612000
HCT116 wt p53	NKRF	43000	tubulin	293000
HCT116 -/- p53	NKRF	83200	tubulin	406000
A549	NKRF	48900	tubulin	284000
U2OS	NKRF	204000	tubulin	956000
CaCo-2	NKRF	63000	tubulin	652000
MCF-7	NKRF	40700	tubulin	526000
HEK293	PINX1	189000	tubulin	29200
HeLa	PINX1	63100	tubulin	30200
HCT116 wt p53	PINX1	148000	tubulin	31400
HCT116 -/- p53	PINX1	108000	tubulin	28500
A549	PINX1	54200	tubulin	18600
U2OS	PINX1	51600	tubulin	18700
CaCo-2	PINX1	63000	tubulin	22900
MCF-7	PINX1	26500	tubulin	25700
HEK293	PINX1	603000	tubulin	9280
HeLa	PINX1	184000	tubulin	7700
HCT116 wt p53	PINX1	399000	tubulin	16800
HCT116 -/- p53	PINX1	144000	tubulin	1860
A549	PINX1	187000	tubulin	3940
U2OS	PINX1	852000	tubulin	13600
CaCo-2	PINX1	69600	tubulin	2180
MCF-7	PINX1	367000	tubulin	3930
HEK293	PINX1	13700	tubulin	24300
HeLa	PINX1	13300	tubulin	22300
HCT116 wt p53	PINX1	27500	tubulin	35700
HCT116 -/- p53	PINX1	54500	tubulin	35700
A549	PINX1	19600	tubulin	29700
U2OS	PINX1	47200	tubulin	101000
CaCo-2	PINX1	27200	tubulin	71000
MCF-7	PINX1	2380	tubulin	13800
HEK293	GPKOW	854000	tubulin	245000
HeLa	GPKOW	577000	tubulin	130000
HCT116 wt p53	GPKOW	437000	tubulin	81200
HCT116 -/- p53	GPKOW	621000	tubulin	141000
A549	GPKOW	435000	tubulin	103000
U2OS	GPKOW	966000	tubulin	311000
CaCo-2	GPKOW	726000	tubulin	180000
MCF-7	GPKOW	125000	tubulin	30600
HEK293	GPKOW	203000	tubulin	1350000
HeLa	GPKOW	69100	tubulin	192000

HCT116 wt p53	GPKOW	42800	tubulin	145000
HCT116 -/- p53	GPKOW	78700	tubulin	241000
A549	GPKOW	63100	tubulin	190000
U2OS	GPKOW	182000	tubulin	1480000
CaCo-2	GPKOW	120000	tubulin	640000
MCF-7	GPKOW	38900	tubulin	144000
HEK293	GPKOW	764000	tubulin	159000
HeLa	GPKOW	428000	tubulin	72400
HCT116 wt p53	GPKOW	199000	tubulin	38700
HCT116 -/- p53	GPKOW	354000	tubulin	41700
A549	GPKOW	238000	tubulin	27500
U2OS	GPKOW	542000	tubulin	60700
CaCo-2	GPKOW	418000	tubulin	30600
MCF-7	GPKOW	196000	tubulin	15800
HEK293	GPATCH4	23700	tubulin	10200
HeLa	GPATCH4	17600	tubulin	6970
HCT116 wt p53	GPATCH4	10100	tubulin	3530
HCT116 -/- p53	GPATCH4	19600	tubulin	8070
A549	GPATCH4	28200	tubulin	13000
U2OS	GPATCH4	29800	tubulin	13300
CaCo-2	GPATCH4	42900	tubulin	19400
MCF-7	GPATCH4	9260	tubulin	3040
HEK293	GPATCH4	90500	tubulin	3630000
HeLa	GPATCH4	33600	tubulin	945000
HCT116 wt p53	GPATCH4	11600	tubulin	700000
HCT116 -/- p53	GPATCH4	15100	tubulin	1590000
A549	GPATCH4	5840	tubulin	5130
U2OS	GPATCH4	33000	tubulin	4400000
CaCo-2	GPATCH4	25100	tubulin	2290000
MCF-7	GPATCH4	2880	tubulin	460000
HEK293	GPATCH4	124000	tubulin	2160000
HeLa	GPATCH4	52700	tubulin	1560000
HCT116 wt p53	GPATCH4	27700	tubulin	796000
HCT116 -/- p53	GPATCH4	32200	tubulin	1240000
A549	GPATCH4	11800	tubulin	975000
U2OS	GPATCH4	149000	tubulin	2220000
CaCo-2	GPATCH4	52300	tubulin	1730000
MCF-7	GPATCH4	12300	tubulin	1060000
HEK293	GPATCH2	114000	tubulin	2990000
HeLa	GPATCH2	60800	tubulin	1810000
HCT116 wt p53	GPATCH2	36100	tubulin	1280000
HCT116 -/- p53	GPATCH2	75000	tubulin	1730000
A549	GPATCH2	86100	tubulin	1260000
U2OS	GPATCH2	107000	tubulin	3110000
CaCo-2	GPATCH2	137000	tubulin	2140000
MCF-7	GPATCH2	64200	tubulin	1280000
HEK293	GPATCH2	77900	tubulin	1000000

HeLa	GPATCH2	54800	tubulin	748000
HCT116 wt p53	GPATCH2	30300	tubulin	503000
HCT116 -/- p53	GPATCH2	61100	tubulin	706000
A549	GPATCH2	62900	tubulin	545000
U2OS	GPATCH2	70400	tubulin	1100000
CaCo-2	GPATCH2	135000	tubulin	813000
MCF-7	GPATCH2	23600	tubulin	188000
HEK293	GPATCH2	37200	tubulin	1790000
HeLa	GPATCH2	17200	tubulin	822000
HCT116 wt p53	GPATCH2	6160	tubulin	385000
HCT116 -/- p53	GPATCH2	19300	tubulin	766000
A549	GPATCH2	22000	tubulin	507000
U2OS	GPATCH2	31100	tubulin	1830000
CaCo-2	GPATCH2	49400	tubulin	1040000
MCF-7	GPATCH2	25500	tubulin	84100
HEK293	RBM6	11400	tubulin	295000
HeLa	RBM6	4110	tubulin	137000
HCT116 wt p53	RBM6	6300	tubulin	188000
HCT116 -/- p53	RBM6	7450	tubulin	110000
A549	RBM6	11800	tubulin	80400
U2OS	RBM6	6040	tubulin	210000
CaCo-2	RBM6	10100	tubulin	62200
MCF-7	RBM6	15600	tubulin	14400
HEK293	RBM6	56600	tubulin	262000
HeLa	RBM6	74800	tubulin	155000
HCT116 wt p53	RBM6	18500	tubulin	127000
HCT116 -/- p53	RBM6	46600	tubulin	153000
A549	RBM6	32700	tubulin	103000
U2OS	RBM6	88500	tubulin	328000
CaCo-2	RBM6	79900	tubulin	168000
MCF-7	RBM6	15600	tubulin	112000
HEK293	RBM6	30600	tubulin	190000
HeLa	RBM6	37700	tubulin	151000
HCT116 wt p53	RBM6	43400	tubulin	241000
HCT116 -/- p53	RBM6	37200	tubulin	180000
A549	RBM6	41900	tubulin	149000
U2OS	RBM6	20200	tubulin	140000
CaCo-2	RBM6	53700	tubulin	129000
MCF-7	RBM6	48000	tubulin	133000
HEK293	CMTR1	44300	tubulin	280000
HeLa	CMTR1	25200	tubulin	128000
HCT116 wt p53	CMTR1	14700	tubulin	115000
HCT116 -/- p53	CMTR1	20500	tubulin	152000
A549	CMTR1	18700	tubulin	106000
U2OS	CMTR1	43600	tubulin	303000
CaCo-2	CMTR1	22900	tubulin	204000
MCF-7	CMTR1	18700	tubulin	115000

HEK293	CMTR1	14600	tubulin	581000
HeLa	CMTR1	13900	tubulin	420000
HCT116 wt p53	CMTR1	17100	tubulin	697000
HCT116 -/- p53	CMTR1	6720	tubulin	708000
A549	CMTR1	5390	tubulin	418000
U2OS	CMTR1	7040	tubulin	353000
CaCo-2	CMTR1	5750	tubulin	283000
MCF-7	CMTR1	11900	tubulin	675000
HEK293	CMTR1	81000	tubulin	28100
HeLa	CMTR1	42000	tubulin	20200
HCT116 wt p53	CMTR1	58800	tubulin	32900
HCT116 -/- p53	CMTR1	63400	tubulin	27600
A549	CMTR1	39300	tubulin	20500
U2OS	CMTR1	27700	tubulin	17400
CaCo-2	CMTR1	15700	tubulin	14500
MCF-7	CMTR1	50300	tubulin	29500
HEK293	DHX15	2020	tubulin	9890
HeLa	DHX15	1610	tubulin	20100
HCT116 wt p53	DHX15	2770	tubulin	32100
HCT116 -/- p53	DHX15	12100	tubulin	62900
A549	DHX15	10200	tubulin	58600
U2OS	DHX15	10500	tubulin	66000
CaCo-2	DHX15	15200	tubulin	42900
MCF-7	DHX15	1240	tubulin	16700
HEK293	DHX15	19600	tubulin	256000
HeLa	DHX15	11600	tubulin	177000
HCT116 wt p53	DHX15	9410	tubulin	104000
HCT116 -/- p53	DHX15	15000	tubulin	107000
A549	DHX15	4030	tubulin	72900
U2OS	DHX15	16600	tubulin	293000
CaCo-2	DHX15	18100	tubulin	205000
MCF-7	DHX15	3860	tubulin	149000
HEK293	DHX15	46600	tubulin	500000
HeLa	DHX15	35800	tubulin	245000
HCT116 wt p53	DHX15	17100	tubulin	294000
HCT116 -/- p53	DHX15	25400	tubulin	286000
A549	DHX15	109000	tubulin	417000
U2OS	DHX15	131000	tubulin	463000
CaCo-2	DHX15	61000	tubulin	395000
MCF-7	DHX15	104000	tubulin	474000
HEK293	DHX16	7780	tubulin	20800
HeLa	DHX16	4530	tubulin	15300
HCT116 wt p53	DHX16	6940	tubulin	33900
HCT116 -/- p53	DHX16	10500	tubulin	44600
A549	DHX16	8780	tubulin	43800
U2OS	DHX16	14700	tubulin	46900
CaCo-2	DHX16	8340	tubulin	28400

MCF-7	DHX16	4610	tubulin	21800
HEK293	DHX16	37300	tubulin	409000
HeLa	DHX16	25000	tubulin	236000
HCT116 wt p53	DHX16	16600	tubulin	150000
HCT116 -/- p53	DHX16	26900	tubulin	208000
A549	DHX16	9510	tubulin	135000
U2OS	DHX16	35200	tubulin	463000
CaCo-2	DHX16	20500	tubulin	327000
MCF-7	DHX16	7900	tubulin	141000
HEK293	DHX16	80100	tubulin	241000
HeLa	DHX16	42600	tubulin	98900
HCT116 wt p53	DHX16	23800	tubulin	64000
HCT116 -/- p53	DHX16	53700	tubulin	116000
A549	DHX16	19300	tubulin	95000
U2OS	DHX16	96000	tubulin	325000
CaCo-2	DHX16	46300	tubulin	193000
MCF-7	DHX16	11500	tubulin	64500
HEK293	GPATCH11	5020	tubulin	97300
HeLa	GPATCH11	4830	tubulin	92300
HCT116 wt p53	GPATCH11	4260	tubulin	120000
HCT116 -/- p53	GPATCH11	8790	tubulin	114000
A549	GPATCH11	11200	tubulin	88800
U2OS	GPATCH11	4100	tubulin	98700
CaCo-2	GPATCH11	6600	tubulin	88300
MCF-7	GPATCH11	3610	tubulin	76400
HEK293	GPATCH11	51800	tubulin	112000
HeLa	GPATCH11	49600	tubulin	92400
HCT116 wt p53	GPATCH11	52800	tubulin	132000
HCT116 -/- p53	GPATCH11	63500	tubulin	147000
A549	GPATCH11	62900	tubulin	135000
U2OS	GPATCH11	62200	tubulin	142000
CaCo-2	GPATCH11	62900	tubulin	89000
MCF-7	GPATCH11	58300	tubulin	81000
HEK293	GPATCH11	2670	tubulin	78200
HeLa	GPATCH11	5210	tubulin	62500
HCT116 wt p53	GPATCH11	2780	tubulin	72000
HCT116 -/- p53	GPATCH11	6230	tubulin	95000
A549	GPATCH11	3260	tubulin	80500
U2OS	GPATCH11	2340	tubulin	93200
CaCo-2	GPATCH11	5530	tubulin	79300
MCF-7	GPATCH11	5980	tubulin	82900

5.3 G-patch protein and RNA helicase mRNA levels in matched-pair fibromyxosarcoma tissue samples

Supplemental table 5: Ratios of G-patch protein and RNA helicase mRNA levels in matched-pair fibromyxosarcoma tissue samples

	round 1	round 2	round 3	mean value	standard deviation	t test	*p* value
GPATCH1							
TIS 1	1	1	1	1	0		
CA 1	0.0953962	0.26648721	0.48609442	0.28265928	0.19585052	-6.3439738	0.02395787
TIS 2	1	1	1	1	0		
CA 2	0.19346279	0.21529743	0.1720792	0.19361314	0.02160951	-64.633728	0.00023929
TIS 3	1	1	1	1	0		
CA 3	2.15838991	1.97086334	1.83452874	1.98792733	0.1626035	10.5233915	0.00890952
GPATCH3							
TIS 1	1	1	1	1	0		
CA 1	1.19672155	0.13189809	0.27647608	0.53503191	0.57758167	-1.3943454	0.29791296
TIS 2	1	1	1	1	0		
CA 2	0.5018857	0.56867231	0.49208571	0.52088124	0.04167733	-19.911498	0.00251277
TIS 3	1	1	1	1	0		
CA 3	2.37200261	2.03908067	1.67625648	2.02911325	0.34798014	5.12235101	0.03606294
GPATCH4							
TIS 1	1	1	1	1	0		
CA 1	1.41292268	0.49179008	1.57843869	1.16105048	0.58547502	0.47644665	0.680733
TIS 2	1	1	1	1	0		
CA 2	0.25543402	0.30909231	0.28709126	0.28387253	0.02697356	-45.984624	0.00047257
TIS 3	1	1	1	1	0		
CA 3	2.45418456	1.81593251	2.10072802	2.12361503	0.31974096	6.08667192	0.02594639
RBM5							
TIS 1	1	1	1	1	0		
CA 1	2.07932269	11.9856258	1.26741855	5.11078903	5.96760697	1.19312406	0.35516651
TIS 2	1	1	1	1	0		
CA 2	0.5103141	0.55582523	0.81681623	0.62765185	0.16539404	-3.8993298	0.05991852
TIS 3	1	1	1	1	0		
CA 3	3.67044383	3.32621257	3.93577186	3.64414275	0.30562958	14.984772	0.00442395
SUGP1							
TIS 1	1	1	1	1	0		
CA 1	0.4982451	0.98127313	0.98766944	0.82239589	0.28074104	-1.0957406	0.38752435
TIS 2	1	1	1	1	0		
CA 2	0.16154555	0.1759526	0.283907	0.20713505	0.06687555	-20.534894	0.00236305
TIS 3	1	1	1	1	0		
CA 3	1.03082908	1.27679794	0.98160375	1.09641026	0.15814731	1.05589823	0.40172819
DHX15							
TIS 1	1	1	1	1	0		
CA 1	0.00036905	1.40115142	0.27791344	0.5598113	0.74171937	-1.0279214	0.41205188
TIS 2	1	1	1	1	0		
CA 2	0.83356123	0.89556853	0.97543765	0.90152247	0.07112536	-2.3981332	0.13862308

TIS 3	1	1	1	1	0		
CA 3	0.23204135	0.74133267	0.67180706	0.54839369	0.27616581	-2.8323747	0.10532356
DHX35							
TIS 1	1	1	1	1	0		
CA 1	0.0750514	0.03835695	0.08103097	0.06481311	0.02310595	-70.102771	0.00020342
TIS 2	1	1	1	1	0		
CA 2	5.1664062	3.03070515	0.79115339	2.99608824	2.18783181	1.5802523	0.25482983
TIS 3	1	1	1	1	0		
CA 3	1.8835949	2.04572621	2.21819498	2.04917203	0.16732665	10.8603097	0.00837211
TFIP11							
TIS 1	1	1	1	1	0		
CA 1	0.05770116	0.03330632	0.0844258	0.05847776	0.02556858	-63.780004	0.00024574
TIS 2	1	1	1	1	0		
CA 2	1.9712234	3.43609143	1.98575166	2.4643555	0.84157936	3.01378368	0.09471458
TIS 3	1	1	1	1	0		
CA 3	1.16673798	0.82580597	0.7373736	0.90997252	0.22671888	-0.6877776	0.56264646
SUGP2							
TIS 1	1	1	1	1	0		
CA 1	0.52055934	0.12495823	0.35730905	0.33427554	0.19880384	-5.8000317	0.02846315
TIS 2	1	1	1	1	0		
CA 2	3.46626826	2.06485944	3.42471781	2.98528183	0.79737987	4.31238504	0.04979113
TIS 3	1	1	1	1	0		
CA 3	2.48024677	1.72785936	2.58995928	2.2660218	0.46927957	4.67272434	0.0428754
NKRF							
TIS 1	1	1	1	1	0		
CA 1	0.5870797	0.76671805	3.06021577	1.47133784	1.37893702	0.59203653	0.61383963
TIS 2	1	1	1	1	0		
CA 2	0.34508137	0.30343834	0.23709728	0.29520566	0.05446075	-22.415033	0.00198439
TIS 3	1	1	1	1	0		
CA 3	1.09592312	3.07943832	2.07324126	2.08286756	0.99179264	1.8911026	0.19916466
ZGPAT							
TIS 1	1	1	1	1	0		
CA 1	0.19434437	0.10547372	0.19170783	0.16384197	0.05056558	-28.641386	0.0012168
TIS 2	1	1	1	1	0		1
CA 2	0.84528424	0.82148162	0.50758858	0.72478481	0.18847359	-2.5291962	0.12717988
TIS 3	1	1	1	1	0		1
CA 3	0.78530015	0.95636246	0.59409273	0.77858511	0.18122819	-2.1161268	0.16857809

Supplemental table 6: Raw data of G-patch protein and RNA helicase mRNA levels in matched-pair fibromyxosarcoma tissue samples as quantified by RT-qPCR

	target/ reference	Ct value	target/ reference	Ct value
round 1				
TIS 1	GPATCH4	30.5585013	TFIP11	30.8071963
CA 1	GPATCH4	24.7106521	TFIP11	29.5732854
TIS 2	GPATCH4	26.3186843	TFIP11	35.3266392
CA 2	GPATCH4	26.6872666	TFIP11	32.7471528

TIS 3	GPATCH4	25.9194735	TFIP11	29.8648504
CA 3	GPATCH4	26.6094744	TFIP11	31.5783559
TIS 1	GPATCH1	27.7023278	GPATCH2	33.232327
CA 1	GPATCH1	25.7430855	GPATCH2	27.2412282
TIS 2	GPATCH1	27.7949162	GPATCH2	27.9261869
CA 2	GPATCH1	27.3696287	GPATCH2	27.9653124
TIS 3	GPATCH1	27.0999677	GPATCH2	29.2856588
CA 3	GPATCH1	26.9694045	GPATCH2	28.0600366
TIS 1	RBM5	30.9880797	GPATCH3	36.3810893
CA 1	RBM5	24.5827993	GPATCH3	30.7728352
TIS 2	RBM5	30.1456634	GPATCH3	35.025601
CA 2	RBM5	27.3458294	GPATCH3	33.6542627
TIS 3	RBM5	26.7692033	GPATCH3	34.0335446
CA 3	RBM5	26.0079611	GPATCH3	33.2593027
TIS 1	SUGP1	30.2247329	SUGP2	31.1128559
CA 1	SUGP1	28.6703892	SUGP2	26.7055547
TIS 2	SUGP1	31.1380839	SUGP2	33.4308203
CA 2	SUGP1	31.058679	SUGP2	30.0370419
TIS 3	SUGP1	29.8180838	SUGP2	28.8267804
CA 3	SUGP1	30.2461423	SUGP2	29.0786241
TIS 1	DHX15	26.6148315	NKRF	33.3258454
CA 1	DHX15	32.6695551	NKRF	25.5451821
TIS 2	DHX15	29.9733911	NKRF	28.8749272
CA 2	DHX15	28.635636	NKRF	27.8185995
TIS 3	DHX15	25.4654416	NKRF	28.1905644
CA 3	DHX15	28.0448514	NKRF	28.5302815
TIS 1	DHX35	32.174635	ZGPAT	32.0641339
CA 1	DHX35	30.5614456	ZGPAT	29.0782801
TIS 2	DHX35	36.6117404	ZGPAT	32.7563079
CA 2	DHX35	32.6421843	ZGPAT	31.3984044
TIS 3	DHX35	31.4344881	ZGPAT	30.2801347
CA 3	DHX35	32.1254414	ZGPAT	31.1006822
TIS 1	PSMB2	27.2760746	PSMB2	27.0982209
CA 1	PSMB2	22.6989823	PSMB2	23.0239219
TIS 2	PSMB2	27.7175812	PSMB2	28.2380695
CA 2	PSMB2	27.4182002	PSMB2	27.2739134
TIS 3	PSMB2	25.08696	PSMB2	25.1216638
CA 3	PSMB2	27.0452502	PSMB2	27.8504063
TIS 1	EMC7	30.4906499	EMC7	30.4906499
CA 1	EMC7	22.1919329	EMC7	22.1919329
TIS 2	EMC7	29.0903747	EMC7	29.0903747
CA 2	EMC7	25.7214777	EMC7	25.7214777
TIS 3	EMC7	24.46217	EMC7	24.46217
CA 3	EMC7	26.0179446	EMC7	26.0179446
TIS 1	COPS6	31.5159966	EMC7	30.4906499
CA 1	COPS6	22.8141954	EMC7	22.1919329
TIS 2	COPS6	30.1094244	EMC7	29.0903747

CA 2	COPS6	27.77207	EMC7	25.7214777
TIS 3	COPS6	25.8824121	EMC7	24.46217
CA 3	COPS6	26.0746283	EMC7	26.0179446
TIS 1	COPS6	31.5159966	PSMB2	27.4967648
CA 1	COPS6	22.8141954	PSMB2	22.7008205
TIS 2	COPS6	30.1094244	PSMB2	27.8432012
CA 2	COPS6	27.77207	PSMB2	27.1686135
TIS 3	COPS6	25.8824121	PSMB2	25.2446775
CA 3	COPS6	26.0746283	PSMB2	28.1650737
TIS 1	COPS6	26.0072351	PSMB2	27.4967648
CA 1	COPS6	30.1094244	PSMB2	22.7008205
TIS 2	COPS6	27.77207	PSMB2	27.8432012
CA 2	COPS6	31.5159966	PSMB2	27.1686135
TIS 3	COPS6	22.8141954	PSMB2	25.2446775
CA 3	COPS6	25.8824121	PSMB2	28.1650737
TIS 1	EMC7	29.637251	EMC7	29.6699504
CA 1	EMC7	22.7442063	EMC7	21.9420609
TIS 2	EMC7	29.3029003	EMC7	29.6356942
CA 2	EMC7	25.93222	EMC7	25.4671816
TIS 3	EMC7	24.1407707	EMC7	23.9216537
CA 3	EMC7	26.11888	EMC7	25.5259907
round 2				
TIS 1	SUGP1	29.879532	DHX35	27.6505296
CA 1	SUGP1	28.8419147	DHX35	30.2110217
TIS 2	SUGP1	31.3550899	DHX35	35.6738506
CA 2	SUGP1	30.8207988	DHX35	31.0331647
TIS 3	SUGP1	29.1726764	DHX35	31.9075682
CA 3	SUGP1	29.6848019	DHX35	31.7396109
TIS 1	DHX15	28.2336232	GPATCH4	23.7464283
CA 1	DHX15	25.7043205	GPATCH4	23.7203628
TIS 2	DHX15	32.43927	GPATCH4	26.935547
CA 2	DHX15	29.4341161	GPATCH4	25.4651592
TIS 3	DHX15	27.6308714	GPATCH4	26.1076487
CA 3	DHX15	29.0694083	GPATCH4	25.8191349
TIS 1	RBM5	30.5992796	TFIP11	25.779989
CA 1	RBM5	24.9733565	TFIP11	28.6453593
TIS 2	RBM5	29.9749071	TFIP11	35.4203297
CA 2	RBM5	27.7811714	TFIP11	30.4221906
TIS 3	RBM5	26.6454242	TFIP11	30.7701089
CA 3	RBM5	25.7761996	TFIP11	31.5543582
TIS 1	DHX35	27.5488681	SUGP2	26.1016988
CA 1	DHX35	30.2105465	SUGP2	27.0594912
TIS 2	DHX35	37.7336862	SUGP2	32.8925863
CA 2	DHX35	31.4270747	SUGP2	28.6822646
TIS 3	DHX35	31.6635252	SUGP2	28.6752656
CA 3	DHX35	31.7567664	SUGP2	28.3715118
TIS 1	GPATCH1	26.2314508	NKRF	26.5443621

CA 1	GPATCH1	26.0966228	NKRF	25.2700441
TIS 2	GPATCH1	27.7513836	NKRF	29.2435161
CA 2	GPATCH1	26.9569774	NKRF	27.6142294
TIS 3	GPATCH1	27.0132364	NKRF	28.0694227
CA 3	GPATCH1	26.9100108	NKRF	27.4534854
TIS 1	GPATCH3	30.9776883	ZGPAT	29.4925009
CA 1	GPATCH3	31.857503	ZGPAT	30.6948556
TIS 2	GPATCH3	35.8881241	ZGPAT	33.6392478
CA 2	GPATCH3	33.7184151	ZGPAT	30.7586694
TIS 3	GPATCH3	34.266205	ZGPAT	30.9540092
CA 3	GPATCH3	34.245016	ZGPAT	32.0251097
TIS 1	EMC7	29.8114333	PSMB2	20.6509374
CA 1	EMC7	22.5346035	PSMB2	22.0799057
TIS 2	EMC7	29.5779029	PSMB2	27.7709351
CA 2	EMC7	25.9340674	PSMB2	25.8513245
TIS 3	EMC7	23.9358001	PSMB2	24.9375929
CA 3	EMC7	25.7940714	PSMB2	26.8584252
TIS 1	EMC7	29.8114333	COPS6	23.5576878
CA 1	EMC7	22.5346035	COPS6	22.5220489
TIS 2	EMC7	29.5779029	COPS6	29.9338447
CA 2	EMC7	25.9340674	COPS6	25.7207642
TIS 3	EMC7	23.9358001	COPS6	26.2428042
CA 3	EMC7	25.7940714	COPS6	25.7663458
TIS 1	EMC7	29.8114333	COPS6	23.5576878
CA 1	EMC7	22.5346035	COPS6	22.5220489
TIS 2	EMC7	29.5779029	COPS6	29.9338447
CA 2	EMC7	25.9340674	COPS6	25.7207642
TIS 3	EMC7	23.9358001	COPS6	26.2428042
CA 3	EMC7	25.7940714	COPS6	25.7663458
TIS 1	COPS6	22.6761085	COPS6	24.1308145
CA 1	COPS6	22.5735601	COPS6	23.6075553
TIS 2	COPS6	30.0588604	COPS6	30.1688696
CA 2	COPS6	25.6795635	COPS6	27.6707693
TIS 3	COPS6	25.8225498	COPS6	26.7701231
CA 3	COPS6	25.4725413	COPS6	26.0355525
TIS 1	COPS6	22.6761085	COPS6	23.8127054
CA 1	COPS6	22.5735601	COPS6	22.8916662
TIS 2	COPS6	30.0588604	COPS6	30.7314237
CA 2	COPS6	25.6795635	COPS6	26.0806387
TIS 3	COPS6	25.8225498	COPS6	26.0521216
CA 3	COPS6	25.4725413	COPS6	25.3496808
TIS 1	COPS6	22.6761085	PSMB2	21.2216561
CA 1	COPS6	22.5735601	PSMB2	23.0160379
TIS 2	COPS6	30.0588604	PSMB2	28.0916519
CA 2	COPS6	25.6795635	PSMB2	26.1779685
TIS 3	COPS6	25.8225498	PSMB2	25.2817869
CA 3	COPS6	25.4725413	PSMB2	27.0095749

round 3				
TIS 1	ZGPAT	29.0366776	TFIP11	26.092098
CA 1	ZGPAT	30.3548058	TFIP11	28.5933797
TIS 2	ZGPAT	33.5712946	TFIP11	35.0328532
CA 2	ZGPAT	31.5085307	TFIP11	30.2110524
TIS 3	ZGPAT	31.6978398	TFIP11	30.7571994
CA 3	ZGPAT	31.6567008	TFIP11	31.8979804
TIS 1	NKRF	26.2049442	SUGP2	26.1958097
CA 1	NKRF	25.5232855	SUGP2	26.6156747
TIS 2	NKRF	28.996944	SUGP2	34.4968932
CA 2	NKRF	27.6764363	SUGP2	28.5809488
TIS 3	NKRF	28.9400925	SUGP2	28.705308
CA 3	NKRF	27.6111544	SUGP2	28.780978
TIS 1	GPATCH1	26.1297806	SUGP1	29.879532
CA 1	GPATCH1	26.1055815	SUGP1	28.8419147
TIS 2	GPATCH1	27.7881316	SUGP1	31.3550899
CA 2	GPATCH1	26.9626962	SUGP1	30.8207988
TIS 3	GPATCH1	27.0361605	SUGP1	29.1726764
CA 3	GPATCH1	26.9219885	SUGP1	29.6848019
TIS 1	GPATCH3	30.8904803	GPATCH4	24.0706093
CA 1	GPATCH3	31.6803631	GPATCH4	24.0296041
TIS 2	GPATCH3	35.6291519	GPATCH4	26.613659
CA 2	GPATCH3	33.40245	GPATCH4	25.3730453
TIS 3	GPATCH3	33.9481717	GPATCH4	25.7106725
CA 3	GPATCH3	34.0675846	GPATCH4	25.7146176
TIS 1	COPS6	23.5956557	EMC7	21.8842421
CA 1	COPS6	23.4530405	EMC7	22.6519656
TIS 2	COPS6	30.581507	EMC7	29.4913787
CA 2	COPS6	26.445806	EMC7	24.8110073
TIS 3	COPS6	26.5913458	EMC7	24.7776896
CA 3	COPS6	26.0219292	EMC7	25.7748941
TIS 1	EMC7	21.9519668	EMC7	21.8842421
CA 1	EMC7	22.4548706	EMC7	22.6519656
TIS 2	EMC7	29.6694962	EMC7	29.3009624
CA 2	EMC7	24.8787597	EMC7	24.8110073
TIS 3	EMC7	24.7750425	EMC7	24.7776896
CA 3	EMC7	26.3708509	EMC7	25.7748941
TIS 1	PSMB2	20.6509374	EMC7	21.8842421
CA 1	PSMB2	22.0799057	EMC7	22.6519656
TIS 2	PSMB2	27.7709351	EMC7	29.4913787
CA 2	PSMB2	25.8513245	EMC7	24.8110073
TIS 3	PSMB2	24.9375929	EMC7	24.7776896
CA 3	PSMB2	26.8584252	EMC7	25.7748941
TIS 1	PSMB2	20.6509374	EMC7	29.8114333
CA 1	PSMB2	22.0799057	EMC7	22.5346035
TIS 2	PSMB2	27.7709351	EMC7	29.5779029
CA 2	PSMB2	25.8513245	EMC7	25.9340674

TIS 3	PSMB2	24.9375929	EMC7	23.9358001
CA 3	PSMB2	26.8584252	EMC7	25.7940714

5.4 G-patch protein and RNA helicase mRNA levels in matched-pair squamous cell carcinoma tissue samples

Supplemental table 7: Internal normalization - Ratios of G-patch protein and RNA helicase mRNA expression in matched-pair squamous cell carcinoma tissue samples

	round 1	round 2	round 3	mean ratio	standard deviation	t test	*p* value
AGGF1							
TIS 1	1	1	1	1	0		
CA 1	0.89009036	0.78630059	0.38168189	0.68602428	0.26862854	-2.0244383	0.18021805
TIS 2	1	1	1	1	0		
CA 2	2.28447874	1.08879486	2.39373159	1.92233506	0.72393093	2.2067453	0.15805729
TIS 3	1	1	1	1	0		
CA 3	0.21122956	0.1473378	0.45642131	0.27166289	0.1631634	-7.7316168	0.01632019
TIS 4	1	1	1	1	0		
CA 4	0.93331587	1.06638171	0.58411347	0.86127035	0.24907545	-0.9647149	0.43647243
CHERP							
TIS 1	1	1	1	1	0		
CA 1	0.9266461	0.86232319	0.53075666	0.77324198	0.21244695	-1.848727	0.20574193
TIS 2	1	1	1	1	0		
CA 2	2.43594023	1.06348144	1.35704993	1.61882387	0.7227067	1.48308349	0.27628944
TIS 3	1	1	1	1	0		
CA 3	0.5788372	0.55376194	1.40789063	0.84682992	0.48605455	-0.5458201	0.63993399
TIS 4	1	1	1	1	0		
CA 4	1.90966009	2.09417457	2.96262932	2.32215466	0.5622875	4.07271908	0.05533173
CMTR1							
TIS 1	1	1	1	1	0		
CA 1	1.18409319	1.06619187	0.93557559	1.06195355	0.124313	0.86319773	0.4790088
TIS 2	1	1	1	1	0		
CA 2	14.8125476	6.97358028	13.8526667	11.8795982	4.27575741	4.40717631	0.04782182
TIS 3	1	1	1	1	0		
CA 3	0.50000944	0.38543852	0.6233605	0.50293615	0.11898799	-7.2355188	0.01857078
TIS 4	1	1	1	1	0		
CA 4	1.36079271	2.33904767	0.72756278	1.47580106	0.81187504	1.01507198	0.41689209
GPATCH1							
TIS 1	1	1	1	1	0		
CA 1	0.53651907	0.50254248	0.45085722	0.49663959	0.04313492	-20.212065	0.00243886
TIS 2	1	1	1	1	0		
CA 2	1.87613585	1.4377687	2.11934088	1.81108181	0.34541161	4.06713287	0.0554714
TIS 3	1	1	1	1	0		
CA 3	0.38776097	0.28368875	0.36728403	0.34624458	0.05513393	-20.537945	0.00236235
TIS 4	1	1	1	1	0		
CA 4	0.9215127	0.56613086	0.62320177	0.70361511	0.19085018	-2.6898255	0.11488059

GPATCH2							
TIS 1	1	1	1	1	0		
CA 1	0.98000778	0.72859237	0.89731755	0.86863924	0.12813767	-1.7756178	0.21778334
TIS 2	1	1	1	1	0		
CA 2	0.35894279	2.00306798	2.48111698	1.61437592	1.11320122	0.95591909	0.43999403
TIS 3	1	1	1	1	0		
CA 3	2.66221403	0.27679439	0.38875414	1.10925419	1.34606722	0.14058273	0.90108055
TIS 4	1	1	1	1	0		
CA 4	1.70516396	2.16422468	1.00652497	1.62530454	0.58296681	1.8578403	0.2043033
GPATCH3							
TIS 1	1	1	1	1	0		
CA 1	1.10817963	1.12201341	1.21379099	1.14799468	0.05739956	4.46578867	0.04666067
TIS 2	1	1	1	1	0		
CA 2	2.46789	3.57216419	2.02521107	2.68842175	0.79670677	3.67065071	0.06686108
TIS 3	1	1	1	1	0		
CA 3	0.35115834	0.36505479	0.47337214	0.39652842	0.06691036	-15.62155	0.00407279
TIS 4	1	1	1	1	0		
CA 4	0.76044348	1.03876278	0.50552611	0.76824413	0.26670391	-1.5050884	0.27123473
GPATCH4							
TIS 1	1	1	1	1	0		
CA 1	1.33170261	2.14654447	1.40520551	1.62781753	0.45073151	2.41254898	0.1372959
TIS 2	1	1	1	1	0		
CA 2	1.10028041	1.17995223	1.3427301	1.20765425	0.12357595	2.91049928	0.10055774
TIS 3	1	1	1	1	0		
CA 3	0.08602478	0.24838422	0.19392409	0.17611103	0.08263248	-17.269451	0.0033363
TIS 4	1	1	1	1	0		
CA 4	2.26255455	1.64111075	1.61832713	1.84066414	0.36554536	3.98328954	0.05763104
GPKOW							
TIS 1	1	1	1	1	0		
CA 1	1.87497971	3.19350512	2.38752154	2.48533545	0.66468262	3.87053368	0.06073352
TIS 2	1	1	1	1	0		
CA 2	4.75501035	3.80568457	3.69655358	4.0857495	0.58215974	9.18077044	0.01165724
TIS 3	1	1	1	1	0		
CA 3	0.16849253	0.35420648	0.31581829	0.27950577	0.09803758	-12.729125	0.00611512
TIS 4	1	1	1	1	0		
CA 4	0.21236694	0.25211945	0.22527883	0.22992174	0.02027888	-65.773595	0.00023107
PINX1							
TIS 1	1	1	1	1	0		
CA 1	2.42033822	2.66317521	2.18641192	2.42330845	0.23839552	10.3409766	0.00922224
TIS 2	1	1	1	1	0		
CA 2	3.46358831	3.21960483	3.45296901	3.37872072	0.13790066	29.8770522	0.0011184
TIS 3	1	1	1	1	0		
CA 3	1.42540252	2.9462202	2.42746244	2.26636172	0.77310199	2.83714552	0.10502344
TIS 4	1	1	1	1	0		
CA 4	0.86811988	1.72654554	2.00209911	1.53225484	0.59142952	1.55875282	0.25938997
RBM5							
TIS 1	1	1	1	1	0		

CA 1	1.17467766	1.14163009	0.98661357	1.10097377	0.1004078	1.74181389	0.22366568
TIS 2	1	1	1	1	0		
CA 2	2.67419911	2.75396805	4.43381528	3.28732748	0.99368832	3.98693166	0.0575347
TIS 3	1	1	1	1	0		
CA 3	0.55602219	0.45174683	0.8088339	0.6055343	0.18362021	-3.720912	0.0652387
TIS 4	1	1	1	1	0		
CA 4	1.30647611	1.22944686	1.61090998	1.38227765	0.2017125	3.28251503	0.08160844
SUGP1							
TIS 1	1	1	1	1	0		
CA 1	1.39467703	1.2314837	1.15404506	1.2600686	0.12283631	3.66709184	0.06697817
TIS 2	1	1	1	1	0		
CA 2	3.23752631	2.44403362	3.61527621	3.09894538	0.59779244	6.08150886	0.02598876
TIS 3	1	1	1	1	0		
CA 3	0.41262349	0.34423622	0.25717144	0.33801038	0.07791281	-14.716446	0.00458563
TIS 4	1	1	1	1	0		
CA 4	0.6886684	0.90913883	0.60130424	0.73303716	0.15864102	-2.9147141	0.10030939
DHX15							
TIS 1	1	1	1	1	0		
CA 1	3.51214112	3.05538043	2.08748251	2.88500135	0.7274509	4.48816287	0.04622829
TIS 2	1	1	1	1	0		
CA 2	3.6703163	2.93868128	3.69494765	3.43464841	0.42969666	9.81374799	0.01022421
TIS 3	1	1	1	1	0		
CA 3	0.13598215	0.13234115	0.17664	0.1483211	0.02459236	-59.984123	0.00027781
TIS 4	1	1	1	1	0		
CA 4	0.57933346	0.64449162	0.3922575	0.53869419	0.13093577	-6.1022676	0.02581902
DHX35							
TIS 1	1	1	1	1	0		
CA 1	0.88886191	0.7882375	0.3881592	0.68841954	0.26485566	-2.0376124	0.17847988
TIS 2	1	1	1	1	0		
CA 2	4.05950652	2.94673367	4.32862014	3.77828678	0.73260901	6.56848851	0.02240175
TIS 3	1	1	1	1	0		
CA 3	0.13720682	0.17800911	0.25983942	0.19168511	0.06244969	-22.418727	0.00198374
TIS 4	1	1	1	1	0		
CA 4	2.22545639	0.94737472	1.72901739	1.6339495	0.64432261	1.7041661	0.23046456
GPATCH8							
TIS 1	1	1	1	1	0		
CA 1	1.31665558	1.02157089	0.46800185	0.93540944	0.43083771	-0.2596665	0.81940701
TIS 2	1	1	1	1	0		
CA 2	1.72753178	1.87768143	2.95265218	2.18595513	0.66820993	3.07408564	0.0915246
TIS 3	1	1	1	1	0		
CA 3	0.12919473	0.12073075	0.20016485	0.15003011	0.04362372	-33.747493	0.00087689
TIS 4	1	1	1	1	0		
CA 4	0.41001412	0.24515778	0.25896537	0.30471242	0.09145489	-13.167949	0.00571777
GPANK1							
TIS 1	1	1	1	1	0		
CA 1	1.46725699	1.1126095	0.93377494	1.17121381	0.27152647	1.09216246	0.38877641
TIS 2	1	1	1	1	0		

CA 2	8.01834482	14.8967362	17.0034011	13.3061607	4.6989634	4.53608463	0.04532173
TIS 3	1	1	1	1	0		
CA 3	1.50467252	1.10872581	2.84929515	1.82089783	0.91235642	1.55842246	0.25946085
TIS 4	1	1	1	1	0		
CA 4	0.51016715	0.79916415	1.46889049	0.92607393	0.49179994	-0.2603573	0.8189423
RBM17							
TIS 1	1	1	1	1	0		
CA 1	0.25450998	0.55620788	0.37298937	0.39456907	0.1520022	-6.8988286	0.02037129
TIS 2	1	1	1	1	0		
CA 2	1.59056402	1.407042	1.82804985	1.60855196	0.21107955	4.99358139	0.03784122
TIS 3	1	1	1	1	0		
CA 3	0.18009118	0.20133566	0.37338057	0.25160247	0.10599651	-12.229294	0.00662015
TIS 4	1	1	1	1	0		
CA 4	0.35755994	0.30933806	0.72622277	0.46437359	0.22804623	-4.0681759	0.05544529
TFIP11							
TIS 1	1	1	1	1	0		
CA 1	2.89936999	5.19128189	5.3467179	4.47912326	1.37031215	4.3975515	0.04801653
TIS 2	1	1	1	1	0		
CA 2	3.45061023	3.34382528	1.76631194	2.85358248	0.94311647	3.40413844	0.07652124
TIS 3	1	1	1	1	0		
CA 3	0.09888814	0.09754656	0.23308595	0.14317355	0.07786931	-19.058432	0.00274181
TIS 4	1	1	1	1	0		
CA 4	0.50871834	0.42709665	0.37814621	0.43798707	0.06596379	-14.757112	0.00456056
GPATCH11							
TIS 1	1	1	1	1	0		
CA 1	1.81825517	1.1126095	0.91424815	1.28170427	0.47513362	1.026924	0.41242534
TIS 2	1	1	1	1	0		
CA 2	1.2067036	14.8967362	1.21101323	5.77148436	7.90270024	1.04577589	0.40542967
TIS 3	1	1	1	1	0		
CA 3	0.21377369	1.10872581	0.50513827	0.60921259	0.45646295	-1.4828447	0.27634494
TIS 4	1	1	1	1	0		
CA 4	0.76276028	0.79916415	0.66564478	0.74252307	0.06902184	-6.4611887	0.02312614
RBM10							
TIS 1	1	1	1	1	0		
CA 1	1.28845481	4.58016231	1.07542131	2.31467948	1.964855	1.15891078	0.36616386
TIS 2	1	1	1	1	0		
CA 2	3.09824951	1.34192235	2.01607261	2.15208149	0.8860277	2.25214593	0.15312278
TIS 3	1	1	1	1	0		
CA 3	0.3554368	0.343649	1.57546177	0.75818252	0.70780913	-0.5917417	0.61400329
TIS 4	1	1	1	1	0		
CA 4	0.3784452	0.18257786	0.18050547	0.24717618	0.11368703	-11.469462	0.00751616
SON							
TIS 1	1	1	1	1	0		
CA 1	2.26720533	2.1013219	1.35300139	1.9071762	0.48704376	3.22614805	0.08413207
TIS 2	1	1	1	1	0		
CA 2	4.08941034	4.33319546	2.95246677	3.79169086	0.73694002	6.56138933	0.02244863
TIS 3	1	1	1	1	0		

CA 3	0.41286585	0.42563587	1.00558862	0.61469678	0.33858247	-1.9710552	0.18749995
TIS 4	1	1	1	1	0		
CA 4	0.64007327	0.50676932	0.28937864	0.47874041	0.17701948	-5.1002754	0.03635894
SUGP2							
TIS 1	1	1	1	1	0		
CA 1	1.08327131	1.07173011	0.74380003	0.96626715	0.19274858	-0.3031255	0.79041819
TIS 2	1	1	1	1	0		
CA 2	2.42515222	3.28506169	5.23655422	3.64892271	1.44058718	3.18486016	0.0860522
TIS 3	1	1	1	1	0		
CA 3	0.2594212	0.25559705	0.56268191	0.35923339	0.17620196	-6.2986831	0.02429115
TIS 4	1	1	1	1	0		
CA 4	0.50530438	0.46070655	0.78423491	0.58341528	0.17533863	-4.1151566	0.05428716
NKRF							
TIS 1	1	1	1	1	0		
CA 1	0.74825449	0.3730056	0.38510433	0.50212147	0.21324327	-4.0439771	0.05605591
TIS 2	1	1	1	1	0		
CA 2	1.35351101	1.40466167	1.49722978	1.41846749	0.07284725	9.94968166	0.00995088
TIS 3	1	1	1	1	0		
CA 3	0.38564231	0.45936642	0.57462728	0.47321201	0.09525023	-9.5792274	0.01072284
TIS 4	1	1	1	1	0		
CA 4	0.93632424	0.54502098	0.367402	0.61624908	0.29107252	-2.2835412	0.14983364
ZGPAT							
TIS 1	1	1	1	1	0		
CA 1	6.77454688	3.17697574	3.94514672	4.63222311	1.89464641	3.32051139	0.0799682
TIS 2	1	1	1	1	0		
CA 2	4.12232435	3.95451528	2.43305552	3.50329838	0.93064752	4.6589497	0.04311312
TIS 3	1	1	1	1	0		
CA 3	0.77548086	0.46979136	0.45781482	0.56769568	0.18004686	-4.1587677	0.05324339
TIS 4	1	1	1	1	0		
CA 4	0.76625556	0.92100819	0.36304048	0.68343474	0.28805634	-1.9034717	0.19729774
RBM6							
TIS 1	1	1	1	1	0		
CA 1	2.5668078	1.83169853	1.86805728	2.08885454	0.4143187	4.55193405	0.04502763
TIS 2	1	1	1	1	0		
CA 2	3.17056925	3.69788649	2.77641298	3.21495624	0.46233755	8.29786969	0.01421443
TIS 3	1	1	1	1	0		
CA 3	0.77727512	0.21651984	0.48970606	0.49450034	0.28040838	-3.1224141	0.08907763
TIS 4	1	1	1	1	0		
CA 4	0.22852815	0.51798464	0.61854045	0.45501775	0.20248709	-4.6617143	0.04306525

Supplemental table 8: Normalization to the three reference genes - ratios of G-patch protein and RNA helicase mRNA levels in matched-pair squamous cell carcinoma tissue samples

	round 1	round 2	round 3	mean value	standard deviation	t value	*p* value
AGGF1							
TIS 1	1	1	1	1	0		

CA 1	0.14979673	0.16181834	0.08298269	0.13153259	0.04247292	-35.416204	0.0007963
TIS 2	1	1	1	1	0		
CA 2	0.27534445	0.14573347	0.31670086	0.24592626	0.08919941	-14.642407	0.0046318
TIS 3	1	1	1	1	0		
CA 3	0.56590943	0.43188961	0.99351777	0.66377227	0.29332473	-1.9853883	0.18550642
TIS 4	1	1	1	1	0		
CA 4	2.8892384	3.80937189	4.50504812	3.73455281	0.81049904	5.84378782	0.0280562
CHERP							
TIS 1	1	1	1	1	0		
CA 1	0.13816696	0.14039253	0.11659742	0.13171897	0.01314284	-114.42785	7.6364E-05
TIS 2	1	1	1	1	0		
CA 2	0.2452949	0.12763273	0.18138692	0.18477152	0.05890406	-23.971475	0.00173572
TIS 3	1	1	1	1	0		
CA 3	6.13537404	7.18504607	3.09197789	5.47079933	2.12592249	3.64249009	0.06779573
TIS 4	1	1	1	1	0		
CA 4	6.15047538	9.09513952	23.0280053	12.7578734	9.01523535	2.25897975	0.15239843
CMTR1							
TIS 1	1	1	1	1	0		
CA 1	0.20276265	0.21945784	0.20232624	0.20818224	0.00976739	-140.41297	5.0717E-05
TIS 2	1	1	1	1	0		1
CA 2	1.82152002	0.93358387	1.82399194	1.52636528	0.51336524	1.77591182	0.21773307
TIS 3	1	1	1	1	0		1
CA 3	1.36375738	1.13003562	1.35174952	1.28184751	0.13160997	3.70924952	0.06561003
TIS 4	1	1	1	1	0		1
CA 4	4.23787998	8.35615751	5.60032699	6.06478816	2.09805758	4.18123435	0.05271708
GPATCH1							
TIS 1	1	1	1	1	0		
CA 1	0.09053134	0.10341966	0.0981981	0.09738303	0.0064827	-241.16162	1.7194E-05
TIS 2	1	1	1	1	0		1
CA 2	0.2284288	0.19246464	0.28039446	0.23376264	0.04420691	-30.0216	0.00110767
TIS 3	1	1	1	1	0		1
CA 3	1.0504114	0.83163267	0.80203673	0.8946936	0.13566504	-1.3444586	0.31099314
TIS 4	1	1	1	1	0		1
CA 4	2.87945651	2.02249708	4.80992756	3.23729372	1.4277527	2.71412997	0.11316681
GPATCH2							
TIS 1	1	1	1	1	0		
CA 1	0.16524774	0.14993768	0.19586838	0.17035127	0.02338679	-61.444677	0.00026476
TIS 2	1	1	1	1	0		
CA 2	0.04290712	0.26813159	0.32925058	0.21342976	0.15080571	-9.0340054	0.01203221
TIS 3	1	1	1	1	0		
CA 3	7.27226504	0.81136368	0.85269193	2.97877355	3.71833012	0.92174073	0.45397017
TIS 4	1	1	1	1	0		
CA 4	5.3147194	7.7317648	7.79701762	6.94783394	1.41469496	7.28210031	0.01834043
GPATCH3							
TIS 1	1	1	1	1	0		
CA 1	0.18276264	0.23081376	0.26754095	0.22703912	0.04251501	-31.490229	0.00100691
TIS 2	1	1	1	1	0		

CA 2	0.2916544	0.47797977	0.27232971	0.34732129	0.11356535	-9.9543799	0.00994162
TIS 3	1	1	1	1	0		
CA 3	0.92017227	1.06960543	1.04890773	1.01289514	0.08096448	0.27586227	0.80854435
TIS 4	1	1	1	1	0		
CA 4	2.28487369	3.70885432	3.97685	3.323526	0.90942531	4.42528379	0.04745863
GPATCH4							
TIS 1	1	1	1	1	0		
CA 1	0.23071669	0.44189098	0.30278561	0.32513109	0.10734587	-10.889168	0.00832834
TIS 2	1	1	1	1	0		
CA 2	0.13665391	0.15799341	0.17619171	0.15694635	0.01978969	-73.786508	0.00018362
TIS 3	1	1	1	1	0		
CA 3	0.23444748	0.7282683	0.42165428	0.46145668	0.24930488	-3.7415408	0.0645893
TIS 4	1	1	1	1	0		
CA 4	7.25013597	5.86491711	12.346241	8.48709804	3.41312853	3.79945674	0.06281542
GPKOW							
TIS 1	1	1	1	1	0		
CA 1	0.32150832	0.65728712	0.51748776	0.49876107	0.16867088	-5.147132	0.03573487
TIS 2	1	1	1	1	0		
CA 2	0.58572502	0.50947546	0.48824705	0.52781584	0.05126174	-15.954335	0.00390564
TIS 3	1	1	1	1	0		
CA 3	0.45521209	1.03829812	0.69139243	0.72830088	0.29328997	-1.6045441	0.24980026
TIS 4	1	1	1	1	0		
CA 4	0.65570217	0.90048431	1.75587432	1.10402026	0.5776373	0.31190573	0.78462534
PINX1							
TIS 1	1	1	1	1	0		
CA 1	0.41171681	0.54812406	0.47434336	0.47806141	0.06827959	-13.240035	0.0056562
TIS 2	1	1	1	1	0		
CA 2	0.42307869	0.43100838	0.45629806	0.43679504	0.01734923	-56.227268	0.00031615
TIS 3	1	1	1	1	0		
CA 3	3.88059757	8.63815263	5.2774235	5.9320579	2.44540225	3.49332093	0.07307629
TIS 4	1	1	1	1	0		
CA 4	2.70597679	6.16809404	15.4564665	8.11017911	6.59336923	1.86781462	0.20274403
RBM5							
TIS 1	1	1	1	1	0		
CA 1	0.20219597	0.23499781	0.21280505	0.21666628	0.01673834	-81.057871	0.00015216
TIS 2	1	1	1	1	0		
CA 2	0.33007376	0.36872306	0.58173944	0.42684542	0.13552697	-7.3249837	0.0181321
TIS 3	1	1	1	1	0		
CA 3	1.52029712	1.324478	1.7533032	1.53269277	0.21468117	4.29777315	0.05010521
TIS 4	1	1	1	1	0		
CA 4	4.14094175	4.39290039	12.3510022	6.96161478	4.6690463	2.21154793	0.15752507
SUGP1							
TIS 1	1	1	1	1	0		
CA 1	0.2354861	0.25342914	0.25121301	0.24670942	0.00978264	-133.37278	5.6212E-05
TIS 2	1	1	1	1	0		
CA 2	0.3920878	0.32713693	0.47942081	0.39954851	0.07641559	-13.609952	0.00535534
TIS 3	1	1	1	1	0		

CA 3	1.10770103	1.0090286	0.56400945	0.89357969	0.28964887	-0.6363753	0.58964649
TIS 4	1	1	1	1	0		
CA 4	2.12240388	3.24738881	4.66706631	3.34561967	1.27517202	3.18602695	0.08599707
DHX15							
TIS 1	1	1	1	1	0		
CA 1	0.60707616	0.62898874	0.44865578	0.56157356	0.09840152	-7.7171256	0.01638004
TIS 2	1	1	1	1	0		
CA 2	0.45134639	0.39345731	0.48499492	0.4432662	0.04630066	-20.826729	0.00229752
TIS 3	1	1	1	1	0		
CA 3	0.36930403	0.38800089	0.38376817	0.3803577	0.00980391	-109.47185	8.3434E-05
TIS 4	1	1	1	1	0		
CA 4	1.80074345	2.30250724	3.01886549	2.37403873	0.61220331	3.88744207	0.06025303
DHX35							
TIS 1	1	1	1	1	0		
CA 1	0.14798519	0.16218462	0.08496543	0.13171175	0.04110133	-36.590528	0.00074606
TIS 2	1	1	1	1	0		
CA 2	0.48856454	0.39439575	0.57331535	0.48542521	0.0895011	-9.9581981	0.00993412
TIS 3	1	1	1	1	0		
CA 3	0.36262384	0.52170494	0.57084714	0.48505864	0.1088414	-8.1945347	0.01456734
TIS 4	1	1	1	1	0		
CA 4	6.85408941	3.38375597	13.3781523	7.87199922	5.07435657	2.3456475	0.14360836
GPATCH8							
TIS 1	1	1	1	1	0		
CA 1	0.22380037	0.21025064	0.10154061	0.17853054	0.06701855	-21.230345	0.00221128
TIS 2	1	1	1	1	0		
CA 2	0.20907494	0.25133048	0.38972818	0.28337787	0.09449431	-13.135457	0.00574585
TIS 3	1	1	1	1	0		
CA 3	0.34733699	0.35388875	0.43668293	0.37930289	0.04980043	-21.587743	0.0021389
TIS 4	1	1	1	1	0		
CA 4	1.26268397	0.87565511	2.00375133	1.3806968	0.57323254	1.15029446	0.36899577
GPANK1							
TIS 1	1	1	1	1	0		
CA 1	0.2427512	0.22889851	0.20540361	0.22568444	0.0188801	-71.035311	0.00019812
TIS 2	1	1	1	1	0		
CA 2	0.95006799	1.99349808	2.27317219	1.73891275	0.69732449	1.83534989	0.2078781
TIS 3	1	1	1	1	0		
CA 3	3.97027594	3.24910491	6.28091378	4.50009821	1.58382448	3.82766399	0.06197698
TIS 4	1	1	1	1	0		
CA 4	1.54116094	2.85377555	11.5102756	5.30173737	5.41665946	1.37553925	0.30276283
RBM17							
TIS 1	1	1	1	1	0		
CA 1	0.0436998	0.11448815	0.08065956	0.07961584	0.03540571	-45.025278	0.00049291
TIS 2	1	1	1	1	0		
CA 2	0.19536849	0.18837537	0.24028177	0.20800854	0.0281673	-48.70078	0.00042136
TIS 3	1	1	1	1	0		
CA 3	0.49036793	0.59026347	0.81082242	0.63048461	0.16396974	-3.9032778	0.05980802
TIS 4	1	1	1	1	0		

CA 4	1.12335388	1.10517921	5.58664624	2.60505978	2.58214561	1.07664149	0.39426103
TFIP11							
TIS 1	1	1	1	1	0		
CA 1	0.49517192	1.06847729	1.15273195	0.90546039	0.35780886	-0.4576393	0.69211903
TIS 2	1	1	1	1	0		
CA 2	0.41759235	0.44757682	0.23393378	0.36636765	0.11566683	-9.488316	0.01092593
TIS 3	1	1	1	1	0		
CA 3	0.26438964	0.28590757	0.50870356	0.35300025	0.13527156	-8.2843463	0.01425988
TIS 4	1	1	1	1	0		
CA 4	1.55862333	1.52539102	2.91860785	2.00087407	0.79495445	2.18070952	0.16098589
GPATCH11							
TIS 1	1	1	1	1	0		
CA 1	0.31152083	0.22889851	0.19759319	0.24600418	0.05885855	-22.188093	0.00202507
TIS 2	1	1	1	1	0		
CA 2	0.14756186	1.99349808	0.15942256	0.7668275	1.06234444	-0.3801654	0.74039863
TIS 3	1	1	1	1	0		
CA 3	0.5770923	3.24910491	1.10004538	1.64208086	1.41607369	0.78535226	0.51450916
TIS 4	1	1	1	1	0		
CA 4	2.39246906	2.85377555	5.11728436	3.45450966	1.45836062	2.91514689	0.10028393
RBM10							
TIS 1	1	1	1	1	0		
CA 1	0.21548355	0.94244213	0.2352064	0.46437736	0.41413366	-2.2401599	0.15440472
TIS 2	1	1	1	1	0		
CA 2	0.3703423	0.17959422	0.26938957	0.2731087	0.09542841	-13.193269	0.00569603
TIS 3	1	1	1	1	0		
CA 3	0.94287332	1.00713729	3.45960709	1.8032059	1.43484534	0.96957727	0.43453875
TIS 4	1	1	1	1	0		
CA 4	1.14518087	0.65196002	1.41311567	1.07008552	0.3860945	0.31440925	0.78297774
SON							
TIS 1	1	1	1	1	0		
CA 1	0.39402702	0.43259882	0.2904007	0.37234218	0.07353741	-14.783431	0.00454445
TIS 2	1	1	1	1	0		
CA 2	0.50872429	0.58023676	0.38603907	0.49166671	0.09821612	-8.9645072	0.01221608
TIS 3	1	1	1	1	0		
CA 3	1.13969081	1.24808753	2.16993881	1.51923905	0.56612286	1.58860996	0.25308485
TIS 4	1	1	1	1	0		
CA 4	2.02591439	1.81070985	2.22044842	2.01902422	0.20495616	8.61160599	0.01321765
NKRF							
TIS 1	1	1	1	1	0		
CA 1	0.12837692	0.0767741	0.08341307	0.09618803	0.02807334	-55.762804	0.00032144
TIS 2	1	1	1	1	0		
CA 2	0.16578442	0.1880499	0.1975499	0.18379474	0.01630464	-86.705946	0.00013299
TIS 3	1	1	1	1	0		
CA 3	1.05721626	1.34692108	1.24711966	1.21708567	0.14716913	2.5549068	0.12509085
TIS 4	1	1	1	1	0		
CA 4	2.9729571	1.94727322	2.82564886	2.58195972	0.55456754	4.94084929	0.03860683

SUGP2							
TIS 1	1	1	1	1	0		
CA 1	0.18342851	0.22057304	0.16098717	0.18832957	0.03009376	-46.715813	0.0004579
TIS 2	1	1	1	1	0		
CA 2	0.29482534	0.43977997	0.68983147	0.47481226	0.19981969	-4.5523635	0.0450197
TIS 3	1	1	1	1	0		
CA 3	0.69798535	0.74927044	1.22407437	0.89044339	0.29006855	-0.654182	0.58016528
TIS 4	1	1	1	1	0		
CA 4	1.56609114	1.64574812	6.047627	3.08648875	2.56473022	1.40907784	0.29418065
ZGPAT							
TIS 1	1	1	1	1	0		
CA 1	1.13667916	0.65373685	0.86254253	0.88431951	0.24220651	-0.8272465	0.49508715
TIS 2	1	1	1	1	0		
CA 2	0.49439254	0.52926007	0.32503267	0.44956176	0.1092454	-8.7270223	0.01287703
TIS 3	1	1	1	1	0		
CA 3	2.0619111	1.37680685	1.00792511	1.48221435	0.53484079	1.56162314	0.25877517
TIS 4	1	1	1	1	0		
CA 4	2.33836828	3.28918532	2.83907825	2.82221061	0.47563289	6.63570878	0.02196495
RBM6							
TIS 1	1	1	1	1	0		
CA 1	0.4389015	0.37701024	0.40431799	0.40674324	0.03101683	-33.128821	0.0009099
TIS 2	1	1	1	1	0		
CA 2	0.38848288	0.49506162	0.36623727	0.41659392	0.06885929	-14.674694	0.00461158
TIS 3	1	1	1	1	0		
CA 3	2.11140891	0.63470948	1.06792946	1.27134928	0.75907511	0.61916237	0.59893982
TIS 4	1	1	1	1	0		
CA 4	0.71017781	1.85045299	4.76105852	2.4405631	2.08891864	1.19445939	0.3547452

Supplemental table 9: Raw data of G-patch protein and RNA helicase mRNA levels in matched-pair squamous cell carcinoma tissue samples as quantified by RT-qPCR

	target/reference	Ct value	target/ reference	Ct value
round 1				
TIS 1	AGGF1	26.7306879	DHX35	28.3529166
CA 1	AGGF1	27.1563664	DHX35	28.7961484
TIS 2	AGGF1	28.087104	DHX35	29.138634
CA 2	AGGF1	27.1529084	DHX35	27.3771268
TIS 3	AGGF1	26.3734387	DHX35	27.8007587
CA 3	AGGF1	28.8907155	DHX35	30.9601329
TIS 4	AGGF1	27.8627459	DHX35	29.8875754
CA 4	AGGF1	28.230201	DHX35	29.0087547
TIS 1	CHERP	28.9495545	GPATCH8	25.797499
CA 1	CHERP	29.4918264	GPATCH8	25.6439712
TIS 2	CHERP	29.7686909	GPATCH8	27.0644234
CA 2	CHERP	29.0012155	GPATCH8	26.5274452
TIS 3	CHERP	30.5785821	GPATCH8	25.1392185
CA 3	CHERP	29.6573507	GPATCH8	28.3607304

TIS 4	CHERP	30.6043398	GPATCH8	27.4592928
CA 4	CHERP	29.8817862	GPATCH8	29.0209435
TIS 1	CMTR1	24.5301717	GPATCH4	22.9418014
CA 1	CMTR1	24.5190644	GPATCH4	22.7443636
TIS 2	CMTR1	27.7621615	GPATCH4	22.5152782
CA 2	CMTR1	24.1021325	GPATCH4	22.5917933
TIS 3	CMTR1	24.9235766	GPATCH4	22.50126
CA 3	CMTR1	26.1719095	GPATCH4	26.2898432
TIS 4	CMTR1	27.5045576	GPATCH4	23.9418218
CA 4	CMTR1	27.3193592	GPATCH4	22.9819581
TIS 1	GPATCH1	25.6031544	GPKOW	24.9874469
CA 1	GPATCH1	26.7553497	GPKOW	24.3112754
TIS 2	GPATCH1	26.2782612	GPKOW	25.8669274
CA 2	GPATCH1	25.6135586	GPKOW	23.8437458
TIS 3	GPATCH1	25.5843751	GPKOW	24.7848707
CA 3	GPATCH1	27.2093405	GPKOW	27.6161798
TIS 4	GPATCH1	26.438541	GPKOW	26.120497
CA 4	GPATCH1	26.8108888	GPKOW	28.6275288
TIS 1	GPATCH2	26.579042	PINX1	26.5600422
CA 1	GPATCH2	26.8630961	PINX1	25.5270745
TIS 2	GPATCH2	26.6601628	PINX1	26.6744503
CA 2	GPATCH2	28.4079159	PINX1	25.1205661
TIS 3	GPATCH2	27.1046155	PINX1	26.7115548
CA 3	GPATCH2	25.9381305	PINX1	26.4511959
TIS 4	GPATCH2	27.7060558	PINX1	26.721651
CA 4	GPATCH2	27.1942066	PINX1	27.1836459
TIS 1	GPATCH3	30.0950293	RBM5	23.7378935
CA 1	GPATCH3	30.2337427	RBM5	23.7308239
TIS 2	GPATCH3	31.1619146	RBM5	24.7332053
CA 2	GPATCH3	30.1446966	RBM5	23.5374587
TIS 3	GPATCH3	30.4444891	RBM5	24.7031722
CA 3	GPATCH3	32.260433	RBM5	25.7947387
TIS 4	GPATCH3	32.0607779	RBM5	24.7963678
CA 4	GPATCH3	32.7668078	RBM5	24.6445532
TIS 1	SUGP1	26.885051	TFIP11	26.2207724
CA 1	SUGP1	26.6580938	TFIP11	24.9215275
TIS 2	SUGP1	27.8686315	TFIP11	28.0692563
CA 2	SUGP1	26.4244967	TFIP11	26.5342029
TIS 3	SUGP1	27.0355832	TFIP11	25.5877953
CA 3	SUGP1	28.5839346	TFIP11	29.2029776
TIS 4	SUGP1	28.0957715	TFIP11	28.5444355
CA 4	SUGP1	28.9082166	TFIP11	29.8023075
TIS 1	DHX15	24.6878058	SUGP2	26.0912575
CA 1	DHX15	23.0946129	SUGP2	26.2247241
TIS 2	DHX15	25.748525	SUGP2	26.8776896
CA 2	DHX15	24.1013318	SUGP2	25.844871
TIS 3	DHX15	23.6888562	SUGP2	26.0289392

CA 3	DHX15	26.8218951	SUGP2	28.2435904
TIS 4	DHX15	26.5615648	SUGP2	26.8009605
CA 4	DHX15	27.6111165	SUGP2	28.0519367
TIS 1	GPATCH11	25.0691276	RBM6	25.8642399
CA 1	GPATCH11	24.4384836	RBM6	24.7390273
TIS 2	GPATCH11	24.9872924	RBM6	26.0823791
CA 2	GPATCH11	24.9530144	RBM6	24.65157
TIS 3	GPATCH11	25.246895	RBM6	26.1707669
CA 3	GPATCH11	27.7359408	RBM6	26.7884808
TIS 4	GPATCH11	25.5939725	RBM6	25.2527735
CA 4	GPATCH11	26.2336166	RBM6	27.6446656
TIS 1	RBM10	28.2085802	GPANK1	30.022177
CA 1	RBM10	28.109687	GPANK1	29.7513832
TIS 2	RBM10	29.7757438	GPANK1	32.4710881
CA 2	RBM10	28.4139263	GPANK1	29.7500992
TIS 3	RBM10	28.6156431	GPANK1	31.4991785
CA 3	RBM10	30.3964271	GPANK1	31.2058591
TIS 4	RBM10	29.9875116	GPANK1	30.6734495
CA 4	RBM10	31.6900804	GPANK1	31.9475763
TIS 1	SON	23.2367022	ZGPAT	30.1132208
CA 1	SON	22.2670922	ZGPAT	27.6151522
TIS 2	SON	24.1655116	ZGPAT	29.6874649
CA 2	SON	22.3456696	ZGPAT	27.9088498
TIS 3	SON	22.8376001	ZGPAT	29.3916651
CA 3	SON	24.3448775	ZGPAT	30.0436028
TIS 4	SON	23.9772063	ZGPAT	29.733348
CA 4	SON	24.8567775	ZGPAT	30.4059902
TIS 1	RBM17	21.9056065	NKRF	23.5782725
CA 1	RBM17	24.1085925	NKRF	24.2265712
TIS 2	RBM17	24.7166054	NKRF	24.9072952
CA 2	RBM17	24.2774494	NKRF	24.7050287
TIS 3	RBM17	23.703221	NKRF	23.7790365
CA 3	RBM17	26.4272044	NKRF	25.3946859
TIS 4	RBM17	24.2549267	NKRF	24.0506074
CA 4	RBM17	25.9852585	NKRF	24.3768531
TIS 1	COPS6	23.5219288	PSMB2	23.1027416
CA 1	COPS6	21.6825386	PSMB2	21.5062715
TIS 2	COPS6	24.71653	PSMB2	23.6967094
CA 2	COPS6	21.3377544	PSMB2	21.898438
TIS 3	COPS6	23.6920766	PSMB2	21.2651897
CA 3	COPS6	24.7461269	PSMB2	24.7827081
TIS 4	COPS6	25.2216496	PSMB2	24.9349307
CA 4	COPS6	25.9943161	PSMB2	27.1579902
TIS 1	EMC7	22.6018563	COPS6	23.6633901
CA 1	EMC7	20.0186759	COPS6	21.6161319
TIS 2	EMC7	24.2831224	COPS6	24.6900582
CA 2	EMC7	20.8372259	COPS6	21.5397851

TIS 3	EMC7	22.4754401	COPS6	23.8574265
CA 3	EMC7	23.2996493	COPS6	24.6935245
TIS 4	EMC7	24.8254203	COPS6	25.6478484
CA 4	EMC7	26.5527625	COPS6	26.3911386
TIS 1	EMC7	22.6532344	COPS6	21.8879665
CA 1	EMC7	19.9028431	COPS6	25.1529722
TIS 2	EMC7	24.4085626	COPS6	21.9201499
CA 2	EMC7	21.0727157	COPS6	23.965189
TIS 3	EMC7	22.325802	COPS6	24.8629051
CA 3	EMC7	23.467351	COPS6	25.5759084
TIS 4	EMC7	25.0637086	COPS6	26.3807887
CA 4	EMC7	26.6031105	COPS6	22.9018674
TIS 1	COPS6	23.7001246	EMC7	22.7986253
CA 1	COPS6	21.5419774	EMC7	19.8965873
TIS 2	COPS6	24.269758	EMC7	24.3250633
CA 2	COPS6	22.4825668	EMC7	21.4725535
TIS 3	COPS6	21.5509134	EMC7	25.1592267
CA 3	COPS6	25.1242979	EMC7	27.0830807
TIS 4	COPS6	25.2829235	EMC7	22.440072
CA 4	COPS6	27.7460712	EMC7	23.6373808
TIS 1	PSMB2	23.6671786	PSMB2	24.493776
CA 1	PSMB2	21.8275251	PSMB2	21.2545561
TIS 2	PSMB2	24.0298899	PSMB2	23.7967074
CA 2	PSMB2	22.0701861	PSMB2	22.1499337
TIS 3	PSMB2	21.5986914	PSMB2	21.6010881
CA 3	PSMB2	25.0671314	PSMB2	24.7739151
TIS 4	PSMB2	25.4947212	PSMB2	22.0325836
CA 4	PSMB2	27.5993179	PSMB2	26.749437
TIS 1	EMC7	23.8905197		
CA 1	EMC7	20.2773736		
TIS 2	EMC7	24.5200876		
CA 2	EMC7	20.988968		
TIS 3	EMC7	22.7268778		
CA 3	EMC7	23.0776381		
TIS 4	EMC7	23.0753444		
CA 4	EMC7	25.7083366		
round 2				
TIS 1	AGGF1	26.247164	RBM5	24.1137648
CA 1	AGGF1	26.5972934	RBM5	23.9256221
TIS 2	AGGF1	27.1905635	RBM5	25.0797865
CA 2	AGGF1	27.0711721	RBM5	23.6211896
TIS 3	CHERP	29.6139143	RBM5	24.761882
CA 3	CHERP	29.6858567	RBM5	25.9114932
TIS 4	AGGF1	25.5960616	RBM5	25.301088
CA 4	AGGF1	28.3623622	RBM5	25.0061645
TIS 1	AGGF1	27.8117816	SUGP1	27.1976993
CA 1	AGGF1	27.7224788	SUGP1	26.9006215

TIS 2	CHERP	28.9907732	SUGP1	28.110753
CA 2	CHERP	29.5458115	SUGP1	26.8247992
TIS 3	CHERP	30.5210737	SUGP1	27.1347751
CA 3	CHERP	29.2311115	SUGP1	28.6768431
TIS 4	CHERP	31.5818989	SUGP1	28.5667571
CA 4	CHERP	30.2370534	SUGP1	28.7077273
TIS 1	CMTR1	24.6251724	DHX15	24.4795472
CA 1	CMTR1	24.5357332	DHX15	22.8710176
TIS 2	CMTR1	27.6008277	DHX15	25.0731453
CA 2	CMTR1	24.8019889	DHX15	23.520879
TIS 3	CMTR1	24.8724206	DHX15	23.3090049
CA 3	CMTR1	26.2510875	DHX15	26.2299082
TIS 4	CMTR1	28.2220537	DHX15	25.9267795
CA 4	CMTR1	26.9994643	DHX15	26.5638242
TIS 1	GPATCH1	25.8393055	DHX35	28.5813298
CA 1	GPATCH1	26.8352997	DHX35	28.9281974
TIS 2	GPATCH1	26.2809461	DHX35	29.2162468
CA 2	GPATCH1	25.7602935	DHX35	27.6605436
TIS 3	GPATCH1	25.7113386	DHX35	27.9107366
CA 3	GPATCH1	27.5323554	DHX35	30.4044658
TIS 4	GPATCH1	26.0802569	DHX35	29.3486045
CA 4	GPATCH1	26.9043695	DHX35	29.4302292
TIS 1	GPATCH2	26.4869167	GPATCH8	25.8265286
CA 1	GPATCH2	26.9470583	GPATCH8	25.7989231
TIS 2	GPATCH2	27.0190467	GPATCH8	27.7075351
CA 2	GPATCH2	26.0200463	GPATCH8	26.8018903
TIS 3	GPATCH2	26.5139537	GPATCH8	25.5710535
CA 3	GPATCH2	28.3705682	GPATCH8	28.6247208
TIS 4	GPATCH2	27.874613	GPATCH8	27.1249692
CA 4	GPATCH2	26.7640656	GPATCH8	29.1567848
TIS 1	GPATCH3	31.4838513	GPANK1	30.4878559
CA 1	GPATCH3	31.3216267	GPANK1	30.3376524
TIS 2	GPATCH3	32.5417943	GPANK1	33.3480073
CA 2	GPATCH3	30.7087855	GPANK1	29.4547178
TIS 3	GPATCH3	32.1009499	GPANK1	31.7110992
CA 3	GPATCH3	33.5589063	GPANK1	31.566092
TIS 4	GPATCH3	33.6224039	GPANK1	31.6177742
CA 4	GPATCH3	33.5716806	GPANK1	31.9451526
TIS 1	GPATCH11	25.6280867	TFIP11	27.5830665
CA 1	GPATCH11	24.5717311	TFIP11	25.2100867
TIS 2	GPATCH11	25.1951281	TFIP11	28.5193952
CA 2	GPATCH11	24.8830053	TFIP11	26.7812006
TIS 3	GPATCH11	25.6257708	TFIP11	26.209449
CA 3	GPATCH11	27.5857642	TFIP11	29.5708634
TIS 4	GPATCH11	25.598525	TFIP11	28.7973929
CA 4	GPATCH11	26.6976524	TFIP11	30.0284641
TIS 1	RBM10	30.5477825	RBM17	23.4802208

CA 1	RBM10	28.355883	RBM17	24.3295271
TIS 2	RBM10	28.7911593	RBM17	24.7664884
CA 2	RBM10	28.3703591	RBM17	24.2768189
TIS 3	RBM10	29.1056706	RBM17	24.2538243
CA 3	RBM10	30.6504453	RBM17	26.5694284
TIS 4	RBM10	29.7831806	RBM17	24.4472518
CA 4	RBM10	32.2405755	RBM17	26.1432218
TIS 1	SON	23.5312738	GPATCH4	24.0330635
CA 1	SON	22.4627486	GPATCH4	22.9338776
TIS 2	SON	24.2384146	GPATCH4	22.964843
CA 2	SON	22.1257137	GPATCH4	22.7289194
TIS 3	SON	23.1366918	GPATCH4	23.4209284
CA 3	SON	24.3720078	GPATCH4	25.4334215
TIS 4	SON	24.1043713	GPATCH4	23.5000585
CA 4	SON	25.0880662	GPATCH4	22.788198
TIS 1	GPKOW	26.9677529	NKRF	23.5507995
CA 1	GPKOW	25.2957337	NKRF	24.9766126
TIS 2	GPKOW	26.9169574	NKRF	25.1856189
CA 2	GPKOW	24.9918855	NKRF	24.6984441
TIS 3	GPKOW	26.6737275	NKRF	23.8907101
CA 3	GPKOW	28.1745419	NKRF	25.0160799
TIS 4	GPKOW	27.6390743	NKRF	24.8790469
CA 4	GPKOW	29.6305515	NKRF	25.7578419
TIS 1	PINX1	26.9312211	ZGPAT	29.6096731
CA 1	PINX1	25.5212232	ZGPAT	27.9454677
TIS 2	PINX1	26.8731173	ZGPAT	30.0571868
CA 2	PINX1	25.1893421	ZGPAT	28.0771508
TIS 3	PINX1	27.3047696	ZGPAT	29.7074701
CA 3	PINX1	25.7490819	ZGPAT	30.8011791
TIS 4	PINX1	27.6385499	ZGPAT	30.7180914
CA 4	PINX1	26.8539754	ZGPAT	30.8406114
TIS 1	SUGP2	25.9444904	RBM6	25.8524684
CA 1	SUGP2	25.8477385	RBM6	24.9823693
TIS 2	SUGP2	26.6660793	RBM6	26.4664384
CA 2	SUGP2	24.9532382	RBM6	24.5827711
TIS 3	SUGP2	25.740374	RBM6	25.6483197
CA 3	SUGP2	27.7118507	RBM6	27.8591865
TIS 4	SUGP2	26.6469821	RBM6	26.2185034
CA 4	SUGP2	27.7684889	RBM6	27.1708753
TIS 1	EMC7	22.8290987	EMC7	22.9189719
CA 1	EMC7	20.1664017	EMC7	20.1445415
TIS 2	EMC7	24.255844	EMC7	24.6553782
CA 2	EMC7	21.5347925	EMC7	21.2593821
TIS 3	EMC7	24.255844	EMC7	22.7212477
CA 3	EMC7	21.5347925	EMC7	23.5017645
TIS 4	EMC7	22.5389643	EMC7	24.0881855
CA 4	EMC7	23.6142679	EMC7	27.0478128

TIS 1	EMC7	25.7661762	EMC7	22.9189719
CA 1	EMC7	26.5765069	EMC7	20.1445415
TIS 2	EMC7	22.8290987	EMC7	24.6553782
CA 2	EMC7	20.1664017	EMC7	21.2593821
TIS 3	EMC7	22.5389643	EMC7	22.7212477
CA 3	EMC7	23.6142679	EMC7	23.5017645
TIS 4	EMC7	25.7661762	EMC7	24.0881855
CA 4	EMC7	26.5765069	EMC7	27.0478128
TIS 1	EMC7	22.8290987	EMC7	22.9189719
CA 1	EMC7	20.1664017	EMC7	20.1445415
TIS 2	EMC7	24.255844	EMC7	24.6553782
CA 2	EMC7	21.5347925	EMC7	21.2593821
TIS 3	EMC7	22.5389643	EMC7	22.7212477
CA 3	EMC7	23.6142679	EMC7	23.5017645
TIS 4	EMC7	25.7661762	EMC7	24.0881855
CA 4	EMC7	26.5765069	EMC7	27.0478128
TIS 1	PSMB2	23.8651045	PSMB2	23.7983221
CA 1	PSMB2	21.8498812	PSMB2	21.852786
TIS 2	PSMB2	24.3104334	PSMB2	24.3592506
CA 2	PSMB2	22.5580368	PSMB2	22.6797286
TIS 3	PSMB2	21.989077	PSMB2	22.0312142
CA 3	PSMB2	25.2376277	PSMB2	25.2664093
TIS 4	PSMB2	26.0285832	PSMB2	25.289011
CA 4	PSMB2	27.86291	PSMB2	27.8813646
TIS 1	PSMB2	23.8651045	PSMB2	23.7983221
CA 1	PSMB2	21.8498812	PSMB2	21.852786
TIS 2	PSMB2	24.3104334	PSMB2	24.3592506
CA 2	PSMB2	22.5580368	PSMB2	22.6797286
TIS 3	PSMB2	21.989077	PSMB2	22.0312142
CA 3	PSMB2	25.2376277	PSMB2	25.2664093
TIS 4	PSMB2	26.0285832	PSMB2	25.289011
CA 4	PSMB2	27.86291	PSMB2	27.8813646
TIS 1	PSMB2	23.8651045	PSMB2	23.7983221
CA 1	PSMB2	21.8498812	PSMB2	21.852786
TIS 2	PSMB2	24.3104334	PSMB2	24.3592506
CA 2	PSMB2	22.5580368	PSMB2	22.6797286
TIS 3	PSMB2	21.989077	PSMB2	22.0312142
CA 3	PSMB2	25.2376277	PSMB2	25.2664093
TIS 4	PSMB2	26.0285832	PSMB2	25.289011
CA 4	PSMB2	27.86291	PSMB2	27.8813646
TIS 1	COPS6	23.969973	EMC7	22.9498129
CA 1	COPS6	21.921234	EMC7	20.1926189
TIS 2	COPS6	25.1086234	EMC7	24.6969944
CA 2	COPS6	21.5728348	EMC7	21.0533422
TIS 3	COPS6	24.0505511	EMC7	22.8631304
CA 3	COPS6	24.9884463	EMC7	23.5653111
TIS 4	COPS6	25.5187795	EMC7	24.98077

CA 4	COPS6	26.5659914	EMC7	27.0591145
TIS 1	COPS6	23.969973	EMC7	24.6969944
CA 1	COPS6	21.921234	EMC7	21.0533422
TIS 2	COPS6	25.1086234	EMC7	22.9498129
CA 2	COPS6	21.5728348	EMC7	20.1926189
TIS 3	COPS6	24.0505511	EMC7	22.8631304
CA 3	COPS6	24.9884463	EMC7	23.5653111
TIS 4	COPS6	25.5187795	EMC7	24.98077
CA 4	COPS6	26.5659914	EMC7	27.0591145
TIS 1	COPS6	24.0594464	EMC7	22.9498129
CA 1	COPS6	21.7952681	EMC7	20.1926189
TIS 2	COPS6	24.6912963	EMC7	24.6969944
CA 2	COPS6	21.3908425	EMC7	21.0533422
TIS 3	COPS6	23.880748	EMC7	22.8631304
CA 3	COPS6	24.0516653	EMC7	23.5653111
TIS 4	COPS6	24.0512056	EMC7	24.98077
CA 4	COPS6	25.5276249	EMC7	27.0591145
TIS 1	COPS6	24.0594464	PSMB2	23.8386807
CA 1	COPS6	21.7952681	PSMB2	21.8382783
TIS 2	COPS6	24.6912963	PSMB2	24.4168949
CA 2	COPS6	21.3908425	PSMB2	22.1465414
TIS 3	COPS6	23.880748	PSMB2	21.9190593
CA 3	COPS6	24.0516653	PSMB2	25.0910804
TIS 4	COPS6	24.0512056	PSMB2	25.3128625
CA 4	COPS6	25.5276249	PSMB2	27.8497506
TIS 1	COPS6	23.9524006		
CA 1	COPS6	21.9239894		
TIS 2	COPS6	25.1414426		
CA 2	COPS6	21.3587712		
TIS 3	COPS6	24.1088452		
CA 3	COPS6	24.781581		
TIS 4	COPS6	25.3525762		
CA 4	COPS6	26.5793266		
round 3				
TIS 1	COPS6	21.9239894	GPATCH4	24.0781531
CA 1	COPS6	25.1414426	GPATCH4	23.481238
TIS 2	COPS6	21.3587712	GPATCH4	23.4006827
CA 2	COPS6	24.1088452	GPATCH4	22.8721326
TIS 3	COPS6	24.781581	GPATCH4	23.7333856

CA 3	COPS6	25.3525762	GPATCH4	25.9823827
TIS 4	COPS6	26.5793266	GPATCH4	23.937656
CA 4	AGGF1	26.6176499	GPATCH4	23.1385677
TIS 1	CMTR1	25.644705	GPKOW	26.7309382
CA 1	CMTR1	25.9861056	GPKOW	25.3607951
TIS 2	CMTR1	24.6562487	GPKOW	26.96272
CA 2	CMTR1	24.6409469	GPKOW	24.9637047
TIS 3	CMTR1	27.8696816	GPKOW	26.6241871
CA 3	CMTR1	23.9692501	GPKOW	28.15974
TIS 4	CMTR1	24.5558131	GPKOW	27.9622505
CA 4	CMTR1	25.1241149	GPKOW	29.9769726
TIS 1	GPATCH1	25.8848454	PINX1	26.9052447
CA 1	GPATCH1	26.91246	PINX1	25.6606946
TIS 2	GPATCH1	26.6961326	PINX1	27.0218602
CA 2	GPATCH1	25.4972707	PINX1	25.1204797
TIS 3	GPATCH1	26.0334942	PINX1	27.3384372
CA 3	GPATCH1	27.3548836	PINX1	25.941733
TIS 4	GPATCH1	26.2828581	PINX1	28.0513433
CA 4	GPATCH1	26.8437546	PINX1	26.9281163
TIS 1	GPATCH2	27.5822075	RBM5	23.8923722
CA 1	GPATCH2	27.6137046	RBM5	23.8042214
TIS 2	GPATCH2	27.8911568	RBM5	25.0902205
CA 2	GPATCH2	26.4605667	RBM5	22.8384434
TIS 3	GPATCH2	27.5365597	RBM5	24.8140106
CA 3	GPATCH2	28.7695928	RBM5	25.0070647
TIS 4	GPATCH2	28.1513494	RBM5	25.5275317
CA 4	GPATCH2	28.0153386	RBM5	24.7278871
TIS 1	GPATCH3	31.1395783	SUGP1	27.0601656
CA 1	GPATCH3	30.7212001	SUGP1	26.732636
TIS 2	GPATCH3	31.8399098	SUGP1	28.2099007
CA 2	GPATCH3	30.6831513	SUGP1	26.2372041
TIS 3	GPATCH3	31.0819633	SUGP1	26.9009536
CA 3	GPATCH3	32.0162051	SUGP1	28.730292
TIS 4	GPATCH3	32.0980762	SUGP1	28.0325191
CA 4	GPATCH3	32.9333617	SUGP1	28.6369148
TIS 1	DHX35	27.2696567	DHX15	23.8333791
CA 1	DHX35	28.5060903	DHX15	22.6691516
TIS 2	DHX35	28.0774544	DHX15	24.9586302
CA 2	DHX35	25.8467215	DHX15	22.9692566
TIS 3	DHX35	27.4703954	DHX15	23.344121
CA 3	DHX35	29.2823486	DHX15	25.7289436
TIS 4	DHX35	28.557477	DHX15	24.7014575
CA 4	DHX35	27.6425817	DHX15	25.9343627
TIS 1	GPATCH8	24.7044157	GPATCH11	24.4270175
CA 1	GPATCH8	25.6837405	GPATCH11	24.4458658
TIS 2	GPATCH8	26.4221596	GPATCH11	24.2883676
CA 2	GPATCH8	24.7482873	GPATCH11	23.9041077

TIS 3	GPATCH8	24.8522785	GPATCH11	25.6133402
CA 3	GPATCH8	27.05075	GPATCH11	26.4789068
TIS 4	GPATCH8	25.822314	GPATCH11	25.1133721
CA 4	GPATCH8	27.6465222	GPATCH11	25.5849053
TIS 1	GPANK1	30.1111577	RBM10	28.4726634
CA 1	GPANK1	30.0740777	RBM10	28.2401176
TIS 2	GPANK1	33.0430989	RBM10	29.8030567
CA 2	GPANK1	28.8250598	RBM10	28.6619586
TIS 3	GPANK1	32.0110036	RBM10	29.9258576
CA 3	GPANK1	30.3631587	RBM10	29.138379
TIS 4	GPANK1	32.3823946	RBM10	29.055862
CA 4	GPANK1	31.6844558	RBM10	31.3838941
TIS 1	RBM17	23.3192519	SON	22.7714505
CA 1	RBM17	24.630716	SON	22.2347871
TIS 2	RBM17	24.3892093	SON	23.3927425
CA 2	RBM17	23.413078	SON	21.7325916
TIS 3	RBM17	24.2719716	SON	23.6733408
CA 3	RBM17	25.5776433	SON	23.558816
TIS 4	RBM17	25.4489171	SON	23.3041313
CA 4	RBM17	25.7938462	SON	24.9801919
TIS 1	ZGPAT	30.2347806	NKRF	23.8794283
CA 1	ZGPAT	28.1275666	NKRF	25.1424645
TIS 2	ZGPAT	30.0007347	NKRF	25.3234634
CA 2	ZGPAT	28.5887459	NKRF	24.6298422
TIS 3	ZGPAT	28.9694216	NKRF	24.7077933
CA 3	ZGPAT	29.9611627	NKRF	25.392323
TIS 4	ZGPAT	29.7206258	NKRF	24.3886129
CA 4	ZGPAT	31.0421148	NKRF	25.7169424
TIS 1	RBM6	25.9193062	TFIP11	26.1874032
CA 1	RBM6	24.9051974	TFIP11	23.6617996
TIS 2	RBM6	26.1332615	TFIP11	26.7705802
CA 2	RBM6	24.5490788	TFIP11	25.833076
TIS 3	RBM6	26.0165277	TFIP11	25.197669
CA 3	RBM6	26.9248409	TFIP11	27.1759015
TIS 4	RBM6	25.4049683	TFIP11	25.5666314
CA 4	RBM6	25.9805976	TFIP11	26.8482627
TIS 1	CHERP	28.8735811	SUGP2	24.5923716
CA 1	CHERP	29.6534268	SUGP2	24.9068075
TIS 2	CHERP	29.3320342	SUGP2	26.6196702
CA 2	CHERP	28.7615597	SUGP2	24.1220222
TIS 3	CHERP	29.7994627	SUGP2	25.4327156
CA 3	CHERP	29.1740623	SUGP2	26.1441539
TIS 4	CHERP	30.7978253	SUGP2	26.340522
CA 4	CHERP	29.0994194	SUGP2	26.5710645
TIS 1	PSMB2	23.4687072	PSMB2	23.8097639
CA 1	PSMB2	21.2553747	PSMB2	21.7557687
TIS 2	PSMB2	23.8759742	PSMB2	24.2754046

CA 2	PSMB2	22.1075672	PSMB2	22.38298
TIS 3	PSMB2	21.1808726	PSMB2	21.9347711
CA 3	PSMB2	23.8487336	PSMB2	24.3820156
TIS 4	PSMB2	22.1348183	PSMB2	22.8145898
CA 4	PSMB2	26.660073	PSMB2	27.3230531
TIS 1	PSMB2	22.1348183	PSMB2	23.8097639
CA 1	PSMB2	26.660073	PSMB2	21.7557687
TIS 2	PSMB2	23.4687072	PSMB2	24.2754046
CA 2	PSMB2	21.2553747	PSMB2	22.38298
TIS 3	PSMB2	23.8759742	PSMB2	21.9347711
CA 3	PSMB2	22.1075672	PSMB2	24.3820156
TIS 4	PSMB2	21.1808726	PSMB2	22.8145898
CA 4	PSMB2	23.8487336	PSMB2	27.3230531
TIS 1	COPS6	24.2064847	PSMB2	23.8097639
CA 1	COPS6	21.8786637	PSMB2	21.7557687
TIS 2	COPS6	25.093842	PSMB2	24.2754046
CA 2	COPS6	21.404688	PSMB2	22.38298
TIS 3	COPS6	23.8925412	PSMB2	21.9347711
CA 3	COPS6	24.287519	PSMB2	24.3820156
TIS 4	COPS6	24.805118	PSMB2	22.8145898
CA 4	COPS6	26.0014284	PSMB2	27.3230531
TIS 1	COPS6	24.2064847	COPS6	24.0392472
CA 1	COPS6	21.8786637	COPS6	22.6691446
TIS 2	COPS6	25.093842	COPS6	24.532297
CA 2	COPS6	21.404688	COPS6	21.328115
TIS 3	COPS6	23.8925412	COPS6	23.8274009
CA 3	COPS6	24.287519	COPS6	24.3612058
TIS 4	COPS6	24.805118	COPS6	24.8199866
CA 4	COPS6	26.0014284	COPS6	25.6917916
TIS 1	COPS6	24.2064847	COPS6	24.0392472
CA 1	COPS6	21.8786637	COPS6	22.6691446
TIS 2	COPS6	25.093842	COPS6	24.532297
CA 2	COPS6	21.404688	COPS6	21.328115
TIS 3	COPS6	23.8925412	COPS6	23.8274009
CA 3	COPS6	24.287519	COPS6	24.3612058
TIS 4	COPS6	24.805118	COPS6	24.8199866
CA 4	COPS6	26.0014284	COPS6	25.6917916
TIS 1	EMC7	22.9368803	COPS6	24.0392472
CA 1	EMC7	20.0595048	COPS6	22.6691446
TIS 2	EMC7	24.7068208	COPS6	24.532297
CA 2	EMC7	20.8160382	COPS6	21.328115
TIS 3	EMC7	22.7608484	COPS6	23.8274009
CA 3	EMC7	22.9780254	COPS6	24.3612058
TIS 4	EMC7	23.6276402	COPS6	24.8199866
CA 4	EMC7	26.4261991	COPS6	25.6917916
TIS 1	EMC7	22.9368803	EMC7	22.969045
CA 1	EMC7	20.0595048	EMC7	20.6636722

TIS 2	EMC7	24.7068208	EMC7	24.2052647
CA 2	EMC7	20.8160382	EMC7	20.8292382
TIS 3	EMC7	22.7608484	EMC7	23.157899
CA 3	EMC7	22.9780254	EMC7	23.0384989
TIS 4	EMC7	23.6276402	EMC7	23.8243423
CA 4	EMC7	26.4261991	EMC7	26.5134642
TIS 1	EMC7	22.9368803	PSMB2	23.7872472
CA 1	EMC7	20.0595048	PSMB2	21.6625523
TIS 2	EMC7	24.7068208	PSMB2	24.1209588
CA 2	EMC7	20.8160382	PSMB2	23.2151731
TIS 3	EMC7	22.7608484	PSMB2	21.7425311
CA 3	EMC7	22.9780254	PSMB2	24.6316324
TIS 4	EMC7	23.6276402	PSMB2	22.1773733
CA 4	EMC7	26.4261991	PSMB2	27.8168744
TIS 1	PSMB2	23.4687072	PSMB2	23.7872472
CA 1	PSMB2	21.2553747	PSMB2	21.6625523
TIS 2	PSMB2	23.8759742	PSMB2	24.1209588
CA 2	PSMB2	22.1075672	PSMB2	23.5649375
TIS 3	PSMB2	21.1808726	PSMB2	21.7425311
CA 3	PSMB2	23.8487336	PSMB2	24.6316324
TIS 4	PSMB2	22.1348183	PSMB2	22.1773733
CA 4	PSMB2	26.660073	PSMB2	28.0577567
TIS 1	COPS6	24.4120383	PSMB2	23.7872472
CA 1	COPS6	22.0609631	PSMB2	21.6625523
TIS 2	COPS6	24.9278342	PSMB2	24.1209588
CA 2	COPS6	22.5579896	PSMB2	23.2151731
TIS 3	COPS6	24.0236184	PSMB2	21.9990309
CA 3	COPS6	24.8175203	PSMB2	24.6316324
TIS 4	COPS6	24.5759007	PSMB2	22.1773733
CA 4	COPS6	26.55885	PSMB2	27.8168744
TIS 1	EMC7	22.6581297	EMC7	23.4080665
CA 1	EMC7	18.8523929	EMC7	20.480496
TIS 2	EMC7	24.4235901	EMC7	24.5642306
CA 2	EMC7	20.1582783	EMC7	20.804701
TIS 3	EMC7	22.0673313	EMC7	22.8130973
CA 3	EMC7	22.0678341	EMC7	22.6645965
TIS 4	EMC7	22.9918534	EMC7	23.0639748
CA 4	EMC7	25.4081067	EMC7	26.8793137
TIS 1	EMC7	22.6581297		
CA 1	EMC7	18.8523929		
TIS 2	EMC7	24.4235901		
CA 2	EMC7	20.1582783		
TIS 3	EMC7	22.0673313		
CA 3	EMC7	22.0678341		
TIS 4	EMC7	22.9918534		
CA 4	EMC7	25.4081067		

a) CHERP

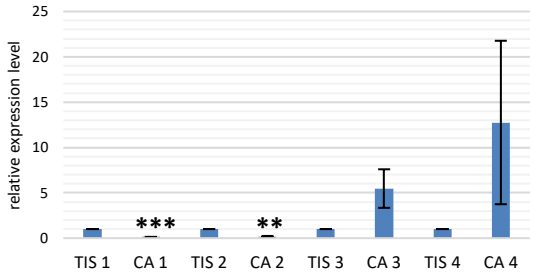

b) CMTR1

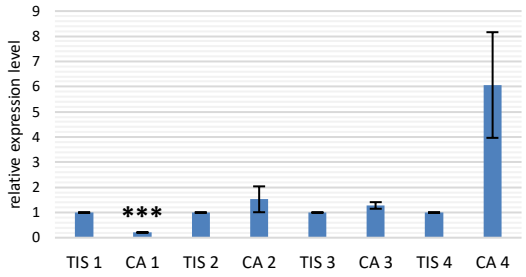

c) GPANK1

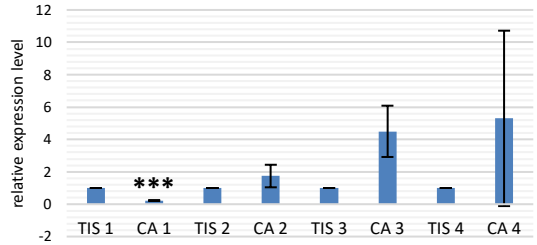

d) GPATCH1

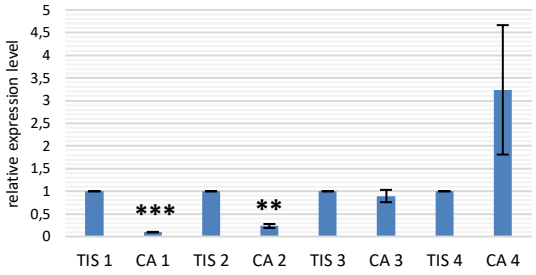

e) GPATCH2

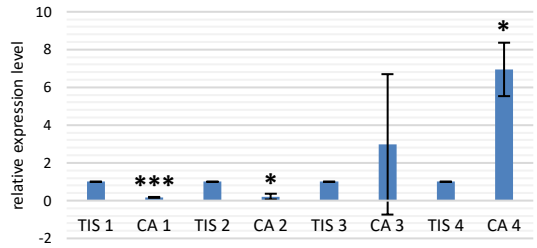

f) GPATCH3

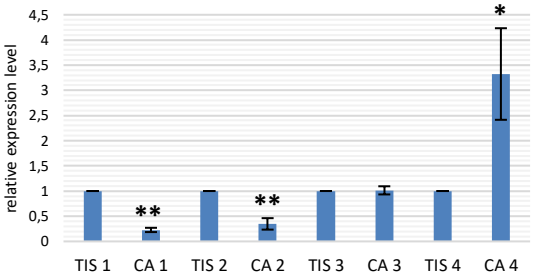

g) GPATCH4

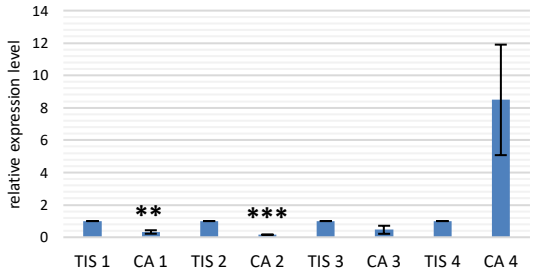

h) GPATCH8

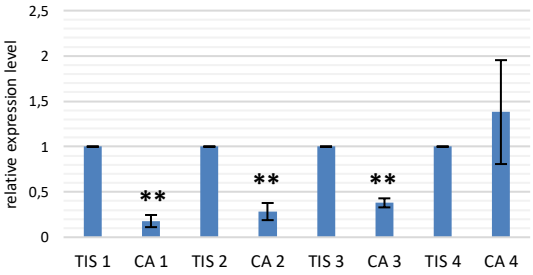

i) GPATCH11

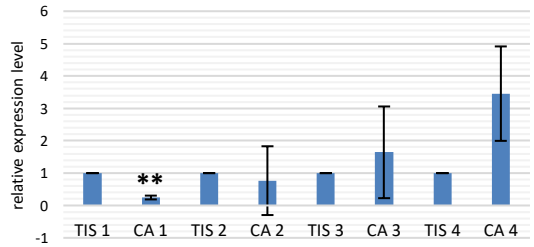

j) GPKOW

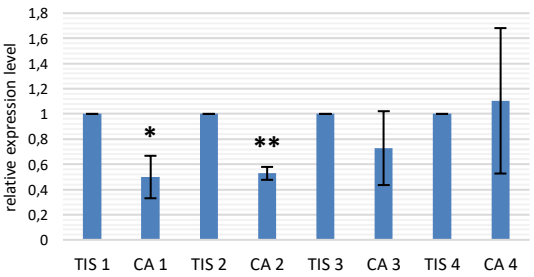

k) NKRF

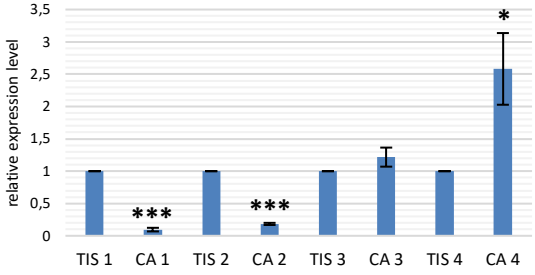

l) PINX1

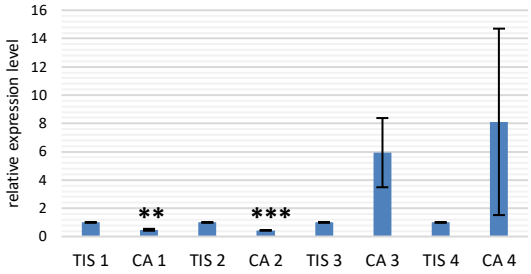

m) RBM6

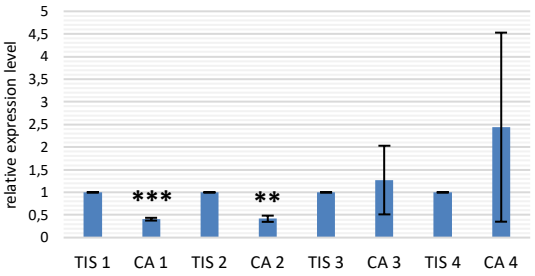

n) RBM10

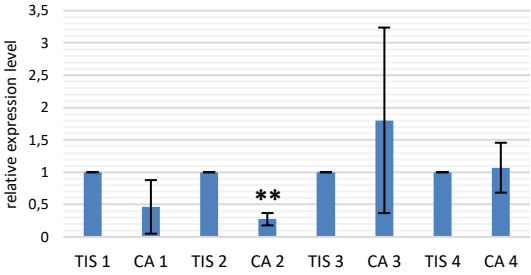

o) RBM17

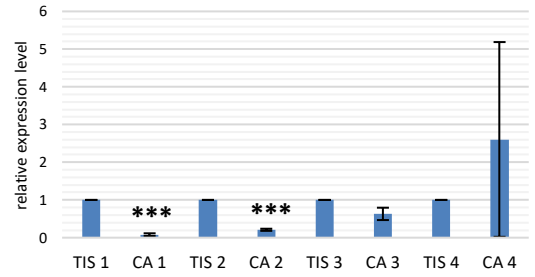

p) SON

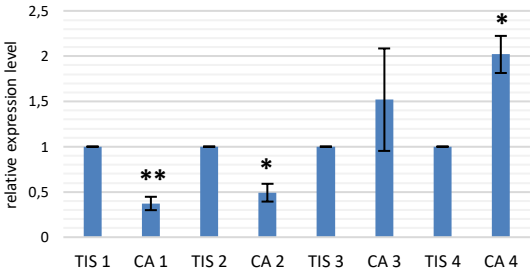

q) SUGP1

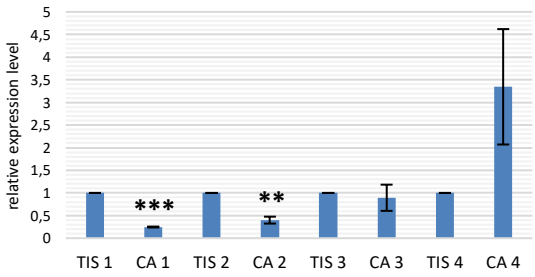

r) SUGP2

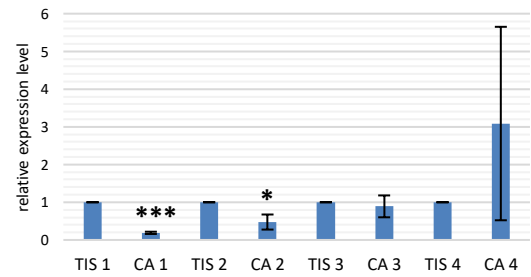

s) TFIP11

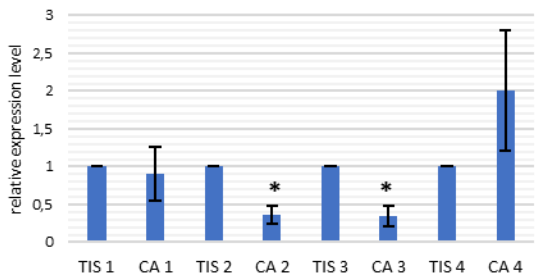

t) ZGPAT

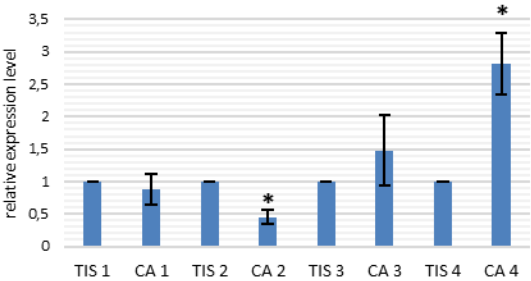

Supplemental figure 1: Normalization to the three reference genes – Ratios of G-patch protein and RNA helicase mRNA expression in matched-pair squamous cell carcinoma tissue samples

6. References

Abdel-Monem M, Dürwald H, Hoffmann-Berling H (1976): Enzymic unwinding of DNA. 2. Chain separation by an ATP-dependent DNA unwinding enzyme. Eur J Biochem 65, 441–449

Abdel-Monem M, Hoffmann-Berling H (1976): Enzymic unwinding of DNA. 1. Purification and characterization of a DNA-dependent ATPase from Escherichia coli. Eur J Biochem 65, 431–440

Ahlquist P (2006): Parallels among positive-strand RNA viruses, reverse-transcribing viruses and double-stranded RNA viruses. Nat Rev Microbiol 4, 371–382

Al-Ayoubi AM, Zheng H, Liu Y, Bai T, Eblen ST (2012): Mitogen-activated protein kinase phosphorylation of splicing factor 45 (SPF45) regulates SPF45 alternative splicing site utilization, proliferation, and cell adhesion. Mol Cell Biol 32, 2880–2893

Albrecht B, Hausmann M, Zitzelsberger H, Stein H, Siewert JR, Hopt U, Langer R, Höfler H, Werner M, Walch A (2004): Array-based comparative genomic hybridization for the detection of DNA sequence copy number changes in Barrett's adenocarcinoma. J Pathol 203, 780–788

Alexandrov A, Colognori D, Shu MD, Steitz JA (2012): Human spliceosomal protein CWC22 plays a role in coupling splicing to exon junction complex deposition and nonsense-mediated decay. Proc Natl Acad Sci U S A 109, 21313–21318

Andersen CBF, Ballut L, Johansen JS, Chamieh H, Nielsen KH, Oliveira CLP, Pedersen JS, Séraphin B, Le Hir H, Andersen GR (2006): Structure of the exon junction core complex with a trapped DEAD-box ATPase bound to RNA. Science 313, 1968–1972

Angeloni D (2007): Molecular analysis of deletions in human chromosome 3p21 and the role of resident cancer genes in disease. Brief Funct Genomic Proteomic 6, 19–39

Aravind L, Koonin EV (1999): G-patch: a new conserved domain in eukaryotic RNA-processing proteins and type D retroviral polyproteins. Trends Biochem Sci 24, 342–344

Arenas JE, Abelson JN (1997): Prp43: An RNA helicase-like factor involved in spliceosome disassembly. Proc Natl Acad Sci U S A 94, 11798–11802

Assenberg R, Mastrangelo E, Walter TS, Verma A, Milani M, Owens RJ, Stuart DI, Grimes JM, Mancini EJ (2009): Crystal structure of a novel conformational state of the flavivirus

NS3 protein: implications for polyprotein processing and viral replication. J Virol 83, 12895–12906

Bai J, Chen YS, Mei PJ, Liu QH, Du Y, Zheng JN (2015): PinX1 is up-regulated and associated with poor patients' survival in gliomas. Int J Clin Exp Pathol 8, 6952–6959

Ballut L, Marchadier B, Baguet A, Tomasetto C, Séraphin B, Le Hir H (2005): The exon junction core complex is locked onto RNA by inhibition of eIF4AIII ATPase activity. Nat Struct Mol Biol 12, 861–869

Banerjee D, McDaniel PM, Rymond BC (2015): Limited portability of G-patch domains in regulators of the Prp43 RNA helicase required for pre-mRNA splicing and ribosomal RNA maturation in Saccharomyces cerevisiae. Genetics 200, 135–147

Bauerová-Zábranská H, Stokrová J, Strísovsky K, Hunter E, Ruml T, Pichová I (2005): The RNA binding G-patch domain in retroviral protease is important for infectivity and D-type morphogenesis of Mason-Pfizer monkey virus. J Biol Chem 280, 42106–42112

Beran RKF, Lindenbach BD, Pyle AM (2009): The NS4A protein of hepatitis C virus promotes RNA-coupled ATP hydrolysis by the NS3 helicase. J Virol 83, 3268–3275

Bernstein J, Patterson DN, Wilson GM, Toth EA (2008): Characterization of the essential activities of Saccharomyces cerevisiae Mtr4p, a 3'->5' helicase partner of the nuclear exosome. J Biol Chem 283, 4930–4942

Bléoo S, Sun X, Hendzel MJ, Rowe JM, Packer M, Godbout R (2001): Association of human DEAD box protein DDX1 with a cleavage stimulation factor involved in 3'-end processing of pre-MRNA. Mol Biol Cell 12, 3046–3059

Bohnsack KE, Ficner R, Bohnsack MT, Jonas S (2021): Regulation of DEAH-box RNA helicases by G-patch proteins. Biol Chem 402, 561–579

Bohnsack MT, Martin R, Granneman S, Ruprecht M, Schleiff E, Tollervey D (2009): Prp43 bound at different sites on the pre-rRNA performs distinct functions in ribosome synthesis. Mol Cell 36, 583–592

Bonnal S, Martínez C, Förch P, Bachi A, Wilm M, Valcárcel J (2008): RBM5/Luca-15/H37 regulates Fas alternative splice site pairing after exon definition. Mol Cell 32, 81–95

Bono F, Ebert J, Lorentzen E, Conti E (2006): The crystal structure of the exon junction complex reveals how it maintains a stable grip on mRNA. Cell 126, 713–725

Bourgeois CF, Mortreux F, Auboeuf D (2016): The multiple functions of RNA helicases as drivers and regulators of gene expression. Nat Rev Mol Cell Biol 17, 426–438

Bowers HA, Maroney PA, Fairman ME, Kastner B, Lührmann R, Nilsen TW, Jankowsky E (2006): Discriminatory RNP remodeling by the DEAD-box protein DED1. RNA 12, 903–912

Bustin S, Huggett J (2017): qPCR primer design revisited. Biomol Detect Quantif 14, 19–28

Bustin SA, Nolan T (2004): Pitfalls of quantitative real-time reverse-transcription polymerase chain reaction. J Biomol Tech 15, 155–166

Cai MY, Zhang B, He WP, Yang GF, Rao HL, Rao ZY, Wu QL, Guan XY, Kung HF, Zeng YX et al. (2010): Decreased expression of PinX1 protein is correlated with tumor development and is a new independent poor prognostic factor in ovarian carcinoma. Cancer Sci 101, 1543–1549

Campbell PJ (2020): Pan-cancer analysis of whole genomes. Nature 578, 82–93

Causevic M, Hislop RG, Kernohan NM, Carey FA, Kay RA, Steele RJ, Fuller-Pace FV (2001): Overexpression and poly-ubiquitylation of the DEAD-box RNA helicase p68 in colorectal tumours. Oncogene 20, 7734–7743

Chang TH, Tung L, Yeh FL, Chen JH, Chang SL (2013): Functions of the DExD/H-box proteins in nuclear pre-mRNA splicing. Biochim Biophys Acta 1829, 764–774

Chaouki AS, Salz HK (2006): Drosophila SPF45: a bifunctional protein with roles in both splicing and DNA repair. PLoS Genet 2, e178

Chen Y, Potratz JP, Tijerina P, Del Campo M, Lambowitz AM, Russell R (2008): DEAD-box proteins can completely separate an RNA duplex using a single ATP. Proc Natl Acad Sci U S A 105, 20203–20208

Chen Z, Gui B, Zhang Y, Xie G, Li W, Liu S, Xu B, Wu C, He L, Yang J et al. (2017): Identification of a 35S U4/U6.U5 tri-small nuclear ribonucleoprotein (tri-snRNP) complex intermediate in spliceosome assembly. J Biol Chem 292, 18113–18128

Christian H, Hofele RV, Urlaub H, Ficner R (2014): Insights into the activation of the helicase Prp43 by biochemical studies and structural mass spectrometry. Nucleic Acids Res 42, 1162–1179

Coccia M, Rossi A, Riccio A, Trotta E, Santoro MG (2017): Human NF-κB repressing factor acts as a stress-regulated switch for ribosomal RNA processing and nucleolar homeostasis surveillance. Proc Natl Acad Sci U S A 114, 1045–1050

Cordin O, Beggs JD (2013): RNA helicases in splicing. RNA Biol 10, 83–95

Cortés-Ciriano I, Gulhan DC, Lee JJ, Melloni GEM, Park PJ (2021): Computational analysis of cancer genome sequencing data. Nat Rev Genet, 1–17

Dai MS, Challagundla KB, Sun XX, Palam LR, Zeng SX, Wek RC, Lu H (2012): Physical and functional interaction between ribosomal protein L11 and the tumor suppressor ARF. J Biol Chem 287, 17120–17129

Dardenne E, Polay Espinoza M, Fattet L, Germann S, Lambert MP, Neil H, Zonta E, Mortada H, Gratadou L, Deygas M et al. (2014): RNA helicases DDX5 and DDX17 dynamically orchestrate transcription, miRNA, and splicing programs in cell differentiation. Cell Rep 7, 1900–1913

De Maio A, Yalamanchili HK, Adamski CJ, Gennarino VA, Liu Z, Qin J, Jung SY, Richman R, Orr H, Zoghbi HY (2018): RBM17 Interacts with U2SURP and CHERP to Regulate Expression and Splicing of RNA-Processing Proteins. Cell Rep 25, 726-736.e7

Donehower LA, Harvey M, Slagle BL, McArthur MJ, Montgomery CA, Butel JS, Bradley A (1992): Mice deficient for p53 are developmentally normal but susceptible to spontaneous tumours. Nature 356, 215–221

Dumont S, Cheng W, Serebrov V, Beran RK, Tinoco I, Pyle AM, Bustamante C (2006): RNA translocation and unwinding mechanism of HCV NS3 helicase and its coordination by ATP. Nature 439, 105–108

Early Breast Cancer Trialists' Collaborative Group (2005): Effects of chemotherapy and hormonal therapy for early breast cancer on recurrence and 15-year survival: an overview of the randomised trials. Lancet 365, 1687–1717

Edamatsu H, Kaziro Y, Itoh H (2000): LUCA15, a putative tumour suppressor gene encoding an RNA-binding nuclear protein, is down-regulated in ras-transformed Rat-1 cells. Genes Cells 5, 849–858

Eisenberg E, Levanon EY (2013): Human housekeeping genes, revisited. Trends Genet 29, 569–574

Emi M, Fujiwara Y, Nakajima T, Tsuchiya E, Tsuda H, Hirohashi S, Maeda Y, Tsuruta K, Miyaki M, Nakamura Y (1992): Frequent loss of heterozygosity for loci on chromosome 8p in hepatocellular carcinoma, colorectal cancer, and lung cancer. Cancer Res 52, 5368–5372

Fairman-Williams ME, Guenther UP, Jankowsky E (2010): SF1 and SF2 helicases: family matters. Curr Opin Struct Biol 20, 313–324

Feng YZ, Zhang QY, Fu MT, Zhang ZF, Wei M, Zhou JY, Shi R (2017): Low expression of PinX1 is associated with malignant behavior in basal-like breast cancer. Oncol Rep 38, 109–119

Flores-Ramírez I, Rivas-Torres MÁ, Rodríguez-Dorantes M, Gutiérrez-Sagal R, Baranda-Avila N, Langley E (2021): Oncogenic role of PinX1 in prostate cancer cells through androgen receptor dependent and independent mechanisms. J Steroid Biochem Mol Biol 210, 105858

Fouraux MA, Kolkman MJM, van der Heijden A, de Jong AS, van Venrooij WJ, Pruihjn GJM (2002): The human La (SS-B) autoantigen interacts with DDX15/hPrp43, a putative DEAH-box RNA helicase. RNA 8, 1428–1443

Fu X-D, Ares M (2014): Context-dependent control of alternative splicing by RNA-binding proteins. Nat Rev Genet 15, 689–701

Fukuda T, Yamagata K, Fujiyama S, Matsumoto T, Koshida I, Yoshimura K, Mihara M, Naitou M, Endoh H, Nakamura T et al. (2007): DEAD-box RNA helicase subunits of the Drosha complex are required for processing of rRNA and a subset of microRNAs. Nat Cell Biol 9, 604–611

Fuller-Pace FV (2013): The DEAD box proteins DDX5 (p68) and DDX17 (p72): multi-tasking transcriptional regulators. Biochim Biophys Acta 1829, 756–763

Godbout R, Packer M, Bie W (1998): Overexpression of a DEAD box protein (DDX1) in neuroblastoma and retinoblastoma cell lines. J Biol Chem 273, 21161–21168

Gorbalenya AE, Koonin EV (1993): Helicases: amino sequence comparisons and structure-function relationships. Curr Opin Struct Biol 3, 419–429

Gorlin RJ, Cervenka J, Anderson RC, Sauk JJ, Bevis WD (1970): Robin's syndrome. A probably X-linked recessive subvariety exhibiting persistence of left superior vena cava and atrial septal defect. Am J Dis Child 119, 176–178

Gross T, Siepmann A, Sturm D, Windgassen M, Scarcelli JJ, Seedorf M, Cole CN, Krebber H (2007): The DEAD-box RNA helicase Dbp5 functions in translation termination. Science 315, 646–649

Halls C, Mohr S, Del Campo M, Yang Q, Jankowsky E, Lambowitz AM (2007): Involvement of DEAD-box proteins in group I and group II intron splicing. Biochemical characterization of Mss116p, ATP hydrolysis-dependent and -independent mechanisms, and general RNA chaperone activity. J Mol Biol 365, 835–855

Hamann F, Schmitt A, Favretto F, Hofele R, Neumann P, Xiang S, Urlaub H, Zweckstetter M, Ficner R (2020): Structural analysis of the intrinsically disordered splicing factor Spp2 and its binding to the DEAH-box ATPase Prp2. Proc Natl Acad Sci U S A 117, 2948–2956

Hardwick SW, Luisi BF (2013): Rarely at rest: RNA helicases and their busy contributions to RNA degradation, regulation and quality control. RNA Biol 10, 56–70

He Y, Andersen GR, Nielsen KH (2010): Structural basis for the function of DEAH helicases. EMBO Rep 11, 180–186

Heininger AU, Hackert P, Andreou AZ, Boon KL, Memet I, Prior M, Clancy A, Schmidt B, Urlaub H, Schleiff E et al. (2016): Protein cofactor competition regulates the action of a multifunctional RNA helicase in different pathways. RNA Biol 13, 320–330

Herschlag D (1995): RNA chaperones and the RNA folding problem. J Biol Chem 270, 20871–20874

Hilbert M, Karow AR, Klostermeier D (2009): The mechanism of ATP-dependent RNA unwinding by DEAD box proteins. Biol Chem 390, 1237–1250

Hilbert M, Kebbel F, Gubaev A, Klostermeier D (2011): eIF4G stimulates the activity of the DEAD box protein eIF4A by a conformational guidance mechanism. Nucleic Acids Res 39, 2260–2270

Hilliker A (2012): Analysis of RNA helicases in P-bodies and stress granules. Meth Enzymol 511, 323–346

Hirawake-Mogi H, Thanh Nhan NT, Okuwaki M (2021): G-patch domain-containing protein 4 localizes to both the nucleoli and Cajal bodies and regulates cell growth and nucleolar structure. Biochemical and biophysical research communications 559, 99–105

Højland AT, Lolas I, Okkels H, Lautrup CK, Diness BR, Petersen MB, Nielsen IK (2018): First reported adult patient with TARP syndrome: A case report. Am J Med Genet A 176, 2915–2918

Hollstein M, Sidransky D, Vogelstein B, Harris CC (1991): p53 mutations in human cancers. Science 253, 49–53

Hooper C, Hilliker A (2013): Packing them up and dusting them off: RNA helicases and mRNA storage. Biochim Biophys Acta 1829, 824–834

Hu Y, Li L, Seidelmann SB, Timur AA, Shen PH, Driscoll DJ, Wang QK (2008): Identification of association of common AGGF1 variants with susceptibility for Klippel-

Trenaunay syndrome using the structure association program. Ann Hum Genet 72, 636–643

Inoue A, Yamamoto N, Kimura M, Nishio K, Yamane H, Nakajima K (2014): RBM10 regulates alternative splicing. FEBS Lett 588, 942–947

Ishaq M, Ma L, Wu X, Mu Y, Pan J, Hu J, Hu T, Fu Q, Guo D (2009): The DEAD-box RNA helicase DDX1 interacts with RelA and enhances nuclear factor kappaB-mediated transcription. J Cell Biochem 106, 296–305

Ito S, Koso H, Sakamoto K, Watanabe S (2017): RNA helicase DHX15 acts as a tumour suppressor in glioma. Br J Cancer 117, 1349–1359

Jackson SP, Bartek J (2009): The DNA-damage response in human biology and disease. Nature 461, 1071–1078

Jacob AG, Driscoll DJ, Shaughnessy WJ, Stanson AW, Clay RP, Gloviczki P (1998): Klippel-Trénaunay syndrome: spectrum and management. Mayo Clin Proc 73, 28–36

Jankowsky E (2011): RNA helicases at work: binding and rearranging. Trends Biochem Sci 36, 19–29

Jankowsky E, Bowers H (2006): Remodeling of ribonucleoprotein complexes with DExH/D RNA helicases. Nucleic Acids Res 34, 4181–4188

Jankowsky E, Gross CH, Shuman S, Pyle AM (2001): Active disruption of an RNA-protein interaction by a DExH/D RNA helicase. Science 291, 121–125

Jarmoskaite I, Russell R (2014): RNA helicase proteins as chaperones and remodelers. Annu Rev Biochem 83, 697–725

Jeske M, Müller CW, Ephrussi A (2017): The LOTUS domain is a conserved DEAD-box RNA helicase regulator essential for the recruitment of Vasa to the germ plasm and nuage. Genes Dev 31, 939–952

Jing Y, Nguyen MM, Wang D, Pascal LE, Guo W, Xu Y, Ai J, Deng FM, Masoodi KZ, Yu X et al. (2018): DHX15 promotes prostate cancer progression by stimulating Siah2-mediated ubiquitination of androgen receptor. Oncogene 37, 638–650

Johnson JM, Castle J, Garrett-Engele P, Kan Z, Loerch PM, Armour CD, Santos R, Schadt EE, Stoughton R, Shoemaker DD (2003): Genome-wide survey of human alternative pre-mRNA splicing with exon junction microarrays. Science 302, 2141–2144

Johnson SJ, Jackson RN (2013): Ski2-like RNA helicase structures: common themes and complex assemblies. RNA Biol 10, 33–43

Johnston JJ, Sapp JC, Curry C, Horton M, Leon E, Cusmano-Ozog K, Dobyns WB, Hudgins L, Zackai E, Biesecker LG (2014): Expansion of the TARP syndrome phenotype associated with de novo mutations and mosaicism. Am J Med Genet A 164A, 120–128

Johnston JJ, Teer JK, Cherukuri PF, Hansen NF, Loftus SK, Chong K, Mullikin JC, Biesecker LG (2010): Massively parallel sequencing of exons on the X chromosome identifies RBM10 as the gene that causes a syndromic form of cleft palate. Am J Hum Genet 86, 743–748

Jonas S, Izaurralde E (2015): Towards a molecular understanding of microRNA-mediated gene silencing. Nat Rev Genet 16, 421–433

Kanai Y, Dohmae N, Hirokawa N (2004): Kinesin transports RNA: isolation and characterization of an RNA-transporting granule. Neuron 43, 513–525

Kaneko H, Kitoh H, Matsuura T, Masuda A, Ito M, Mottes M, Rauch F, Ishiguro N, Ohno K (2011): Hyperuricemia cosegregating with osteogenesis imperfecta is associated with a mutation in GPATCH8. Human genetics 130, 671–683

Kang J, Han K, Kim HJ, Park JH, Kong JS, Park S, Myung JK (2018): The clinical significance of PINX1 expression in papillary thyroid carcinoma. Hum Pathol 81, 176–183

Kapranov P, Cheng J, Dike S, Nix DA, Duttagupta R, Willingham AT, Stadler PF, Hertel J, Hackermüller J, Hofacker IL et al. (2007): RNA maps reveal new RNA classes and a possible function for pervasive transcription. Science 316, 1484–1488

Kibbe WA (2007): OligoCalc: an online oligonucleotide properties calculator. Nucleic Acids Res 35, W43-6

Koodathingal P, Novak T, Piccirilli JA, Staley JP (2010): The DEAH box ATPases Prp16 and Prp43 cooperate to proofread 5' splice site cleavage during pre-mRNA splicing. Mol Cell 39, 385–395

Kosar M, Giannattasio M, Piccini D, Maya-Mendoza A, García-Benítez F, Bartkova J, Barroso SI, Gaillard H, Martini E, Restuccia U et al. (2021): The human nucleoporin Tpr protects cells from RNA-mediated replication stress. Nat Commun 12, 3937

Křížová I, Hadravová R, Štokrová J, Günterová J, Doležal M, Ruml T, Rumlová M, Pichová I (2012): The G-patch domain of Mason-Pfizer monkey virus is a part of reverse transcriptase. J Virol 86, 1988–1998

Kruiswijk F, Labuschagne CF, Vousden KH (2015): p53 in survival, death and metabolic health: a lifeguard with a licence to kill. Nat Rev Mol Cell Biol 16, 393–405

Kuang J, Yan X, Genders AJ, Granata C, Bishop DJ (2018): An overview of technical considerations when using quantitative real-time PCR analysis of gene expression in human exercise research. PLoS One 13, e0196438

Kurpinski KT, Magyari PA, Gorlin RJ, Ng D, Biesecker LG (2003): Designation of the TARP syndrome and linkage to Xp11.23-q13.3 without samples from affected patients. Am J Med Genet A 120A, 1–4

Lebaron S, Papin C, Capeyrou R, Chen YL, Froment C, Monsarrat B, Caizergues-Ferrer M, Grigoriev M, Henry Y (2009): The ATPase and helicase activities of Prp43p are stimulated by the G-patch protein Pfa1p during yeast ribosome biogenesis. EMBO J 28, 3808–3819

Leitão AL, Costa MC, Enguita FJ (2015): Unzippers, resolvers and sensors: a structural and functional biochemistry tale of RNA helicases. Int J Mol Sci 16, 2269–2293

Levin MK, Gurjar M, Patel SS (2005): A Brownian motor mechanism of translocation and strand separation by hepatitis C virus helicase. Nat Struct Mol Biol 12, 429–435

Li C, Ge S, Zhou J, Peng J, Chen J, Dong S, Feng X, Su N, Zhang L, Zhong Y et al. (2020): Exploration of the effects of the CYCLOPS gene RBM17 in hepatocellular carcinoma. PLoS One 15, e0234062

Li HL, Song J, Yong HM, Hou PF, Chen YS, Song WB, Bai J, Zheng JN (2016): PinX1: structure, regulation and its functions in cancer. Oncotarget 7, 66267–66275

Li L, Wei Y, To C, Zhu CQ, Tong J, Pham N an, Taylor P, Ignatchenko V, Ignatchenko A, Zhang W et al. (2014): Integrated omic analysis of lung cancer reveals metabolism proteome signatures with prognostic impact. Nat Commun 5, 5469

Li R, Zhang H, Yu W, Chen Y, Gui B, Liang J, Wang Y, Sun L, Yang X, Zhang Y et al. (2009): ZIP: a novel transcription repressor, represses EGFR oncogene and suppresses breast carcinogenesis. EMBO J 28, 2763–2776

Li W, Fu Q, Man W, Guo H, Yang P (2019): LncRNA OR3A4 participates in the angiogenesis of hepatocellular carcinoma through modulating AGGF1/akt/mTOR pathway. Eur J Pharmacol 849, 106–114

Lin ML, Fukukawa C, Park JH, Naito K, Kijima K, Shimo A, Ajiro M, Nishidate T, Nakamura Y, Katagiri T (2009): Involvement of G-patch domain containing 2 overexpression in breast carcinogenesis. Cancer Sci 100, 1443–1450

Linder P, Jankowsky E (2011): From unwinding to clamping - the DEAD box RNA helicase family. Nat Rev Mol Cell Biol 12, 505–516

Liu J, Wang D, Zhang C, Zhang Z, Chen X, Lian J, Liu J, Wang G, Yuan W, Sun Z et al. (2018): Identification of liver metastasis-associated genes in human colon carcinoma by mRNA profiling. Chin J Cancer Res 30, 633–646

Liu Y, Conaway L, Rutherford Bethard J, Al-Ayoubi AM, Thompson Bradley A, Zheng H, Weed SA, Eblen ST (2013): Phosphorylation of the alternative mRNA splicing factor 45 (SPF45) by Clk1 regulates its splice site utilization, cell migration and invasion. Nucleic Acids Res 41, 4949–4962

Luo D, Xu T, Hunke C, Grüber G, Vasudevan SG, Lescar J (2008): Crystal structure of the NS3 protease-helicase from dengue virus. J Virol 82, 173–183

Mallam AL, Del Campo M, Gilman B, Sidote DJ, Lambowitz AM (2012): Structural basis for RNA-duplex recognition and unwinding by the DEAD-box helicase Mss116p. Nature 490, 121–125

Martin R, Straub AU, Doebele C, Bohnsack MT (2013): DExD/H-box RNA helicases in ribosome biogenesis. RNA Biol 10, 4–18

Memet I, Doebele C, Sloan KE, Bohnsack MT (2017): The G-patch protein NF-κB-repressing factor mediates the recruitment of the exonuclease XRN2 and activation of the RNA helicase DHX15 in human ribosome biogenesis. Nucleic Acids Res 45, 5359–5374

Mitsuhashi M (1996): Technical report: Part 1. Basic requirements for designing optimal oligonucleotide probe sequences. J Clin Lab Anal 10, 277–284

Mourtada-Maarabouni M, Keen J, Clark J, Cooper CS, Williams GT (2006): Candidate tumor suppressor LUCA-15/RBM5/H37 modulates expression of apoptosis and cell cycle genes. Exp Cell Res 312, 1745–1752

Mourtada-Maarabouni M, Sutherland LC, Meredith JM, Williams GT (2003): Simultaneous acceleration of the cell cycle and suppression of apoptosis by splice variant delta-6 of the candidate tumour suppressor LUCA-15/RBM5. Genes Cells 8, 109–119

Muller PAJ, Vousden KH (2013): p53 mutations in cancer. Nat Cell Biol 15, 2–8

Nakagawa Y, Yoshida A, Numoto K, Kunisada T, Wai D, Ohata N, Takeda K, Kawai A, Ozaki T (2006): Chromosomal imbalances in malignant peripheral nerve sheath tumor detected by metaphase and microarray comparative genomic hybridization. Oncol Rep 15, 297–303

Napetschnig J, Kassube SA, Debler EW, Wong RW, Blobel G, Hoelz A (2009): Structural and functional analysis of the interaction between the nucleoporin Nup214 and the DEAD-box helicase Ddx19. Proc Natl Acad Sci U S A 106, 3089–3094

Nishidate T, Katagiri T, Lin ML, Mano Y, Miki Y, Kasumi F, Yoshimoto M, Tsunoda T, Hirata K, Nakamura Y (2004): Genome-wide gene-expression profiles of breast-cancer cells purified with laser microbeam microdissection: identification of genes associated with progression and metastasis. Int J Oncol 25, 797–819

Niu Z, Jin W, Zhang L, Li X (2012): Tumor suppressor RBM5 directly interacts with the DExD/H-box protein DHX15 and stimulates its helicase activity. FEBS Lett 586, 977–983

Oh JJ, Grosshans DR, Wong SG, Slamon DJ (1999): Identification of differentially expressed genes associated with HER-2/neu overexpression in human breast cancer cells. Nucleic Acids Res 27, 4008–4017

Oh JJ, Razfar A, Delgado I, Reed RA, Malkina A, Boctor B, Slamon DJ (2006): 3p21.3 tumor suppressor gene H37/Luca15/RBM5 inhibits growth of human lung cancer cells through cell cycle arrest and apoptosis. Cancer Res 66, 3419–3427

Oh JJ, West AR, Fishbein MC, Slamon DJ (2002): A candidate tumor suppressor gene, H37, from the human lung cancer tumor suppressor locus 3p21.3. Cancer Res 62, 3207–3213

O'Leary NA, Wright MW, Brister JR, Ciufo S, Haddad D, McVeigh R, Rajput B, Robbertse B, Smith-White B, Ako-Adjei D et al. (2016): Reference sequence (RefSeq) database at NCBI: current status, taxonomic expansion, and functional annotation. Nucleic Acids Res 44, D733-45

Ordway JM, Bedell JA, Citek RW, Nunberg A, Garrido A, Kendall R, Stevens JR, Cao D, Doerge RW, Korshunova Y et al. (2006): Comprehensive DNA methylation profiling in a human cancer genome identifies novel epigenetic targets. Carcinogenesis 27, 2409–2423

Ozgur S, Buchwald G, Falk S, Chakrabarti S, Prabu JR, Conti E (2015): The conformational plasticity of eukaryotic RNA-dependent ATPases. FEBS J 282, 850–863

Pahl HL (1999): Activators and target genes of Rel/NF-kappaB transcription factors. Oncogene 18, 6853–6866

Pan C, Russell R (2010): Roles of DEAD-box proteins in RNA and RNP Folding. RNA Biol 7, 667–676

Pan L, Li Y, Zhang HY, Zheng Y, Liu XL, Hu Z, Wang Y, Wang J, Cai YH, Liu Q et al. (2017): DHX15 is associated with poor prognosis in acute myeloid leukemia (AML) and regulates cell apoptosis via the NF-kB signaling pathway. Oncotarget 8, 89643–89654

Pavlova NN, Thompson CB (2016): The Emerging Hallmarks of Cancer Metabolism. Cell Metab 23, 27–47

Pena V, Jovin SM, Fabrizio P, Orlowski J, Bujnicki JM, Lührmann R, Wahl MC (2009): Common design principles in the spliceosomal RNA helicase Brr2 and in the Hel308 DNA helicase. Mol Cell 35, 454–466

Pfaffl MW (2004): Real-time RT-PCR: Neue Ansätze zur exakten mRNA Quantifizierung. BIOspektrum 10, 92–95

Phan T, Kohlway A, Dimberu P, Pyle AM, Lindenbach BD (2011): The Acidic Domain of Hepatitis C Virus NS4A Contributes to RNA Replication and Virus Particle Assembly. J Virol 85, 1193–1204

Piccininni S, Varaklioti A, Nardelli M, Dave B, Raney KD, McCarthy JEG (2002): Modulation of the hepatitis C virus RNA-dependent RNA polymerase activity by the non-structural (NS) 3 helicase and the NS4B membrane protein. J Biol Chem 277, 45670–45679

Ponting CP (2000): Novel eIF4G domain homologues linking mRNA translation with nonsense-mediated mRNA decay. Trends Biochem Sci 25, 423–426

Putnam AA, Jankowsky E (2013): DEAD-box helicases as integrators of RNA, nucleotide and protein binding. Biochim Biophys Acta 1829, 884–893

Qian D, Cheng J, Ding X, Chen X, Chen X, Guan Y, Zhang B, Wang J, Er P, Qiu M et al. (2016): PinX1 suppresses tumorigenesis by negatively regulating telomerase/telomeres in colorectal carcinoma cells and is a promising molecular marker for patient prognosis. Onco Targets Ther 9, 4821–4831

Qian D, Zhang B, He LR, Cai MY, Mai SJ, Liao YJ, Liu YH, Lin MC, Bian XW, Zeng YX et al. (2013): The telomere/telomerase binding factor PinX1 is a new target to improve the radiotherapy effect of oesophageal squamous cell carcinomas. J Pathol 229, 765–774

Ramaswamy S, Ross KN, Lander ES, Golub TR (2003): A molecular signature of metastasis in primary solid tumors. Nat Genet 33, 49–54

Ranji A, Boris-Lawrie K (2010): RNA helicases: emerging roles in viral replication and the host innate response. RNA Biol 7, 775–787

Rasmussen R: Quantification on the LightCycler; In: Rapid cycle real-time PCR: Methods and applications, edited by Meuer SC, Wittwer C, Nakagawara K: Springer. Berlin, New York 2001, 21–34

Raymaekers M, Smets R, Maes B, Cartuyvels R (2009): Checklist for optimization and validation of real-time PCR assays. J Clin Lab Anal 23, 145–151

Rintala-Maki ND, Goard CA, Langdon CE, Wall VE, Traulsen KEA, Morin CD, Bonin M, Sutherland LC (2007): Expression of RBM5-related factors in primary breast tissue. J Cell Biochem 100, 1440–1458

Rintala-Maki ND, Sutherland LC (2004): LUCA-15/RBM5, a putative tumour suppressor, enhances multiple receptor-initiated death signals. Apoptosis 9, 475–484

Robert-Paganin J, Halladjian M, Blaud M, Lebaron S, Delbos L, Chardon F, Capeyrou R, Humbert O, Henry Y, Henras AK et al. (2017): Functional link between DEAH/RHA helicase Prp43 activation and ATP base binding. Nucleic Acids Res 45, 1539–1552

Robert-Paganin J, Réty S, Leulliot N (2015): Regulation of DEAH/RHA helicases by G-patch proteins. Biomed Res Int 2015

Robertson JM, Walsh-Weller J (1998): An introduction to PCR primer design and optimization of amplification reactions. Methods Mol Biol 98, 121–154

Romond EH, Perez EA, Bryant J, Suman VJ, Geyer CE, Davidson NE, Tan-Chiu E, Martino S, Paik S, Kaufman PA et al. (2005): Trastuzumab plus adjuvant chemotherapy for operable HER2-positive breast cancer. N Engl J Med 353, 1673–1684

Roth J, Lenz-Bauer C, Contente A, Löhr K, Koch P, Bernard S, Dobbelstein M (2003): Reactivation of mutant p53 by a one-hybrid adaptor protein. Cancer Res 63, 3904–3908

Russell R (2008): RNA misfolding and the action of chaperones. Front Biosci 13, 1–20

Sales-Lee J, Perry DS, Bowser BA, Diedrich JK, Rao B, Beusch I, Yates JR, Roy SW, Madhani HD (2021): Coupling of spliceosome complexity to intron diversity. Curr Biol 31, 4898-4910.e4

Sampath J, Long PR, Shepard RL, Xia X, Devanarayan V, Sandusky GE, Perry WL, Dantzig AH, Williamson M, Rolfe M et al. (2003): Human SPF45, a Splicing Factor, Has Limited Expression in Normal Tissues, Is Overexpressed in Many Tumors, and Can Confer a Multidrug-Resistant Phenotype to Cells. Am J Pathol. 163, 1781–1790

Sampson ND, Hewitt JE (2003): SF4 and SFRS14, two related putative splicing factors on human chromosome 19p13.11. Gene 305, 91–100

Schütz P, Bumann M, Oberholzer AE, Bieniossek C, Trachsel H, Altmann M, Baumann U (2008): Crystal structure of the yeast eIF4A-eIF4G complex: an RNA-helicase controlled by protein-protein interactions. Proc Natl Acad Sci U S A 105, 9564–9569

Schütz P, Karlberg T, van den Berg S, Collins R, Lehtiö L, Högbom M, Holmberg-Schiavone L, Tempel W, Park HW, Hammarström M et al. (2010): Comparative structural analysis of human DEAD-box RNA helicases. PLoS One 5

Semlow DR, Blanco MR, Walter NG, Staley JP (2016): Spliceosomal DEAH-Box ATPases remodel pre-mRNA to activate alternative splice sites. Cell 164, 985–998

Semlow DR, Staley JP (2012): Staying on message: ensuring fidelity in pre-mRNA splicing. Trends Biochem Sci 37, 263–273

Shajani Z, Sykes MT, Williamson JR (2011): Assembly of bacterial ribosomes. Annu Rev Biochem 80, 501–526

Shiryaev SA, Chernov AV, Aleshin AE, Shiryaeva TN, Strongin AY (2009): NS4A regulates the ATPase activity of the NS3 helicase: a novel cofactor role of the non-structural protein NS4A from West Nile virus. J Gen Virol 90, 2081–2085

Shiryaev SA, Chernov AV, Shiryaeva TN, Aleshin AE, Strongin AY (2011): The acidic sequence of the NS4A cofactor regulates ATP hydrolysis by the HCV NS3 helicase. Arch Virol 156, 313–318

Si W, Zhou B, Xie W, Li H, Li K, Li S, Deng W, Shi P, Yuan C, Ke T et al. (2021): Angiogenic factor AGGF1 acts as a tumor suppressor by modulating p53 post-transcriptional modifications and stability via MDM2. Cancer Lett 497, 28–40

Sloan KE, Bohnsack MT (2018): Unravelling the Mechanisms of RNA Helicase Regulation. Trends Biochem Sci 43, 237–250

Steckelberg AL, Boehm V, Gromadzka AM, Gehring NH (2012): CWC22 connects pre-mRNA splicing and exon junction complex assembly. Cell Rep 2, 454–461

Steimer L, Klostermeier D (2012): RNA helicases in infection and disease. RNA Biol 9, 751–771

Story RM, Steitz TA (1992): Structure of the recA protein-ADP complex. Nature 355, 374–376

Story RM, Weber IT, Steitz TA (1992): The structure of the E. coli recA protein monomer and polymer. Nature 355, 318–325

Strunk BS, Karbstein K (2009): Powering through ribosome assembly. RNA 15, 2083–2104

Studer MK, Ivanović L, Weber ME, Marti S, Jonas S (2020): Structural basis for DEAH-helicase activation by G-patch proteins. Proc Natl Acad Sci U S A 117, 7159–7170

Stumpf CR, Ruggero D (2011): The cancerous translation apparatus. Curr Opin Genet Dev 21, 474–483

Sutherland LC, Rintala-Maki ND, White RD, Morin CD (2005): RNA binding motif (RBM) proteins: a novel family of apoptosis modulators? J Cell Biochem 94, 5–24

Svec M, Bauerová H, Pichová I, Konvalinka J, Strísovský K (2004): Proteinases of betaretroviruses bind single-stranded nucleic acids through a novel interaction module, the G-patch. FEBS Lett 576, 271–276

Swiech K, Picanço-Castro V, Covas DT (2012): Human cells: new platform for recombinant therapeutic protein production. Protein Expr Purif 84, 147–153

Talbot SJ, Crawford DH (2004): Viruses and tumours – an update. Eur J Cancer 40, 1998–2005

Tauchert MJ, Fourmann JB, Lührmann R, Ficner R (2017): Structural insights into the mechanism of the DEAH-box RNA helicase Prp43. Elife 6, e21510

The UniProt Consortium (2019): UniProt: a worldwide hub of protein knowledge. Nucleic Acids Res 47, 506–515

The UniProt Consortium (2021): UniProt: the universal protein knowledgebase in 2021. Nucleic Acids Res 49, D480-D489

Thomas P, Smart TG (2005): HEK293 cell line: a vehicle for the expression of recombinant proteins. J Pharmacol Toxicol Methods 51, 187–200

Tian XL, Kadaba R, You SA, Liu M, Timur AA, Yang L, Chen Q, Szafranski P, Rao S, Wu L et al. (2004): Identification of an angiogenic factor that when mutated causes susceptibility to Klippel-Trenaunay syndrome. Nature 427, 640–645

Tian XP, Qian D, He LR, Huang H, Mai SJ, Li CP, Huang XX, Cai MY, Liao YJ, Kung HF et al. (2014): The telomere/telomerase binding factor PinX1 regulates paclitaxel sensitivity depending on spindle assembly checkpoint in human cervical squamous cell carcinomas. Cancer Lett 353, 104–114

Timur AA, Driscoll DJ, Wang Q (2005): Biomedicine and diseases: the Klippel-Trenaunay syndrome, vascular anomalies and vascular morphogenesis. Cell Mol Life Sci 62, 1434–1447

Vallejo-Illarramendi A, Marciano DK, Reichardt LF (2013): A novel method that improves sensitivity of protein detection in PAGE and Western blot. Electrophoresis 34, 1148–1150

Vargo-Gogola T, Rosen JM (2007): Modelling breast cancer: one size does not fit all. Nat Rev Cancer 7, 659–672

Vermeulen J, de Preter K, Lefever S, Nuytens J, Vloed F de, Derveaux S, Hellemans J, Speleman F, Vandesompele J (2011): Measurable impact of RNA quality on gene expression results from quantitative PCR. Nucleic Acids Res 39

Wang W, Cassidy J, O'Brien V, Ryan KM, Collie-Duguid E (2004): Mechanistic and predictive profiling of 5-Fluorouracil resistance in human cancer cells. Cancer Res 64, 8167–8176

Wang Y, Gogol-Döring A, Hu H, Fröhler S, Ma Y, Jens M, Maaskola J, Murakawa Y, Quedenau C, Landthaler M et al. (2013): Integrative analysis revealed the molecular mechanism underlying RBM10-mediated splicing regulation. EMBO Mol Med 5, 1431–1442

Watkins NJ, Bohnsack MT (2012): The box C/D and H/ACA snoRNPs: key players in the modification, processing and the dynamic folding of ribosomal RNA. Wiley Interdiscip Rev RNA 3, 397–414

Weir JR, Bonneau F, Hentschel J, Conti E (2010): Structural analysis reveals the characteristic features of Mtr4, a DExH helicase involved in nuclear RNA processing and surveillance. Proc Natl Acad Sci U S A 107, 12139–12144

Witten JT, Ule J (2011): Understanding splicing regulation through RNA splicing maps. Trends Genet 27, 89–97

Wong ML, Medrano JF (2005): Real-time PCR for mRNA quantitation. BioTechniques 39, 75–85

Xie C, Liao H, Zhang C, Zhang S (2019): Overexpression and clinical relevance of the RNA helicase DHX15 in hepatocellular carcinoma. Hum Pathol 84, 213–220

Yang Q, Jankowsky E (2005): ATP- and ADP-dependent modulation of RNA unwinding and strand annealing activities by the DEAD-box protein DED1. Biochemistry 44, 13591–13601

Yang Q, Jankowsky E (2006): The DEAD-box protein Ded1 unwinds RNA duplexes by a mode distinct from translocating helicases. Nat Struct Mol Biol 13, 981–986

Yao HH, Zhao YJ, He YF, Da Huang B, Wang W (2019): Knockdown of AGGF1 inhibits the invasion and migration of gastric cancer via epithelial-mesenchymal transition through Wnt/β-catenin pathway. Cancer Cell Int 19, 41

Ye J, Coulouris G, Zaretskaya I, Cutcutache I, Rozen S, Madden TL (2012): Primer-BLAST: a tool to design target-specific primers for polymerase chain reaction. BMC Bioinformatics 13, 134

Yokota T, Yoshimoto M, Akiyama F, Sakamoto G, Kasumi F, Nakamura Y, Emi M (1999): Localization of a tumor suppressor gene associated with the progression of human breast carcinoma within a 1-cM interval of 8p22-p23.1. Cancer 85, 447–452

Yoo JE, Park YN, Oh BK (2014): PinX1, a telomere repeat-binding factor 1 (TRF1)-interacting protein, maintains telomere integrity by modulating TRF1 homeostasis, the process in which human telomerase reverse Transcriptase (hTERT) plays dual roles. J Biol Chem 289, 6886–6898

Yuan JS, Reed A, Chen F, Stewart CN (2006): Statistical analysis of real-time PCR data. BMC Bioinformatics 7, 85

Zhang T, Yao Y, Wang J, Li Y, He P, Pasupuleti V, Hu Z, Jia X, Song Q, Tian XL et al. (2016): Haploinsufficiency of Klippel-Trenaunay syndrome gene Aggf1 inhibits developmental and pathological angiogenesis by inactivating PI3K and AKT and disrupts vascular integrity by activating VE-cadherin. Hum Mol Genet 25, 5094–5110

Zhang X, Sun H, Chen W, He X (2019): Elevated expression of AGGF1 predicts poor prognosis and promotes the metastasis of colorectal cancer. BMC Cancer 19

Zhao H, Sun Q, Li L, Zhou J, Zhang C, Hu T, Zhou X, Zhang L, Wang B, Li B et al. (2019): High Expression Levels of AGGF1 and MFAP4 Predict Primary Platinum-Based Chemoresistance and are Associated with Adverse Prognosis in Patients with Serous Ovarian Cancer. J Cancer 10, 397–407

Zhao L, Li R, Shao C, Li P, Liu J, Wang K (2012): 3p21.3 tumor suppressor gene RBM5 inhibits growth of human prostate cancer PC-3 cells through apoptosis. World J Surg Oncol 10, 247

Zhou XZ, Huang P, Shi R, Lee TH, Lu G, Zhang Z, Bronson R, Lu KP (2011): The telomerase inhibitor PinX1 is a major haploinsufficient tumor suppressor essential for chromosome stability in mice. J Clin Invest 121, 1266–1282

Zhou XZ, Lu KP (2001): The Pin2/TRF1-interacting protein PinX1 is a potent telomerase inhibitor. Cell 107, 347–359

Acknowledgements

First, I would like to thank everyone who continuously supported and motivated me in writing this thesis.

I especially want to thank …

…my supervisor Prof. Dr. Markus T. Bohnsack for his excellent supervision and support, your patience and all the helpful recommendations.

…Dr. Katherine Bohnsack for her remarkable supervision, ideas and help with any concern, as well as the proofreading.

… Dr. Indira Memet for the good initial incorporation training and help.

…Dr. Jens Kretschmer for the help with data analysis.